Log Book

Log Book

Philippe

Ph.W. Courteille
Universidade de São Paulo
Instituto de Física de São Carlos
22/08/2025

2

.

Part I

Log books

Chapter 0

Strontium lattices

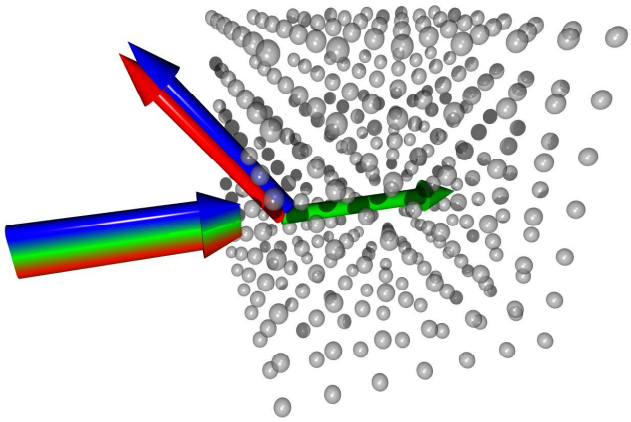

0.1 15.05.2009 First ideas

In the first years the experiment on ***Collective scattering from Bose-condensates*** will be the main experiment to be set up at São Carlos. The project ***Cavity QED with sub-recoil resolution*** is technically more demanding and can only be considered in the eventuality of good financial funding. The project ***Many-body physics with fermions in lattices*** needs to be worked out. All other projects are either based on experimental setups at Tübingen (Zimmermann, Guérin), Nice (Kaiser) or São Carlos (Bagnato), or small side projects supporting those experiments.

My projects for IRSES could be ***Crystallography of optical lattices***, i.e. demonstrate various types of lattices with ultracold Rb (e.g. 2D plaquettes, Mott insulators), demonstrate bcc and diamond lattice with strontium photonic bands.

0.1.1 Collective scattering from Bose-condensates

Cooperativity and disorder govern the interaction of ultracold atomic clouds with light. Due to their small sizes and low temperatures Bose-Einstein condensates are ideal test objects for measuring the impact of collective effects on light scattering via the radiation pressure.

The question is which species to chose. Rubidium is nice and easy, but we will need to be able to adjust the interatomic interaction with Feshbach resonances.

Goals, questions, visions

- identify collective effects in light scattering
- radiation pressure measurements for BECs
- outlook on photon condensation or subradiant entanglement

Methods, equipment

- cold atoms in a magneto-optical trap
- setup for Bose-Einstein condensation of rubidium
- dipole trap for strong confinement
- possibility of addressing a Feshbach resonance

Manpower, tasks

- 1-2 PhD thesis for setting up the whole experiments and doing the measurements
- access to good mechanical and electronic workshops

Time schedule

- year 1: equipment of a lab, optical table, oscilloscopes, power supplies and current drives, vacuum chambers, etc.
- year 2: setting up lasers, optics, sensitive cameras, computer control systems for setting up the MOT and the BEC
- year 3: reaching the quantum-degenerate regime and measuring the response of BECs to incident light

Collaboration

- Nice (France) and Milano (Italy)

Financing

- FAPESP , FP7 (Marie Curie IRSES und INCO)

0.1.2 Cavity QED with sub-recoil resolution

The aim of this project is the construction of a high-level experiment combining Bose-Einstein condensates with CQED in a new regime, where the cavity finesse is high enough to resolve the atomic motion on the sub-recoil level.

Goals, questions, visions

- reach the strong coupling regime with a condensate in a "long cavity"
- study collective cavity QED with "dual" quantization of the atomic motion and the light field

Methods, equipment

- Bose-Einstein condensation of strontium (or calcium)
- development of ultrahigh finesse ring cavities
- laser frequency stabilization of diode lasers on ultrahigh finesse cavities

Manpower, tasks

- 2 graduate students for more than three years

Time schedule

- ¿3 years

Collaboration

- perhaps Prof. Dr. D. Magalhães with a common project of developing a Pound-Drever-Hall servo electronics

Financing

- FAPESP

0.1.3 Many-body physics with fermions in lattices

Fermions or mixtures of fermions and bosons in optical lattices bear the potentiality of simulating more complicated many-body systems such as electron gases in solids, superfluids and superconductors. They offer the advantage of high purity, wide tuning ranges for relevant parameters and thermodynamic potentials and controllable impurities. The goal of this project is the implementation of ^{6}Li-^{7}Li mixtures as quantum simulator. For practicability and versatility I would use a. lithium (or potassium) and b. dipole traps for high repetition rates.

Goals, questions, visions

- study few and many-body physics with lithium

Methods, equipment

- Bose-Einstein condensates of ^{7}Li and Fermi gas of ^{6}Li
- purely optical trap (high power 1 μm fiber laser) fed by a 2D-MOT
- Feshbach resonances, reduced dimensions, very small volumes
- design should be able to accommodate a ring cavity at a later stage
- evtl. use potassium because for easier handling

Manpower, tasks

- 1-2 graduate students

Time schedule

- $>$ 3 years

Collaboration

- Prof. Dr. K. Capelle from the ABC University of São Paulo

Financing

- FAPESP

0.1.4 Photonic bands in optical lattices

The project consists of two branches. The first branches consists in a continuation of an experiment started at the University of Tübingen in mid 2009. The second branch will be an experiment to be started in São Carlos studying band structure of exotic optical lattices with ultracold strontium. The exchange of students between São Carlos and Tübingen is highly recommended.

Goals, questions, visions

- detecting photonic bands in an optical lattice
- study the impact of disorder
- watch for signatures of localization of light
- consider complete 3D bandgaps in lattices of ^{174}Yb or $84Sr$

Methods, equipment

- the Tübingen experiment consists of a MOT feeding a 1D optical lattice made by an optical standing wave
- we analyze the spectrum of Bragg-scattered light

Manpower, tasks

- 1 PhD from São Carlos

Time schedule

- 2 years

Collaboration

- Prof. Dr. C. Zimmermann from the University of Tübingen (Germany)
- Dr. W. Guerin from the University of Tübingen (Germany)
- Dipl.-Phys. A. Schilke from the University of Tübingen (Germany)

Financing

- FAPESP for travel expenses, FP7, Humboldt-Stiftung

0.1.5 Ultracold fusion with Bose-condensates

The aim if this project is the continuation of the Tübingen CARL experiment in collaboration with my São Carlos group. Together with a graduate student from São Carlos I would give practical and conceptual advise and theoretical support.

At a later stage, one could consider supporting research in the form of smaller side projects. For example, the development of an ultrahigh finesse cavity, design of a stable Pound-Drever-Hall servo for diode lasers, etc.). Even later, one would head for a thermal CARL experiment in São Carlos or introduce a cavity in an existing BEC apparatus.

Goals, questions, visions

- numerical simulation of Ramsey experiment, develop intuitive picture of the process
- predictions for Raman CARL
- quantum CARL and quantum synchronization
- ideas for the very good cavity limit
- manipulate the scattering of light and hence tailoring the atomic motion with optical cavities, ring cavities in the quantum-good-cavity limit (Cavity-enforced Atomic Quantum Dynamics, CAQD). The ETH experiment is in the CQED regime, where the atomic quantum dynamics is obtained via ultra-low pumping.
- micro ring cavities and squeezed light
- Mott-isolator with cavity for 1D
- why is "ring" cavity necessary for JJ experiment?
- BEC damping: calculate, consider two-sided incoupling

Methods, equipment

- the Tübingen BEC equipment

Manpower, tasks

- 1 graduate student for theoretical support, will establish a link to Tübingen
- 1 undergraduate student for constructing a supercavity and locking a laser to it
- my conceptual support, supervision and guidance of Tübingen PhD thesis

Time schedule

- 3 years, beyond the end of Simone's thesis

Collaboration

- Prof. Dr. C. Zimmermann from the University of Tübingen (Germany)
- Prof. Dr. D. Magalhães, common project of developing a PDH servo electronics
- follow-up of DFG CARL project with C. Gnahm

Financing

- DFG-FAPESP? for travel and a São Carlos student's stay in Tübingen
- FP7?

0.2 03.03.2010 More ideas

- BEC and macroscopic particles, nanotubes, walls, colloids or fullerenes trapped in optical tweezers
- photonic condensates
- full band gaps in Bravais lattices
- adiabatic potentials, electric Feshbach resonance, plasmons and cold atoms

Start a strontium CARL experiment in parallel, use it as a first step to subrecoil resolution CQED.

0.3 15.04.2010 Proposal

I decided to go for strontium and wrote a proposal to FAPESP. The first goal is to obtain cold strontium in an optical trap. The motivation is long-termed. The selling arguments for strontium are 1. optical frequency standards, 2. gaseous photonic crystals, 3. CQED with subrecoil resolution, 4. superradiance on slower decay rates. Vanderlei takes it with him for reading and correcting the portuguese.

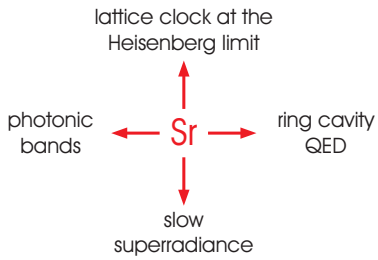

Figure 1: (code) Sr projects.

Strontium apparatus
- mechanical setup
- oven
- Zeeman slower
- main chamber
- magnetic field
- optical setup
- laser at 461 nm
- heatpipe
- laser at 689 nm
- stable cavity
- PDH stabilization
- bandwidth broadening
- laser at 497 nm
- laser at 1064 nm
- crossed dipole trap
- optical lattice

0.4 17.04.2010 Level scheme

The level scheme of strontium is shown in Fig. 2 [95]. The experiment can be devided into several stages, starting with the blue MOT, then loading onto the red MOT, then into the lattice. The first level of construction requires the vacuum chamber and a laser at 461 nm. At a second stage, we want a laser 689 nm. This laser must be stabilized to a cavity using a Pound-Drever-Hall servo.

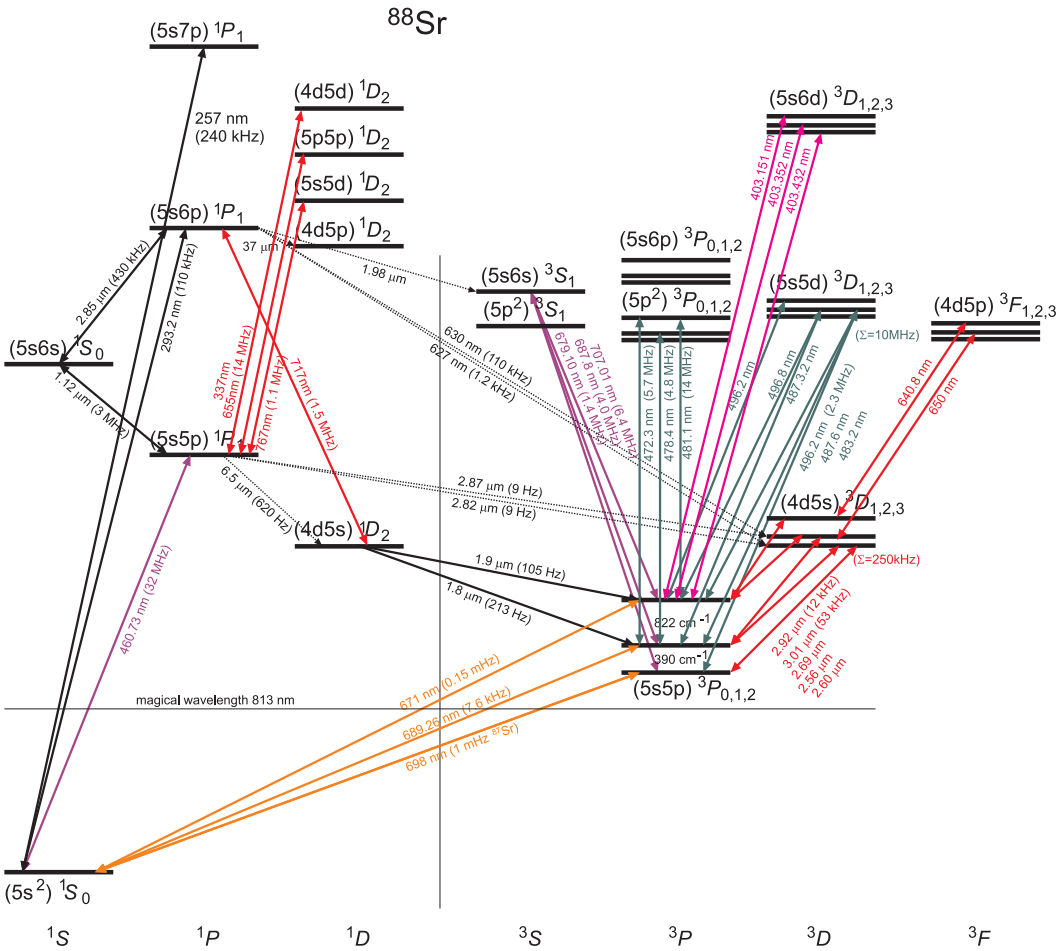

Figure 2: (code) Grotian diagram of strontium.

0.5 18.04.2010 Strontium data

***Isotopes.*—**

Sr isotope	nuclear spin	natural abundance	scattering length	shift of 461nm line
88	0	82.6%	$-2a_B$	0
87	9/2	7%		$-60\,\mathrm{MHz}$
86	0	9.8%	$+800a_B$	$-125\,\mathrm{MHz}$
84	0	0.56%	$+122.7a_B$	$-270\,\mathrm{MHz}$

Interspecies scattering length $a_{88-87} = 55a_B$.
$\nu_{461}^{88} = 434.829\,121\,311\,(10)\,\mathrm{THz}$, $\nu_{461}^{86} = \nu_{461}^{88} - 163.817\,4\,(2)\,\mathrm{MHz}$.

***Strontium transition wavelengths.*—**

$c = 299792458\,\mathrm{m/s}$

term	energy [cm^{-1}]	[nm]	[THz]
^{88}Sr $5s^2\ {}^1S_0$	0	0	0
^{88}Sr $5s5p\ {}^1P_1$	21698.452	460.86237	650.50323
^{88}Sr $5s5p\ {}^3P_0$	14317.507	698.44562	429.228 066 418 008 3
^{88}Sr $5s5p\ {}^3P_1$	14504.3382416	689.448896836	434.829 121 311
^{87}Sr $5s5p\ {}^3P_1$			$\nu_{87} - 60\,\mathrm{MHz}$
^{86}Sr $5s5p\ {}^3P_1$			$\nu_{86} - 163.816\,\mathrm{MHz}$
^{84}Sr $5s5p\ {}^3P_1$			$\nu_{84} - 270\,\mathrm{MHz}$
^{88}Sr $5s5p\ {}^3P_2$	14898.545	671.20648	446.64714
^{88}Sr $5s5p\ {}^3P_2 - 5s5d\ {}^1D_2$	20133.11	496.6943	603.5754
^{88}Sr $5s5p\ {}^3P_2 - 5s5d\ {}^3D_1$	20108.47	497.3028	602.8368
^{88}Sr $5s5p\ {}^3P_2 - 5s5d\ {}^3D_2$	20123.55	496.9303	603.2887
^{88}Sr $5s5p\ {}^3P_2 - 5s5d\ {}^3D_3$	20146.58	496.3621	603.9793

***Characteristic frequencies.*—**

transition	linewidth	Doppler limit	recoil shift
formula		$\frac{1}{2}\hbar\Gamma$	$\frac{\hbar^2 k^2}{2m}$
461 nm	32 MHz	770 µK	10.7 kHz = 512 nK
689 nm	7.6 kHz	180 nK	4.8 kHz = 229 nK
767 nm	1.1 MHz	26 µK	3.9 kHz = 185 nK

0.6 30.04.2010 Possible vacuum system

I am slowly starting to plan the vacuum apparatus and lasers. Here are some points to consider:

Oven. —

Generation of an atomic beam via an effusion oven. Temperature of the oven 575° and of the nozzle 850° [66].

Transverse cooling by a 2D molasses needs 20 mW.

Slowing by a 20 cm long constant deceleration σ_- Zeeman slower with a peak magnetic field of 600 G needs 60 mW @461 nm.

Chamber. —

We want a main chamber with very good optical access. This is very important for testing various lattice geometries e.g. diamond configurations. Evtl. we want space for accomodating a ring cavity.

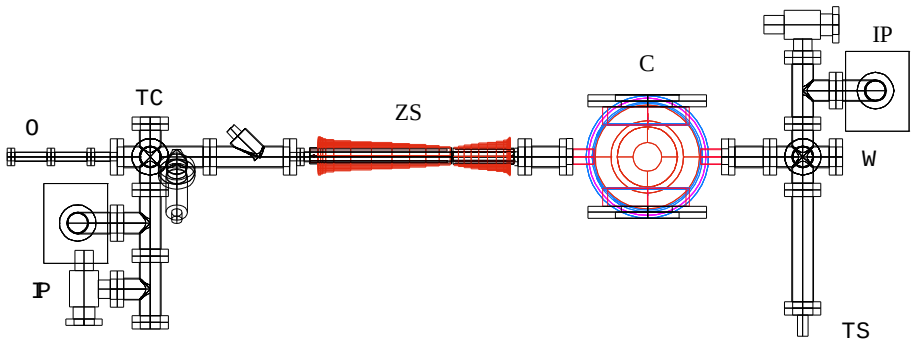

Fig. 16. Vacuum aparatus. O: oven for St sublimation; IP: ion pumps; TC: cell for transverse cooling; ZS: differential pumping tube for the Zeeman slower; C: MOT cell; TS: titanium sublimation pump; W: sapphire window for the Zeeman slower laser beam.

Figure 3: (code) Possible vacuum apparatus according to [Sorrentino06].

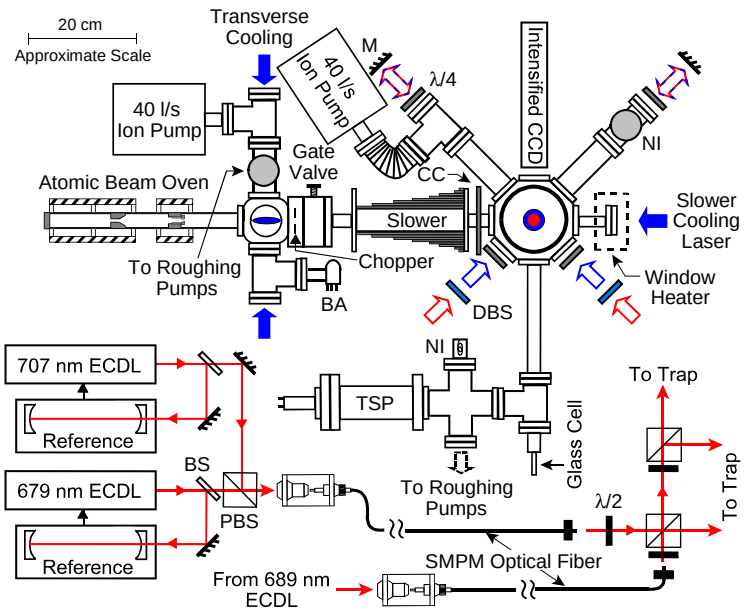

Figure 4: (code) Possible vacuum apparatus according to [Ludlow-09].

0.7 01.05.2010 Possible laser system

Blue MOT.—

A laser at 461 nm is needed with about 200 mW.

Option 1: TA-SHG pro laser from Toptica: fast but expensive 90000 Eur

Option 2: Master-slave with master locked by opt. feedback to stable cavity and slave with

Option 3: stilbene 3 dye laser: certainly not

Control of laser frequency with a heatpipe for saturation spectroscopy.

Red MOT.—

A laser at 689 nm is needed with about 30 mW.

Option 1: TA-SHG pro laser from Toptica: fast but expensive 90000 Eur

Option 2: Extended cavity diode laser (ECDL) with a Hitachi HL6738MG mounted in the Littrow configuration which delivers typically 15 mW [Ferrari03]

Magnetic trap.—

magnetic trap for metastable $^2P_{1/2}$ atoms

depopulator at 497 nm

10s MOT loading time + 6s evaporation time

Optical lattice.—

Using Vanderlei's IPG?

0.8 02.05.2010 Planing PhD and diploma thesis

Andrés. —

The working title is *Construção de uma armadilha magnéto-óptica para estrôncio.*

Dominik. —

Set up an ECLD at 689 nm and stabilize it to a stable cavity. This would be an interesting collaboration project with Daniel. Especially, because of the existence of mHz transitions at 698 nm. The optics should thus be planned broadband between 670..700 nm. The working title is *Aufbau eines frequenzstabilen Lasers bei 689 nm für eine magneto-optische Falle für Strontium auf dem* $^1S_0 -^3 P_1$ *Übergang.*

Alexander. —

Set up the blue and then the red Sr MOT. Construction of laser at 461 nm and of a heatpipe for Lamb-dip spectroscopy. Designing the Sr oven, the Zeeman slower, and the chamber. Optimization for good optical access.

Some infos to consider: -480 MHz for Zeeman slowing beam, transverse molasses cooling, 500° hot heatpipe with sapphire windows, > 100 G/cm^2 for MOT gradient, use 922 nm for an optical trap,...

Helmar. —

Planing the apparatus, exotic lattice calculations, band calculations.

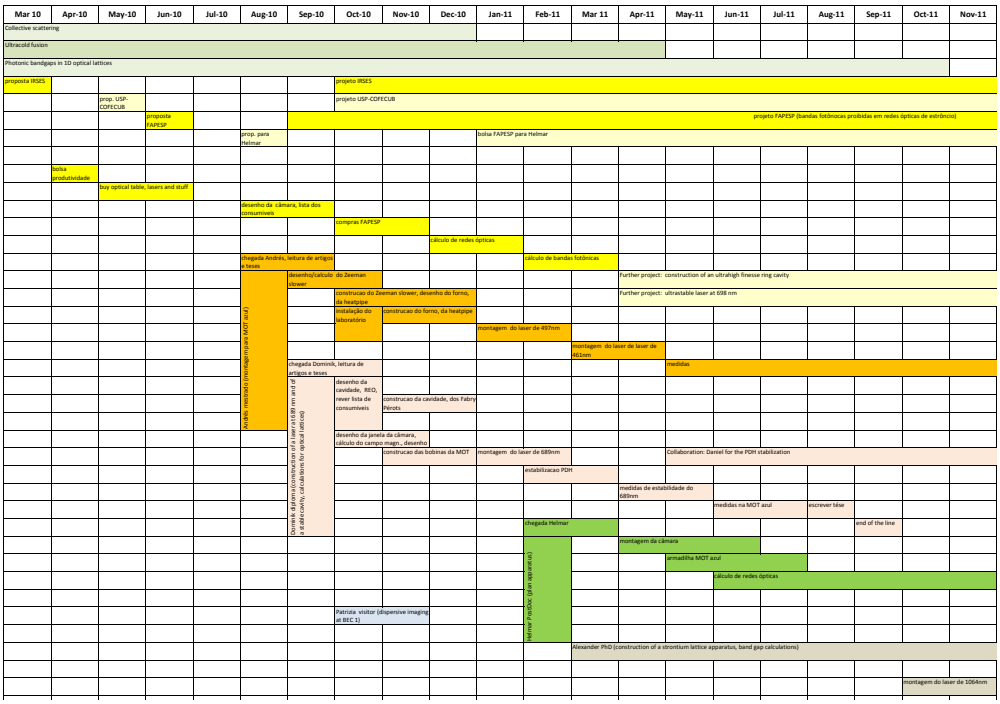

Figure 5: (code) Workplan.

0.9 03.05.2010 Proposition for a collaboration with Daniel

The goal of the project the development of an optical frequency standard based on clock transitions in ultracold strontium lattices. The strontium part will be set up by myself. Daniel would collaborate on the metrology part of the project.

The metrology part is conceived in two stages: **1.** Construction of a kHz stable ECDL laser system at 689 nm. This laser is also needed for second stage cooling of strontium. **2.** In a second stage this laser system will be duplicated, but at 698 nm and with an improved stability. This is because the interesting clock transition in strontium at 698 nm has mHz linewidth. Hence this laser will be locked in a second step to an ultrastable cavity. Once the strontium lattice is available, we will set up an optical clock.

For the first stage, the main components of the laser system are:
a. an ECDL at 689 nm (with peltier, grating and piezo, evtl. buy from Toptica), (Toptica) current supply and temperature stabilizer, an optical isolator, 2 AOMs, mirrors and polarization optics for 670 nm to 700 nm;
b. a stable cavity in a vacuum chamber (2l ion pump) with mechanical damping and temperature stabilization, quartz spacer, piezo, EOM, fast electronics;
c. a pump-probe spectroscopy on a strontium heat pipe.

For the second stage (after 2 years?) the technology developped for 689 nm will

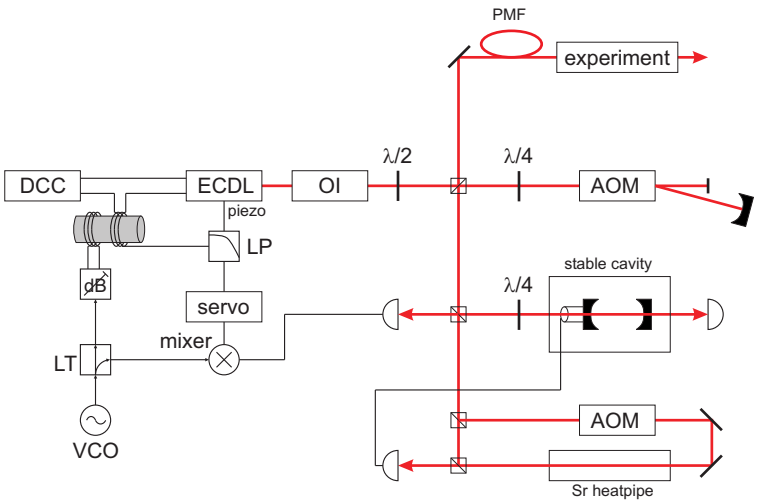

Figure 6: (code) Possible laser system at 689 nm according to [Poli06].

also be applied to 698 nm. In parallel, an apparatus for ultracold strontium in a lattice will be set up. The tasks for the collaborative projects are then
a. develop a 2nd stage stabilization to an ultrastable cavity without piezo;
b. locking the laser to the mHz clock transition.

0.10 29.06.2010 Design of magnetic trap and Zeeman slower

Using the approach of [53] we need a quadrupole magnetic field with 160 G/cm^2. Having a Zeeman slower, we probably don't need large MOT beam diameters, so that the coils can be quite close. BEC1 experiment: distance of coils 40 mm, maximum current I=25 A, gradient 160 G/cm^2.

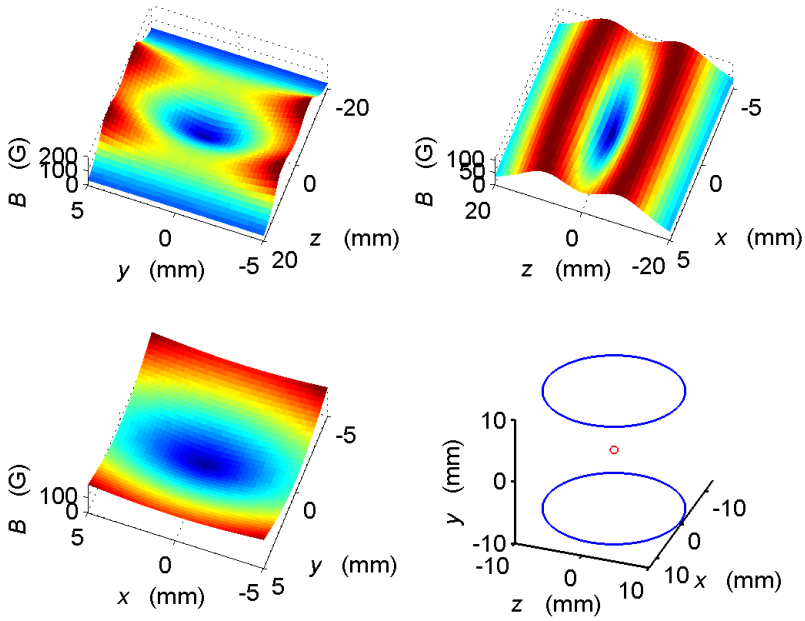

Figure 7: (code) Magnetic quadrupole trap.

30 cm Zeeman slower with -270 MHz shifted cooling light or
30 cm Zeeman slower -+300 G with 0 crossing and -500 MHz shifted cooling light (30 mW)or

Think of: optical feedback stabilization to a 100 kHz cavity (finesse $F \simeq 10000$). Dichroic mirrors for 461 nm and 689 nm.

0.11 20.07.2010 Optical binding in a 1D lattice?

Condition for Bragg reflection at a 1D lattice of atomic sheets separated by $\lambda_D/2$

$$\frac{\lambda_d}{2}\cos\beta_i + \frac{\lambda_d}{2}\cos\beta_s = n\lambda_b \tag{1}$$

$$\beta_i = -\beta_s \ . \tag{2}$$

Condition for Bragg scattering at a transverse grating with periodicity λ_D

$$\lambda_d \sin\beta_i - \lambda_d \sin\beta_t = n\lambda_b \ . \tag{3}$$

This yields with $n = 1$

$$\sin\beta_t = \sin\beta_i - \frac{\lambda_b}{\lambda_D} = \sin\beta_i - \cos\beta_i \ . \tag{4}$$

For $\beta_i = 3°$ we obtain $\beta_t = -71°$.

Goos-Hähnchen shift in a 1D lattice? Look for angular variations of β_f upon a scan of λ_{dip}.

0.12 04.08.2010 List of papers 1 for strontium

Early work on the strontium hyperfine structure [49].

At the INLN people built a strontium apparatus for studies of localization of light, [8], [9], [17], [19], [18], [118].

At Innsbruck [108, 111], and Rice [75, 91, 113, 29, 30, 31, 33, 72] they made the first condensate of ^{84}Sr.

At LENS they are interested in metrology [38, 82, 83, 39, 106], just like in Japan [53, 73], at NIST [121, **?**, **?**, 67, 66], at BNPM [25], and at Pisa [110].

About ytterbium [64, 40]. In particular a Mott state was achieved [41].

0.13 06.08.2010 Design of oven 1

At INLN they use a stack of 100 tubes with $\simeq 0.2$ mm diameter for channelling the strontium jet. On how to design an oven see [8] page 97 and [**?**] page 23.

0.14 06.09.2010 Conflat norms 1

sensible	idiotic
CF10	1
CF16	$1\frac{1}{3}$
CF25	$2\frac{1}{8}$
CF40 (ou CF35)	$2\frac{3}{4}$
CF50	$3\frac{3}{8}$
CF63	$4\frac{1}{2}$
CF75	$4\frac{5}{8}$
CF100	6
CF125	$6\frac{3}{4}$
CF160 (ou CF150)	8
CF200	10
CF250	12

0.15 07.09.2010 List of tasks and problems 1

461 nm part list for saturation spectroscopy

part list for MOT setup

497 nm

689 nm

1064 nm

Heatpipe no need for pressure gauge?
sapphire windows?
part list: home made tube, +4× FlangeCF16ThruNot, +2× WindowCF16, ValveGateCF16

Referencecavity suspension?
thermal insulation?
buy ULE Spacer from REO optics
design of windows
part list: homemade tube, +2× FlangeCF100ThruNot, +2× FlangeCF40ThruRot, +2× windows, +1× Feedthrough, ValveGateCF40

Etalon which type of mirror? piezos?
check design carefully

Strontium oven oven design
type of heating wire?
where to obtain the small tubes?

Strontium low vacuum station design of custom-made chamber
type of ion pump and turbo pump? is CF63 or even CF40 OK?
type of pressure gauge?

Strontium slower design?

Strontium main chamber design?
are the deeper CF100 windows feasible?
are 160 G/cm feasible with the coils?

Strontium high vacuum station type of titanium non-sublimation pump?

0.16 07.09.2010 Heating of coils

Consider a $L = 100$ m long wire with $A = 1$ mm^2 cross section carrying a current of $I = 10$ A for 1 h. Resistivity of copper $\rho = 0.02\,\Omega\text{mm}^2/\text{m}$, density $\rho_{\text{Cu}} = 8.93\,\text{kg/dm}^3$, specific heat $c_{\text{Cu}} = 389.4$ J/kg K.

The total resistence is then $R = \rho\frac{l}{A} = 2\ \Omega$. The electrical power transformed into heat is $P = RI^2 = 200$ W. The produced heat is $Q = Pt = 216000$ J. With the mass of the wire, $m_{Cu} = \rho_{Cu}V = 0.893$ kg, we obtain the temperature increase $\Delta T = \frac{Q}{c_{Cu}m_{Cu}} = 621$ K, if no heat is dissipated.

0.17 06.10.2010 Zeeman slower 1

Estimation of the maximum velocity we need to be able to decelerate, if we want to capture 90% of the atoms of the atoms moving in $+z$-direction. The Maxwell-Boltzmann velocity distribution for $T = 600°C$ is,

$$f(v_z)dv_z = \sqrt{\frac{m}{2\pi k_B T}} e^{-mv_z^2/2k_B T} dv_z \ . \tag{5}$$

We normalize the distribution of interesting atoms to 1, $\int_0^\infty 2f(v_z)dv_z = 1$. Hence, the condition

$$\int_0^{v_{mx}} 2f(v_z)dv_z = \mathrm{erf}\left(v_{mx}\sqrt{\frac{m}{2k_B T}}\right) \equiv 0.9 \ . \tag{6}$$

yields $v_{mx} = 1.1631\sqrt{2k_B T/m} \simeq 490$ m/s. The maximum Doppler shift that has to be compensated by a Zeeman shift is then $kv_{mx}/2\pi \simeq 600$ MHz. Assuming constant deceleration, $v = v_{mx}\sqrt{1 - z/L}$.

The Zeeman shift of the transition frequency between a ground and an excited state is

$$\Delta E = (g_e m_e - g_g m_g)\mu_B B \ . \tag{7}$$

For the ^{84}Sr transition $^1S_0$ - $^1P_1$, we have $g_g = g_e = 1$, $m_g = 0$ and $m_e = 1$. Hence,

$$\Delta E = \mu_B B \ . \tag{8}$$

The resonance condition

$$\Delta_{sl} + kv = \tfrac{1}{\hbar}\Delta E \tag{9}$$

yields

$$B(z) = \frac{\hbar\Delta_{sl}}{\mu_B} + \frac{\hbar k v_{mx}}{\mu_B}\sqrt{1 - \frac{z}{L}} \ . \tag{10}$$

For example for an increasing field Zeeman slower, $\Delta_{sl} = 0$, $B_{mx} = \frac{\hbar k v_{mx}}{\mu_B} = 760$ G.

The necessary length L of the Zeeman slower can be estimated from the maximum achievable deceleration,

$$F = \hbar k \frac{I}{\hbar\omega}\sigma(\Delta_{sl} + kv - \mu_B B) = \hbar k \frac{\Omega^2}{\Gamma}\frac{\Gamma^2}{(\Delta_{sl} + kv - \mu_B B)^2 + 2\Omega^2 + \Gamma^2} \ . \tag{11}$$

In resonance and saturation,

$$a_{mx} = \frac{F}{m} = \frac{\hbar k \Gamma}{2m} \ . \tag{12}$$

The minimum length is therefore, $L = v_{mx}^2/2a_{mx} = 12$ cm. For safety, the length is commonly doubled. We go for 25 cm.

0.18 22.10.2010 William's experiment 1

Question 1: Is it correct that a photonic band gap is formed any time, when multiple scattering between subsequent layers comes into play? Homogeneous or inhomogeneous broadening may, of course, hide the band gap, but it should be there.

Question 2: It is true that the presence of a band gap (visible or not) is equivalent to a modification of the DOS, even if it is only small or only 1D? What does it mean, when we say that our band gap is only 1D? In my opinion, it means that, within the band gap the angular integration of the DOS is not considerably modified. HOWEVER, in the direction of the Bragg angle the modification can be huge. This is analog to Simone's observation. She observes a very strong modification of cooperativity, although the solid angle of the cavity is extremely small. Despite the fact that the superradiant enhancement of Γ is small, the observed effects are huge, because along the optical axis the amplification is huge.

In the case of an optical lattice, the optical axis is given by the Bragg angle, and the solid angle of the cavity corresponds to the divergence of the Bragg-scattered light. In both cases, for the cavity and for the 1D lattice, the underlying process is single-photon scattering.

Question 3: Can you calculate the one-dimensional DOS inversely from a given reflection profile?

If the above picture is correct, in order to find the holy grail of a DOS modification, it would be sufficient to watch out for an anisotropy of cooperative light emission. Well, we already know, that Bragg scattering is an effect of anisotropic cooperative scattering. But in this case, the isotropy is broken by the direction of the incident beam, i.e. the absorption plays a decisive role.

Perhaps, an angular modification of the DOS could easier be detected by exciting the atoms NOT under the Bragg angle, but some arbitrary angle. Experimentally, one would search for an increased probability that the atoms are SPONTANEOUSLY emitted into the Bragg angles.

The problem is, how to arrange for spontaneous emission, without being disturbed by the cooperativity linked to the absorption process. Perhaps, populating the $P_{3/2}$ by decay from a higher-lying level? We should try to estimate the amplification of spontaneous emission in Bragg direction. We could also estimate the angular distribution of cooperativity, e.g. using the formalism of [Courteille et al., Euro. Phys. J. D 58, 69 (2010)]. We could calculate the structure factor for a spatially ordered cloud, and reinterprete the anisotropy of the structure factor in terms of an anisotropy of the atom-vacuum mode coupling constant g_k, which is directly related to the DOS.

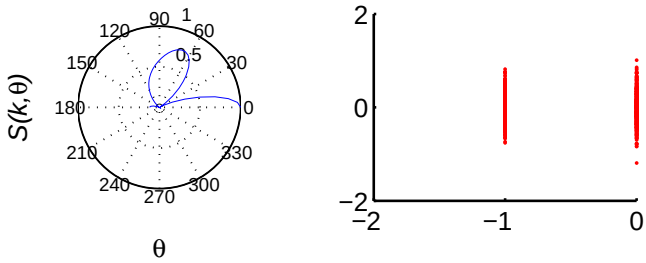

Figure 8: (code) Cooperation of a lattice.

Question 4: Perhaps signatures of a band gap are easier seen if the optical lattice is split in two parts by depleting the central region of the lattice. In some sense, the parts then represent the mirrors of an optical cavity. (This is a little bit like going from Rabi to Ramsey spectroscopy.) Can you calculate the reflection spectrum?

Answer 1: Multiple reflection is a particular case of multiple scattering, which is not covered by our cooperative model.

0.19 22.10.2010 Not to forget 1

Arduino
Synergy plus monitor synchronization
Mechanical shutter by Andrés
Windows for main chamber CJT 680178 CF100

0.20 01.11.2010 List of papers 2 for diamond lattices

Band structure of diamond lattices [22], [97], [50], [80], [89], [114], [2], [3].

Proposals on how to make useful bandgaps [34], [10], [116], [45], [115], [6], [5], [120], [123], [112], [56], [1].

Atomic band gaps in optical lattices [37].

Tasks for Dominik:
- Calculations for optical lattice (Kagome lattice, diamond lattice): Configuration of laser beams (frequency, polarization, direction)
- Depth, steepness of sites, geometrical arrangement
- Band structure

0.21 01.11.2010 Zeeman slower 2

Question: How much light power can we provide? 250 mW is the total laser power at 461 nm.
What is the isotope shift between ^{88}Sr and ^{84}Sr? About 280 MHz [106].
What is the effective length of the slower?
What is the mean velocity of the atoms leaving the oven?
Which paper talks about complete simulations? [77].

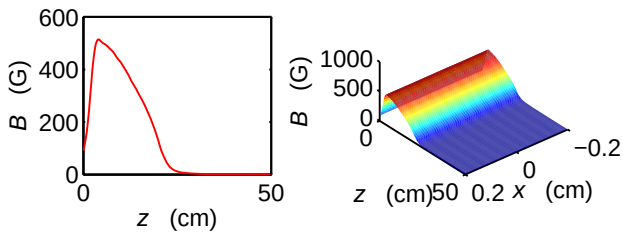

Figure 9: (code) Calculation of the magnetic field.

The detuning of the slower laser must be chosen carefully in order for the atoms to have a well design final velocity, and be not repelled back into the slower

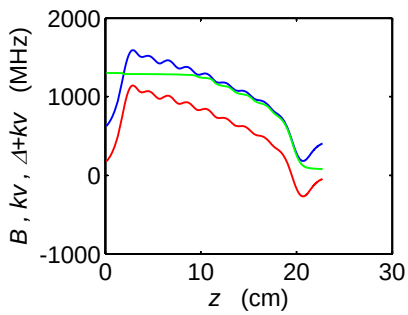

Figure 10: (code) Simulation of the atomic trajectory.

0.22 12.11.2010 AOM scheme 1

Scheme from Bidel for ^{88}Sr:

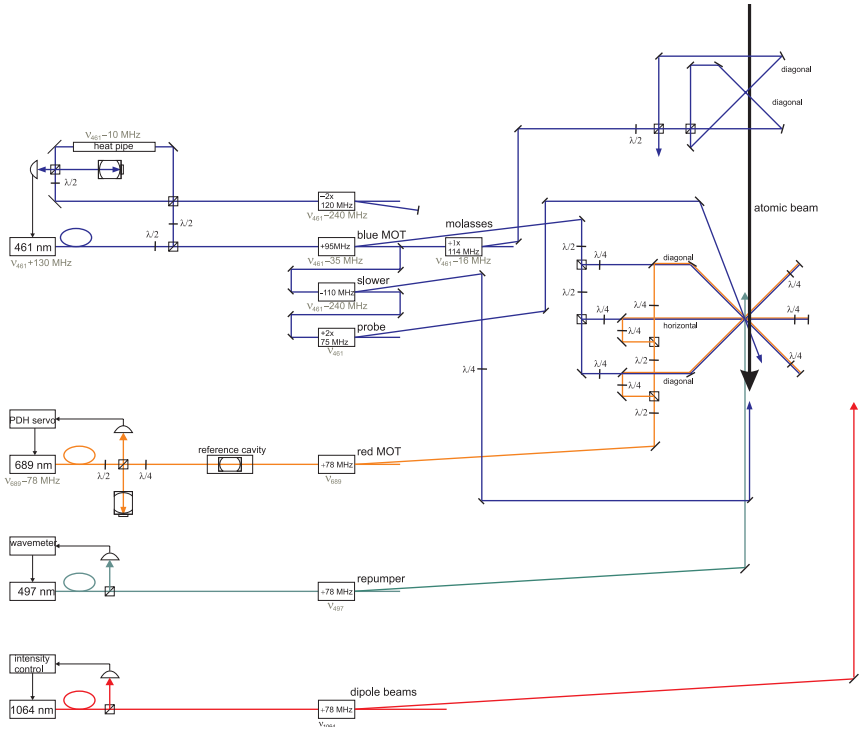

Figure 11: (code) Possible MOT AOM scheme.

If we switch to ^{84}Sr, how must we change the scheme.

0.23 25.11.2010 Evaporation in dipole trap 1

Implememt David's idea [117].

0.24 24.01.2011 PDH stabilization 1

I got the PDH servo of the 689 nm laser working. The laser is stabilized to a Toptica scanning etalon only using the fast branch. It seems very stable. From the transmission signal of the scanning etalon, using the 20 MHz sidebands to calibrate the frequency axis, we estimate a cavity linewidth of $\kappa = (2\pi)$ 7 MHz. This corresponds to a finesse of $F = 600$. The free spectral range is $\delta_{fsr} = 4$ GHz. The noise in the transmission signal when the laser is locked is lower than 5%. With

$$\frac{1}{\Delta^2 + \kappa^2} = \frac{0.95}{\kappa^2} \ . \tag{13}$$

This means that the laser linewidth with respect to the cavity is smaller than $\Delta = 0.2\kappa = (2\pi)$ 1.6 MHz. This can be improved by tighter locking and better cavities.

Some theory : The frequency-modulated light exiting the DL-pro is described by

$$e^{i(\omega t + N \sin \Omega t)} = e^{i\omega t}[-J_1(N)e^{i\Omega t} + J_0(N) + J_1(N)e^{-i\Omega t}] \ , \tag{14}$$

where $\Omega = (2\pi)$ 20 MHz is the modulation frequency. The cavity response is close to resonance

$$E_r(\omega) = E_0(\omega)\sqrt{R}\frac{1 - e^{-2\pi i\omega/\delta_{fsr}}}{1 - R\ e^{-2\pi i\omega/\delta_{fsr}}} \simeq E_0(\omega)\frac{1}{\sqrt{R}}\frac{i\Delta_c}{i\Delta_c + \frac{\delta_{fsr}}{2F\sqrt{R}}} \ , \tag{15}$$

by expanding the exponentials. Absolute value and phase follow from $E_r(\omega) = |E_r(\omega)|e^{i\phi(\omega)}$.

Inserting into the sideband spectrum and only considering terms oscillating with Ω we obtain for the photocurrent after demodulation with the local oscillator $e^{-i\Omega t + i\theta}$

$$S_{PDH} = |E_{tot}|^2 e^{-i\Omega t + i\theta} = J_0(N)J_1(N)\mathrm{Re}\{e^{i\theta}[E_r^*(\omega)E_r(\omega+\Omega) - E_r(\omega)E_r^*(\omega-\Omega)]\} + \dots \ . \tag{16}$$

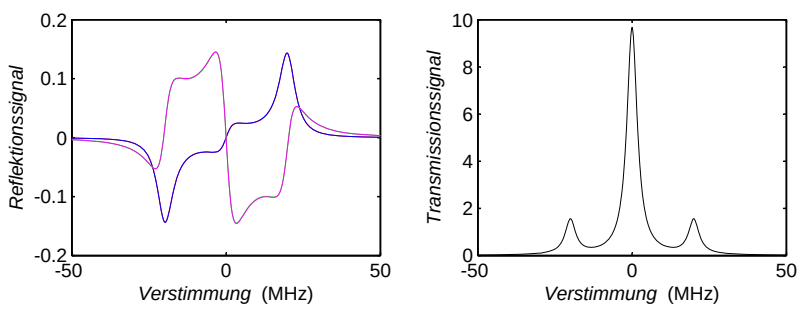

Figure 12: (code) PDH signal.

$$S_{PDH} = \frac{J_0(N)J_1(N)E_0(\omega)E_0(\omega+\Omega)}{R}\mathrm{Re}\left(e^{i\theta}\frac{i\Delta}{i\Delta+\kappa}\frac{-i(\Delta+\Omega)}{-i(\Delta+\Omega)+\kappa} - e^{i\theta}\frac{-i\Delta}{-i\Delta+\kappa}\frac{i(\Delta-\Omega)}{i(\Delta-\Omega)+\kappa}\right) \tag{17}$$

$$= \frac{J_0(N)J_1(N)E_0(\omega)E_0(\omega+\Omega)}{R}\left(-\frac{2}{\kappa}\frac{\Omega^2}{\kappa^2+\Omega^2}\Delta + O\left(\Delta^2\right)\right) .$$

I.e. the steepness of the slope of the PDH signal for $\theta = \pi/2$ is about $J_0(N)J_1(N)E_0(\omega)E_0(\omega+\Omega)\frac{2}{\kappa}$. With this we can use the slope to discriminate the frequency noise.

0.25 28.01.2011 Pressure in our vacuum system

For the calculation of flow and loading rates see Sec. ??.

Pumping through our Zeeman slower: The flow rate through our Zeeman slower can be expressed as

$$S_{zee} \equiv S_{net} \tag{18}$$
$$= \frac{1}{\frac{1}{S_{D4mm}} + \frac{1}{S_{L10cmD4mm}} + \frac{1}{S_{D6mm}} + \frac{1}{S_{L10cmD6mm}} + \frac{1}{S_{D8mm}} + \frac{1}{S_{L10cmD8mm}} + \frac{1}{S_{D10mm}} + \frac{1}{S_{L10cmD10mm}}}$$
$$= 0.14 \text{ l/s}.$$

The small tubes contribute most to the flow rate reduction.

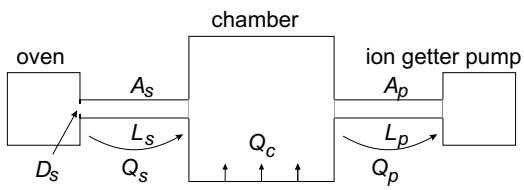

Figure 13: (code) Vacuum scheme.

Let us now consider the low vacuum pumping station including the oven as a simple gas cell whose partial pressure is $p_{res} \simeq 2 \times 10^{-7}$ mbar. The main vacuum chamber (chb) is then fed with Sr atoms by the oven (res) through the Zeeman slower at a loading rate

$$Q_{zee} = p_{res} S_{zee} = 1.4 \cdot 10^{-8} \text{ mbar l/s} . \tag{19}$$

Outgasing of the chamber: Our main chamber has a volume of $V_{chb} = 1.3$ l and a surface of about $F_{chb} = 700$ cm^2. Hence, it outgases at a rate

$$Q_{out} = R_{stl} F_{chb} = 0.35 \cdot 10^{-8} \text{ mbar l/s} . \tag{20}$$

This adds to the feeding rate

$$Q_{fee} = Q_{zee} + Q_{out} . \tag{21}$$

Quintessence: The pressure in the oven chamber needs to be reduced by an order of magnitude.

Pumping through apertures: Typical flow rates through apertures are $S_{CF40} =$ 151 l/s and $S_{CF63} = 374$ l/s. This means for example that a simple CF40 aperture would not reduce the (anyhow low) pumping speed of a $S_{pmp} = 75$ l/s ion pump. If the CF40 tube is 30 cm long, $S_{L30cmCF40} = 80$ l/s, the pumping speed would only be reduced by a factor of 2. Here, a CF63 tube would be advantageous, $S_{L30cmCF63} =$ 314 l/s. **Quintessence:** We should use CF63 tubing for the high vacuum pumping station.

Let us assume that the full pumping speed of the ion pump is available at the main chamber. The pumping rate is then

$$Q_{pmp} = p_{chb} S_{pmp} \ . \tag{22}$$

Pressure in the chamber: The pressure in the chamber p_{chb} results from an equilibrium between the feeding and the pumping,

$$Q_{pmp} = Q_{fee} \ , \tag{23}$$

so that

$$p_{chb} = Q_{tot}/S_{pmp} \simeq \ 2.3 \cdot 10^{-10} \text{ mbar} \ . \tag{24}$$

Quintessence: We need to improve the pumping rate by more than two orders of magnitude. Titanium sublimation pumps or nonevaporable getter pumps can yield pumping rates of 1000 l/s.

Feeding from coated walls: We use the same approach as above, but assume that the chamber walls are all coated with Rb degasing at rate Q_{Rb} and being readsorbed at a rate $p_c S_{Rb}$. Thus,

$$Q_c + Q_{Rb} = Q_p + p_c S_{Rb} = p_c S_{pmp} + p_c S_{Rb} \ . \tag{25}$$

Neglecting dirt and assuming that readsorption is much slower then pumping, we

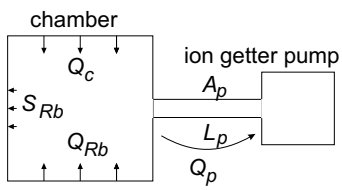

Figure 14: (code) Vacuum scheme.

may be able to estimate the Rb degasing rate

$$Q_{Rb} = Q_p = p_c S_{pmp} \ . \tag{26}$$

Then, when the pump is switched off, the readsorption rate follows from

$$S_{Rb} = Q_{Rb}/p_{Rb} \ , \tag{27}$$

where $p_{Rb} = 1.5 \times 10^{-7}$ mbar is the Rb partial pressure at room temperature.

In practice, dirt is likely to be produced by the ion getter pump at a rate exceeding Q_{Rb}. This dirt will drift into the chamber when the ion getter pump is turned off. For this reason, no improvement of the absorption signal is observed, when the pump is turned off.

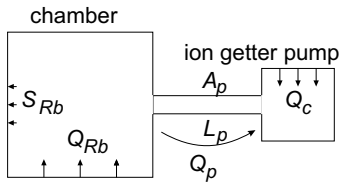

Figure 15: (code) Vacuum scheme.

Partial pressure of Rb: Let us now consider a Rb cell. The partial pressure at room temperature of $p_{Rb} = 1.5 \times 10^{-7}$ mbar is due to an equilibrium of Rb outgassing and adsorption, i.e. the Rb coated walls of the cell releases atoms into the gas phase, and the cell walls act like a pump, $\tilde{p}_{Rb} = Q_{Rb}/S_{Rb}$. The partial pressure depends very much on temperature. Now we consider a Rb cell connected to a vacuum chamber. If the Rb coated area is much smaller (e.g. ten times) than the chamber,

$$\tilde{p}_{Rb} = \frac{\tilde{Q}_{Rb} A_{oven}}{\tilde{S}_{Rb} A_{cell}} = p_{Rb} \frac{A_{oven}}{A_{cell}} \approx 1.5 \times 10^{-8} \text{ mbar} . \tag{28}$$

In the presence of an additional pump

$$\tilde{p}_{Rb} = \frac{\tilde{Q}_{Rb} A_{oven}}{\tilde{S}_{Rb} A_{cell} + \tilde{S}_{igp} A_{cell}} . \tag{29}$$

Now we introduce an additional source (e.g. Rb atoms from a cell or a dispenser),

$$\tilde{p} = \frac{\tilde{Q}_{Rb} A_{oven} + \tilde{Q}_{dirt} A_{cell}}{\tilde{S}_{Rb} A_{cell} + \tilde{S}_{igp} A_{cell}} . \tag{30}$$

Our vacuum gauges: We use various types of Pfeiffer vacuum gauges:
IKR 070, range $10^{-11}..5 \times 10^{-3}$ mbar for the UHV part
IKR 050, range $2 \times 10^{-9}..5 \times 10^{-3}$ mbar for the oven chamber part
TPR 018, $8 \times 10^{-4}..1500$ mbar for the Sr cells

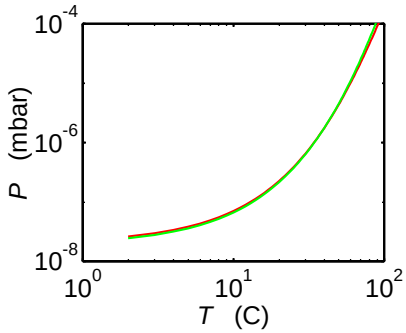

Figure 16: (code) Vacuum Temperature dependence of Rb partial pressure [107].

0.26 31.01.2011 Adjustment of the DL-TA-SHG-pro

Procedure : 1. coarse-tune wavelength at screw
2. fine-tune offset at SC110
3. coarse-adjust first mirror mount after the two optical isolators optimizing the ring cavity spectrum
4. fine-tune with the two mirrors preceding the SHG
5. lock the SHG and tune the crystal temperature optimizing the output power
A. only if necessary: adjust the doubling crystal with the upper left screw
B. only if necessary: adjust the ring cavity with the right curved mirror using the upper right screw

0.27 02.02.2011 PDH stabilization 2

We need about 30mW power.

Single-mode operation is not easy at 60 mA. It is much easier to get this at 46 mA. Here, I even get the PDH working with the following parameters $P_{DLpro} = 8.4$ mW, $P_{cavity} = 840$ μW, $P_{PDHdetector} = 240$ μW, $P_{wavemeter} = 1.4$ mW, $\lambda = 689.4536$ nm.
For the DCC: $T = 34.4°$C, $I = -44.5$ mW
For the PDH: ModAmp=4, gain=5, phase=0.3
For the FALC: InpOff1=0, InpOff2=0, SLI=10, FLD=1, FLI=7, XSLI=10, ULI-R=1, ULI-C=4, ULI-pol=+, ULI-range=1,1, main gain=3

0.28 03.02.2011 Toptica laser installation 1

Andreas Nendel from Toptica installed two lasers:

The 497nm laser S/N12014 laser works nicely. At the wavelengths 496, 497, 498nm the threshold currents are 75, 70, 68mA. With the set currents 304, 305, 299mA, the laser diode temperatures 20, 20, 20° and the crystal temperatures 41.9, 45.6, 48.6^{c}irc, we measure powers of the laser diode of 107, 109, 103mW, of the test beam of 12.7, 13.4, 12mW behind the fiberdock without fiber, and 57, 54, 54mW for the SHG behind the fiberdock without fiber.

The 689nm laser S/N17119 has problems. Bei einem Laserstrom von ca. 65mA hat der Laser eine Leistung von 22mW, scheint jedoch nicht sauber single-mode zu sein. Das Wavemeter zeigt zwar 20GHz modensprungfreien Durchstimmbereich an, das mit einem FPI gemessene Modenspektrum ist jedoch nicht im ganzen Bereich einwandfrei einmodig. Bei niedrigen Leistungen (ca.10mW) funktioniert die Pound-Drever-Hall (PDH) Stabilisierung mit dem FALC-Einschub gut, bei höheren Leistungen (ca. 20mW) scheinen die Modulationsseitenbänder am Rande der Singlemodeplateaus zu verschwinden. Hier funktioniert die Stabilisierung nicht. Die Amplitude des PDH-Signals ist folglich grösser bei niedrigeren Leistungen, obwohl die Lichtleistung vor dem Resonator grösser ist. Das legt die Vermutung nahe, dass die Kontroll- und Regelelektronik zwar gut funktioniert, die Laserdiode die Spezifikationen jedoch nicht einhält. Für den Einsatz im Experiment sind 20mW mindestens bei guter spektraler Reinheit notwendig.

0.29 13.12.2011 689nm

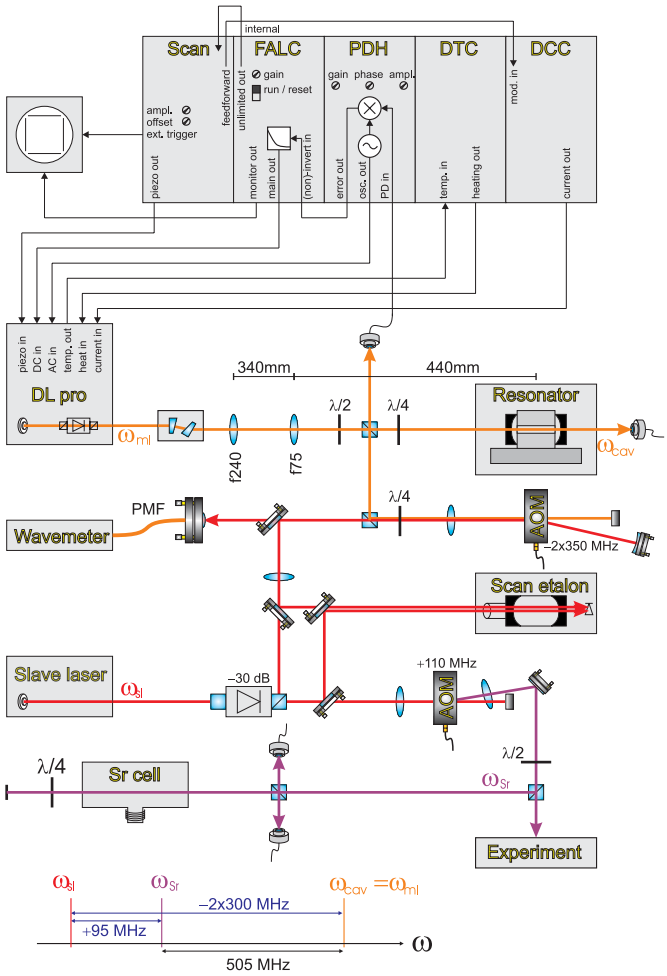

Figure 17: (code) Scheme.

0.30 03.01.2012 Modematching the reference cavity

Fast method for prealigning the beam:

$$\frac{\tilde{P}(\tilde{x})}{P} = \int_{-\infty}^{\tilde{x}} \int_{-\infty}^{\infty} \frac{2}{\pi w_0^2} e^{-2r^2/w_0^2} dx dy = \frac{1}{\pi} \int_{-\infty}^{\infty} e^{-\theta^2} d\theta \int_{-\infty}^{\tilde{\xi}} e^{-\xi^2} d\xi = \tfrac{1}{2} \operatorname{erf}\left(\frac{\tilde{x}\sqrt{2}}{w_0}\right) + \tfrac{1}{2} \,. \tag{31}$$

Using $\tilde{P}(-w_0/2) = P \cdot 16\%$ and $\tilde{P}(w_0/2) = P \cdot 84\%$, we cut the beam with a razor blade mounted on a micrometric table. The distance necessary for ramping from 16% to 84% is just w_0.

According to Dominik the cavity has a waist of $w_0 = 180\ \mu$m. The DL pro after the anamorphic prism pair has $w_0 = 620\ \mu$m. Modematching of the DL pro at 689 nm with the SLS cavity requires two lenses.

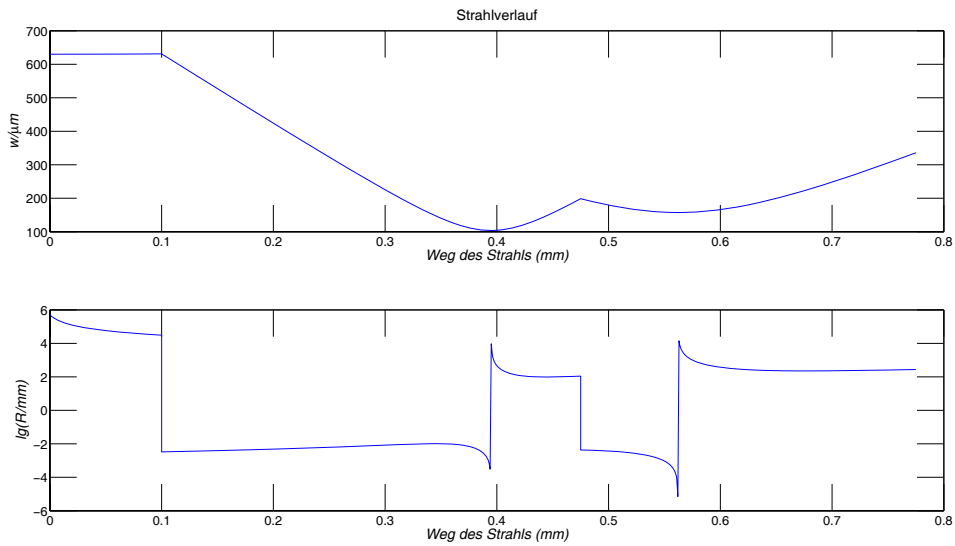

Figure 18: (code) Mode matching of ring cavity.

0.31 24.01.2012 Laser diode connections

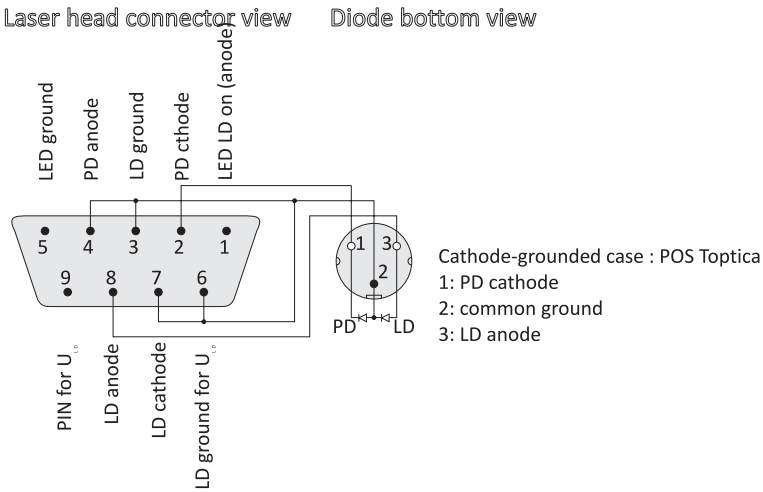

Figure 19: (code) Scheme.

0.32 11.02.2012 MOT is working

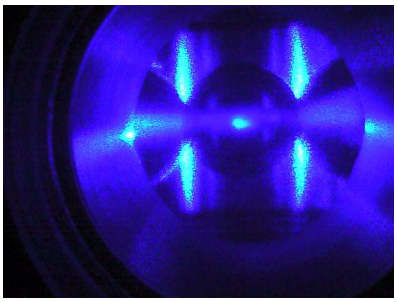

Figure 20: (code) Sr MOT.

0.33 19.02.2012 Optical pumping of strontium

Let us consider a strontium atom, where the blue 461nm transition and the green 497nm repumper transition are driven.

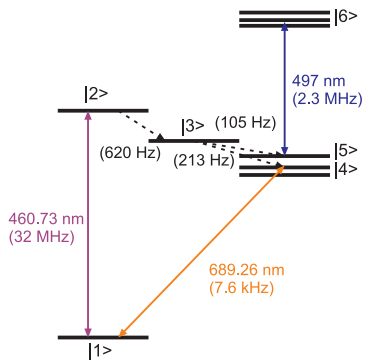

Figure 21: (code) Sr scheme.

Defining the Bloch vector by $\vec{\rho} \equiv \begin{pmatrix} \rho_{11} & \rho_{22} & \rho_{12} & \rho_{21} & \rho_{33} & \rho_{44} & \rho_{55} & \rho_{66} & \rho_{56} & \rho_{65} \end{pmatrix}$, the population dynamics can be described by the following matrix,

$$M \equiv$$

$$\begin{pmatrix}
0 & \Gamma_{12} & \frac{i}{2}\Omega_{12} & -\frac{i}{2}\Omega_{12} & 0 & \Gamma_{14} & 0 & 0 & 0 & 0 \\
0 & -\Gamma_{12}-\Gamma_{23} & -\frac{i}{2}\Omega_{12} & \frac{i}{2}\Omega_{12} & 0 & 0 & 0 & 0 & 0 & 0 \\
\frac{i}{2}\Omega_{12} & -\frac{i}{2}\Omega_{12} & -\frac{\Gamma_{12}}{2}+i\Delta_{12} & 0 & 0 & 0 & 0 & 0 & 0 & 0 \\
-\frac{i}{2}\Omega_{12} & \frac{i}{2}\Omega_{12} & 0 & -\frac{\Gamma_{12}}{2}-i\Delta_{12} & 0 & 0 & 0 & 0 & 0 & 0 \\
0 & \Gamma_{23} & 0 & 0 & -\Gamma_{34}-\Gamma_{35} & 0 & 0 & 0 & 0 & 0 \\
0 & 0 & 0 & 0 & \Gamma_{34} & -\Gamma_{14} & 0 & \Gamma_{46} & 0 & 0 \\
0 & 0 & 0 & 0 & \Gamma_{35} & 0 & 0 & \Gamma_{56} & \frac{i}{2}\Omega_{56} & -\frac{i}{2}\Omega_{5} \\
0 & 0 & 0 & 0 & 0 & 0 & 0 & -\Gamma_{46}-\Gamma_{56} & -\frac{i}{2}\Omega_{56} & \frac{i}{2}\Omega_{56} \\
0 & 0 & 0 & 0 & 0 & 0 & \frac{i}{2}\Omega_{56} & -\frac{i}{2}\Omega_{56} & -\frac{\Gamma_{56}}{2}+i\Delta_{56} & 0 \\
0 & 0 & 0 & 0 & 0 & 0 & -\frac{i}{2}\Omega_{56} & \frac{i}{2}\Omega_{56} & 0 & -\frac{\Gamma_{56}}{2}-
\end{pmatrix}$$

With the decay rates $\Gamma_{12} = (2\pi)32$ MHz, $\Gamma_{14} = (2\pi)7.6$ kHz, $\Gamma_{23} = (2\pi)620$ Hz, $\Gamma_{34} = (2\pi)213$ Hz, $\Gamma_{35} = (2\pi)105$ Hz, $\Gamma_{46} = (2\pi)2.3$ MHz, $\Gamma_{56} = (2\pi)2.3$ MHz.

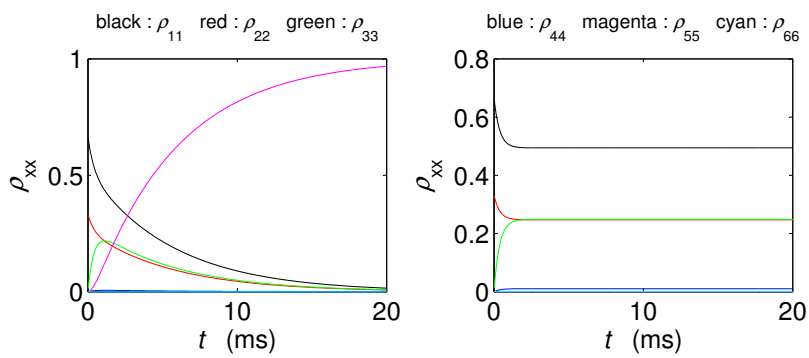

Figure 22: (code) Optical pumping without (left) and with repumper (right) $\Omega_{56} = \Gamma_{56}$.

Describing all transitions by rate equations, the matrix is,

$$M \equiv \begin{pmatrix} -B_{12} - B_{14} & \Gamma_{12} + B_{12} & 0 & \Gamma_{14} + B_{14} & 0 & 0 \\ B_{12} & -\Gamma_{12} - \Gamma_{23} - B_{12} & 0 & 0 & 0 & 0 \\ 0 & \Gamma_{23} & -\Gamma_{34} - \Gamma_{35} & 0 & 0 & 0 \\ B_{14} & 0 & \Gamma_{34} & -\Gamma_{14} - B_{14} & 0 & \Gamma_{46} \\ 0 & 0 & \Gamma_{35} & 0 & -B_{56} & \Gamma_{56} + B_{56} \\ 0 & 0 & 0 & 0 & B_{56} & -\Gamma_{46} - \Gamma_{56} - B_{56} \end{pmatrix}$$

where B_{xy} are the laser induced transition rates (Einstein B coefficients).

0.34 20.02.2012 Estimations for the dipole potential depth

Using [47], we calculate the dipole potential via,

$$U_d(\mathbf{r}) = \frac{3\pi c^2 \Gamma_{461}}{2\omega_{461}^3} \frac{1}{\omega_d - \omega_{461}} I(\mathbf{r}) \ ,$$

with the maximum intensity,

$$I_0 = \frac{2P}{\pi w_0^2} \ .$$

we expect a potential depth,

$$U_0 = \frac{3\pi c^2 \Gamma_{461}}{2\omega_{461}^3} \frac{1}{\omega_d - \omega_{461}} I_0 \ ,$$

of 13 μK for $\lambda_d = 922$ nm, $P_d = 2$ W, and $w_0 = 50\mu$ m, and 12 μK for $\lambda_d = 1064$ nm. Replacing the strong 461 nm line with the 689 nm line we obtain contribution to the trap depth on the order of 30 nK. For overlapping laser beams the intensity I_0 would be the sum of the intensities of the individual laser beams, e.g. for a 3D optical lattice $I_0 = 6I_{indiv}$. Let I_{laser} be the available laser power. For a 3D lattice, the beam has to be split

The trap frequencies depend on the geometry. For a single focused laser beam,

$$\omega_r = \sqrt{\frac{2U_0}{m}} \frac{\sqrt{2}}{w_0} \qquad and \qquad \omega_z = \sqrt{\frac{2U_0}{m}} \frac{1}{z_R} \ .$$

For a 1D optical lattice,

$$\omega_z = \sqrt{2\frac{2U_0}{m}} k \ .$$

0.35 23.02.2012 Magnetic potential depth & g-factors for strontium

The ground state hs no Zeeman effect. For the other levels, the splitting is,

$$\Delta E_{zee} = \mu_B m_J g_J |B| \ ,$$

with the Landé-factor,

$$g_J = 1 + \frac{J(J+1) + S(S+1) - L(L+1)}{2J(J+1)} \ .$$

In particular, $g_J(^1S_1) = 1.5$, $g_J(^1P_1) = 1$, and $g_J(^3P_J) = 1.5$.

Using the *magnetic trap* field calculations routine *201006_MagnTrap.m* and the experimental parameters for mean diameter, $2R = 21$ cm, for the distance, $2A = 13$ cm, for the current, $I = 35$ A, and for the winding number, $N = 200$, I find the gradients, $\partial_x B = \partial_z B = 33$ G/cm and $\partial_y B = 66$ G/cm. The minimum trap depth is 320 G corresponding to 20 mK.

Using

$$g_F \simeq g_J \frac{F(F+1) + J(J+1) - I(I+1)}{2F(F+1)} - g_J \frac{\mu_K}{\mu_B} \frac{F(F+1) - J(J+1) - I(I+1)}{2F(F+1)} \ , \tag{32}$$

for the isotopes ^{88}Sr, ^{86}Sr, and ^{84}Sr, which have the nuclear spin $I = 0$ and $F = J$,

$$g_F = g_J \ . \tag{33}$$

The nuclear spin of ^{87}Sr is $I = 9/2$. Hence, the g_F-factors of the various levels are [73, 33],

$$\begin{aligned} g_F(^1S_0, F = \tfrac{9}{2}) &= ... \\ g_F(^{1,3}P_1, F = \tfrac{7}{2}) &= ... \\ g_F(^{1,3}P_1, F = \tfrac{9}{2}) &= ... \\ g_F(^{1,3}P_1, F = \tfrac{11}{2}) &= ... \ . \end{aligned} \tag{34}$$

0.36 24.02.2012 Plans for Nicola's stay

1. Collective halos:
- Abraham-Minkowski
- Red-blue asymmetry
- interpretation of interferences (artifact due to homogeneous density, the Fourier transform should exhibit oscillations)
- do the projection to compare with experiment
- estimate the rate of scattered photons

2. Optical binding:
- negative force components

3. Mie resonances:
- generalization for elliptic shapes

4. Collective Lamb shift:
- multiple scattering avoided in strontium

5. Collective scattering in three-level systems:
- independent tuning of dispersion and absorption
- interesting for making $n < 1$

6. Photonic bands in 3-level systems:

7. MWSR in the ring cavity:
- coupling strength problem

0.37 29.02.2012 Strontium MOTs in the gravity field

What are the strengths of the blue and red Sr MOTs as compared to gravity? The expression for the radiation pressure force in vertical direction is,

$$F_z(z, v_z) = \frac{\hbar k \Gamma}{2} \sum_{\pm} \frac{\pm \Omega^2}{4\left[\Delta \mp k v_z \mp g_J \mu_B z \partial_z B/\hbar\right]^2 + 6\Omega^2 + \Gamma^2} - mg \tag{35}$$

$$\partial_z \omega_{zeem} = g_J \mu_B \partial_z B/\hbar \ . \tag{36}$$

Linearization for small

$$F_z(\mathbf{r}) = e^{\mathbf{r}\cdot\nabla} F_z(\mathbf{0}) = F(0,0) + z\frac{\partial}{\partial z}F(0,0) + v_z \frac{\partial}{\partial v_z} F(0,0) + .. \tag{37}$$

$$= 0 + z\frac{16\hbar k \Gamma \Omega^2 \Delta}{\left(4\Delta^2 + 2\cdot 6\Omega^2 + \Gamma^2\right)^2}\partial_z \omega_{zeem} + v_z \frac{16\hbar k \Gamma \Omega^2}{\left(4\Delta^2 + 2\cdot 6\Omega^2 + \Gamma^2\right)^2} k + .. \tag{38}$$

$$= -\kappa z - v_z \alpha \tag{39}$$

$$\kappa = \frac{-16\hbar k \Gamma \Omega^2 \Delta \partial_z \omega_{zeem}}{\left(4\Delta^2 + 2\cdot 6\Omega^2 + \Gamma^2\right)^2} \quad , \quad \alpha = \kappa \frac{k}{\partial_z \omega_{zeem}} \ . \tag{40}$$

For $\Omega = -\Delta = \Gamma$

$$\kappa z = \frac{k g_J \mu_B z \partial_z B}{16} = mg \tag{41}$$

$$\omega = \sqrt{\frac{\kappa}{m}} = \sqrt{\frac{k g_J \mu_B \partial_z B}{16 m}} = (2\pi) 300 Hz \ . \tag{42}$$

Gravity has a much larger impact on narrow transitions, since the MOT force scales with the scattering rate. With a gradient of $\partial_z B_z = 10$ G/cm, an earth field of $B_e = 1$ G produces a displacement of $B_e/\partial_z B_z = 1$ mm.

$$\frac{m}{2}\omega^2 = \frac{\kappa}{2} \ .$$

0.38 12.03.2012 Refractive index of air

Using the formula [36]

$$n_s = 1 + 10^{-8}\left(8342.13 + \frac{2406030}{130 - 10^{12}/\lambda^2} + \frac{15997}{38.9 - 10^{12}/\lambda^2}\right)$$
$$n_f = 1 + (n_s - 1)\frac{0.00185097P}{1 + 0.003671T} \ .$$

where P is the pressure of air in mbar, T is the temperature in °C, and $\lambda = 689$ nm the wavelength, we find that at $T = 20$°C a pressure change from $P = 10^{-4}$ mbar to $P = 10^{-5}$ mbar changes the refraction index by $\Delta n \simeq 10^{-11}$, which corresponds to a frequency change on the order of 6 kHz.

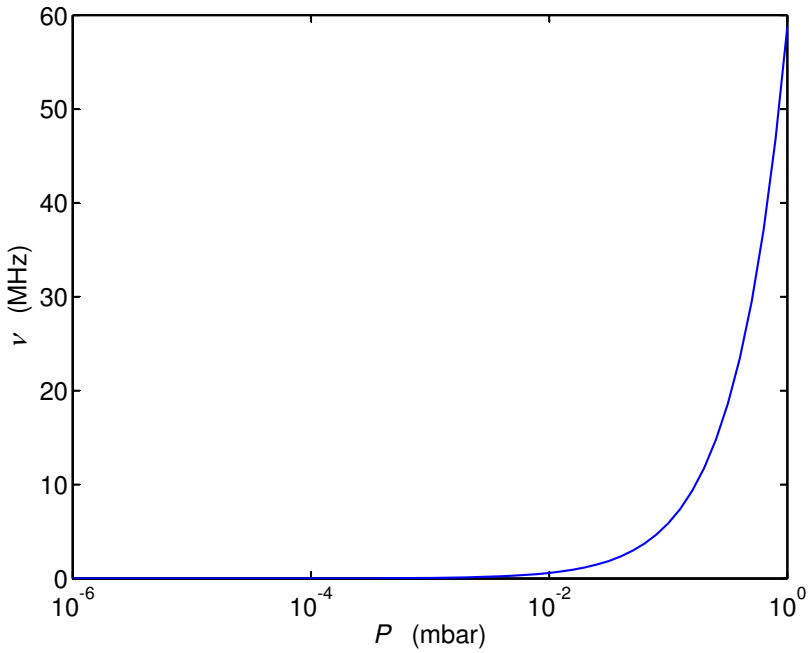

Figure 23: (code) Pressure dependence of the strontium intercombination line $\nu = \frac{c}{\lambda(n_f - 1)}$.

At $P = 10^{-4}$ mbar, the temperature dependence of the refraction index is completely negligible.

0.39 14.03.2012 Green repumper

The green repumper is working, the MOT is much brighter than without. The blue laser is now locked using the DigiLock.

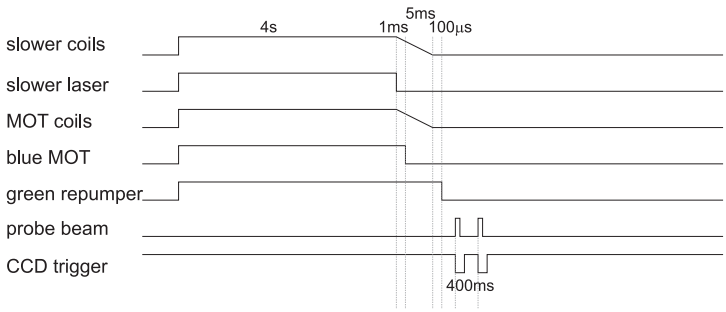

Figure 24: (code) Helmar's experimental sequence.

0.40 17.05.2012 Fiber coupling the 689 nm

Got 74% efficiency with Thorlabs single mode fiber for the 689 nm laser. I installed the FiberDock and obtain about 70%. The perfect Gaussian beam facilitates enormously the coupling of the ring cavity. Without mode matching I obtain about 60% transmission.

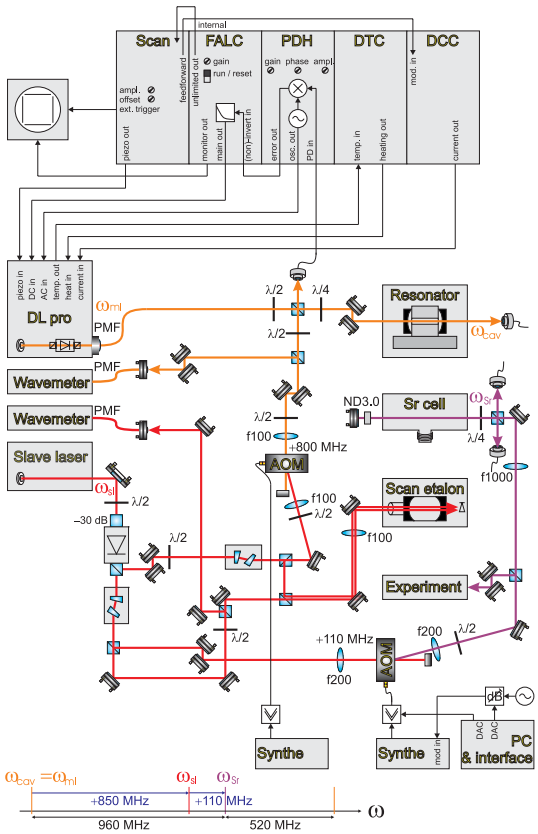

Figure 25: (code) Scheme.

0.41 18.05.2012 Locking the 461nm

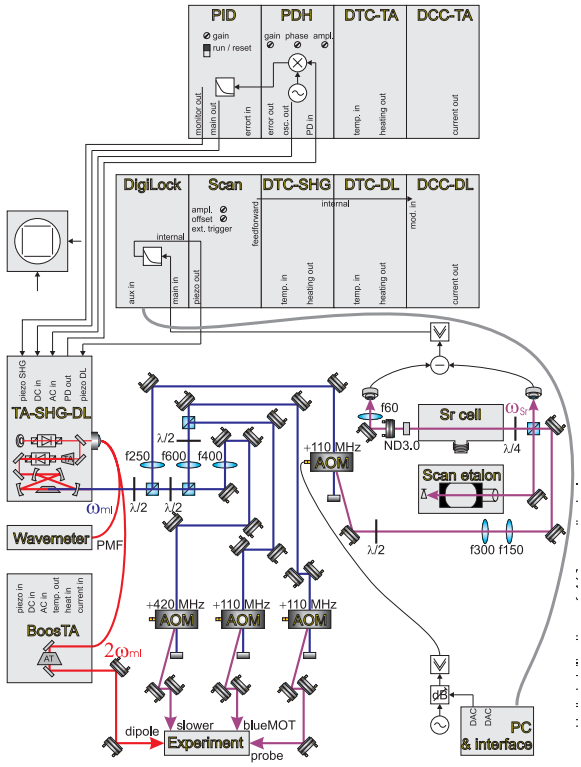

Figure 26: (code) Scheme.

0.42 19.05.2012 Locking the 497nm

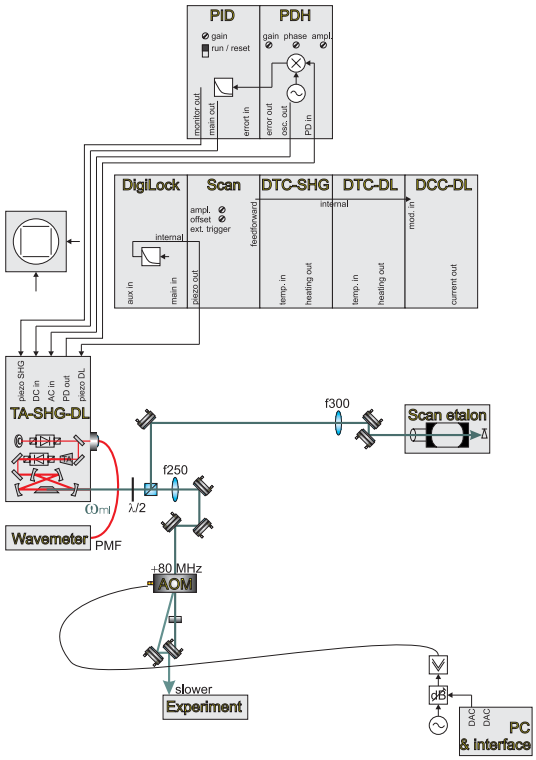

Figure 27: (code) Scheme.

0.43 03.06.2012 Optical pumping of strontium

We now extend the scheme of 19.2.2012 by including a laser driving the red MOT transition. I.e. we consider a strontium atom, where the blue 461nm transition, the green 497nm repumper transition and the red 689nm transition are driven.

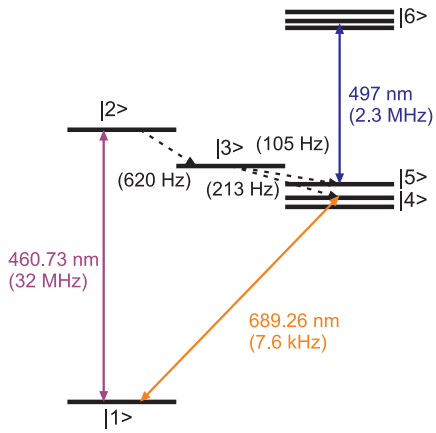

Figure 28: (code) Sr scheme.

Defining the Bloch vector by $\vec{\rho} \equiv \begin{pmatrix} \rho_{11} & \rho_{22} & \rho_{12} & \rho_{21} & \rho_{33} & \rho_{44} & \rho_{55} & \rho_{66} & \rho_{56} & \rho_{65} \end{pmatrix}$, the population dynamics can be described by the following matrix, $M =$

$$\begin{pmatrix}
0 & \Gamma_{12} & 0 & \Gamma_{14} & 0 & 0 & \frac{i}{2}\Omega_{12} & -\frac{i}{2}\Omega_{12} & \frac{i}{2}\Omega_{14} & -\frac{i}{2}\Omega_{14} & 0 & 0 \\
0 & -\Gamma_{12}-\Gamma_{23} & 0 & 0 & 0 & 0 & -\frac{i}{2}\Omega_{12} & \frac{i}{2}\Omega_{12} & 0 & 0 & 0 & 0 \\
0 & \Gamma_{23} & -\Gamma_{34}-\Gamma_{35} & 0 & 0 & 0 & 0 & 0 & 0 & 0 & 0 & 0 \\
0 & 0 & \Gamma_{34} & -\Gamma_{14} & 0 & \Gamma_{46} & 0 & 0 & -\frac{i}{2}\Omega_{14} & \frac{i}{2}\Omega_{14} & 0 & 0 \\
0 & 0 & \Gamma_{35} & 0 & 0 & \Gamma_{56} & 0 & 0 & 0 & 0 & 0 & 0 \\
0 & 0 & 0 & 0 & 0 & -\Gamma_{46}-\Gamma_{56} & 0 & 0 & 0 & 0 & 0 & 0 \\
\frac{i}{2}\Omega_{12} & -\frac{i}{2}\Omega_{12} & 0 & 0 & 0 & 0 & \Lambda_{12} & 0 & 0 & 0 & -\frac{i}{2}\Omega_{14} & 0 \\
-\frac{i}{2}\Omega_{12} & \frac{i}{2}\Omega_{12} & 0 & 0 & 0 & 0 & 0 & \Lambda_{12}^{*} & 0 & 0 & 0 & -\frac{i}{2}\Omega \\
\frac{i}{2}\Omega_{14} & 0 & 0 & 0 & 0 & -\frac{i}{2}\Omega_{14} & 0 & 0 & \Lambda_{14} & 0 & -\frac{i}{2}\Omega_{12} & 0 \\
-\frac{i}{2}\Omega_{14} & 0 & 0 & 0 & 0 & \frac{i}{2}\Omega_{14} & 0 & 0 & 0 & -\Lambda_{14}^{*} & 0 & \frac{i}{2}\Omega_{1} \\
0 & 0 & 0 & 0 & 0 & 0 & -\frac{i}{2}\Omega_{14} & 0 & -\frac{i}{2}\Omega_{12} & 0 & \Lambda_{14} & 0 \\
0 & 0 & 0 & 0 & 0 & 0 & 0 & -\frac{i}{2}\Omega_{14} & 0 & \frac{i}{2}\Omega_{12} & 0 & -\Lambda_{1} \\
0 & 0 & 0 & 0 & \frac{i}{2}\Omega_{56} & -\frac{i}{2}\Omega_{56} & 0 & 0 & 0 & 0 & 0 & 0 \\
0 & 0 & 0 & 0 & -\frac{i}{2}\Omega_{56} & \frac{i}{2}\Omega_{56} & 0 & 0 & 0 & 0 & 0 & 0
\end{pmatrix}$$

with $\Lambda_{ij} \equiv i\Delta_{ij} - \gamma_{ij}$, $\Delta_{24} = \Delta_{12} - \Delta_{14}$, $\gamma_{12} = \frac{1}{2}(\Gamma_{12} + \Gamma_{23})$, $\gamma_{14} = \frac{1}{2}\Gamma_{14}$, $\gamma_{24} = \frac{1}{2}(\Gamma_{12} + \Gamma_{23} + \Gamma_{14})$, and $\gamma_{56} = \frac{1}{2}\Gamma_{56}$. The decay rates are $\Gamma_{12} = (2\pi)32$ MHz, $\Gamma_{14} = (2\pi)7.6$ kHz, $\Gamma_{23} = (2\pi)620$ Hz, $\Gamma_{34} = (2\pi)213$ Hz, $\Gamma_{35} = (2\pi)105$ Hz, $\Gamma_{46} = (2\pi)2.3$ MHz, $\Gamma_{56} = (2\pi)2.3$ MHz.

We find that, when the red MOT is operated, a tiny bit of blue light is sufficient to populate the metastable $^3D_2$ state very rapidly (see Fig. 29(a)). This shows that it is unavoidable to use a mechanical shutter for the blue light.

If however the repumper is also shone in.

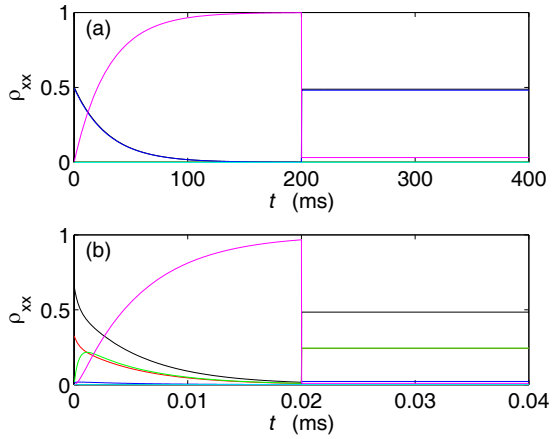

Figure 29: (code) (a) Optical pumping without repumper in the presence of a red MOT $\Omega_{14} = 10\Gamma_{14}$ and only weak blue light $\Omega_{12} = 0.01\Gamma_{12}$. The repumper is switched after 200 ms with only $\Omega_{56} = 0.001\Gamma_{56}$. (b) Same as (a), but with $\Omega_{14} = 10\Gamma_{14}$ and saturating blue light $\Omega_{12} = \Gamma_{12}$. The repumper is switched after 20 μs with only $\Omega_{56} = 0.1\Gamma_{56}$. Legend: Black ρ_{11}, red ρ_{22}, green ρ_{33}, blue ρ_{44}, magenta ρ_{55}, cyan ρ_{66}.

0.44 05.06.2012 PDH settings

PDH-locking is working with the following settings: $I_{laser} = 48.8$ mA, $P_{fiber} = 6.91$ mW, $P_{cavity-in} = 1$ mW, PDH-Ampl=5, PDH-Gain=9, PDH-Phase=0, FALC-non-invert, FALC-fast-diff=5+7.

0.45 07.06.2012 Thorlabs $\lambda/2$-waveplates

For the zero-order $\lambda/2$ waveplates at 670nm Thorlabs specifies 0.48λ retardance at 690nm. This means that we should expect a maximum extinction of

$$\left\| \begin{pmatrix} 1 & 0 \\ 0 & 0 \end{pmatrix} \begin{pmatrix} \cos\frac{\pi}{4} & -\sin\frac{\pi}{4} \\ \sin\frac{\pi}{4} & \cos\frac{\pi}{4} \end{pmatrix} \begin{pmatrix} 1 & 0 \\ 0 & e^{0.48\cdot 2i\pi} \end{pmatrix} \begin{pmatrix} \cos\frac{\pi}{4} & \sin\frac{\pi}{4} \\ -\sin\frac{\pi}{4} & \cos\frac{\pi}{4} \end{pmatrix} \begin{pmatrix} 1 \\ 0 \end{pmatrix} \right\|^2 = 0.004 \quad (43)$$

behind a polarizer. What we find is rather 30% with one of the zero-order $\lambda/2$ waveplates.

We returned the incriminated waveplate to Javier, who borrowed us a zero-order $\lambda/2$ plate at 633 nm, which works nice for 689 nm.

0.46 08.06.2012 Ring cavity calibration

Using the WSU wavemeter we found the Sr Lamb-dip using $3 \cdot 10^{-3}$mbar at $\nu_{689} =$ 434.82907THz. Two cavity modes are found at $\nu_{cav1} =$ 434.82959MHz and $\nu_{cav2} =$ 434.82811THz. Consequently, $\nu_{cav1} - \nu_{689} = 520$ MHz and $\nu_{689} - \nu_{cav2} = 960$ MHz. ν_{cav1} is close to the value 505 MHz measured earlier by Dominik. This seems to show that the cavity is stable and we might not need the Lamb dip for calibration.

The HL6738MG laser diodes are specified for 690 nm with uncertainties between 680 nm and 695 nm. Ours seems quite far from ν_{689}. At 28°C I find for diode (1) 685.9 nm, for diode (2) 685.7 nm, for diode (3) 686.0 nm, for diode (4) 687.4 nm, and for diode (5) 687.5 nm.

I only get about 20% for the Brimrose 800 MHz AOM at -5dBm feeding a Minicircuit +29dB/1W/1GHz amplifier. The beam is focused with a $f = 150$ mm lens.

For the Brimrose 110 MHz AOM at -5dBm feeding a Minicircuit +33dB/2W/500MHz amplifier, I get 80% focussing the with a $f = 240$ mm lens.

The Rohde&Schwarz amplifier is perfect for frequency-modulating with an external source. With a 2 kHz sawtooth signal and 200 kHz/V modulation depth, I observe 500 kHz (with error message up to 5 MHz) broad signals.

The tuning stability of the Minicircuit ZOS-150 VCO is 5.8 MHz/V. This means that for 1 kHz frequency stability, we need 170 μV tuning voltage stability.

0.47 14.06.2012 Scanning etalon

Helmar ajusted the *scanning etalon*. The cavity has a length of $L = 5$ cm and a free spectral range of $\delta_{fsr} = c/4L = 1.5$ GHz. We use a 100 kHz shunt resistor and measure a transmission line width of $\Delta = 16$ MHz by calibration with the 20 MHz sidebands of the PDH stabilization. From this we deduce the finesse of at least $F = \delta_{fsr}/\Delta = 94$.

From the mirror reflectivity $R = 99.2\%$ the finesse should be $F = \frac{\pi\sqrt{R}}{1-R} = 390$.

0.48 23.06.2012 Spectroscopy in the strontium cell

The *partial pressure of strontium* can be calculated from the following curve. The strontium density follows from $n = P/k_B T$.

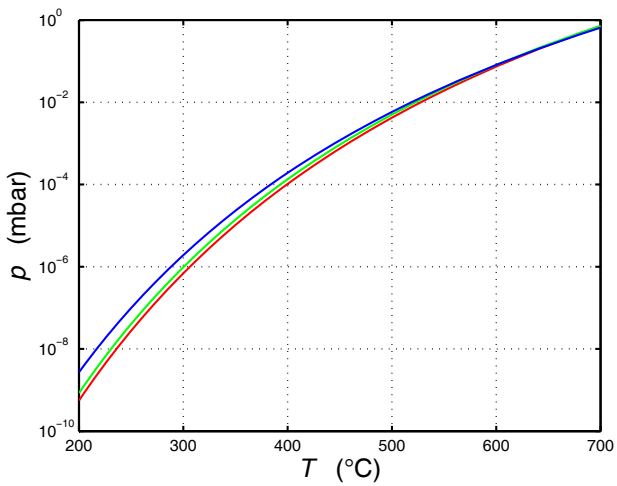

Figure 30: (code) Vapor pressure of strontium.

Let's consider saturation spectroscopy on the 689 nm line in the $L = 0.5$ mm long cell. At $T = 700$ K the strontium gas pressure is about $p = 10^{-4}$ mbar$= 10^{-2}$ Pa, which gives a density of

$$n = \frac{p}{k_B T} = 10^{12} \text{ cm}^{-3} \tag{44}$$

$$b_0 = \sigma_0 n L = 40000 \ . \tag{45}$$

With an estimated Doppler broadening of $\Delta\omega_D = (2\pi)$ 10 GHz, we expect an optical density of $b \simeq \frac{\Gamma_{689}}{\Delta\omega_D} b_0 = 0.005$.

0.49 24.06.2012 Spectroscopy in the blue MOT

Can we expect an *absorption signal* at 689 nm from the blue MOT? The atom number in the blue MOT is about$N = 10^8$ and its estimated radius is $\bar{r} = 1$ mm

$$n(\mathbf{r}) = n_0 e^{-r^2/2\bar{r}^2} \tag{46}$$

$$N = \int n(\mathbf{r}) d^3\mathbf{r} = n_0 (2\pi)^{3/2} \bar{r}^3 \tag{47}$$

$$b_0 = \int_{-\infty}^{\infty} \sigma_0 n(\mathbf{r}) dy = \frac{\lambda^2}{2\pi} \frac{N}{2\pi \bar{r}^2} \ . \tag{48}$$

We expect $n_0 = 6 \cdot 10^9$ cm^{-3}, $b_0 = 1.2$. The blue Doppler limit the line broadening will be about 1 MHz, so that the optical density will be $b \simeq \frac{\Gamma_{689}}{\Gamma_{461}} b_0 = 2.85 \times 10^{-4}$.

On the other hand, the blue MOT will generate a saturation broadening of the ground state on the order of Γ_{461}, so that the Doppler broadening might be negligible. This is confirmed by simulation:

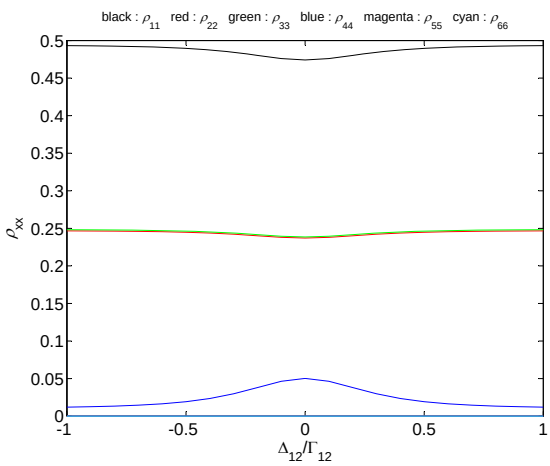

Figure 31: (code) Excitation probability of the weak transition for $\Omega_{12}/\Gamma_{12} = 1$, $\Omega_{14}/\Gamma_{12} = 20$, and $\Omega_{56}/\Omega_{12} = 5$.

0.50 27.06.2012 Try red MOT 1

We tried to find the red MOT without success. However, the red light has a clear impact on the blue MOT: the cloud is slightly shifted and the atom number enhanced when the AOM frequency is tuned to about 863.5 MHz. MOT beam intensity $I \simeq 40$ mW/cm^2.

The red laser works very stable

master laser	temperature	$T = 23.5$C
	current	$I = 43.5$ mA
	fiber output power	$P = 4.4$ mW
	power before cavity	$P = 3.1$ mW
	power behind cavity	$P = 1.6$ mW
	power to injection	$P = 76$ μW
	power to etalon	$P = 300$ μW
	power before 800MHz AOM	$P = 840$ μW @855MHz
	power behind 800MHz AOM	$P = 210$ μW
	WS6 wavemeter reading	$\lambda = 434.8282$ THz
slave laser	temperature	$T = 39$C
	current	$I = 113$ mA
	output power	$P = 36.3$ mW
	power before 110MHz AOM	$P = 20$ mW
	WS6 wavemeter reading	$\lambda = 434.8290$ THz

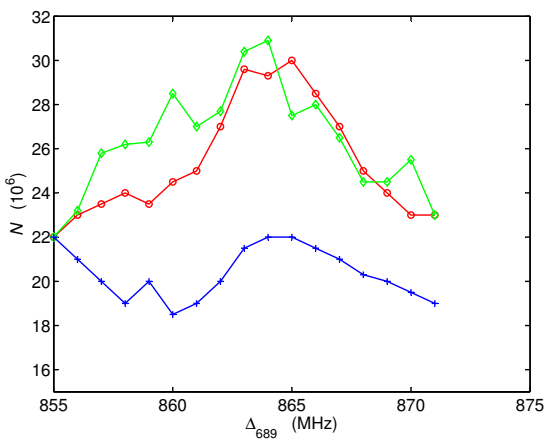

Figure 32: (code) Measured atom number as a function of the red light detuning. (Red) A 689nm beam traverses the blue MOT. (Green) The blue MOT intensity has been reduces by 4. (Blue) A red MOT superposed to the blue MOT.

0.51 28.06.2012 Try red MOT 2, self-induction

The red MOT is now clearly visible. We estimate $N = 10^6$ at roughly $T = 20\ \mu$K.

The Agilent current supply needs 50 ms for switching off. Is this due to *eddy currents* due to *self-induction* in the MOT coils? We know that smaller coils can be switched off in about 100 μs. How does the self-induction scale with the coil diameter? We calculate the self-inductivity of a current loop.

The current density can be parametrized as $\vec{j}(\vec{r}) = I\delta(\rho - R)\delta(z)\hat{e}_\phi$. The vector potential is

$$\vec{A}(\vec{r}) = \frac{\mu_0}{4\pi}\int \frac{\vec{j}(\vec{r}')}{|\vec{r}-\vec{r}'|}d^3\vec{r}' \ .$$

According to the Biot-Savart law, the magnetic field is

$$\begin{aligned}\vec{B}(\vec{r}) &= \frac{\mu_0}{4\pi}\int \nabla\times\frac{\vec{j}(\vec{r}')}{|\vec{r}-\vec{r}'|}d^3\vec{r}' = \frac{\mu_0}{4\pi}\int d^3\vec{r}'\frac{(\vec{r}-\vec{r}')\times\vec{j}(\vec{r}')}{|\vec{r}-\vec{r}'|^3} \\ &= \frac{\mu_0 I}{4\pi}\int Rd\phi' \frac{\begin{pmatrix} -z\cos\phi' \\ -z\sin\phi' \\ (\rho\cos\phi - R\cos\phi')\cos\phi' + (\rho\sin\phi - R\sin\phi')\sin\phi' \end{pmatrix}}{\sqrt{(\rho\cos\phi - R\cos\phi')^2 + (\rho\sin\phi - R\sin\phi')^2 + z^2}^3} \ .\end{aligned}$$

The field across the $z = 0$ plane is

$$\begin{aligned}B_z(x,y) &= \frac{\mu_0 IR}{4\pi}\int_0^{2\pi} d\phi' \frac{(\rho\cos\phi - R\cos\phi')\cos\phi' + (\rho\sin\phi - R\sin\phi')\sin\phi'}{\sqrt{(\rho\cos\phi - R\cos\phi')^2 + (\rho\sin\phi - R\sin\phi')^2}^3} \\ &= \frac{\mu_0 IR}{4\pi}\int_0^{2\pi} d\alpha \frac{\rho\cos\alpha - R}{\sqrt{\rho^2 + R^2 - 2\rho R\cos\alpha}^3} \ ,\end{aligned}$$

and the flux across the $z = 0$ plane,

$$\begin{aligned}\Phi &= \int_A B_z(x,y)dA = \frac{\mu_0 IR}{4\pi}\int_0^{2\pi} d\phi \int_0^R \rho d\rho \int_0^{2\pi} d\alpha \frac{\rho\cos\alpha - R}{\sqrt{\rho^2 + R^2 - 2\rho R\cos\alpha}^3} \\ &= \frac{\mu_0 IR}{4\pi}2\pi\int_0^{2\pi} d\alpha \frac{-2\cos\alpha + \left(\cos\alpha\ln(-\cos\alpha + 1 + \sqrt{2-2\cos\alpha})\right)\sqrt{2-2\cos\alpha} + 1 - (\cos\alpha\ln(-\cos\alpha +}{\sqrt{2-2\cos\alpha}} \\ &= \frac{\mu_0 IR}{4\pi}2\pi 4 = 2\mu_0 IR \ .\end{aligned}$$

Finally, the self-inductivity becomes

$$L = \frac{\Phi}{I} = 2\mu_0 RN^2 \ ,$$

where N is the number of turns.

I.e. the self-inductivity scales linearly with the diameter. Of course, the permeability of metallic material, such as the coil holders is not taken into account, here. But it seems anyway unlikely that self-induction is much more than an order of magnitude larger in our setup, and hence a switch-off time of few ms should be feasible.

For $R = 12$ cm and $N = 200$ turns, we expect $L = 12$ mH. If the coils has a resistance of $R' = 0.5\ \Omega$, the decay time will be $\tau = L/R' = 24$ ms.

According to [H.A. Wheeler, Proc. I.R.E. 16, 1398 (1928), doi:10.1109/JRPROC.1928.221309, *Simple inductance formulae for radio coils*] the inductivity can be calculated as

$$L = \frac{4}{5}\frac{R^2N^2}{6R+9l+10d}\frac{10^{-6}}{25.4} \ .$$

0.52 06.07.2012 Cooperative scattering projects

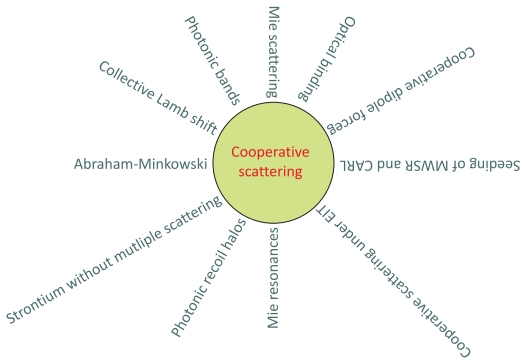

Figure 33: (code) Links.

0.53 31.07.2012 Setup of the strontium apparatus

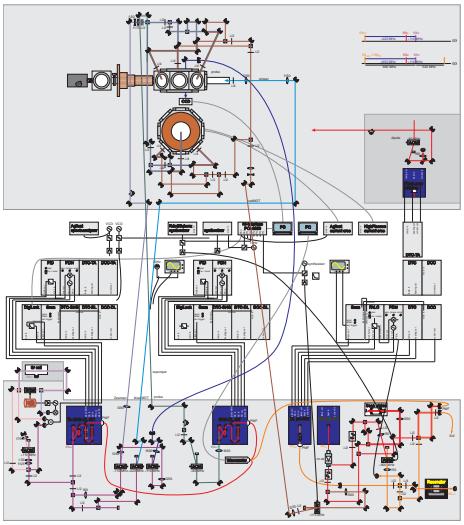

Figure 34: (code)

0.54 01.08.2012 Unlock-relock logic

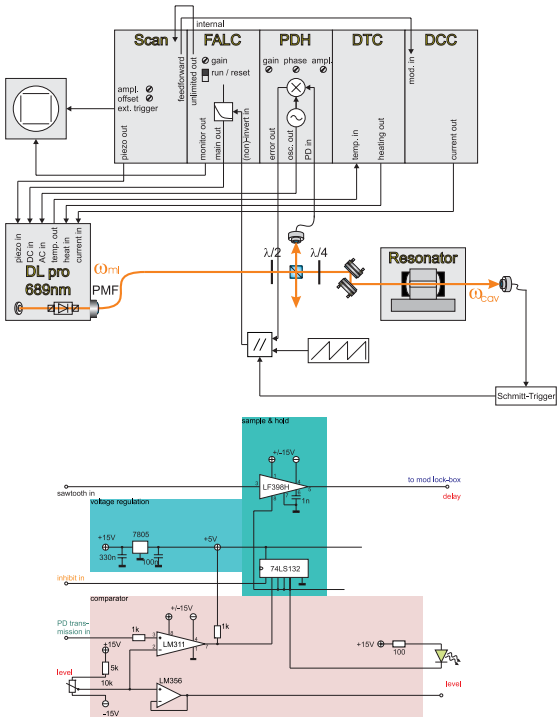

Figure 35: (code) Unlock-relock logic for simplifying the Pound-Drever-Hall servo.

0.55 16.08.2012 Intensity stabilization

We will son need an intensity control for an optical dipole trap. In the following scheme, the variable attenuator controls the amplitude of the guided to the AOM Radio frequency amplitude: low voltage (0 V) blocks at the control input to the attenuator, high voltage (+16 V) switches through him. The sketched controller realizes a negative feedback so if the photodiode outputs a positive voltage.

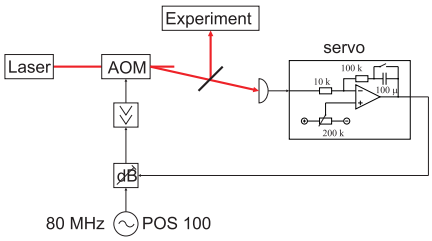

Figure 36: (code) Scheme of an intensity control.

0.56 21.08.2012 Three-level cooling

Flavio Cruz proposes to use Sr for testing the viability of three-level cooling. The lower transition is the 32 MHz large $(5s^2)^1S_0$ - $(5s5p)^1P_1$ blue cooling transition at 461 nm, the upper transition is a 1.1 MHz $(5s5p)^1P_1$ - $(5s5d)^1D_2$ NIR transition at 767 nm. For the saturation parameters $s_{low} = 0.2$ and $s_{up} = 11000$, he predicts that for suitable detunings temperatures down to 8 μK may be reached. The saturation intensities are: $I_{s,low} = \frac{g_1}{g_2}\frac{2\pi^2 c\hbar}{3\lambda^3}\Gamma = 43$ mW/cm^2 for the lower transition. and $I_{s,up} = 0.5$ mW/cm^2 for the upper transition.

If we can borrow a potassium Toptica laser from Kilvia, the experiment might be simple. The laser can provide $P = 100$ mW. Using 1 cm beam diameter and retroreflecting the beams, we can make the total intensity as high as $I = 200$ mW/cm^2, which corresponds to a saturation parameter of $s = 400$.

Good point made by Robin: Is it necessary to have two phase-coherent beams to reach sub-Doppler temperatures for both single-resonances? If this is the case, it could represent a problem, because typical laser linewidth are 1 MHz. For the simulations, laser phase jitter can be accounted for by including some phase-damping term (transversal decay) into the Bloch equations.

0.57 29.08.2012 Matter wave Mie resonances

Do they exist? Can we apply our scalar Mie scattering theory to the problem of scattering BECs at a small perturbation (like a localized potential hole)? Small we expect an evanescent wave entering the hole? Will it develop a whispering gallery mode? How about the Goos-Hänchen shift? How about scattering the BEC at an optical lattice made by another atomic species? How about matter wave band gaps for the BEC propagating inside the optical lattice? Can we detect those band gaps via Bragg diffraction suppression?

0.58 06.09.2012 Magnetic field compensation

Compensation of magnetic field is important for the red transition in order to control *gravitational sag* [18] and inhomogeneous broadening by magnetic field fluctuations: For resonant imaging we need the inhomogeneous Zeeman broadening to be smaller than 7.6 kHz,

$$\mu_B g_F m_F \Delta B < \hbar\Gamma \ .$$

This corresponds to 5 mG. For comparison, the *earth magnetic field* is about 300 mG.

It will be essential to synchronize the duty cycle with the 60 Hz line.

0.59 07.09.2012 Atomic light house effect 1

Robin suggests to look for a reorientation of the collective force via a transversal B-field gradient. He calls this effect the *lighthouse effect*. To have a noticeable impact,

$$\mu_B g_F m_F y |\partial_y B| \sim |\Delta| \gg \Gamma \ .$$

Assuming we can make $|\partial_y B| \sim 70$ G/cm and the cloud is 1 mm large, we may expect a Zeeman shift of 7 G, which is in the same order magnitude as $\Gamma = (2\pi)32$ MHz.

We have to check, whether cooperative effect can be observed with the parameters of our MOT. Check N, ρ, T, b_0! How reproducable can we make our MOT? Can we manipulate the atom numbers without modifying the volume. Eventually, use magnetically trapped atoms repumping the $^3D_2$ atoms at the very last and then quickly appling a blue or red push beam.

We also have to check, whether a Stern-Gerlach type acceleration can easily be distinguished from the interesting effect. The transverse gradient gives rise to a force on the magnetic dipole moment of,

$$F_y = -\partial_y H_{zeem} = -\mu_B g_F m_F \partial_y B \ .$$

For the ground state, $m_F = 0$, so that no force is to be expected. However, the push beam may generate a small population of excited Zeeman states, $m'_F = 0, \pm 1$.

Finally, we want a simple estimation of the observable force deviation, e.g. recalculating the structure factor within the timed Dicke approximation.

0.60 11.09.2012 Discussion with Robin

Understand single-atom scattering term in the matter wave quantized theory.

Failure of smooth density approximation: Robin realizes that mean-field theory (introduction of refraction index in the smooth density approximation) breaks down at high densities with lots of multiple scattering. This is analogous to the unitarity limit in a gas driven into a Feshbach resonance. The simple two-body collision picture breaks down. The scattering length looses its meaning. Is it obvious that many-body theory is always valid? Is it fair to compare the TDS including some coarse graining to the partial wave approximation?

Atomic clouds under stress: The cooperative dipole force: Force fluctuations: $b_0 = 0..10..50$, $\Delta = -3.. + 3\Gamma$, variance transverse et longitudinale, reduction due to shared photons

Need high $b_0 = 3$, $N = 10^7$ with 10% precision. How to change atom number without changing size?

Assuming we have $N = 10^8$ and $\bar{r} = 3$ mm. Then $b_0 = \frac{3N}{\sigma_r^2} = 1.6$, which is small.

0.61 18.11.2012 Strontium levels

Ryan checked some possible transitions for three-level schemes. The values found at http://x-ray.gist.ac.kr/spec/strontiumtable5.htm must be derived from calculated values of the level energies, which are only approximate. The nist.gov site provides more accurate data, as listed below.

Term	Level	τ	(5s5s) 1S0	Γ	(5s5p) 1P1	Γ	(5s5p) 3P°0	Γ	(5s5p) 3P°1	Γ	(5s5p) 3P°2	Γ
	(cm-1)	(s)	(nm)	(Hz)	(nm)	(Hz)	(nm)	(Hz)	(nm)	(Hz)	(nm)	(Hz)
Sr II (2S1/2)	45932,0900	Limit										
(5s5s) 1S0	0,0000		-		-	32M	-		-		-	
(5s6s) 1S0	30591,8250		326,884715		1124,432766	3M	614,465073		621,600969		637,215420	
(5s5p) 1P1	**21698,4520**	**5,0n**	**460,862369**	**32M**	-		1354,840065		1390,024462		1470,608348	
(5s6p) 1P1	34098,4040		293,268858	110k	806,454735		505,538247		510,358491		520,837158	
(5s7p) 1P1	38906,8580		257,024096	240k	581,111348		406,680111		409,793675		416,522394	
(4d5p) 1P1	41172,0540		242,883195		513,515681		372,376417		374,985188		380,611513	
(5s8p) 1P1	42462,1360		235,503932		481,610103		355,307579		357,681909		362,797431	
(4d5s) 1D2	20149,6850		496,285674		-		1714,625308		1771,369043		1904,348389	
(4d5p) 1D°2	33826,8990		295,622723		824,507870		512,573636		517,529634		528,307955	
(5s5d) 1D2	34727,4470		287,956670		767,518907	1,1M	489,957344		494,483713		504,314359	
(5p5p) 1D2	36960,8420		270,556607		655,205377	14M	441,631058		445,305210		453,261961	
(5s6d) 1D2	39733,0670		251,679539		554,489242		393,459755		396,373452		402,665290	
(5s7d) 1D2	41831,4480		239,054598		496,697064		363,452113		365,936923		371,293061	
(5s8d) 1D2	43021,0580		232,444307		468,985827		348,388950		350,671417		355,586999	
(5s6s) 3S1	29038,7730		344,367167		1362,338241		**679,289404**		**688,021051**		**707,202175**	
(5s5p) 3P°0	14317,5070		698,445616	1m	-		-		-		-	
(5s5p) 3P°1	**14504,3340**		**689,449098**	**7,6k**	-		53525,454030		-		-	
(5s5p) 3P°2	14898,5450		671,206484	0,15m	-		17210,578310		25367,125727		-	
(5s6p) 3P°0	33853,4900		295,390520		822,704133		511,875957		516,818408		527,566817	
(5s6p) 3P°1	33868,3170		295,261202		821,701802		511,487759		516,422680		527,154464	
(5s6p) 3P°2	33973,0650		294,350834		814,689636		508,761949		513,644161		524,259588	
(5p5p) 3P0	35193,4420		284,143847		741,015740		479,020461		483,346116		492,734701	
(5p5p) 3P1	35400,1050		282,485038		729,838947		474,324844		478,565735		487,767760	
(5p5p) 3P2	35674,6370		280,311191		715,502836		468,227707		472,359796		481,322474	
(4d5p) 3P°0	37292,0740		268,153496		641,287829		435,263916		438,832460		446,557575	
(4d5p) 3P°1	37302,7310		268,076887		640,849859		435,062108		438,627330		446,345161	
(4d5p) 3P°2	37336,5910		267,833772		639,462279		434,422152		437,976850		445,671606	
(5s7p) 3P°0	39411,6690		253,731959		564,550189		398,499061		401,488156		407,944740	
(5s7p) 3P°1	39426,4420		253,636887		564,079741		398,264602		401,250167		407,699038	
(5s7p) 3P°2	39457,3830		253,437994		563,096957		397,774436		400,752629		407,185389	
(4d5s) 3D1	18159,0400		550,689904		-		2603,127449		2736,198206		**3067,018965**	
(4d5s) 3D2	18218,7840		548,884053		-		2563,263260		2692,188615		**3011,831377**	53k
(4d5s) 3D3	18319,2610		545,873548		-		2498,904230		2621,282137		**2923,364582**	12k
(5s5d) 3D1	**35006,9080**		285,657905		751,401966		483,339271		487,743636		**497,305524**	
(5s5d) 3D2	**35021,9890**		285,534896		750,551449		482,987210		487,385132		**496,932831**	**2.3M**
(5s5d) 3D3	**35045,0190**		285,347256		749,256344		482,450571		486,838681		**496,364773**	
(4d5p) 3D°1	36264,1510		275,754422		686,544463		455,650531		459,562688		468,041955	
(4d5p) 3D°2	36381,7460		274,863114		681,046092		453,222067		457,092457		465,479981	
(4d5p) 3D°3	36559,4920		273,526777		672,900416		449,600159		453,408677		461,660333	
(4d5p) 3F°2	33266,8510		300,599537		864,423850		527,722754		532,977532		544,416017	
(4d5p) 3F°3	33589,7090		297,710230		840,953988		518,882067		523,961410		535,012159	
(4d5p) 3F°4	33919,3150		294,817274		818,272818		510,157022		515,066175		525,741071	
(5s6d) 3D1	**39685,8656**		251,978881		555,944297		394,191842		397,116433		**403,432068**	
(5s6d) 3D2	**39690,7951**		251,947586		555,791980		394,115259		397,038709		**403,351852**	
(5s6d) 3D3	**39703,0986**		251,869510		555,412179		393,924245		396,844852		**403,151783**	

Figure 37: (code) Sr levels and transitions.

0.62 11.06.2013 Compensation coils

Calculation of the magnetic field of the compensation coils using a numeric integration of the Biot-Savart law.

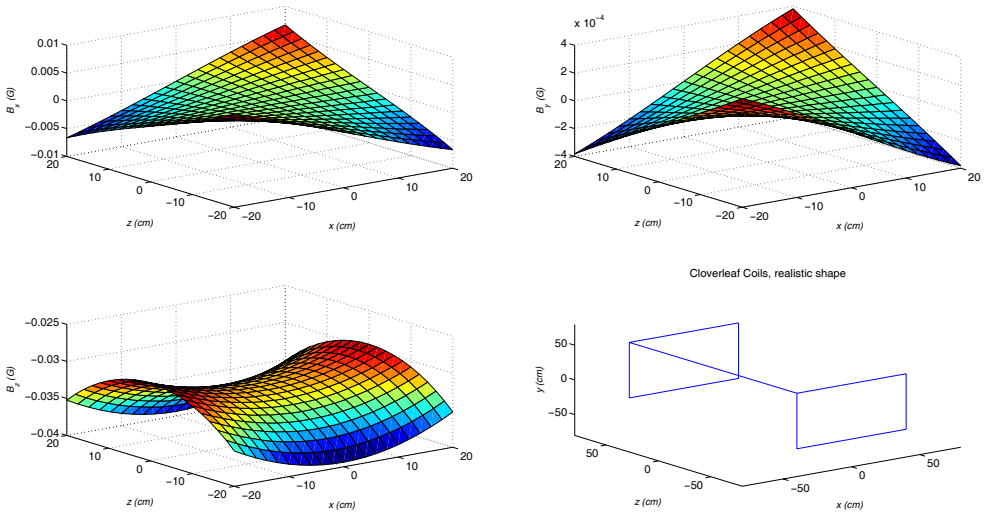

Figure 38: (code) Magnetic field of the compensation coils.

0.63 28.06.2013 Doppler broadening for strontium

The *Doppler cooling limit* is given by

$$T_D = \frac{\hbar}{k_B}\Gamma \ .$$

Using $k_B T = m\bar{v}^2$ we can estimate the width of a Doppler broadened line

$$k\bar{v} = k\sqrt{\frac{k_B T_D}{m}} = k\sqrt{\frac{\hbar\Gamma}{m}}$$

or scaled to Γ

$$\frac{k\bar{v}}{\Gamma} = \sqrt{\frac{\hbar k^2}{m\Gamma}} = \sqrt{\frac{\omega_{rec}}{\Gamma}} \ .$$

This formula shows that there is a trade-off between advantages and disadvantages of cooling on a narrow line: On one hand, for $\omega_{rec} > \Gamma$ one avoids photon reabsorption and radiation trapping; on the other hand, *Doppler broadening* starts to play an eminent role.

For the blue Sr line we have $k_{blue}\bar{v}/\Gamma_{blue} = 0.026$. For the red line, $k_{red}\bar{v}/\Gamma_{red} = 1.1$. This means that, although the temperature of the red MOT is much lower than that of the blue MOT, spectroscopy in the red line will be affected by Doppler broadening.

wavelength	blue MOT	red MOT
linewidth $\Gamma/2\pi$	32 MHz	7.6 kHz
theoretical Doppler limit T_D	1.5 mK	365 nK
measured temperature T_m	4 mK	10 μK
Doppler width $k\bar{v}/2\pi$ @ 461 nm @ T_D	817 kHz	12.7 kHz
Doppler width $k\bar{v}/2\pi$ @ 689 nm @ T_D	546 kHz	8.5 kHz
Doppler width $k\bar{v}/2\pi$ @ 461 nm @ T_m	1.3 MHz	67 kHz
Doppler width $k\bar{v}/2\pi$ @ 689 nm @ T_m	892 kHz	45 kHz
recoil temperature T_{rec} @ 461 nm	2 μK	
recoil temperature T_{rec} @ 689 nm	917 nK	

Here, the recoil temperature is calculated via $T_{rec} = \frac{2\hbar^2 k^2}{k_B m}$.

In order to cool all atoms from the blue MOT into the red MOT, we apply a triangular frequency modulation to the red MOT light. The question is what is the best modulation excursion and the best modulation frequency.

1. The modulation excursion should be larger than the Doppler width @ 689 nm, i.e.

$$\Delta\omega_{red} \simeq k v_m \ ,$$

so the 90% of the Doppler-shifted atoms get in resonance at one point with the modulated red MOT light.

2. In order to drive transitions, the interaction time Δt of the red MOT light with an atom should be longer than a Rabi cycle,

$$\Omega\Delta t > \pi \ .$$

3. The interaction time depends on the resonance width $\Gamma = (2\pi) \cdot 7.6$ kHz and the ramp speed, whose duration is T and frequency excursion is $\Delta\omega_{red}$,

$$\frac{\Delta t}{T} = \frac{\Gamma}{\Delta\omega_{red}} \ .$$

4. The Rabi frequency can be estimated from the red MOT intensity $I = 30\,\mathrm{mW/cm}^2$ and the saturation intensity $I_s = 3\ \mu\mathrm{W/cm}^2$, since

$$\frac{I}{I_s} = \frac{\Omega^2}{2\Gamma^2} \ .$$

5. Finally, we obtain that the ramp speed should be slower than

$$T^{-1} < \frac{\Gamma}{\Delta\omega_{red}\Delta t} < \frac{\Gamma\Omega}{\Delta\omega_{red}\pi} = \frac{\Gamma^2\sqrt{2I/I_s}}{kv_m\pi} \simeq 12 \text{ kHz} \ .$$

0.64 21.01.2014 Magnetic trap

Atoms decaying into the $(5s5p)\ ^3P_2$, $m_J = 2$, $g_J = 3/2$ Zeeman state are magnetically trapped in the MOT magnetic field, $\partial_z B = 2\partial_r B = 70$ G/cm. The temperature of the blue MOT is about 5 mK. The depth of the magnetic trap is about 300 G (see Sec. 29.6.2010), which corresponds to 420 MHz or $U_0 = 20$ mK. Generally, the temperature equilibrates at a fifth of the trap depth, which is $T = 4$ mK.

The magnetic trapping potential can be approximated by $U(\mathbf{r}) \simeq \mu_B g_J m_J \partial_r B \sqrt{r^2 + 4z^2}$. With the definition

$$\bar{r} \equiv \frac{k_B T}{\mu_B g_J m_J \partial_r B} \ ,$$

the density can be written

$$n(\mathbf{r}) = n_0 e^{-U(\mathbf{r})/k_B T} = n_0 e^{-\sqrt{r^2+4z^2}/\bar{r}} \ .$$

The atom number is $N = n_0 V_{eff} = n_0 4\pi \bar{r}^3$. For our parameters,

$$\bar{r} \approx 6 \text{ mm} \ .$$

From $m\omega_r^2 \bar{r}^2 = k_B T$,

$$\omega_r = \frac{\mu_B g_J m_J \partial_r B_{qua}}{\sqrt{m k_B T}} \ . \tag{49}$$

Upon adiabatic ramping the phase space density $\rho = n_0 \lambda_{dB}^3$ stays constant,

$$\lambda_{dB} = \sqrt{\frac{2\pi\hbar^2}{m k_B T}} \ . \tag{50}$$

With $g_J = 7/6$, $m_J = 1, 2$, $T = 5$mK, $\partial_r B_{qua} = 70$ G/cm, we get

$$\bar{r} = \frac{k_B T}{\mu_B g_J m_J \partial_r B_{qua}} = 4.6\text{mm} \ . \tag{51}$$

Hence,

$$t \propto (\partial_r B_{qua})^{2/3} \tag{52}$$
$$\bar{r} \propto (\frac{1}{\partial_r B_{qua}})^{1/3} \ .$$

For example, ramping from 70 G/cm to 7 G/cm we reduce the temperature from 5 mK to about 1 mK and increase the size from 3 mm to 6 mm. The 29.6.2010 we estimated a trap depth of about 300 G, which would scale down to 30 G or 2 mK.

0.65 13.02.2014 Questions to think about

1. Can the Rice excited ^{86}Sr molecular BEC production scheme be implemented with ^{88}Sr provided we put the atoms in an optical lattice.

2. Can we use the strontium intercombination line be used for sideband cooling in a dipole trap, lattice, or cavity? Ask Celso for help!

0.66 07.04.2014 Atomic light house effect 2

0.66.1 Optical density of the red MOT

A typical situation for a red MOT is that one of Maryvonne Chalony: $N = 2 \cdot 10^7$, $T = 4\ \mu$K, $\bar{R} = 70\ \mu$m, and $b_0 = 50$ for the blue transition.

Actually, the optical density should not depend on Γ. In practice, however, narrow transitions are generally dominated by Doppler broadening. For example, at 4 μK the Doppler broadening of the intercombination line is: $k\bar{v} = k\sqrt{k_B T/m} = (2\pi)$ 28 kHz. Even if the temperature is at the Doppler limit $T_D = \hbar\Gamma/k_B = 365$ nK, the Doppler width still is (2π) 8.5 kHz.

To prevent blurring of the light house deflection by the thermal atomic motion, it is important that the Doppler shift be smaller than the Zeeman shift, $k\bar{v} \ll \bar{R}\partial_r B$. In this case, the main effect of the thermal motion is to reduce the optical thickness of the atomic cloud, by a factor corresponding to the spectral overlap between the natural linewidth and the Doppler broadened width, $b_D = b_0\Gamma/kv = 12$.
Note that reducing the optical thickness is always possible by ballistically expanding the cloud.

0.66.2 Beam divergence

Setting $w_0 = \bar{R} = 70\ \mu$m, we obtain the divergence angle $\alpha = \lambda/\pi w_0 = 0.18°$.

0.67 24.04.2014 Bloch equations for the blue transition

0.68 26.04.2014 Resonance fluorescence of the S-P transitions

The four-level Bloch equations allow to calculate time-evolutions, absorption spectra and fluorescence spectra, after having specified the Rabi frequency, the laser polarization vector, the magnetic field vector and its amplitude: The splitting of the

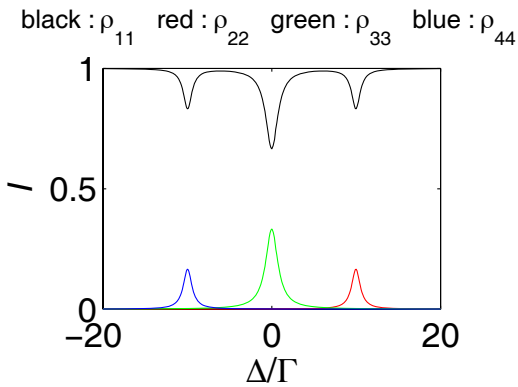

Figure 39: (code) Absorption spectrum.

absorption spectrum is due to the Zeeman effect. In the shown example, the laser polarization is chosen such as to drive all transitions.

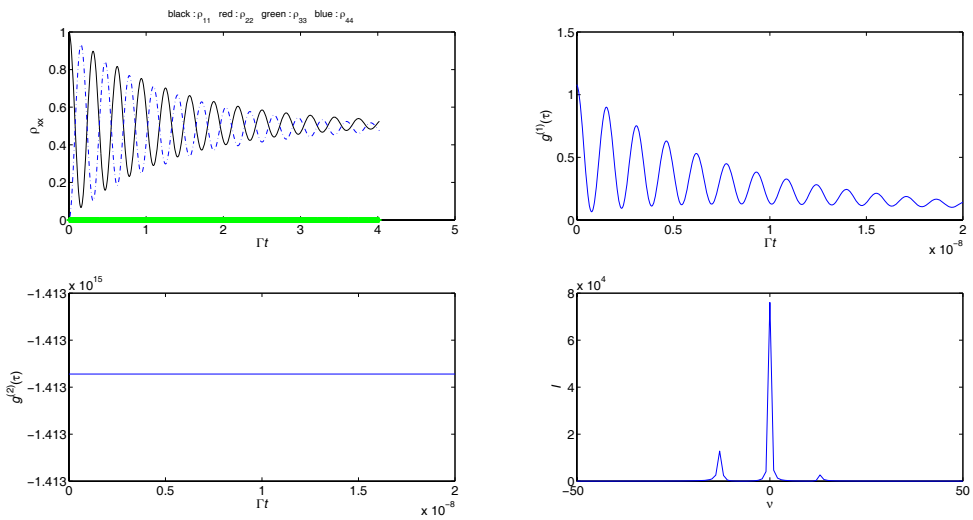

Figure 40: (code) Time evolution, first and second-order correlation functions, and generalized Mollow spectrum.

Calculating the fluorescence spectrum is more complicated.

The question is whether we should plan to measure the fluorescence spectrum for

our blue or red strontium MOT and watch out for cooperative modifications of the Mollow spectrum.

0.69 07.04.2014 Atomic light house effect 3

0.69.1 Displacing the MOT via radiation pressure

The light house signature could be simplified by applying a strong offset magnetic field and tuning the probe laser to one of the Zeeman-shifted transitions. If $\mu_B B \gg \hbar\Gamma \simeq \hbar|\Delta|$, the other Zeeman sublevels might be disregarded.

0.69.2 Deflection by the blue MOT

A typical situation for a blue MOT is: $N = 1{\cdot}10^8$, $T = 4$ mK, $\bar{R} = 3$ mm, $b = 70$ G/cm and $b_0 = 1$. The maximum deflection angle is:

$$\theta_L = \arcsin \frac{1 - \sqrt{1 + 4\alpha^2\sigma^2}}{2\alpha\sigma^2} = -\alpha = \frac{2\mu_B b}{\hbar k_0 \Gamma} \simeq 0.0026^\circ \ .$$

On a distance of 1 m this angle produces a deflection of 55 μm which can be readily detected with a quadrant detector.

0.69.3 Beam divergence

Setting $w_0 = \bar{R} = 3$ mm, we obtain the divergence angle $\alpha_{div} = \lambda/\pi w_0 = 0.003^\circ$. Hence, the condition to resolve the deflection is

$$1 \ll \frac{\theta_L}{\alpha_{div}} = \frac{\mu_B b w_0}{\hbar\Gamma} \ .$$

0.70 12.06.2014 Gradient for lighthouse deflection

0.70.1 What is the impact of the magnetic field?

The question is how to maximize the magnetic field gradient responsible for inducing the atomic lighthouse deflection.

The Zeeman effect is for $J = 1$,

$$V(B) = -\vec{\mu} \cdot \mathbf{B} = -\frac{\mu_B}{\hbar}(\hat{J}_x B_x + \hat{J}_y B_y + \hat{J}_z B_z) = -\frac{\mu_B}{\hbar}\left[\frac{1}{2}(B_x - iB_y)\hat{J}_+ + \frac{1}{2}(B_x + iB_y)\hat{J}_- + \hat{J}_z B_z\right.$$
$$= -\mu_B \begin{pmatrix} B_z & \frac{1}{\sqrt{2}}(B_x - iB_y) & 0 \\ \frac{1}{\sqrt{2}}(B_x + iB_y) & 0 & \frac{1}{\sqrt{2}}(B_x - iB_y) \\ 0 & \frac{1}{\sqrt{2}}(B_x + iB_y) & -B_z \end{pmatrix}$$

gives rise to a level shift, which only depends on the absolute value of the magnetic field,

$$\langle J, m_z | V(B) | J, m_z \rangle = -\frac{\mu_B}{\hbar} m_z |\mathbf{B}| \ .$$

0.70.2 How to calculate the lighthouse deflection?

The atomic lighthouse-deflected radiation pattern is given by [69],

$$E(k) = \frac{\hbar\Gamma}{id}\frac{e^{ik_0 r}}{r}\int d^3r' \rho(\mathbf{r}')\beta^{(1)}(\mathbf{r}')e^{-i\mathbf{k}\cdot\mathbf{r}'} \ ,$$

where $\rho(\mathbf{r}) = \frac{N}{(2\pi)^{3/2}R^3}e^{-(x^2+y^2+z^2)/2R^2}$ is the atomic density distribution and

$$\beta^{(1)}(\mathbf{r}) = \frac{\Omega_0}{\Gamma}\frac{e^{i\mathbf{k}_0\cdot\mathbf{r}}}{i + 2\Delta(\mathbf{r})/\Gamma}$$

the local atomic dipole moment. As shown above, the local detuning, $\Delta(\mathbf{r}) = \frac{\mu_B m_j |\mathbf{B}(\mathbf{r})|}{\hbar}$, is proportional to the absolute value of the local magnetic field.

0.70.3 What is the shape of the inhomogeneous magnetic field?

We consider the quadrupole field given by $\mathbf{B} = b(x, y, -2z)^T$ shifted sideways via a homogeneous magnetic field, $\mathbf{B}_0 = B_0\hat{\mathbf{e}}_z$, so that the absolute value is

$$|\mathbf{B}_s| = b\sqrt{x^2 + y^2 + (2z - B_0/b)^2} \ .$$

The local gradient is then,

$$\nabla|\mathbf{B}_s| = \frac{1}{\sqrt{x^2 + y^2 + (2z - B_0/b)^2}}\begin{pmatrix} x \\ y \\ 4z - 2B_0/b \end{pmatrix} \ .$$

e may also expand the absolute value of the magnetic field for $x, y, z \ll B_0/b$ within the cloud:

$$|\mathbf{B}_s| \simeq B_0\sqrt{1-\frac{4b}{B_0}z} \simeq B_0 - 2bz \ .$$

Choosing the laser detuning $\Delta_0 = \mu_B B_0/\hbar$,

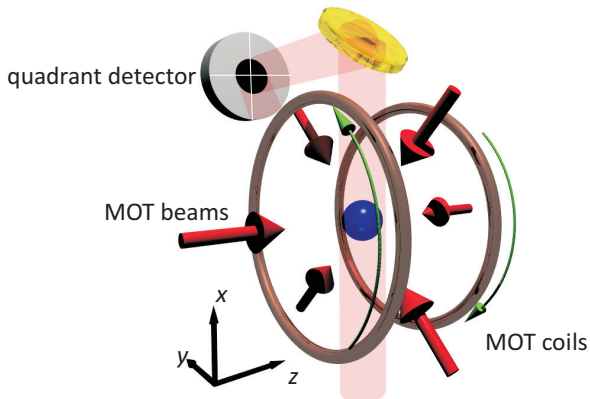

Figure 41: (code) Experimental scheme.

$$\Delta(\mathbf{r}) = \Delta_0 + \frac{\mu_B m_j |\mathbf{B}(\mathbf{r})|}{\hbar} \simeq \frac{\mu_B B_0}{\hbar} - \frac{\mu_B(B_0 - 2bz)}{\hbar} = \frac{2\mu_B bz}{\hbar} = k_0\Gamma\alpha z \ ,$$

with $\alpha = \frac{2\mu_B b}{\hbar k_0 \Gamma}$. Hence,

$$\beta^{(1)}(\mathbf{r}) = \frac{\Omega_0}{\Gamma}\frac{e^{i\mathbf{k}_0\cdot\mathbf{r}}}{i + 2\Delta(\mathbf{r})/\Gamma} = \frac{\Omega_0}{\Gamma}\frac{e^{i\mathbf{k}_0\cdot\mathbf{r}}}{i + 2\alpha k_0 z} \ .$$

For the blue Sr line, if we want to detune by $|\Delta| = 2\Gamma$, we have to apply $B_0 = \frac{2\hbar}{\mu_B}\Gamma \approx 46$ G. With an axial gradient of $2b = 70$ G/cm, the magnetic field at the edge of the cloud $z_e = 3$ mm is $|\mathbf{B}(z_e)| - B_0 = 2bx_e \approx 21$ G.

0.70.4 What (anti-)Helmholtz currents should be chosen?

The magnetic field generated by our (anti-)Helmholtz coils, $R = d$, along the symmetry axis is

$$\mathbf{B}_H(z) = -\frac{8}{5\sqrt{5}}\frac{\mu_0 N I_H \hat{e}_z}{R}[1+O(z^2)] \quad \text{resp.} \quad \mathbf{B}_{aH}(z) = -\frac{48}{25\sqrt{5}}\frac{\mu_0 N I_{aH}\hat{e}_z}{R^2}[z+O(z^3)] \ .$$

Hence, the total field in the case of asymmetric currents, $I_{1,2} = I_H \pm I_{aH}$, is

$$B_{tot}(z) = B_{aH}(z) + B_H(z) \simeq -\frac{8}{25\sqrt{5}}\frac{N\mu_0}{R^2}(6zI_{aH} + 5RI_H) \ .$$

We know that for $I_{aH} = 35$ A and $N = 100$ the gradient of the magnetic field is

$$2b = \frac{48}{25\sqrt{5}}\frac{\mu_0 N I_{aH}}{R^2} = 70 \text{ G} \ ,$$

which gives $R = 7.35$ cm. Finally,

$$\mathbf{B}_H(z) = -\frac{8}{5\sqrt{5}}\frac{\mu_0 N I_H}{R} = -I_H \cdot 12.23 \text{ G/A} \ .$$

Hence, to obtain the $\mathbf{B}_H = 46$ G estimated above, we need $I_H = 4$ A.

0.71 08.09.2014 Kuramoto synchronization of atomic dipoles in clouds

The notion of superradiance is, nowadays, a matter of dispute. A frequently adopted designation involves a synchronization of the atomic dipole moments to incident light field [99]. But in this sense, even the Bragg scattering would be a superradiant process, in fact, this scattering is accelerated by the number of scatterers [101]. Here we propose to reserve this word, in the original sense of Dicke, for processes due to a spontaneous self-synchronization of atomic dipole moments due to mutual interaction.

We believe that the spontaneous Kuramoto-type synchronization gives rise to islands of synchronized atomic dipoles. This leads to CARL type forces, which in turn influences the local density distribution leading to CARL type self-organization leading to the formation of transverse patterns.

If $\bar{n} = N/\bar{R}^3$ is the mean atomic density, the mean distance between two atoms is $\bar{d} = \bar{n}^{-1/3}$. The mean velocity of the atoms at a given temperature is $\bar{v} = \sqrt{k_B T/m}$. I.e. due to the atomic thermal motion a new realization of the atomic disorder is realized before a time

$$\Delta t = \frac{\bar{d}}{\bar{v}} = \frac{\sqrt{m}}{\bar{n}^{1/3}\sqrt{k_B T}} = \frac{\bar{R}\sqrt{m}}{N^{1/3}\sqrt{k_B T}} \ .$$

For strontium and $N = 10^5$, $T \approx 4$ mK and $\bar{R} = 3$ mm, we expect $\Delta t \simeq 100$ μs.

Let us now assume a pulsed probe beam with pulse duration Δt. Its intensity is related to the Rabi frequency via,

$$I = \frac{\hbar\omega}{\sigma_0}\frac{\Omega^2}{\Gamma} \ ,$$

where $\sigma_0 = 3\lambda^2/2\pi$ is the resonant optical cross section. Operating at saturation intensity $\Omega_s = \Gamma$, we would expect $I = I_s = 85$ mW/cm^2. In order to resolve the speckle in a direction orthogonal to $\vec{k}_0$, we need a detector with a limited aperture given by a solid angle $\Delta\Omega_s$. The question is therefore, how many photons are scattered from the probe beam into this solid angle within time Δt. For a single atom, we would expect

$$n_{ph} = \frac{\Delta P_s}{\hbar\omega}\Delta t = \frac{\sigma_0 I \Delta\Omega_s}{\hbar\omega}\Delta t = \frac{\Omega^2}{\Gamma}\Delta\Omega_s \Delta t \ .$$

At saturation and for $\Delta\Omega = 1^\circ \times 1^\circ = 3\cdot 10^{-4}$ sr, we would expect $n_{ph} = \Gamma\Delta\Omega_s\Delta t \simeq 6$ photons in 100 μs. For $N = 10^5$ atoms, we have more photons but also more forward scattering.

An experiment, where we don't look for angular resolution, but analyze the time-dependent fluctuations of the photon number as a function of aperture size seems feasible with a blue strontium MOT.

0.72 13.07.2014 Lighthouse deflection detection

To detect the deflection, we propose to use a quadrant detector (PDQ80A, Thorlabs) for transient signals and a CCD camera for measurements of beam deformations.

PDQ80A – Thorlabs

- Old connector – Hirose connector HS10A-7P-6P (male)

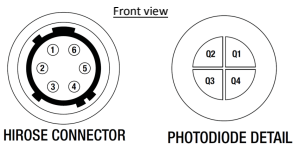

	Pin assignment	Cable color
PIN 1	X-axis: $(Q_2 + Q_3) - (Q_1 + Q_4)$	Orange
PIN 2	Y-axis: $(Q_1 + Q_2) - (Q_3 + Q_4)$	Blue
PIN 3	SUM: $Q_1 + Q_2 + Q_3 + Q_4$	Green
PIN 4	$+V$ ($+5\ V$ to $+15\ V$)	Red
PIN 5	COMMON	White
PIN 6	$-V$ ($-5\ V$ to $-15\ V$)	Yellow

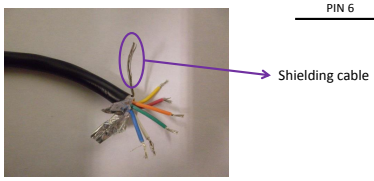

- New connector – DB9 connector (female)
  - Same number pattern used
  - Shielding wire is connected to PIN 7
  - PINs 8 and 9 not used

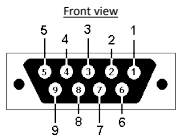

Figure 42: (code) Quadrant detector connections.

0.73 14.07.2014 Lighthouse deflection sequence?

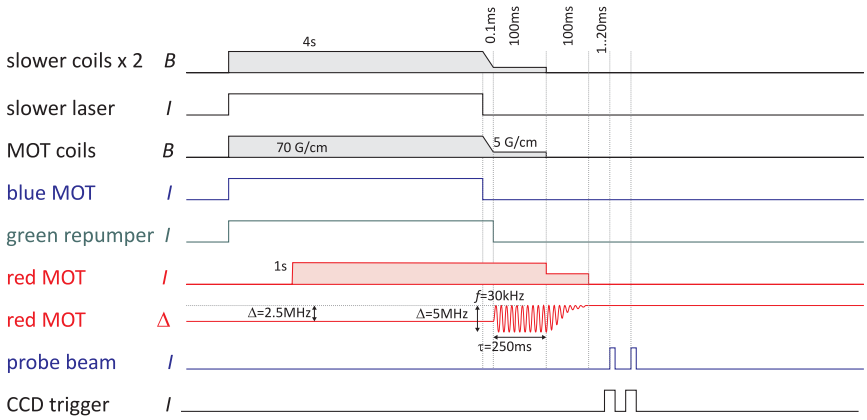

Figure 43: (code) Experimental sequence.

0.74 15.07.2014 Lighthouse deflection signal

Estimation of the quadrant detector signal

$$
\begin{aligned}
S = P_{left} - P_{right} &= \int_{-\infty}^{\infty}\int_{-\infty}^{\Delta x_{LH}} \frac{2P}{\pi w(z)^2} e^{-2r^2/w(z)^2} dxdy - \int_{-\infty}^{\infty}\int_{-\infty}^{-\Delta x_{LH}} \frac{2P}{\pi w(z)^2} e^{-2r^2/w(z)^2} dxdy \\
&= \frac{2P}{\pi w(z)^2}\frac{w(z)^2}{2}\sqrt{\pi}\left[\int_{-\infty}^{\sqrt{2}\Delta x_{LH}/w(z)} e^{-x^2}dx - \int_{-\infty}^{-\sqrt{2}\Delta x_{LH}/w(z)} e^{-x^2}dx\right] \\
&= \frac{P}{\sqrt{\pi}}\left[\int_{-\infty}^{\sqrt{2}\Delta x_{LH}/w(z)} e^{-x^2}dx - \int_{-\infty}^{-\sqrt{2}\Delta x_{LH}/w(z)} e^{-x^2}dx\right] \\
&= \frac{P}{\sqrt{\pi}}\left[\frac{\sqrt{\pi}}{2}\left[1+\operatorname{erf}\left(\tfrac{\sqrt{2}\Delta x_{LH}}{w(z)}\right)\right] - \frac{\sqrt{\pi}}{2}\left[1+\operatorname{erf}\left(-\tfrac{\sqrt{2}\Delta x_{LH}}{w(z)}\right)\right]\right] = P\operatorname{erf}\left(\tfrac{\sqrt{2}\Delta x_{LH}}{w(z)}\right) .
\end{aligned}
$$

For gaussian beams, $w(z)^2 = w_0^2\left[1+\left(\frac{\lambda z}{\pi w_0^2}\right)^2\right]$, so that the signal becomes

$$
S = P\operatorname{erf}\left(\frac{\sqrt{2}\Delta x_{LH}}{w_0\sqrt{1+(\lambda z/\pi w_0^2)^2}}\right) = P\operatorname{erf}\left(\frac{\sqrt{2}\theta_{LH}}{w_0\sqrt{z^{-2}+z_R^{-2}}}\right) = P\operatorname{erf}\left(\frac{\sqrt{2}\theta_{LH}}{\sqrt{\left(\frac{w_0}{z}\right)^2+\left(\frac{\lambda}{\pi w_0}\right)^2}}\right) ,
$$

using $\theta_{LH} = \Delta x_{LH}/z$. Provided the deflection angle does not depend strongly on w_0, the argument becomes maximal, when $z = z_R$. I.e. for a given z the waist producing the largest signal is just

$$
w_0 = \sqrt{\frac{\lambda z}{\pi}} .
$$

Unfortunately, numerical simulations show that the deflection angle is so small, that huge Rayleigh lengths z_R and observation distances z must be chosen. Chosing a reasonable distance $z = z_R = 2$ m, we find that $w_0 = 540$ μm should be a good choice. It corresponds to a diffraction angle of $\theta_D = \frac{w(z)}{z}\sqrt{1+\left(\frac{\lambda z}{\pi w_0^2}\right)} \approx 0.015°$. Assuming a deflection angle of $\theta_{LH} \approx 0.0025°$, we then expect a signal of,

$$
S = P\operatorname{erf}\left(\frac{z\theta_{LH}}{w_0}\right) = P\operatorname{erf}\left(\frac{\sqrt{2}\theta_{LH}}{\theta_D}\right) \simeq P\frac{\sqrt{8}\theta_{LH}}{\sqrt{\pi}\theta_D} \approx 0.27P ,
$$

using the expansion $\sqrt{\pi}\operatorname{erf}(x) = 2x - \frac{2}{3}x^3 + \frac{1}{5}x^5 + ...$

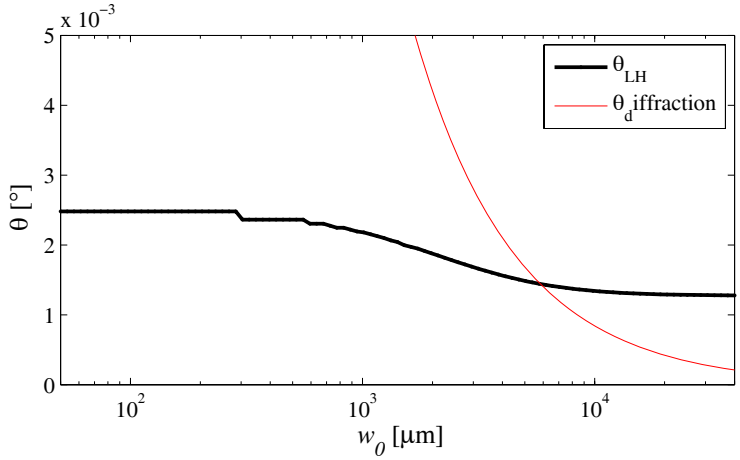

Figure 44: (code) Deflection and diffraction angle.

0.75 25.07.2014 Detectability of speckle patterns in a blue Sr MOT

If $\bar{n} = N/\bar{R}^3$ is the mean atomic density, the mean distance between two atoms is $\bar{d} = \bar{n}^{-1/3}$. The mean velocity of the atoms at a given temperature is $\bar{v} = \sqrt{k_B T/m}$. I.e. due to the atomic thermal motion a new realization of the atomic disorder is realized before a time

$$\Delta t = \frac{\bar{d}}{\bar{v}} = \frac{\sqrt{m}}{\bar{n}^{1/3}\sqrt{k_B T}} = \frac{\bar{R}\sqrt{m}}{N^{1/3}\sqrt{k_B T}} \ .$$

For strontium and $N = 10^5$, $T \approx 4$ mK and $\bar{R} = 3$ mm, we expect $\Delta t \simeq 100$ μs.

Let us now assume a pulsed probe beam with pulse duration Δt. Its intensity is related to the Rabi frequency via,

$$I = \frac{\hbar\omega}{\sigma_0}\frac{\Omega^2}{\Gamma} \ ,$$

where $\sigma_0 = 3\lambda^2/2\pi$ is the resonant optical cross section. Operating at saturation intensity $\Omega_s = \Gamma$, we would expect $I = I_s = 85$ mW/cm^2. In order to resolve the speckle in a direction orthogonal to $\vec{k}_0$, we need a detector with a limited aperture given by a solid angle $\Delta\Omega_s$. The question is therefore, how many photons are scattered from the probe beam into this solid angle within time Δt. For a single atom, we would expect

$$n_{ph} = \frac{\Delta P_s}{\hbar\omega}\Delta t = \frac{\sigma_0 I \Delta\Omega_s}{\hbar\omega}\Delta t = \frac{\Omega^2}{\Gamma}\Delta\Omega_s \Delta t \ .$$

At saturation and for $\Delta\Omega = 1^\circ \times 1^\circ = 3\cdot 10^{-4}$ sr, we would expect $n_{ph} = \Gamma\Delta\Omega_s\Delta t \simeq 6$ photons in 100 μs. For $N = 10^5$ atoms, we have more photons but also more forward scattering.

An experiment, where we don't look for angular resolution, but analyze the time-dependent fluctuations of the photon number as a function of aperture size seems feasible with a blue strontium MOT.

0.76 26.07.2014 Plans for Robin's stay

- Measurement of the light deflection
- Detectability of speckle patterns in a blue Sr MOT
- Detectability of cooperative effects in resonance fluorescence
- Alternative approaches based on homodyne detection
- Projects for post-docs and PhD students

0.77 25.11.2014 Measurement attempt of CBS in a Sr heatpipe

- combat stray light
- get wedged beam splitter BSW10
- try helicity ∥ helicity and h ⊥ h
- do not saturate atoms
- clean old cell and/or make new cell, improve temperature isolation
- can pressure broadening dephase the dipoles?

0.78 30.12.2014 Measuring CBS in a hot gas: Some estimations

The starting point of this experiment is the allegation that even a hot atomic cloud may exhibit coherent backscattering (CBS) provided the incident laser ω is tuned far enough from the atomic resonance, $\Delta \equiv \omega - \omega_0$. The elastic (Rayleigh) scattering then occurs on a time scale so short that the atoms do not move considerably during the time it take a photon to be scattered at least twice before being reradiated into backward direction.

0.78.1 What is the minimum detuning?

1. ***Cold atoms:*** Without thermal motion we consider the scattering as elastic, if the photon is bound by an atom for a time shorter than it takes the atom to travel, *accelerated by the photonic recoil* over a distance λ. If τ is the time the photon stays near an atom, the travel distance l needs to satisfy

$$\lambda \gg l = v\tau = \frac{p}{m}\tau = \frac{\hbar k}{m}\tau = \omega_{rec}\tau\frac{\lambda}{2\pi} \ , \tag{53}$$

where ω_{rec} is the recoil frequency. Hence,

$$\frac{2\pi}{\tau} \gg \omega_{rec} \ , \tag{54}$$

which is always satisfied for broad transitions, for which on resonance $2\pi/\tau = \Gamma$ and off resonance $2\pi/\tau = |\Delta|$. Hence, there is no minimum detuning for cold atoms.
2. ***Hot atoms:*** With thermal motion the scattering as elastic, if the photon is bound by an atom for a time shorter than it takes the atom to travel, *due to thermal motion* over a distance λ. With the mean thermal velocity $\bar{v} \equiv \sqrt{k_B T/m}$ (which is also the *rms* width of the Maxwell velocity distribution), the condition reads,

$$\lambda \gg l = \bar{v}\tau \ . \tag{55}$$

Hence, if $\tau = 2\pi/|\Delta|$ is the time the photon stays near an atom, the minimum detuning for CBS is,

$$|\Delta| \gg k\bar{v} \ . \tag{56}$$

This means that by tuning the incident laser outside the Doppler-broadened line, $|\Delta| \gg k\bar{v}$, there may be many atoms with velocities v satisfying $|\Delta - kv| \gg k\bar{v}$ and therefore qualifying for CBS. A problem may, however, occur due to the fact that the optical cross section for off-resonant scattering is weak and that even a small amount of atoms with $|\Delta - kv| < k\bar{v}$ and thus having a large optical cross section may completely dominate and impede CBS.

To check this we calculate the detuning dependent optical density of a Doppler-broadened hot cloud trying to separate the contributions of atoms with $|\Delta - kv| > k\bar{v}$ from those of atoms with $|\Delta - kv| < k\bar{v}$.

0.78.2 Do resonantly scattered photons impede CBS?

We want calculate the optical density of a Doppler-broadened Sr cloud heated to $T = 495°\mathrm{C}$ inside a 15cm long vapor cell as a function of the laser detuning from the 461nm resonance, whose width is $\Gamma = (2\pi)$ 32MHz. The vapor pressure of Sr at this temperature is $P = 4.3 \cdot 10^{-3}$ mbar (see Sec. 23.6.2013). The rms Doppler width is $k\bar{v} = (2\pi)$ 580 MHz $\approx 18\Gamma$.

The optical cross section for an atom with resonance frequency ω_0 moving with velocity v and irradiated by a laser beam at frequency ω is,

$$\sigma(v) = \frac{6\pi}{k^2} \frac{\Gamma^2}{4(\omega - \omega_0 - kv)^2 + \Gamma^2} \ . \tag{57}$$

The one-dimensional Maxwell velocity distribution is,

$$\rho(v)dv = \sqrt{\frac{m}{2\pi k_B T}} e^{-mv^2/2k_B T} dv \ , \tag{58}$$

which is normalized to 1. The density of the atoms is

$$n(T) = \frac{P}{k_B T} \approx 10^{18} \ \mathrm{m}^{-3} \ . \tag{59}$$

The optical density is

$$\begin{aligned} b(T,\omega) &= Ln(T)(\sigma \star \rho)(\delta) = Ln(T) \int_{-\infty}^{\infty} \sigma(v)\rho(v)dv \\ &= L\frac{P}{k_B T}\sqrt{\frac{m}{2\pi k_B T}} \frac{6\pi}{k^2} \int_{-\infty}^{\infty} \frac{\Gamma^2 e^{-mv^2/2k_B T}}{4(\omega - \omega_0 - kv)^2 + \Gamma^2} dv \ . \end{aligned} \tag{60}$$

0.78.3 Checking the zero temperature limit

At zero temperature (assuming a fixed density n), we may approximate the Gaussian (respecting its normalization) by a δ-distribution:

$$\sqrt{\frac{m}{2\pi k_B T}} e^{-mv^2/2k_B T} dv \to \delta(kv)d(kv) \ . \tag{61}$$

Hence,

$$b(0,\omega) = Ln\frac{6\pi}{k^2} \int_{-\infty}^{\infty} \frac{\Gamma^2}{4(\omega - \omega_0 - kv)^2 + \Gamma^2} \delta(kv)d(kv) = Ln\frac{6\pi}{k^2} \frac{\Gamma^2}{4(\omega - \omega_0)^2 + \Gamma^2} \ , \tag{62}$$

which means, that we recover the standard optical density

$$b(0,\omega) = Ln\sigma(\omega) \ . \tag{63}$$

0.78.4 Checking the narrow linewidth limit

If the atomic linewidth is very narrow, we may approximate the Lorentzian (respecting its normalization) by a δ-distribution:

$$\frac{2k}{\pi\Gamma}\frac{\Gamma^2}{4(\omega-\omega_0-kv)^2+\Gamma^2}dv \to \delta(\omega-\omega_0-kv)d(kv) \ . \tag{64}$$

Hence,

$$\begin{aligned} b(T,\omega) &= Ln\sqrt{\frac{m}{2\pi k_B T}}\frac{6\pi}{k^2}\int_{-\infty}^{\infty} e^{-mv^2/2k_BT}\frac{\pi\Gamma}{2k}\delta(\omega-\omega_0-kv)d(kv) \\ &= Ln\sqrt{\frac{m}{2\pi k_B T}}\frac{6\pi}{k^2}\frac{\pi\Gamma}{2k}e^{-m(\omega-\omega_0)^2/2k_BTk^2} \ . \end{aligned} \tag{65}$$

On resonance,

$$b(T,\omega_0) = Ln\sqrt{\frac{\pi}{2}}\frac{\sigma_0\Gamma}{2k\bar{v}} \ . \tag{66}$$

The fraction $\Gamma/2k\bar{v}$ can be interpreted as the spectral overlap between the Lorentzian absorption linewidth and the Maxwell distribution. The Figs. **??**(a,b) traces the optical density profile in the various limits. The narrow linewidth limit (blue) coincides with the Voigt profile (green).

0.78.5 Elastic and inelastic scattering

Let us now separate resonant and Rayleigh scattering by classifying the atoms in those satisfying $|\Delta - kv| < k\bar{v}$ and the others. The inelastic optical density would be,

$$\begin{aligned} b_{inel}(T,\omega) &= Ln(T)\int_{-\infty}^{\infty}\chi_{|\omega-\omega_0-kv|<k\bar{v}}\sigma(v)\rho(v)dv \\ &\simeq Ln\sqrt{\frac{\pi}{2}}\frac{\sigma_0\Gamma}{2k\bar{v}}\chi_{|\omega-\omega_0-kv|<k\bar{v}}\ e^{-m(\omega-\omega_0)^2/2k_BTk^2} \ . \end{aligned} \tag{67}$$

The elastic optical density would be

$$b_{el} = b - b_{inel} \simeq Ln\sqrt{\frac{\pi}{2}}\frac{\sigma_0\Gamma}{2k\bar{v}}\chi_{|\omega-\omega_0-kv|>k\bar{v}}\ e^{-m(\omega-\omega_0)^2/2k_BTk^2} \ . \tag{68}$$

The result is shown in Fig. **??**(c). It seems that elastically scattered photons represent a considerable contribution to the optical density at detunings just outside of the Doppler wings.

0.78.6 CBS angle

We may now calculate the mean free path and the CNS angle. The mean free path is given by

$$l_{mfp} = \frac{L}{b(T,\omega)} \ . \tag{69}$$

The angle is given by

$$\alpha_{cbs} = \frac{0.7}{kl_{mfp}} = \frac{b(T,\omega)}{kL} \ . \tag{70}$$

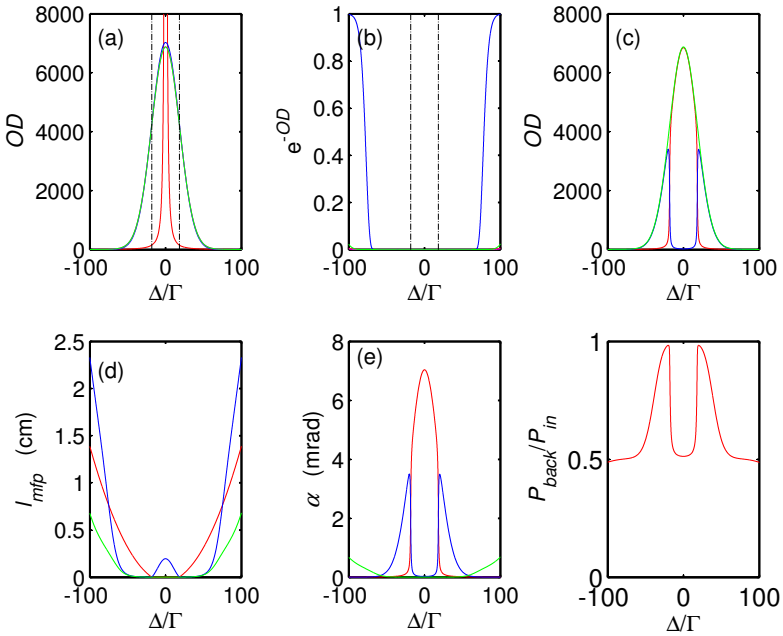

Figure 45: (code) (a) Optical density and (b) absorption for (red) the zero temperature limit, (blue) the narrow linewidth limit, and (green) the full Voigt profile. (c) Optical density generated by atoms within (red) and beyond (blue) the Doppler width, and (green) all atoms. (d) Mean free path, same color code as (c). (e) Angle of the CBS cone, same color code as (c). (f) Simple model for the back scattered peak intensity. Parameters see text.

0.79 31.12.2014 CBS experiment

We performed an experiment with our 15 cm long hot strontium cell. However, due to the presence of an argon buffer gas, the estimated active length is rather $L_{cell} = 5$ cm. The temperature was set to $T = 495°$C. We irradiated a blue laser with $P = 62$ μW of power (at resonance)and the beam diameter $w_0 = 1$ mm, so that the intensity was well below saturation. The laser frequency was tuned to various positions between ± 1.8 GHz and the backscattered light was passed through a $f100$ lens in the focus of which was placed a CCD camera (see Fig. **??**).

We are interested in the *angular distribution* of the CBS cone. To map this distribution we image the cone through a lens whose focus lies on the CCD camera. In this way, all parallel beams are *imaged into a single spot* and all beams emitted from a single point into different directions within the cone α are *imaged at different points* on the CCD camera at distances $f\alpha$ from the optical axis. For example, a beams backscattered under an angle of $\alpha = 3$ mrad hits the CCD camera at a distance $\Delta x = f\alpha \simeq 300\mu$m from the center. Our CCD camera having 7.5 μm large pixels, the cone would extend over 40 pixels.

This means that, once the focus is perfectly set, the depth of field of along the optical axis is infinite. Or in other words, the light collected at $\Delta x = 0$ contains the true information of the backscattering ($\alpha = 0$) independently on the mean free path.

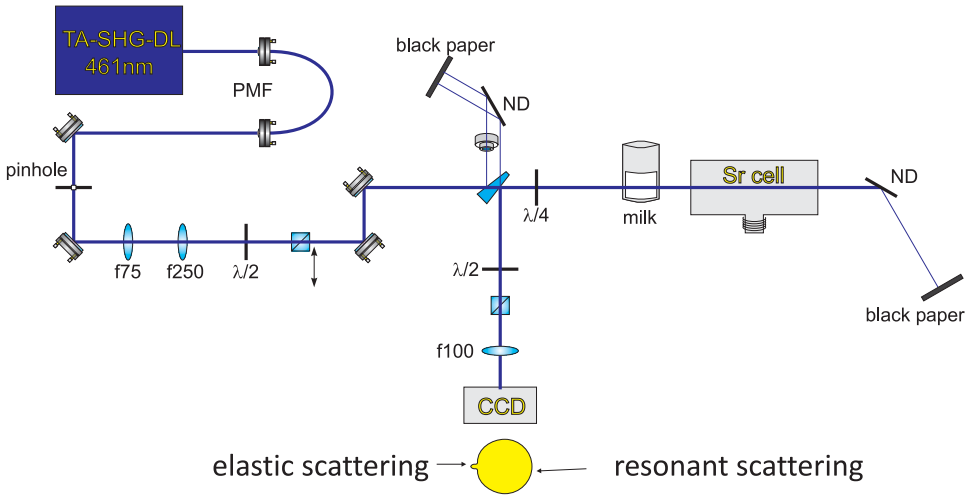

Figure 46: (code) Deflection and diffraction angle.

In contrast, any light at $|\Delta x| > 0$ originates from different angles α depending on how deep in cloud the scattering atom was located.

The results of our measurement are shown in the Figs. **??**.

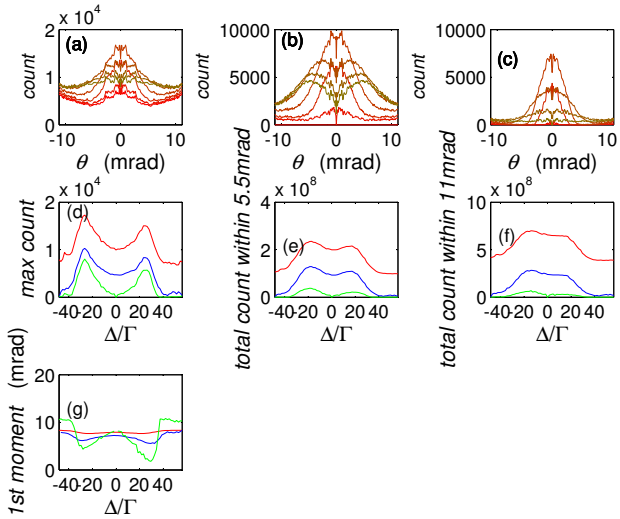

Figure 47: (code) (a) Cut through azimuthally averaged backscattered CCD images taken at various laser detunings. The x-axis has been rescaled to angle (see text). (b) Same as (a), but from the backscattered images an image taken off resonance was subtracted before azimuthal average. (c) Same as (a), but from the backscattered images an image taken on resonance was subtracted before azimuthal average. (d) Peak height at the center the azimuthally averaged images (red) obtained from the images (a), (blue) obtained from the images (b) (green) obtained from the images (c). (e) Total count integrated over 5.5 mrad using the same color coding as in (d). (f) Total count integrated over 11 mrad using the same color coding as in (d). (g) First moment of the distribution using the same color coding as in (d).

0.80 01.01.2015 CBS measurement analysis

The measured curves shown Fig. **??**(b) exhibits a narrowing of the angular distribution for detunings close to the Doppler width. The width of the "cone" is $\Delta\alpha \simeq 3$ mrad, which is compatible with our estimation in figure Fig. **??**(e). The amount of light emitted near $\alpha \simeq 0$ shown in Fig. **??**(d) exhibits peaks at the detunings $|\Delta| \simeq k\bar{v}$, which agrees with the positions, where the "elastic" optical density shown in Fig. **??**(c) has its peaks.

0.80.1 Contribution of incoherent scattering

We see from Fig. **??**(d) that the mean free path varies over huge ranges, when we vary the laser detuning. As long as the mean free path is shorter than the cell, the amount of incoherently isotropically scattered light is constant and equal to the incident light. I.e. the light power P_{incoh} collected inside a given backward solid angle is independent on the laser detuning. To verify this, we may integrate the counts recorded on the CCD camera, plot the result as a function of Δ and check whether the curve is flat. Figs. **??**(d,e) where we integrate over 5.5 mrad, respectively 11 mrad indeed show a weaker dependence within the detuning range, where $l_{mfp} < L_{cell}$.

This is not incompatible with CBS. The CBS light P_{cbs} adds up to the incoherently scattered light and will have its strongest impact close to the optical axis [within $\alpha < 3$ mrad according to Fig. **??**(e)]. The larger we chose the integration region, and consequently the detected solid angle, the more we emphasize incoherent with respect to elastic scattering.

Fig. **??**(g) illustrates the narrowing of the cone near $|\Delta - k\bar{v}| \simeq 0$ via a calculation of the first moment:

$$\frac{\int_{cone} \rho Image \ \rho d\rho d\theta}{\int_{cone} Image \ \rho d\rho d\theta} \ . \tag{71}$$

0.80.2 How to compare the data to a model?

Our simplistic model is based the assumption that we can separate the optical densities of elastically scattering atoms, b_{el}, and incoherently scattering ones, b_{incoh}. Let us now, for a try, assume that the amount of incoherently backscattered light be,

$$P_{incoh} \propto 1 - e^{-b_{incoh}} = 1 - e^{-L_{cell}/l_{mfp}} \ . \tag{72}$$

The amount of CBS light is only due to a fraction of the elastic optical density, let us say $b_{cbs} = b_{el}/1000$, such that

$$P_{cbs} \propto 1 - e^{-b_{cbs}} = 1 - e^{-b_{el}/1000} \ . \tag{73}$$

Fig. **??**(f) plots $P(\Delta) = P_{incoh} + P_{cbs}$. The curve looks not too different from the one observed in Fig. **??**(d). However, it is clear that we need a more sophisticated model taking into account, e.g., the anisotropic angular distribution of the CBS light.

We may conclude that, at this stage of the data analysis, our measurement are not incompatible with CBS. Nevertheless, further verification may be necessary to eliminate possible experimental artifacts.

0.80.3 Further tests

For instance, we may want to check issues due to finite apertures. Indeed, the imaging system was optimized for the highest optical density. However, at low optical density (e.g. at the edges of the Doppler profile) the mean free path may we on the order of centimeters. The light scattered from atoms which are deep in the cloud (seen along the optical axis)into an angle α may be clipped at the aperture, which artificially reduces the count rate around the edges of the Doppler profile. This effect is contrary to the observed one, provided the focusing was well done. Furthermore, the field of view considered in our measurement is pretty small, 11 mrad = 0.63°.

Nevertheless, it would be a good idea to measure simultaneously the amount light transmitted through the cell in order to detect when the condition $l_{mfp} < L_{cell}$ breaks down.

Furthermore, it may be interesting to evaluate the width of the cone as a function of Δ, thus checking Fig. **??**(e).

0.81 01.05.2015 CBS halfcone

Jean-Jacques Greffet, Waves in Random Media 3, S65 (1991)

0.82 11.05.2015 Strontium hollow cathode project

Locking 461nm to hollow cathode, J. Phys. Soc. Japan 81, 034401 (2012)

Blue ray laser should work, arXiv14060409, J. Phys. Chem. Ref. Data, 033103, 201 (2010)

heatpipe construction, Rev. Sci. Instr. 42, 1779 (1971)

Spectroscopy on Sr-hollow cathode, Physica Scripta. 26, 183 (1982)

Feshbach resonances in Sr, PRL 110, 173201 (2013)

0.83 30.11.2015 Saturation spectroscopy for the repumper

We consider setting up a saturation spectroscopy for the repumper at 497 nm using the $L = 10$ cm long Sr cell heated to $T = 500$ K, where the partial pressure o the strontium is about $P = 10^{-1}$ mbar (see Fig. **??**. To calculate the Lamb-dip we write the Maxwell velocity distribution like,

$$\rho(v)dv = \sqrt{\frac{m}{2\pi k_B T}} e^{-mv^2/2k_B T} dv \ .$$

The probe laser intensity is below saturation, such that the optical cross section for atom moving with velocity v is,

$$\sigma(\Delta_{67}) = \frac{6\pi}{k^2} \frac{\Gamma_{67}^2}{4\Delta_{67}^2 + \Gamma_{67}^2} \ .$$

The saturation laser has high intensity, $\Omega_{67} \equiv 10\Gamma_{67}$. We calculate the steady-state population

$$\rho_{66}(\Delta_{67})$$

in the ground state of the $|6\rangle$-$|7\rangle$ transition using optical Bloch equations. Finally, we obtain the spectrum of the probe laser via,

$$OD(\omega) = Ln \int_{-\infty}^{\infty} \rho_{66}(\Delta_{67} + kv) \ \sigma(\Delta_{67} - kv) \ \rho(v)dv$$

and the intensity of the transmitted light via, $\frac{I}{I_0} = e^{-OD}$.

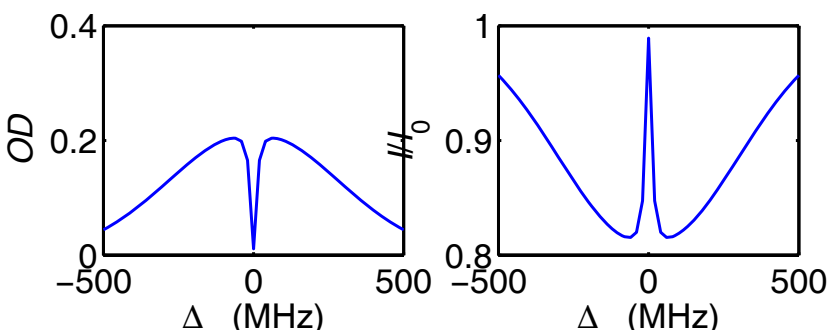

Figure 48: (code) Saturation spectrum on the repumping transition.

0.84 14.12.2015 Green MOT

Viability of green MOT for cooling atoms via molasses cooling.

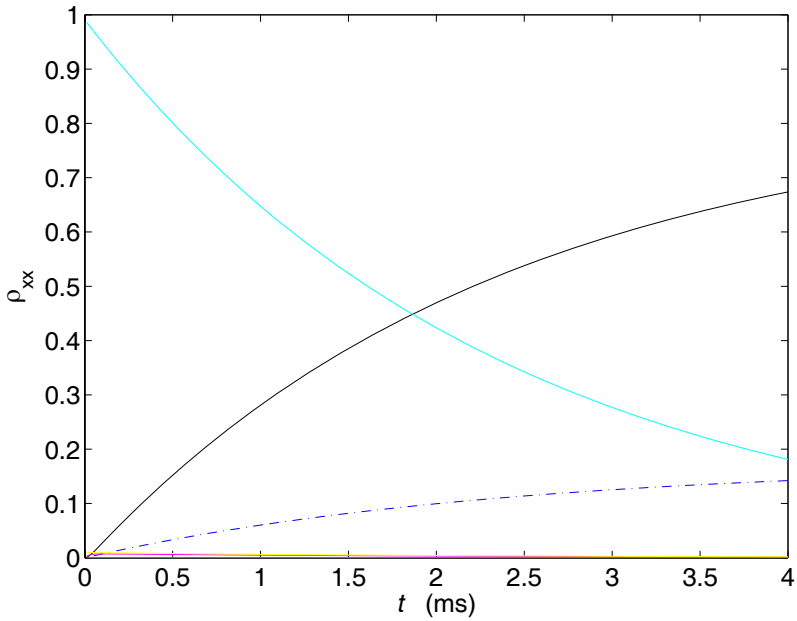

Figure 49: (code) Optical pumping.

Paulo tried to run green and blue MOT simultaneously, without seing any impact of the green laser. We gave up the idea, as the simulations show as well that the leak of the green is too large.

0.85 11.01.2016 Reference cavity calibration

On the 24.7.2015 we did the following measurement of the reference cavity's free spectral range:

1. The red laser was locked at two different modes (a) e (b) of the reference cavity, whose frequencies measured with the wavemeter were found to be close to

$$\nu_{wm,a} = 434.7848 \text{ THz} \quad \text{and} \quad \nu_{wm,b} = 434.7788 \text{ THz} .$$

The two modes were 4 free spectral ranges (fsr) apart from each other. From this we derive a first estimation of the fsr,

$$\delta_{fsr} = \tfrac{1}{4}(\nu_{wm,a} - \nu_{wm,b}) = 1.5 \text{ GHz} .$$

2. Simultaneously, comparison of the laser frequency with the frequency comb yielded,

$$\nu_{fc,a} = 434.784\ 786\ 94 \text{ THz} \quad \text{and} \quad \nu_{fc,b} = 434.778\ 803\ 79 \text{ THz} ,$$

which are 4 modes of the reference cavity away from each other.

3. Finally, we locked the laser to a third mode closer to the strontium line. Literature claims for the strontium line, $\nu_{sr} = 434.829\ 121\ 311$ THz. We observe this line shining the red laser into a blue MOT increasing the master laser frequency resonant to its cavity by +837 MHz and +150 MHz. The uncertainty in hitting the resonance with the red laser coming from the Doppler width of the blue MOT is about ±1 MHz. Hence, the cavity resonance is around,

$$\nu_{sr,c} = 434.828\ 134 \text{ THz} ,$$

which is 29 modes away from $\nu_{fc,a}$ and 33 modes away from $\nu_{fc,b}$. I.e. we have three measurements of the free spectral range: $\delta_{fsr,a} = \nu_{fc,a}/(N-29)$, $\delta_{fsr,b} = \nu_{fc,b}/(N-33)$, and $\delta_{fsr,c} = \nu_{sr,c}/N$, where N is the mode number of the mode, which is close to the reference cavity. Now, two treatments are possible:

4a. We treat all measurements as equivalent. Since there can be only one value for the free spectral range, we vary N minimizing,

$$\chi(N) = \sqrt{(\delta_{fsr,a} - \delta_{fsr,b})^2 + (\delta_{fsr,b} - \delta_{fsr,c})^2 + (\delta_{fsr,c} - \delta_{fsr,a})^2} .$$

Doing so we find a minimum at, $N = 290\ 892$. We calculate the free spectral range by,

$$\delta_{fsr} = \sqrt{\delta_{fsr,a}^2 + \delta_{fsr,a}^2 + \delta_{fsr,a}^2} = 1.494\ 809\ 531\ (3) \text{ GHz} .$$

4b. We only consider ther comb measurements, which are more precise. Since there can be only one value for the free spectral range, we vary N minimizing,

$$\chi(N) = \sqrt{(\delta_{fsr,a} - \delta_{fsr,b})^2} .$$

Doing so we find a minimum at, $N = 290\ 700$. We calculate the free spectral range by,

$$\delta_{fsr} = \sqrt{\delta_{fsr,a}^2 + \delta_{fsr,a}^2} = 1.495\ 796\ 921\ (3) \text{ GHz} .$$

In this case, we expect the cavity resonance at,

$$\nu_{sr,c} = N\delta_{fsr} = 434.828\ 164\ 739\ 84 \text{ THz} ,$$

which is 30 MHz higher than the expected value.

0.86 28.01.2016 Red light spectrum in blue MOT

Irradiating and scanning the red laser, we observe in the blue MOT fluorescence a clear dip and two sidebands at about 18 MHz. Where do they come from? Furthermore, we observe that, during the scan, for a short time, the fluorescence gets higher than the stationary blue MOT fluorescence. How is that possible.

0.86.1 Sidebands

We suspect that the sidebands are due to the fact that the atomic cloud is not in the center of the magnetic field, but displaced from the center by an amount

$$\Delta z = \frac{\hbar \Delta\omega / \mu_B}{\partial B_q} = 1.8 \text{ mm} ,$$

where $\partial B_q = 70$ G/cm and $\Delta\omega = 18$ MHz. We confirmed this hypothesis by the following experiment: We displaced the MOT on purpose along the magnetic field symmetry axis $\hat{\mathbf{e}}_z$, such that the atoms are predominantly in a region with $\mathbf{B} \simeq \pm B_z \hat{\mathbf{e}}_z$. We then shine the red laser along the z-axis with circular polarization $\sigma^\pm$ without retroreflection. We find that for the combination $+B_z$ and σ^+ the upper sideband is suppressed, and by either changing the polarization or the moving the cloud to the other side, the lower sideband is suppressed. This is because the $m_J = \pm 1$ Zeeman state is up(down)-shifted in positive magnetic fields and the other way round in negative magnetic fields. This observation confirms, that the spitting is due to the Zeeman effect.

But it also shows that the atomic cloud is not in the center of the magnetic field. The signal is useful for measuring the temperature and positioning the MOT in the centre of the magnetic field. Find out the reasons for the displacement and how to remedy.

0.86.2 Overshooting

When irradiating the red laser, we observe a fluorescence reduction of the blue MOT. This is understood by a depletion of the ground state population due to excitation into the $^3P_1$ by the red laser. When the red laser is now suddenly switched off, we observe an enhancement of fluorescence beyond the fluorescence of the blue MOT. The enhancement decays on the time scale of second. ???

0.87 01.02.2016 Magnetic field switching

We consider the magnetic coil drive circuit shown in the figure. At time $t = -\infty$ the transistor (IGBT) is closed. Then, at time $t = 0$ it is opened, a process which is described by a temporal increase of its resistence, $R(t) = \frac{R_\infty}{2}(1 + \tanh \frac{t}{\tau})$. We know $R_{coil} = 0.5\Omega$, $L = 8$ mH, $\tau = 10$ μs, and $R_\infty = 100$ kΩ.

With $N = 100$ turns and $r = 12$ cm, we expect, $L_N = 2N\mu_0 r = 30\mu$H, while Rodrigo measures about 8 mH.

0.87.1 1. approach

The diferential equation is,

$$U_0 = L\dot{I} + R_{coil}I + R_{fet}(t)I \ .$$

A solução numérica pode ser obtida por,

$$I(t + dt) = I + dt\ L^{-1}(U_0 - R_{cl}I - R(t)I) \ .$$

The induced voltage is $U_L = L\dot{I}$.

However, this does not explain the slow linear decay of the current. Perhaps, the strong overvoltage U_L inhibits the proper operation of the IGBT.

0.87.2 2. approach

Let us now assume, that the current I emitted by the power supply is not stopped, but redirected from the coil to a shunt resistor R_{snht}, which is in serie with a capacitor C_{snt}, $I_L \to I_C$, by opening the FET1 and closing FET2. Then,

$$\begin{aligned} I &= I_L + I_C \\ U_0 - R_0 I &= U_L + U_{R,coil} + U_{fet,1} = U_{fet,2} + U_{R,shnt} + U_{C,shnt} + U_{fet,2} \\ L\dot{I}_L + R_{coil}I_L + R_{fet1}I_L &= U_0 - R_0(I_L + I_C) \ , \end{aligned}$$

which gives

$$\begin{aligned} R_{fet,2}I_C + RI_C + C^{-1}\int I_C dt + R_{fet,2}I_C &= U_0 - R_0(I_L + I_C) \\ R_{fet,2}\dot{I}_C + R\dot{I}_C + C^{-1}I_C + R_{fet,2}\dot{I}_C &= -R_0(\dot{I}_L + \dot{I}_C) = -R_0\Bigg((-\frac{R}{L}I_L - \frac{R_{fet1}}{L}I_L + \frac{1}{L}U_0 - \end{aligned}$$

and

$$\begin{aligned} I_L(t + dt) &= I_L + dt\frac{1}{L}\left[-RI_L - R_{fet1}I_L + U_0 - R_0(I_L + I_C)\right] \\ I_C(t + dt) &= I_C + dt\frac{1}{R_{fet,2} + R + R_{fet,2} + R_0}\Bigg[-C^{-1}I_C - \frac{R_0}{L}\left[-RI_L - R_{fet1}I_L + U_0 - R_0(I_L + I_C\right. \end{aligned}$$

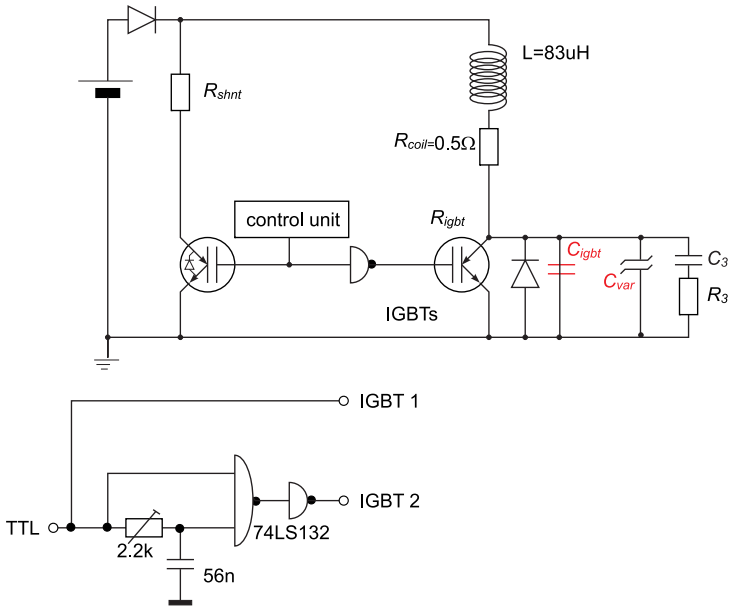

Figure 50: (code) Current drive.

0.88 18.05.2016 Blue-ray repumping

The seven-level Bloch equations allow to calculate time-evolutions, absorption spectra and fluorescence spectra, after having specified the Rabi frequency, the laser polarization vector, the magnetic field vector and its amplitude:

The level excited by the blue-ray laser might have a small decay rate into the $^2P_0$ state. For loading from the magnetic trap this is not a problem, but perhaps for a continuous blue MOT.

Raul set up the laser in November and saw that it is able to repump. Unfortunately, the laser seems damaged after New Year. We had to buy new diodes. Now, Michal has setup another ECDL and got it to work at 403.318 nm with up to 4 mW.

The simulation of the figure shows that without repumping, all atoms end up in the $^3P_2$ state within 10 μs. When the blue-ray repumper is switched on, this metastable state is depleted, and most atoms return to the ground state. There are, however, some atoms (blue dash-dotted line) populating the metastable $^3P_0$, which is not depleted.

Tests for the experiment:

1. Blue MOT in steady-state with/out green or blue-ray repumper
2. Blue MOT for a few seconds, then shine irradiate green or blue-ray repumper watching the rise time (should be quasi instantaneous) and the final fluorescence level (might be larger for the green repumper)

According to http://physics.nist.gov/cgi-bin/ASD/lines1.pl the intensity of the repumper lines at 497nm and 403 nm is 120 and 160, respectively. I expect that the linewidths should scale in a similar way.

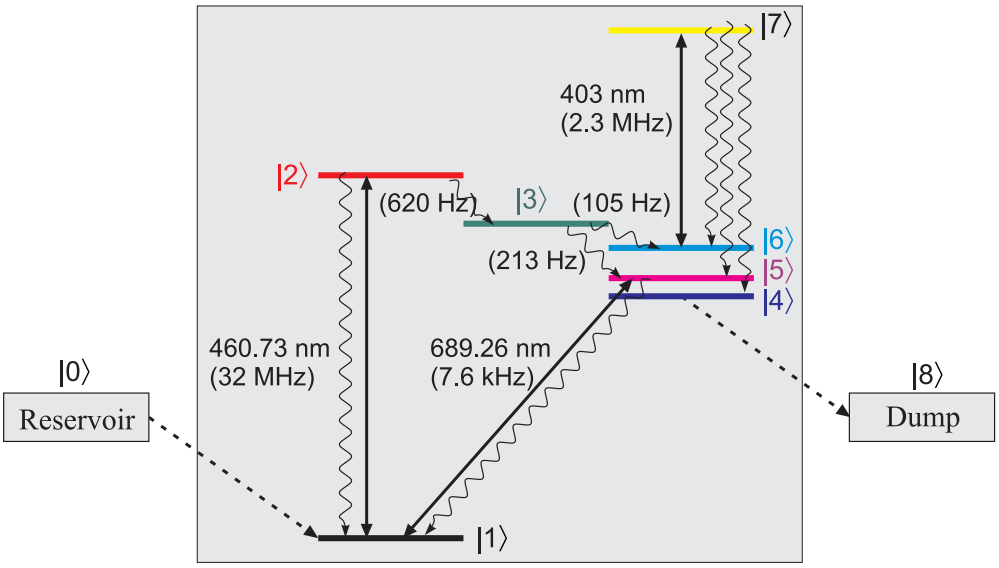

Figure 51: (code) Repumping scheme with a leak. The colors correspond to the colors of the simulations below.

0.89 30.05.2016 Spontaneous emission inhibition

It is possible to inhibit spontaneous emission by a series of short pulses. However, the pulse duration must be shorter than the inverse level spacing. On the other, putting the atom inside a cavity The hamiltonian (not Jaynes-Cummings) for a two-level atom in a cavity with periodic dispersive phase shift of the upper state is

$$\hat{H} = \hbar\omega_0\hat{\sigma}^+\hat{\sigma}^- + \Omega\hat{\sigma}^- + \Omega\hat{\sigma}^+ \ . \tag{74}$$

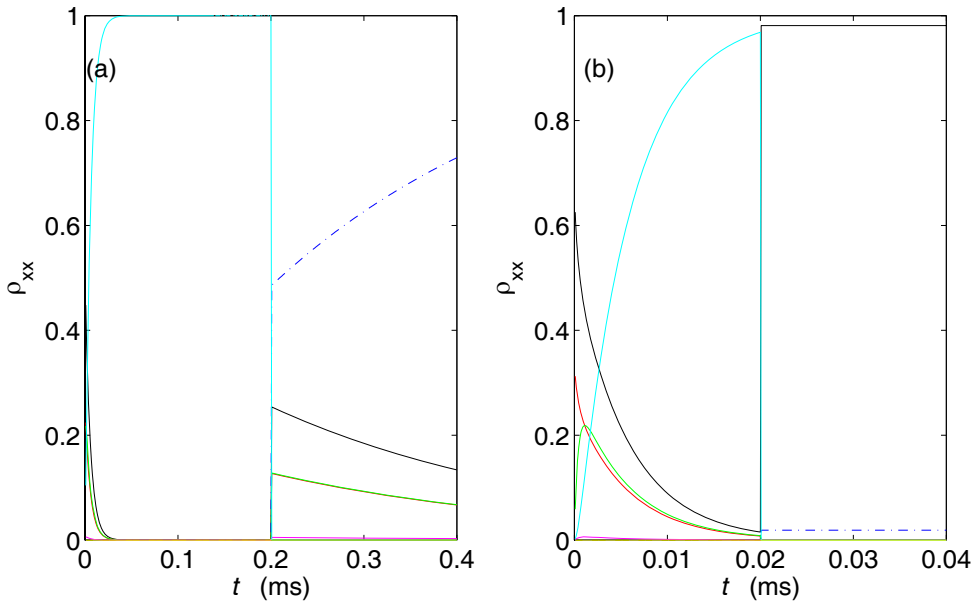

Figure 52: (code) Repumping with a leak. (a) In the first phase only the blue MOT is irradiated, in the second phase the blue MOT and the blue-ray repumper. (b) In the first phase only the blue MOT is irradiated, in the second phase only the blue-ray repumper.

0.90 03.08.2016 Switching on and off Sr1

0.90.1 Switch-on sequence

1. Verify vacuum pressures:

oven chamber	1.8 10^{-8} mbar
science chamber	4.1 10^{-10} mbar
reference cavity	4.0 10^{-7} mbar
Sr-cell	6.8 10^{-1} mbar

2. Turn on chiller, verify green light and water flux, let precool for 10 minutes
3. Verify currents for Sr-oven (1.7 A) and μ-tubes (2.5 A) with inductive Ampèremeter
4. Open gate valve
5. Set Zeeman slower coil current drive from analog to digital at 38 A
6. Set MOT coils current drives both to 29 A
7. Switch-on blue MOT laser (325.2516 nm and ... mW at output) and lock the doubling cavity
8. Activate DigiLock
9. Switch-on green repumper (300.1700 nm ... mW at output), lock the doubling cavity, and adjust frequency optimizing MOT fluorescence
10. Adjust blue MOT spectroscopy AOM optimizing MOT fluorescence
11. Realign efficiency of Zeeman slower AOM and correct the slower alignment
12. Verify 35 mW before the blue MOT AOM
13. Switch-on red MOT laser
14. Switch on LabView, run Sr1-Totalmanualcontrol-v0

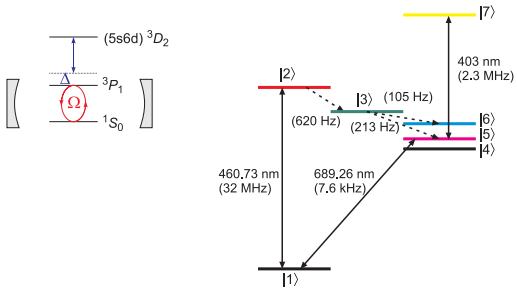

Figure 53: (code) Principle.

15. Calibration data are stored on L:/
16. To start an experimental sequence run L:/Sr1/MainProgram/Sr_v0p0.vi

0.90.2 Switch-off sequence

1. Turn off DigiLock (unlock, scan, unconnect)
2. Unlock doubling cavities of blue MOT laser and repumper and switch-off the respective lasers
3. Unlock red MOT PDH and switch-off the respective laser
4. Set Zeeman slower coil current drive from digital to analog
5. Close gate valve
6. Over week-ends turn down currents for Sr-oven (0.7 A) and μ-tubes (1.2 A) with inductive Ampèremeter
7. Turn off chiller, verify green light to be off

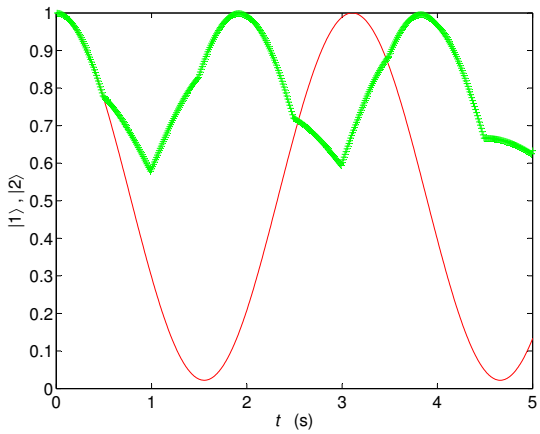

Figure 54: (code) Inhibit of transitions by applying short pulses on a connected strong transition.

0.91 03.09.2016 MOT switching problems

Checking the idea of operating the blue MOT ($N_b = 200$) and the red MOT with a separate coils. Simulations show that for the red MOT coils $N_r = 25$ windings on a single-layer solenoid with $R_r = 9.7$ cm radius, inserted into the center of the blue MOT coils, and beginning at $A_z = 5.5$ cm axial distance from the trap center and extending, outwards are enough to produce a 4 G/cm gradient with $I_r = 12$ A. First we estimate the voltage induced in the red coil when the blue MOT is switched off in $\tau = 100$ μs: The field produced by the blue MOT coil is

$$B = \frac{\mu_0 I_b}{2\pi R_b} N_b \approx 150 \text{ G} .$$

It produces a flux through the red MOT coil

$$\phi = BA_r = \frac{\mu_0 I_b}{2\pi R_b} N_b N_r \pi R_r .$$

Switching off this flux linearly in a time interval τ like $I = I_{b0}(1 - t/\tau)$ induces a voltage

$$U_i = -\dot{\Phi} = -\frac{\mu_0 I_{b0}}{2\tau}\frac{N_b N_r R_r}{R_b} \ .$$

With $N_b = 200$, $N_r = 15$, $I_{b0} = 30$ A, and simplifying $R_r \simeq R_b$, we get

$$U_i = -\frac{\mu_0 I_{b0}}{2\tau}\frac{N_b N_r R_r}{R_b} \approx 565 \text{ V} \ .$$

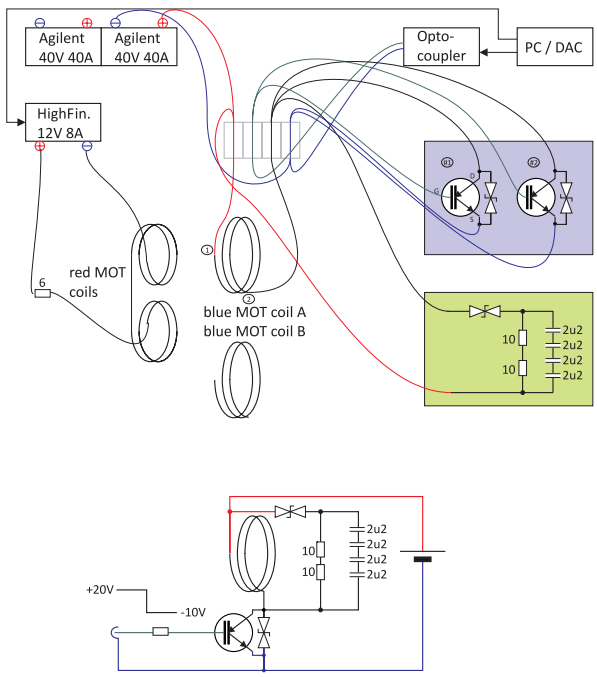

Figure 55: (code) Controlling blue and red MOT magnetic fields without homemade PID servo.

In the past, we tried many circuits for the rapid magnetic field switching, including PID-controled MOSFETs and various protection components, such as diodes, Zener diodes, varistors and Transils. Without success: Either the MOSFETs burned or overheated, or we observed huge spikes, noise, and transient oscillations. The problem is that (1) we want switch the magnetic field to finite non-zero values, and (2) the inductance is huge ($L = 10$ mH). I decide to use 2 separare coils for generating the fields for the blue and red MOT. Both fields will only be switched on and off completely, thus avoiding operation of the MOSFETs and at intermediate settings, where they are particularly stressed. A coil that I made (20 windings, $L = 200$ μH, $r = 4$ cm) could be switched off in 100 μs. Paulo made new coils that he placed directly on the flanges of the viewport. Those needed 3 mH, which shows the huge impact of eddy currents when the metal is very close to the coils.

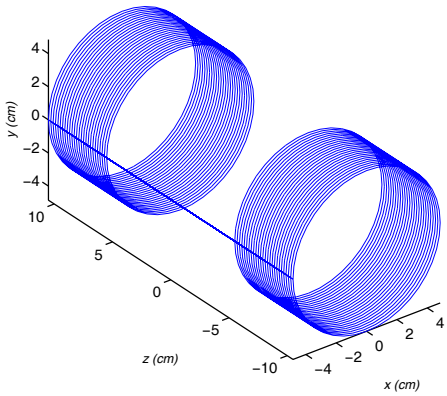

Figure 56: (code) Red MOT layout.

There was the idea to shield the magnetic field from the flanges with a *μ-metal* layer inserted between the coil and the flange hoping that this would not impact the magnetic field in the center of the coil. However, some tests we did showed that the μ-metal (even when isolated from the flange and not forming a closed loop) drastically reduces the magnetic field, while it has almost no impact on the switching speed.

0.92 22.08.2018 Transfer cavity for the repumper

We study the impact of a mode hop for a transfer cavity of $\delta_{fsr} = 1.5$ GHz changing its free spectral range from δ_{fsr} to $\tilde{\delta}_{fsr}$,

$$\nu_{ref} = N_{ref}\delta_{fsr} = (N_{ref} - 1)\tilde{\delta}_{fsr} \ .$$

If, before the mode hop, we had for the repumper frequency,

$$\nu_{rep} = N_{rep}\delta_{fsr} \ ,$$

after the hop we'll have,

$$\tilde{\nu}_{rep} = (N_{rep} - 1)\tilde{\delta}_{fsr} = \frac{N_{rep} - 1}{N_{ref} - 1}\nu_{ref} = \frac{\nu_{rep} - \delta_{fsr}}{\nu_{ref} - \delta_{fsr}}\nu_{ref} \ ,$$

such that,

$$\nu_{rep} - \tilde{\nu}_{rep} = \nu_{rep} - \frac{\nu_{rep} - \delta_{fsr}}{\nu_{ref} - \delta_{fsr}}\nu_{ref} \ .$$

For $\nu_{ref} = c/461$ nm and $\nu_{rep} = 497$ nm we expect $\nu_{rep} - \tilde{\nu}_{rep} = 109$ MHz. For $\nu_{ref} = c/689$ nm and $\nu_{ref} = 707$ nm we expect $\nu_{rep} - \tilde{\nu}_{rep} = 38$ MHz. For $\nu_{ref} = c/689$nm and $\nu_{ref} = 679$ nm we expect $\nu_{rep} - \tilde{\nu}_{rep} = 22$ MHz.

0.93 04.09.2018 Reflection from 2D-lattices

Shahmoon et al. [100] propose a 2D-lattice of atoms that act as mirror via cooperative scattering. The idea is closely linked to our 1D-photonic band gap papers [94, 93]!

Like in our work, [100] assumes frozen atoms (no external degrees of freedom considered), hence elastic scattering (no recoil shift). Is this realistic considering strong confinement (Lamb-Dicke regime)? The optical lattice beams are neglected (no light-shift).

Can the idea be tested with 3D-lattices? The lattice constant should be $a < \lambda$. We could make a lattice constant $a = 1064/2$ nm $= 532$ nm and probing with 689 nm $=$ 532 nm/0.772. Can Romain do some calculations?

0.94 10.09.2018 Pablo Saldanhas negative force proposal

Just upfront some parameters estimations:

In the Tübingen experiment we have typically $N = 100000$ and for ^{87}Rb, we get $g = \frac{4\pi\hbar^2}{m} a_s \approx 5.6 \cdot 10^{-51}$ with the scattering length $a_s = 110 a_B$. The trap frequency is typically $\omega = (2\pi)100$ Hz, such that

$$\mu = \left(\frac{15Ng}{8\pi}\right)^{2/5} \left(\frac{m\omega^2}{2}\right)^{3/5} \approx h \cdot 1.8 \text{ kHz}$$

can be calculated, as well as

$$D = \sqrt{\frac{2\mu}{m\omega^2}} \approx 6.5 \ \mu m$$

such that

$$\phi(\mathbf{r}) = \sqrt{\frac{\mu}{g} - \frac{m\omega^2 x^2}{2g}} = \sqrt{\frac{\mu}{g}\left(1 - \frac{x^2}{D^2}\right)} \ .$$

Gradients of $\nabla B = 50$ G/cm can easily be realized and switched quickly. Since the experiment has to be done after the trapping potential has been switched off, everything needs to go fast. If possible within 1 ms. Within $\Delta t = 100$ μs the gradient can generate a momentum change of

$$\Delta p = F\Delta t = \mu_B \nabla B \Delta t = \hbar \Delta k = \frac{\hbar}{D} \cdot 28 \ ,$$

which should be plenty.

0.95 17.01.2019 2D optical lattice

The atomic cloud has been transferred to a crossed beam dipole trap. What optical lattices could be interesting? Let's study a 2D optical lattice made of two identical retroreflected beams along the x and y-directions,

$$\begin{aligned}
U(\mathbf{r},t) &= \frac{3\pi c^2}{2\omega_0^3}\frac{\Gamma}{\Delta}I(\mathbf{r}) \\
&= \frac{3\pi c^2}{2\omega_0^3}\frac{\Gamma}{\Delta}\frac{2P}{\pi w_0^2}\left[e^{(-2x^2-2z^2)/w_0^2}e^{-y^2/y_R^2}(e^{iky}+e^{-iky})^2 + e^{(-2y^2-2z^2)/w_0^2}e^{-x^2/x_R^2}(e^{ikx}+e^{-ikx})\right. \\
&\simeq \frac{3\pi c^2}{2\omega_0^3}\frac{\Gamma}{\Delta}\frac{2P}{\pi w_0^2}8\left(1-\frac{k^2x^2}{2}-\frac{k^2y^2}{2}-\frac{x^2}{w_0^2}-\frac{y^2}{w_0^2}-\frac{x^2}{x_R^2}-\frac{y^2}{y_R^2}-\frac{2z^2}{w_0^2}\right) \\
&\simeq U_0\left(1-\frac{k^2x^2}{2}-\frac{k^2y^2}{2}-\frac{2z^2}{w_0^2}\right) .
\end{aligned}$$

We have $\lambda = 1064$ nm and only consider the strong resonance at 461 nm, whose linewidth is $\Gamma = (2\pi)$ 30.5 MHz. We assume $w_0 = 10$ μm and $P = 1$ W per beam. Then,

$$U_0 = \frac{12\pi c^2}{\omega_0^3}\frac{\Gamma}{\Delta}\frac{2P}{\pi w_0^2} \approx 3.2\cdot 10^{-25}\ \text{J} = k_B\cdot 20\ \text{mK} = h\cdot 484\ \text{MHz} .$$

The trap frequencies are

$$\omega_z = \frac{2}{w_0}\sqrt{\frac{U_0}{m}} \approx (2\pi)58\ \text{kHz} \quad , \quad \omega_x = \omega_y = k\sqrt{\frac{U_0}{m}} \approx (2\pi)1.4\ \text{MHz} .$$

That means we are in the well-resolved sideband limit with respect to every direction of space,

$$\Gamma_{689} = (2\pi)\ 7.6\ \text{kHz} \quad , \quad \omega_{rec} = \frac{\hbar k_{689}^2}{2m} = (2\pi)\ 4.7\ \text{kHz} .$$

If the beams are not identical and not even elliptical,

$$\begin{aligned}
U(\mathbf{r},t) &= \frac{3\pi c^2}{2\omega_0^3}\frac{\Gamma}{\Delta}4\left[\frac{2P_y}{\pi w_{yz}w_{yx}}e^{-2z^2/w_{yz}^2}e^{-2x^2/w_{yx}^2}e^{-y^2/y_R^2}\cos^2 ky + \frac{2P_x}{\pi w_{xz}w_{xy}}e^{-2z^2/w_{xz}^2}e^{-2y^2/w_{xy}^2}e^{-x}\right. \\
&\simeq \frac{3\pi c^2}{2\omega_0^3}\frac{\Gamma}{\Delta}4\left[\frac{2P_y}{\pi w_{yz}w_{yx}}\left(1-\frac{2z^2}{w_{yz}^2}-\frac{2x^2}{w_{yx}^2}-\frac{y^2}{y_R^2}-k^2y^2\right)+\frac{2P_x}{\pi w_{xz}w_{xy}}\left(1-\frac{2z^2}{w_{xz}^2}-\frac{2y^2}{w_{xy}^2}-\frac{x^2}{x_R^2}\right.\right. \\
&\simeq U_0\left(1-\zeta_x\frac{2z^2}{w_{xz}^2}-\zeta_y\frac{2z^2}{w_{yz}^2}-\zeta_x k^2x^2-\zeta_y k^2y^2\right) ,
\end{aligned}$$

where,

$$U_0 \equiv \frac{3\pi c^2}{2\omega_0^3}\frac{\Gamma}{\Delta}4\left(\frac{2P_x}{\pi w_{xz}w_{xy}}+\frac{2P_y}{\pi w_{yz}w_{yx}}\right) \quad , \quad \zeta_x \equiv \frac{P_x w_{yz}w_{yx}}{P_x w_{yz}w_{yx}+P_y w_{xz}w_{xy}} \equiv 1-\zeta_y .$$

The trap frequencies are now,

$$\omega_x = k\sqrt{\frac{2U_0\zeta_x}{m}} \quad , \quad \omega_y = k\sqrt{\frac{2U_0\zeta_y}{m}} \quad , \quad \omega_z = 2\sqrt{\frac{U_0}{m}\left(\frac{\zeta_x}{w_{xz}^2} + \frac{\zeta_y}{w_{yz}^2}\right)} \, .$$

One can verify that the old formulae are recovered for $P_x = P_y$ and $w_{xz} = w_{xy} = w_{yz} = w_{yx}$.

0.96 18.01.2019 2D optical dipole trap

A similar calculation for a running wave dipole trap with the same geometry as in the last section:

$$
\begin{aligned}
U(\mathbf{r},t) &= \frac{3\pi c^2}{2\omega_0^3}\frac{\Gamma}{\Delta}I(\mathbf{r}) \\
&= \frac{3\pi c^2}{2\omega_0^3}\frac{\Gamma}{\Delta}\left(\frac{2P_y}{\pi w_{yz}w_{yx}}e^{-2z^2/w_{yz}^2}e^{-2x^2/w_{yx}^2}e^{-y^2/y_R^2}+\frac{2P_x}{\pi w_{xz}w_{xy}}e^{-2z^2/w_{xz}^2}e^{-2y^2/w_{xy}^2}e^{-x^2/x_R^2}\right) \\
&= \frac{3\pi c^2}{2\omega_0^3}\frac{\Gamma}{\Delta}\left[\frac{2P_y}{\pi w_{yz}w_{yx}}\left(1-\frac{2x^2}{w_{yx}^2}-\frac{2z^2}{w_{yz}^2}-\frac{y^2}{y_R^2}\right)+\frac{2P_x}{\pi w_{xz}w_{xy}}\left(1-\frac{2y^2}{w_{xy}^2}-\frac{2z^2}{w_{xz}^2}-\frac{x^2}{x_R^2}\right)\right] \\
&\simeq U_0\left(1-\zeta_x\frac{2x^2}{w_{yx}^2}-\zeta_y\frac{2y^2}{w_{xy}^2}-\zeta_x\frac{2z^2}{w_{xz}^2}-\zeta_y\frac{2z^2}{w_{yz}^2}\right) ,
\end{aligned}
$$

where,

$$
U_0 \equiv \frac{3\pi c^2}{2\omega_0^3}\frac{\Gamma}{\Delta}\left(\frac{2P_y}{\pi w_{yz}w_{yx}}+\frac{2P_x}{\pi w_{xz}w_{xy}}\right) \quad , \quad \zeta_x \equiv \frac{P_x w_{yz}w_{yx}}{P_x w_{yz}w_{yx}+P_y w_{xz}w_{xy}} = 1-\zeta_y .
$$

The trap frequencies are now,

$$
\omega_x = \frac{2}{w_{yx}}\sqrt{\frac{U_0\zeta_x}{m}} \quad , \quad \omega_y = \frac{2}{w_{xy}}\sqrt{\frac{U_0\zeta_y}{m}} \quad , \quad \omega_z = 2\sqrt{\frac{U_0}{m}\left(\frac{\zeta_x}{w_{xz}^2}+\frac{\zeta_y}{w_{yz}^2}\right)} .
$$

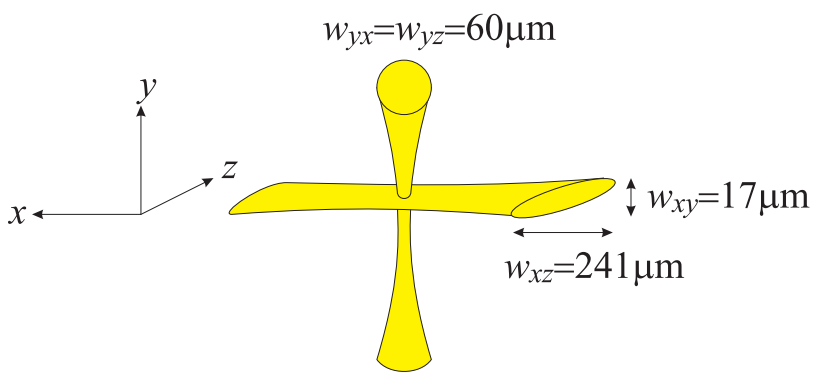

Figure 57: (code) .

With $P_x = P_y = 3$ W and the waists indicated in Fig. 57, one expects,

$$
\omega_x \approx (2\pi)\ 753\ \text{Hz} \quad , \quad \omega_y \approx (2\pi)\ 2836\ \text{Hz} \quad , \quad \omega_z \approx (2\pi)\ 825\ \text{Hz} .
$$

0.97 06.02.2019 SWAP MOT

Can the SWAP MOT idea be used to improve the transfer to an optical dipole trap [76], [74]?

Katori shows [54] that the $^1S_0$-state and the three $^3P_1$-states are Stark-shifted by different amounts depending on the wavelength of the (linearly polarized) optical dipole light. Around 822 nm they are equal (magical wavelength). The shifts of the $^3P_1$-states are different for linearly polarized light driving $\Delta m = 0$ transitions, linearly polarized light driving $\Delta m = \pm 1$ transitions, and circularly polarized light driving $\Delta m = \pm 1$ transitions. However, at 1064 nm the shifts of the $^3P_1$-states are negligibly small compared to the shift of the $^1S_0$-state.

0.98 21.03.2019 Critical temperature

Let us assume a cloud of $N = 500000$ ultracold ^{88}Sr atoms in a trap characterized by the harmonic trapping frequencies $\omega r, r, z/2\pi = 300, 300, 800$ Hz. We measure a temperature of $T = 800$ nK. What are the features of this cloud?

The critical temperature is given by,

$$k_B T = \frac{N^{1/3}}{1.202}\hbar\bar{\omega} \approx k_B \cdot 1.3\ \mu\text{K} \ .$$

Ultracold ^{88}Sr density for the case of a Gaussian shape,

$$n_0 = \frac{N}{(2\pi)^{3/2}\bar{x}\bar{y}\bar{z}} \simeq 2.2 \cdot 10^{17}\ \text{cm}^{-3} \ .$$

The collision rate is,

$$\gamma_{cll} = \bar{v} n_0 \sigma = \sqrt{\frac{k_B T}{m}}\ n_0\ 4\pi a_s^2 \approx 343\ \text{s}^{-1} \ .$$

If the cloud were condensed, we would expect in the Thomas-Fermi limit,

$$|\psi(\mathbf{r})|^2 = \frac{\mu - V_{trp}(\mathbf{r})}{g} \ .$$

The chemical potential follows from the normalization condition,

$$N = \int_{n(\mathbf{r})>0} n(\mathbf{r}) d^3\mathbf{r} \ .$$

In the case of an ellipsoidal harmonic oscillator, $V_{trp}(r,z) = \frac{m}{2}(\omega_r^2 r^2 + \omega_z^2 z^2)$, the chemical potential is,

$$\mu = \left(\frac{15Ng}{8\pi}\right)^{2/5} \left(\frac{m}{2}(\omega_r^2\omega_z)^{2/3}\right)^{3/5} \approx \hbar \cdot 61\ \text{kHz} \ ,$$

where $g \equiv 4\pi\hbar^2 a_s/m$. The peak density is,

$$n_0 = |\psi(0)|^2 = \frac{\mu}{g} \approx 6.3 \cdot 10^{16}\ \text{cm}^{-3} \ .$$

The radial size σ of the condensate follows from $n(r_{hw}, 0) = \frac{n(0,0)}{2}$,

$$r_{hw} = \sqrt{\frac{\mu}{m\omega_r^2}} \ .$$

For a thermal cloud influenced by quantum statistics,

Calculate cloud shape (Thomas-Fermi) for $a_s = -2a_B$!

However, the maximum number of atoms imposed by the negative scattering length $a_s = -2a_B$ is, for the same conditions [90, 28],

$$N_{max} = 0.575\frac{a_{trp}}{|a_s|} \simeq 2856 \ ,$$

with $a_{trp} = \sqrt{\hbar/m/\bar{\omega}_{trp}}$.

Trap depth,

$$U_0 = ???$$

In case of evaporation the equilibrium temperature would be roughly $U_0/5$.

Interference of two beams crossing under right angle,

$$\mathbf{E}_v(\mathbf{r},t)+\mathbf{E}_h(\mathbf{r},t) = \begin{pmatrix} \alpha_v \\ \beta_v e^{i\phi_v} \\ 0 \end{pmatrix} E_0 e^{i(kz-\omega t)} + \begin{pmatrix} \alpha_h \\ 0 \\ \beta_h e^{i\phi_h} \end{pmatrix} E_0 e^{i(ky-\omega t)} = \begin{pmatrix} \alpha_v e^{ikz} + \alpha_h e^{iky} \\ \beta_v e^{i\phi_v} e^{ikz} \\ \beta_h e^{i\phi_h} e^{iky} E_0 e^{-i\omega t} \end{pmatrix}$$

For example, $\alpha_h = 0$, $\beta_h e^{i\phi_h} = 1$, $\alpha_v = 1$, $\beta_v = 1$,

$$\mathbf{E}_v(\mathbf{r},t) + \mathbf{E}_h(\mathbf{r},t) = \begin{pmatrix} e^{ikz} \\ e^{i\phi_v} e^{ikz} \\ e^{iky} \end{pmatrix} E_0 e^{-i\omega t}$$

For example, $\alpha_h = 1$, $\beta_h e^{i\phi_h} = 0$, $\alpha_v = 1$, $\beta_v = 1$,

$$\mathbf{E}_v(\mathbf{r},t) + \mathbf{E}_h(\mathbf{r},t) = \begin{pmatrix} e^{ikz} + e^{iky} \\ e^{i\phi_v} e^{ikz} \\ 0 \end{pmatrix} E_0 e^{-i\omega t}$$

0.99 25.04.2019 Three-body collisions

Between ground and excited states *fine changing collision*s and *radiative escape* are possible. Between two ground states only *hyperfine changing collision*s may occur.

The nature of the collision process, whether it is a one- [1], two-, or three-body collision, reveals itself via the temporal behavior of trap losses. Using the abbreviation,

$$\langle \eta \rangle \equiv \frac{1}{N} \int \eta(\mathbf{r}) n(\mathbf{r}) d^3 r \ , \tag{75}$$

we can write the loss rates due to inelastic one-, two-, and three-body collisions,

$$B\langle 1 \rangle N \quad , \quad K\langle n \rangle N \quad , \quad L\langle n^2 \rangle N \ . \tag{76}$$

the prefactors depend on the collision velocity (that is, the temperature of the sample) and atomic parameters (for example, the collision cross section for two-body collisions, which may itself depend on temperature). Hence, the total number of trapped atoms evolves according to,

$$\boxed{\dot{N} = -B\langle 1 \rangle N - K\langle n \rangle N - L\langle n^2 \rangle N} \ . \tag{77}$$

Assuming a gaussian density distribution,

$$n(\mathbf{r}) = \frac{N}{(2\pi)^{3/2}\bar{r}^3} e^{-r^2/2\bar{r}^2} \ , \tag{78}$$

we calculate,

$$\dot{N} = -BN - B_K N^2 - B_L N^3 \quad \text{with} \quad B_K \equiv \frac{K}{(4\pi)^{3/2}\bar{r}^3} \quad \text{and} \quad B_L \equiv \frac{L}{3^{3/2}(2\pi)^3\bar{r}^6} N^3 \ . \tag{79}$$

Fig. 58 shows a simulation of Eq. (79).

For condensates in the Thomas-Fermi limit [103] found the following differential equations for two- and three-body collisions,

$$\frac{\dot{N}}{N} = -Gc_2 N^{2/5} - \frac{1}{\tau} \quad \text{and} \quad \frac{\dot{N}}{N} = -Lc_3 N^{4/5} - \frac{1}{\tau} \ . \tag{80}$$

[1] By one-body collision we mean collisions with atoms of the background gas.

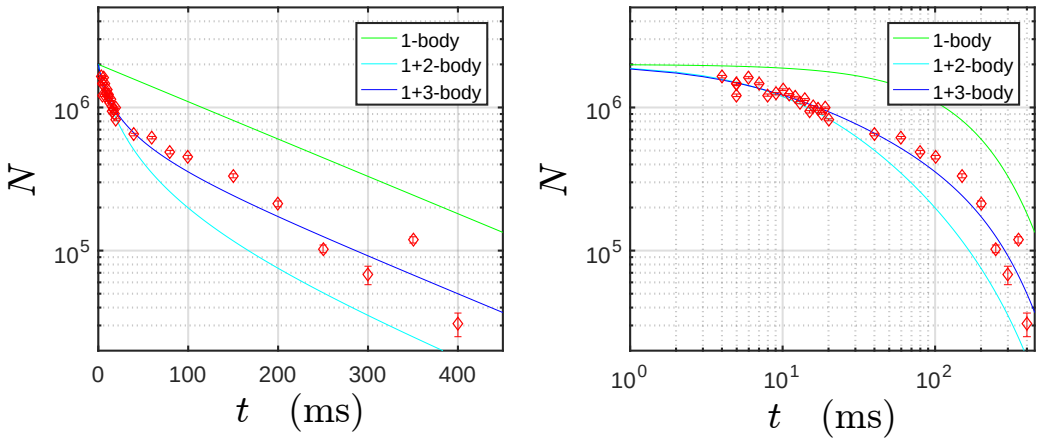

atom number $N = 2000000$

radial trap frequency $w_{rd} = (2\pi)\ 300$ Hz

axial trap frequency $w_{ax} = (2\pi)\ 200$ Hz

peak density $n_0 = 620 \cdot 10^{12}$ cm^{-3}

temperature $T = 1\ \mu$K

critical temperature $T_c = 1.3\ \mu$K

collision rate $\gamma_{coll} = 0.84$ s^{-1}

maximum condensed atom number $N_{max} = 32000$

Figure 58: (code) Measured decay rate of the ODT. The fits are done assuming 1 and 3-body decay with $N_0 = 3.2 \cdot 10^6$, $B = 4$ s^{-1} and $B_L = 3 \cdot 10^{-11}$ s^{-1}.

0.100 25.04.2019 Cooperative forces on dipole-trapped strontium clouds

How about redoing Hellmar's collective force experiments [Bender10]?

At 1 μK temperature the Doppler width with respect to the transition is about 12 μK.

0.101 29.08.2019 blue MOT mCBS

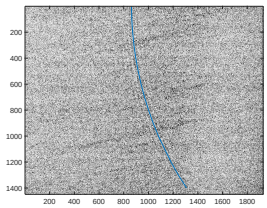

Figure 59: (code)

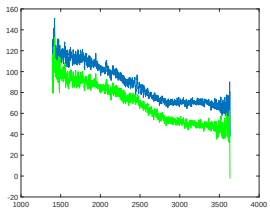

Figure 60: (code)

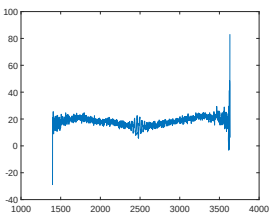

Figure 61: (code)

0.102 18.08.2020 Beam propagation through funnel or waveguide

For comparison with the coupled dipole model calculations done by Marcia to check the Lambert-Beer law for a cloud of atoms arranged in cylinder. Fig. 62 shows a Fourier optics calculation of a beam propagation through a cylindrical waveguide. Fig. 63 shows that not only dispersive phase shifts, but also resonant absorption

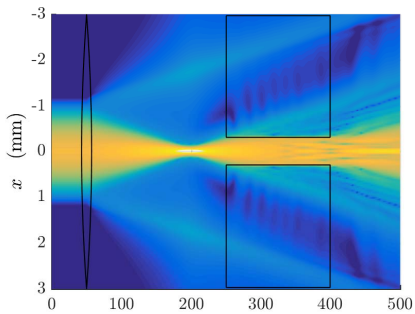

Figure 62: (code)

deforms a phase front.

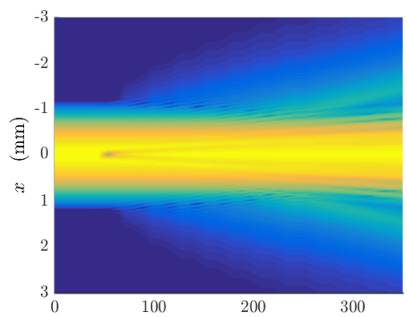

Figure 63: (code)

0.103 14.05.2024 Saturation in a slab of Sr atoms

A laser beam focused down to $w_0 \approx 3\,\mu\text{m}$ traverses an atomic cloud having the shape of a thin slab of thickness $L \approx 8\,\mu\text{m}$. The mode volume formed by the overlap region is then,

$$V_m = \frac{\pi}{2} L w_0^2 \approx 7 \times 1.1^{-16}\,\text{m}^3 \ . \tag{81}$$

One photon in that volume then generates a intensity of

$$I = \varepsilon_0 c \sqrt{\frac{\hbar\omega}{2\varepsilon_0 V_m}}^2 = c\frac{\hbar\omega}{2V_m} \approx 590000\,\text{W/m}^2 \approx 15000 I_{sat} \frac{1}{1+4\Delta^2/\Gamma^2} \tag{82}$$

with the saturation intensity $I_{sat} = 40.6\,\text{mW/cm}^2$.

On average, however, we will have less than one photon in the cloud. Considering the cloud as a cavity, the residence time of a photon in the mode volume will depend on the cavity's finesse. We first estimate the refraction index of the cloud from its density assumed as $n_0 \approx 10^{14}\,\text{cm}^{-3}$. The susceptibility is,

$$\chi = -\frac{\lambda_{461}^3 n_0}{2\pi^2(2\Delta/\Gamma + \imath)} \approx \frac{0.5}{2\Delta/\Gamma + \imath} \ . \tag{83}$$

That is, the real part of the refraction index describes a dispersive profile,

$$\mathfrak{Re}\,\eta_{cloud} = \sqrt{1+\chi} \simeq 1 + \mathfrak{Re}\,\tfrac{\chi}{2} = 1 - \frac{\lambda_{461}^3 n_0}{4\pi^2} \frac{1}{2\Delta/\Gamma + \Gamma/2\Delta} \tag{84}$$

with maximum amplitude,

$$|\mathfrak{Re}\,\eta_{cloud} - 1| < 0.25 \ . \tag{85}$$

The reflectivity of an interface with sudden change of the refraction index from 1 to η_{cloud} is according to the Fresnel formulas,

$$R = \left(\frac{1-\eta_{cloud}}{1+\eta_{cloud}}\right)^2 = 0.04 \ . \tag{86}$$

The finesse of the cavity is then at most,

$$F = \frac{\pi\sqrt{R}}{1-R} \approx 0.65 \ . \tag{87}$$

The free spectral range is,

$$\delta_{fsr} = \frac{c}{2L} \approx 3\,\text{THz} \ . \tag{88}$$

The cavity intensity decay rate is,

$$\kappa_{int} = \frac{2\pi\delta_{fsr}}{F} \approx 2 \times 10^{13}\,\text{s}^{-1} \ . \tag{89}$$

In a time $\Delta t = \kappa_{int}^{-1}$ a photon can perform

$$\frac{c\Delta t}{L} \approx 0.3 \tag{90}$$

round trips. That is, the intensity enhancement factor is 0.3, which means that the light is still strongly saturating the cavity.

The number of photon really entering the cavity depends, of course, on the pump power. For a very low pump power of $P_{input} = 140\,\mathrm{pW}$, we expect inside the cavity a power of,

$$P_{cav} = \frac{F}{\pi} P_{input} \tag{91}$$

corresponding to a photon number of

$$n_{cav} = \frac{P_{cav}}{\hbar\omega\delta_{fsr}} = \frac{2P_{input}}{\hbar\omega\kappa_{int}} \approx 3.7 \times 10^{-5} \ , \tag{92}$$

which in turn yields an intracavity intensity of,

$$n_{cav} I \approx 0.54 I_{sat} \ . \tag{93}$$

A Gaussian density profile will further reduce the finesse of the cavity. On the other hand, the intensity is not expected to be uniform within the slab.

0.104 24.10.2024 Ground state Hanle effect

In collaboration with Mayerlin we start to develop a model for describing the ground state Hanle effect in ^{133}Cs, $I = \frac{7}{2}$. The system is room temperature gas cell, the signals are obtained via pump-probe saturation spectroscopy.

Restricting to closed transitions we need only consider Zeeman structure of $F = 3, 4$ and $F' = 3, 4$ for the D1 line and $F' = 2, 3, 4, 5$ for the D2 line. That is we have between $(2F + 1)(2F' + 1) = 6$ and 20 levels.

Chapter 1

Strontium cavities

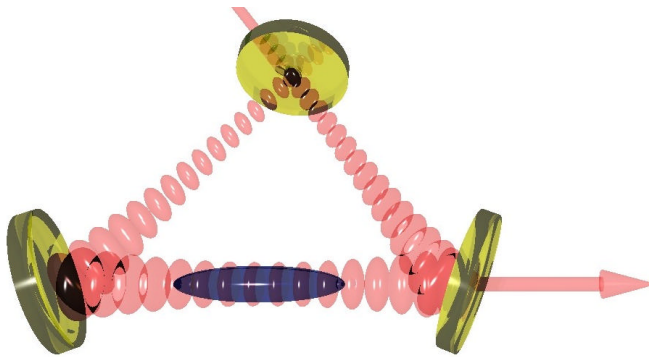

1.1 01.04.2013 Characterizing the ring cavity

The cavity detuning is mostly close to resonance $|\Delta_c| \ll 2\pi\delta_{fsr}$, where

$$\delta_{fsr} \equiv \tau_c^{-1} = \frac{c}{L}$$

is the cavity's *free spectral range* (given in real frequency units). Assuming a $L = 10\,\text{cm}$ round trip length, we have $\delta_{fsr} = 3\,\text{GHz}$. τ_c is the round trip time. Assuming a finesse of $F = 2000$ for s-polarization of the long ring cavity, the *cavity field decay rate*,

$$\kappa = \tau_\kappa^{-1} = \frac{\pi\delta_{fsr}}{F}$$

is $\kappa \simeq (2\pi)\ 750\,\text{kHz}$. The *intensity decay rate* measured by cavity ring-down would be 2κ. Note that κ is also the HWHM of the *intensity transmission* curve.

For the ^{88}Sr $^1S_0 -^3 P_1$ intercombination line at $\lambda = 689\,\text{nm}$ we have the natural linewidth $\Gamma = 2\pi \times 7.6\,\text{kHz}$. The *dipole moment* is

$$d = \sqrt{\frac{3\pi\varepsilon_0\hbar\Gamma}{k^3}}\ .$$

Question: Does it make sense to calculate a dipole moment for a transition, which is not a dipole transition?

For a given cavity, the intracavity power P fixes the intensity

$$I(\mathbf{r}) = \frac{2P}{\pi w^2(z)} e^{-2\rho^2/w^2(z)} \qquad \text{and} \qquad w(z) = w_0\sqrt{1 + \left(\frac{\lambda z}{\pi w_0^2}\right)^2}\ .$$

We define the **mode volume** via $I(0)V_m \equiv \int I(\mathbf{r})dV$. Evaluation of the integral over the Gaussian mode over the length L of the cavity yields

$$V_m = \frac{\pi}{4} L w_0^2\ .$$

Assuming waists of the mode of $w_x = w_y = 50\,\mu\text{m}$, the ring cavity mode volume is $V_m \approx 50\,\mu\text{m} \times 50\,\mu\text{m} \times 10\,\text{cm} \approx 0.2\,\text{mm}^3$.

1.1.1 Calculating the coupling strength

If we fix the *one-photon field amplitude* via

$$I(\mathbf{r}) = n\varepsilon_0 c \mathcal{E}_1^2(\mathbf{r})\ ,$$

where n is the number of photons in the cavity, the energy stored in the cavity is

$$\int \varepsilon_0 |\mathcal{E}_1(\mathbf{r})|^2 dV = \varepsilon_0 \int \frac{I(\mathbf{r})}{n\varepsilon_0 c} \rho d\rho d\phi dz = \frac{1}{nc}\int \frac{2P}{\pi w^2(z)} e^{-2\rho^2/w^2(z)} \rho d\rho d\phi dz = \frac{1}{nc}\frac{P}{2}L = \frac{1}{nc}\frac{n\hbar\omega\delta_{fsr}}{2}L$$

So

$$\mathcal{E}_1(0) = \sqrt{\frac{I(0)}{n\varepsilon_0 c}} = \sqrt{\frac{1}{n\varepsilon_0 c}\frac{2P}{\pi w_0^2}} = \sqrt{\frac{1}{n\varepsilon_0 c}\frac{Ln\hbar\omega\delta_{fsr}}{2V_m}} = \sqrt{\frac{\hbar\omega}{2\varepsilon_0 V_m}}\ .$$

We get $\mathcal{E}_1 \approx 9$ V/m.

The light power can now be expressed as

$$P = \frac{\pi w_0^2}{2} I(0) = \frac{2V_m}{L} n\varepsilon_0 c\mathcal{E}_1^2(0) = 2V_m \delta_{fsr} n\varepsilon_0 \frac{\hbar\omega}{2\varepsilon_0 V_m} = \delta_{fsr} n\hbar\omega \ .$$

To estimate the *cavity pumping rate* (how does it depend on phase matching?), we assume that the power P_{input} is measured in transmission. The coefficient η for resonant pumping of one propagation direction is related to the number n of photons inside the cavity

$$n = |\alpha|^2 = \frac{\eta^2}{\kappa^2} \ .$$

The intracavity field is resonantly enhanced by the finesse

$$\alpha = \frac{F}{\pi}\alpha_{input} = \frac{\delta_{fsr}}{\kappa}\alpha_{input} \ .$$

This yields $\eta = \kappa\alpha = \kappa\sqrt{I/c\hbar\omega \cdot V_m} = \delta_{fsr}\alpha_{input} = \delta_{fsr}\sqrt{I_{input}/c\hbar\omega \cdot V_m}$.

The *atom-field coupling constant* (which is HALF the single-photon Rabi frequency) is

$$g \equiv \frac{d\mathcal{E}_1(0)}{\hbar} = \sqrt{\frac{3\pi\Gamma\omega}{2k^3 V_m}} = \sqrt{\frac{3\Gamma\delta_{fsr}}{k^2 w^2}} \ .$$

$g \approx 2\pi \times 142$ kHz. Therefore the coupling strength is almost an order of magnitude larger than the cavity decay rate.

1.1.2 Cooperativity in cavities

The detuning of the atomic resonance from the laser frequency is typically $\Delta_a = 2\pi \times 1000\,\text{GHz}$ (2 nm). The single-atom reflection coefficient is

$$\beta_\Delta = \frac{k}{\pi w^2}\frac{|\operatorname{Re}\alpha|}{\varepsilon_0} = \frac{k}{\pi w^2}\frac{6\pi}{k^3}\left|\frac{\Gamma}{2\Delta_a + i\Gamma}\right| = \frac{6}{k^2 w^2}\left|\frac{\Gamma}{2\Delta_a + i\Gamma}\right| \ ,$$

where α is the complex atomic polarizability and $\Delta_a = \omega_{dip} - \omega_0$. The resonant reflection coefficient can be interpreted in terms of a phase shift which depends on the matching of the optical cross section $\sigma = 3\lambda^2/2\pi$ of the atom and the field mode cross section,

$$\beta_0 = \frac{\sigma_0}{\pi w^2} = \frac{6}{k^2 w^2} = \frac{2g^2}{\delta_{fsr}\Gamma} \ .$$

The frequency shift accumulated over one round trip $\delta_{fsr}\beta_0$ gets noticeable if it exceed the cavity linewidth κ. From this we get the single-pass optical depth of the atomic sample multiplied by the cavity finesse, which is a quantity known as the *cooperativity parameter* or *cavity-to-free space ratio*,

$$\eta \equiv \frac{\delta_{fsr}\beta_0}{\kappa} = \frac{F}{\pi}\frac{6}{k^2 w^2} = \frac{2g^2}{\kappa\Gamma} \ .$$

The atom sensitivity may be measured in terms of a critical atom number N_{crt}, which can be resolved by the system. It goes to infinity as the resonant single-atom reflection coefficient vanishes, $\beta_0 \to 0$, and converges to zero if $\beta_0 \to 1$:

$$N_{crt} = \frac{4\pi}{F\beta_0} = 4\pi\frac{k^2w^2}{6F} = 2\pi\frac{\Gamma\delta_{fsr}}{Fg^2} = \frac{2\kappa\Gamma}{g^2} = \frac{4}{\eta} \ .$$

The total reflection coefficient is enhanced by the number of atoms N and the number of round trip of a photon in a cavity F, which gives off resonance

$$NF\beta_\Delta \approx NF\frac{6}{k^2w^2}\frac{\Gamma}{2\Delta_a} = NF\frac{g^2}{\Delta_a}\frac{kV}{\omega\pi w^2} = NU_0\frac{L}{c}F = \frac{NU_0}{\kappa} \ ,$$

where we defined the single photon light-shift far-off resonance

$$U_0 \approx \frac{g^2}{\Delta_a}$$

and the single photon Rayleigh scattering rate

$$\gamma_0 \approx \frac{g^2\Gamma}{\Delta_a^2} \ .$$

1.1.3 Collective cooperativity

While the strong coupling regime of CQED requires $\eta > 1$ with a single atom, collective cooperativity is attained with N atoms if $N\eta > 1$ [15, 23]. Then the ensemble couples to the mode as a single "superatom" with a coupling strength increased to $g_N = g_1\sqrt{N}$. This can be seen easily by setting up the Jaynes-Cummings Hamiltonian for two atoms and a light mode and assuming indistinguishable which of the atoms is excited by going to Dicke states.

1.1.4 Saturation parameter in cavities

The optical single photon *saturation parameter* is given

$$s = \frac{g^2}{\Gamma^2}$$

Hence, the number of photons that drives the system to saturation is

$$n_{sat} = \frac{\Gamma^2}{2g^2} = \frac{\Gamma}{\delta_{fsr}}\frac{k^2w^2}{6} = \frac{1}{2s} \ .$$

We see that there is a ***symmetry between η and s, or between N_{crt} and n_{sat}. The regime $N\eta > 1$ denotes collective behavior of N atoms in the same way as $ns > 1$ means saturation***. While η only depends on the phase matching of the atomic antenna and the cavity, s also depends on the cavity mode volume and the natural decay rate.

1.2 02.04.2013 Intracavity metrology and gravimetry

Conventional frequency standards are based on a double servo loop. A laser oscillator is simultaneously locked to high finesse cavity, which provides good short term stability, and to a narrow atomic resonance, which provides good long term stability. The goal of our project is to study a new approach consisting in combining the servo loops by directly inserting the atoms in the cavity. This idea is the base for our CNPq project (english version) for the development of a gravitational sensor.

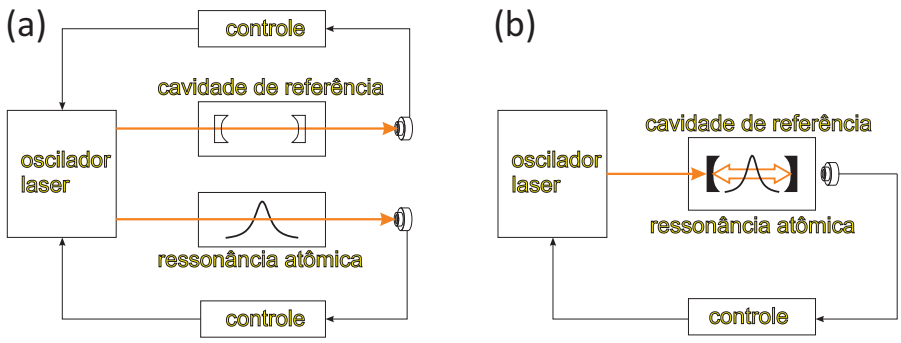

Figure 1.1: (code) Left: conventional concept. Right: New concept.

Possible starting point for theoretical investigations: [70, 78].

1.3 04.04.2013 Total setup

Vision of a complete setup aiming at cooling ^{84}Sr clouds to quantum degenerate temperatures inside a vertical optical ring cavity, letting the atoms perform Bloch oscillations in a 1D optical lattice generated by two intersecting laser beams at 1064 nm and observing the influence of the atomic acceleration on the ring cavity modes.

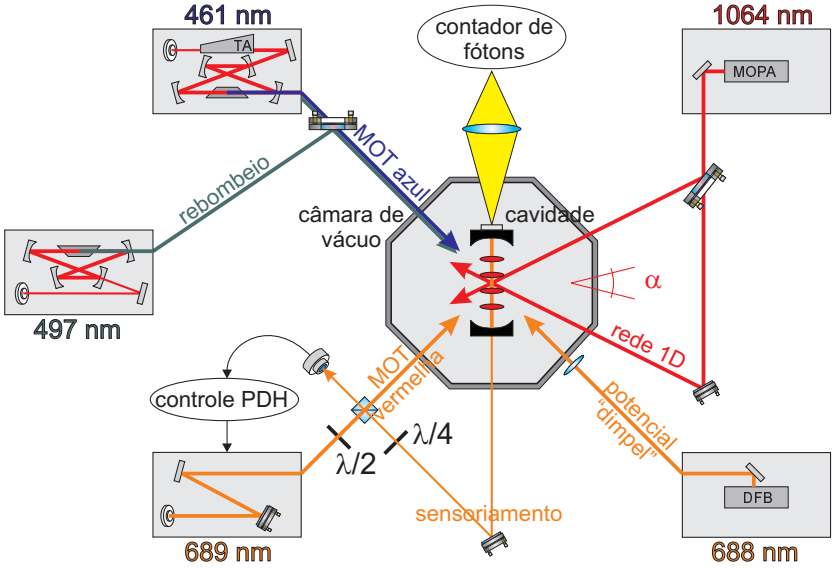

Figure 1.2: (code)

1.4 05.04.2013 Ring cavity laser setup at 689 nm

Exciting the narrow intercombination line of strontium atoms in free space requires, except for the light necessary to operate the red MOT, a *pump laser* beam ν_{pmp} whose frequency can be detuned precisely from the *atomic resonance* ν_{Sr}. If the atom-field interaction is to occur inside a cavity, the cavity mode must also be controlled. A possible scheme for this is shown in the figure:

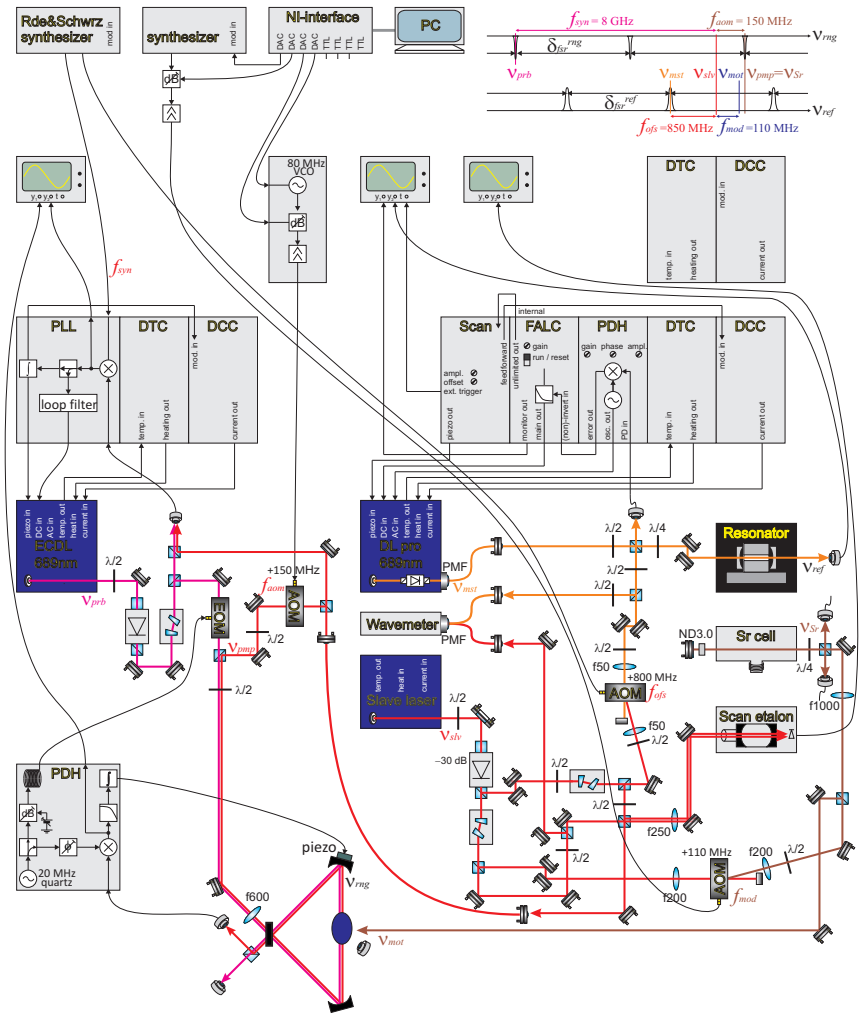

Figure 1.3: (code)

If we want to control the detuning of the laser which is pumping the ring cavity, we need a second independent *probe laser*, ν_{prb}, which is locked to a ring cavity mode and to which the *pump laser*, ν_{pmp}, is phase-locked with an offset frequency, f_{syn}. In order to prevent the probe laser from being too close to the atomic transition, ν_{Sr}, it is tuned close to another longitudinal mode of the ring cavity, distant by $2\delta_{rng}^{fsr}$ or $3\delta_{rng}^{fsr}$,

and this distant cavity mode is locked via a Pound-Drever-Hall servo controlling a piezo mounted to the ring cavity to the probe laser ν_{prb}. The pump laser ν_{pmp} and the original cavity mode are, in contrast, close to the atomic transition. In summary, we have:

$\nu_{mst} = \nu_{ref} = N_{ref}\delta_{ref}^{fsr}$	Pound-Drever-Hall to the stable reference cav
$\nu_{slv} = \nu_{mst} + f_{ofs}$	injection lock on a frequency-shifted laser bea
$\nu_{mot} = \nu_{slv} + f_{mod}$	control of the light for the red MOT
$\nu_{prb} = \nu_{slv} - f_{syn}$	PLL lock on a frequency-shifted laser beam
$\nu_{rng} = \nu_{prb} = N_{rng}\delta_{rng}^{fsr}$	Pound-Drever-Hall lock of the ring cavity
$\nu_{pmp} = \nu_{slv} + f_{aom}$	control of the light pumping the ring cavity
$\Delta_a = \nu_{pmp} - \nu_{Sr} = \nu_{ref} + f_{ofs} + f_{aom} - \nu_{Sr} \simeq 0$	detuning between pump light and atomic tra
$\Delta_c = \nu_{pmp} - \nu_{rng} = f_{syn} + f_{aom} \simeq 0$	detuning between pump light and ring cavity

The detuning Δ_a of the pump laser from ν_{Sr} is controlled via the AOM f_{ofs}, while the detuning Δ_c of the pump laser from ν_{rng} is controlled via a synthesizer.

1.5 05.04.2013 Step-up transformer

1.5.1 Self-resonant step-up transformer from a $50\ \Omega$ rf source providing 0.5 W of $f_m = 4.6$ MHz

The sidebands are generated with an EOM, which typically needs to be driven by up to $U_{eom} \approx 500$ V sine modulation amplitude. The capacity of the EOM to about $C_{eom} = 82$ pF. The modulation frequency is set to $\omega = (2\pi)20$ MHz. We generate the high voltage via a capacitively driven transformer as shown in the figure. for the driving loop we can write:

$$U_{gen} = U_0 e^{i\omega t} = -L_{cpl}\dot{I} + R_i I + \frac{1}{C_{cpl}} \int I dt \ ,$$

where the voltage $U_0 = 15$ V available from the source generates a current

$$\frac{U_0}{I_0} = R_i + i\omega L_{cpl} + \frac{1}{i\omega C_{cpl}}$$

neglecting the impact of the EOM loop.

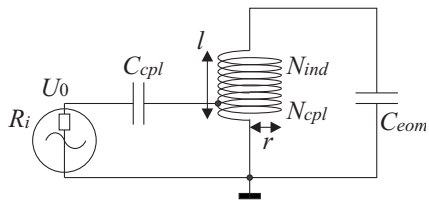

Figure 1.4: (code) Step-up transformer.

Assuming a short coupling coil with N_{cpl} turns and radius r, the magnetic field can be calculated via[1]

$$B = \frac{\mu_0 N_{cpl} I}{2r} \ ,$$

The flux through the secondary coil with area A and N_{ind} turns is now

$$\Phi = N_{ind} B A \ .$$

The induced voltage is

$$U_{ind} = -\dot{\Phi} = -N_{ind} \frac{\mu_0 I_0 i\omega e^{i\omega t}}{2r} A \simeq U_{eom} \ ,$$

so that its amplitude is

$$U_{ind,0} = -N_{ind} \frac{\mu_0}{2} \pi r \frac{i\omega U_0}{R_i + i\omega L_{cpl} + \frac{1}{i\omega C_{cpl}}} \ .$$

[1] For a long coil it would be $B = \frac{\mu_0 N_{cpl} I}{l_{cpl}}$.

To maximize the induced voltage we chose C_{cpl} tal que

$$\omega = \frac{1}{\sqrt{L_{cpl}C_{cpl}}} \qquad \text{with} \qquad L_{cpl} = \frac{\mu_0 N_{cpl}^2 A}{l} \ .$$

We chose $N_{ind}A$ tal que

$$\omega = \frac{1}{\sqrt{L_{ind}C_{eom}}} \qquad \text{with} \qquad L_{ind} = \frac{\mu_0 N_{ind}^2 A}{l} \ .$$

1.5.2 Dimensioning

Choosing $A = \pi r^2$ with $r \approx 1.35$ cm, $l \approx 5.5$ cm, and $N_2 \approx 14$, we get pretty close to $\omega = (2\pi)$ 20 MHz. $U_0 = 15$ V.

1.5.3 Phase modulator specifications

Transmission (measured without/with polarizing beam splitter cube)
Extinction (measured with VIS continuous laser beam between crossed polarizers) $> 1:250$
Wavefront deformation (@ 633 nm): $< \lambda/4$
Bandwidth (3 dB): 100 MHz
Capacity: 82 pF
Max. continuous voltage: 800 V

1.6 05.04.2013 Ideas for projects

Tasks:

- Construct an ECDL laser at 688 nm for the strontium dimpel trap.
- Construct electronic feedback loops for stabilizing lasers and ring cavity.
  - Construct a GHz PLL offset lock for an ECDL reference laser to the master laser.
  - Construct a PDH servo loop for locking the cavity to the reference laser.
- Construct a low finesse ring cavity:
  - Decide geometry, finesse, order the curved mirror at the Oficina Óptica
  - Find UHV suitable piezos and buy them
  - Calculate free spectral range δ_{fsr}, finesse F, waist w_0, phase and impedance matching of the cavity
  - Calculate decay width κ, coupling strength g, saturation photon number s, cooperativity η
  - Calculate heating rate for a reference laser detuned by $\nu_r - \omega_a = 2\delta_{fsr}$ from atomic resonance.
- Design chamber and mechanical parts of the cavity.
  - Design support for the resonator and give the design to the Oficina Mecânica.
  - Design Zeeman slower or 2D MOT, Sr dispensers, etc..
  - buy cylindrical lenses, glas cell, Sr dispensers, ion pumps
- Other tasks.
  - install 2nd interface board

Paulo will design the ring cavity.
Mike will design the chamber and the ring cavity support.
Faisah will work simultaneously on the realization and stabilization of a ring cavity on the 689 nm DL pro and on the vacuum system for the MOT (coils) and the 2D MOT (or Zeeman slower).
Philippe and Daniel start assembling an ECDL.
Projects for Leticia / Vitor: resonant coils for 500 V modulation

1.7 12.04.2013 Tentative time line for the ring cavity project

- Stable laser at 689 nm until end of 2013
- Second vacuum system for a MOT until end of 2013
- Signal from Sr in ring cavity mid of 2014

1.8 16.04.2013 Designing the ECDL

We want to construct a stable ECDL in Littrow configuration. Various plans are available [86, 4, 48, 65, **?**]. Daniel Steck provides a complete design for a very stable uni-body construction.

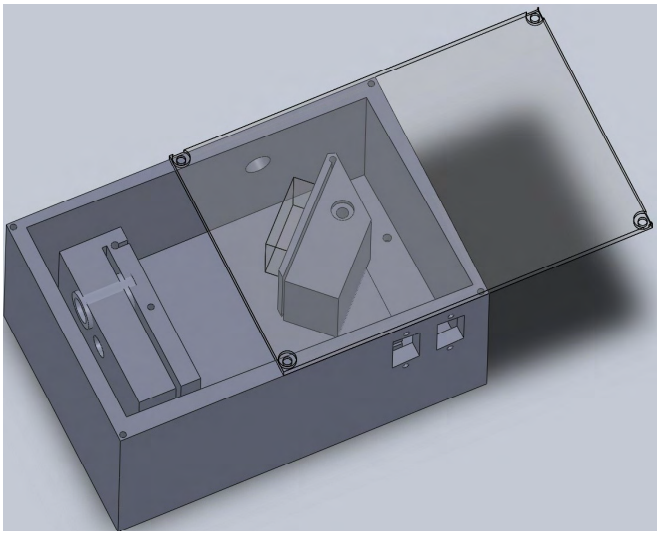

Figure 1.5: (code)

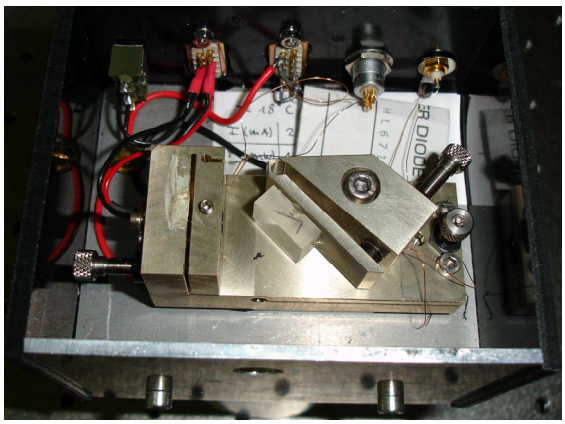

Figure 1.6: (code)

Electronic parts								
20 MHz quartz	TTL		4					
adapter	SM-SM50+	**MiniCircuits**	4	US$	5,95	US$	23,80	
adapter	SF-SF50+	**MiniCircuits**	4	US$	4,95	US$	19,80	
20 MHz bandpass filter	PIF-21.4+	**MiniCircuits**	4	US$	17,20	US$	68,80	
mixer	RDP-1+	**MiniCircuits**	4	US$	20,70	US$	82,80	
mixer	RDP-2	**MiniCircuits**	4	US$	23,20	US$	92,80	
mixer	RAY-11	**MiniCircuits**	4	US$	74,95	US$	299,80	
mixer	SRA-2000+	**MiniCircuits**	4	US$	23,95	US$	95,80	
attenuator	TOAT-3610+	**MiniCircuits**	4	US$	64,45	US$	257,80	
attenuator	TOAT-51020+	**MiniCircuits**	4	US$	64,45	US$	257,80	
directional coupler	TDC-10-1	**MiniCircuits**	2	US$	20,20	US$	40,40	
power splitter	PSCQ-2-21.4	**MiniCircuits**	4	US$	18,20	US$	72,80	
power splitter	PSC2-11	**MiniCircuits**	4	US$	36,95	US$	147,80	
amplifier	MAN-1	**MiniCircuits**	8	US$	18,20	US$	145,60	
amplifier	AD829	**MiniCircuits**	4	US$	20,00	US$	80,00	
synthesizer			0					
current control	DCC 110/0,5A	**Toptica**	0	EUR	1.080,00	US$	-	
temperature control	DTC 110 30W	**Toptica**	0	EUR	1.080,00	US$	-	
						US$	1.685,80	
Nacional								
curved mirrors for ring cavity		**Oficina Óptica**	1	US$	3.000,00	US$	1.500,00	
						US$	1.500,00	
Optics parts								
achromat for IR	AC254-100-B-ML	**Thorlabs**	1	US$	103,00	US$	103,00	
achromat for IR	AC254-200-B-ML	**Thorlabs**	1	US$	103,00	US$	103,00	
achromat for IR	AC254-300-B-ML	**Thorlabs**	1	US$	103,00	US$	103,00	
polarizing beamsplitter 10mm size	PBS102	**Thorlabs**	4	US$	174,00	US$	696,00	
mounted zero order 1/2 Waveplate 670nm	WPH05M-670	**Thorlabs**	2	US$	410,00	US$	820,00	
mounted zero order 1/4 Waveplate 670nm	WPQ05M-670	**Thorlabs**	2	US$	410,00	US$	820,00	
Hitachi laser diode @689nm	HL6750MG	**Thorlabs**	2	US$	99,75	US$	199,50	
Hitachi laser diode @689nm	HL6738MG	**Thorlabs**	6	US$	55,10	US$	330,60	
Si photodiode	FDS02	**Thorlabs**	2	US$	73,50	US$	147,00	
Si photodiode	FDS010	**Thorlabs**	2	US$	42,10	US$	84,20	
Si photodiode	FDS100	**Thorlabs**	2	US$	13,10	US$	26,20	
high-speed InGaAs photodiode	FGA10	**Thorlabs**	2	US$	158,10	US$	316,20	
anamorphic prism	PS871-B	**Thorlabs**	1	US$	150,36	US$	150,36	
free space isolator	IO-3D-660-VLP	**Thorlabs**	1	US$	850,00	US$	850,00	
collimation tube	LT230P-B	**Thorlabs**	1	US$	115,00	US$	115,00	
temperature transducer	AD590	**Thorlabs**	3	US$	13,30	US$	39,90	
1/4"-100 Polaris hex adjuster for vacuum	P25SB100V	**Thorlabs**	2	US$	25,00	US$	50,00	New Focus 9376-K
piezoelectric actuator	AE050S008F	**Thorlabs**	2	US$	130,80	US$	261,60	Noliac NAC2003 (SCMAP02)
piezoelectric and manual actuator	PE4	**Thorlabs**	1	US$	479,60	US$	479,60	
aspheric fiber port coupler	PAF-X-5-B	**Thorlabs**	1	US$	428,40	US$	428,40	Oz HPUC-23A
fast photodetector	PDA8GS	**Thorlabs**	0	US$	3.998,00	US$	-	
DC blocking filter	T8S35	**Thorlabs**	0	US$	96,90	US$	-	
peltier		**Farnell**	0	US$	99,00	US$		Laird 56460-501
grating		**Richardson**	2	US$	200,00	US$	400,00	
						US$	6.214,56	
Vacuum parts								
dispensers		**Alvatec**	0	EUR	147,03	US$	-	
windows		**MDC**	0	US$	399,00	US$	-	
reentrant windows		**Hositrad**	0	EUR	975,00	US$	-	
						US$	-	
						US$	9.400,36	

Figure 1.7: (code) Purchase list for the ring cavity project

1.8.1 Dimensioning the grating

The Bragg condition yields:

$$d(\sin\alpha + \sin\beta) = m\lambda \ .$$

In Littrow configuration the first order is back-reflected into the direction of incidence and the zeroth order is reflected: $\alpha = \beta = \theta_B$, so that

$$2d\sin\theta_B = 689 \text{ nm} \ .$$

Hence, for a grating with $d = 2000$ lines/mm, we expect $\theta_B = 43°$.

1.9 16.04.2013 Meeting with Daniel

We decide to start the construction of an ECDL, perhaps based on the Steck design. Mike will look into the details of the drawings and components. Daniel has some Peltier coolers and 1200 grooves gratings.

Daniel will initiate the construction of a current and a temperature stabilization for the ECDL. He will also look into the assembling of a 9 GHz photodetector providing enough signal to be demodulated with a local oscillator by a mixer.

Philippe will look into the realization of the electronics of the PLL and the PDH.

1.10 26.04.2013 Dimensioning the ring cavity

When dimensioning the ring cavity, we have to consider a. the cavity enhancement (impedance matching), b. the Gaussian geometry and stability (phase matching), c. the cavity configuration, d. the mode structure, e. the characteristic parameters (coupling strength, cooperativity, resolution).

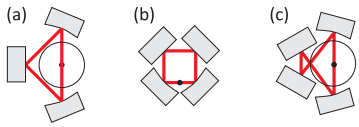

Figure 1.8: (code) Possible schemes for a ring cavity.

1.10.1 Impedance matching

We base ourselves on the formulae given in Kruse's PhD thesis [59] for a three-mirror ring cavity with two high reflectors characterized by their reflection R_{hr}, transmission T_{hr}, and absorption $A_{hr} = 1 - T_{hr} - R_{hr}$, and one input coupler, $A_{cp} = 1 - T_{cp} - R_{cp}$. The cavity enhancement factor is

$$\frac{I_{cav}}{I_0} = \frac{4T_{cp}(1 - A_{tot})}{(A_{tot} + T_{cp})^2} \ ,$$

where A_{tot} is the sum of all cavity losses not resulting from transmission through the input coupler, i.e. $A_{tot} = 2(T_{hr} + A_{hr}) + A_{cp}$. The enhancement factor exhibit a maximum varying T_{cp}, which lies at $T_{cp} = A_{tot}$.

Our oficina óptica specifies as the maximum feasible reflection $R_{hr} = 99.7\%$ and losses of about $A_k = 0.1\%$ for every mirror. Hence, the total losses are $A_{tot} \approx 0.7\%$, and the best reflection for the input coupling would be at $T_{cp} = 99.2\%$. The calculated finesse is then

$$\mathcal{F} = \frac{\pi \sqrt[6]{R_{hr}^2 R_{in}}}{1 - \sqrt[3]{R_{hr}^2 R_{in}}} = 671 \ .$$

Same calculations for a four-mirror ring cavity, $A_{tot} = 3(T_{hr} + A_{hr}) + A_{cp}$ yield a total loss of $A_{tot} \approx 1\%$, and a best reflection for the input coupling of $T_{cp} = 98.9\%$. The calculated finesse is then

$$\mathcal{F} = \frac{\pi \sqrt[8]{R_{hr}^3 R_{cp}}}{1 - \sqrt[4]{R_{hr}^3 R_{cp}}} \approx 625 \ .$$

1.10.2 Geometry of bow-tie cavity with 2 curved and 2 plane mirrors

We first consider a vertical four-mirror ring cavity with 30 cm round-trip length pumped by a 2D MOT. The mirrors will have diameters $\phi = 7.75$ mm and thickness

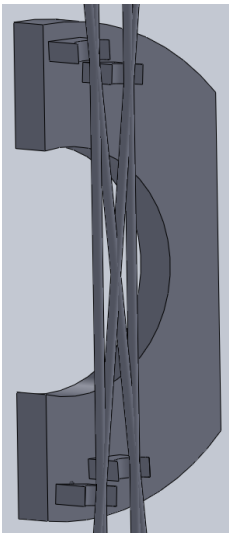

Figure 1.9: (code)

$d = 4$ mm. Standard curvatures are $\rho = 50$ mm and $\rho = 100$ mm. We discard the latter one, as it will yield too large waists.

Based on the sketch geometry, chosing the distance between the parallel beams to be $y = 8$ mm, we calculate the stability diagram of the ring cavity. Starting from the location of the atomic cloud, the round-trip transfer matrix is given by [85]

$$\begin{pmatrix} A & B \\ C & D \end{pmatrix} = \begin{pmatrix} 1 & a/2 \\ 0 & 1 \end{pmatrix} \begin{pmatrix} 1 & 0 \\ -2/\rho & 1 \end{pmatrix} \begin{pmatrix} 1 & b+c+d \\ 0 & 1 \end{pmatrix} \begin{pmatrix} 1 & 0 \\ -2/\rho & 1 \end{pmatrix} \begin{pmatrix} 1 & a/2 \\ 0 & 1 \end{pmatrix} ,$$

where $b = d = \sqrt{(a/2 + c/2)^2 + y^2}$. The radius of curvature is different for the sagittal and tangential plane

$$\rho_s = \frac{\rho}{\cos\frac{\alpha}{2}} \quad , \quad \rho_t = \rho \cos\frac{\alpha}{2} .$$

The waist at the atomic location follows as

$$w_0 = \left(\frac{\lambda}{\pi}\right)^{1/2} \frac{|B|^{1/2}}{\left[1 - \frac{1}{4}(D+A)^2\right]^{1/4}} .$$

The calculation shows, that a distance between the curved mirrors of $a = 85$ mm and $c = 75$ mm between the plane mirrors seems reasonable. It yields waists of $w_{0s} = 30.3$ μm and $w_{0t} = 28.8$ μm, respectively.

For mode matching an incoupled beam it is also important to know the size of the second waist. It is calculated in the same manner:

$$\begin{pmatrix} \tilde{A} & \tilde{B} \\ \tilde{C} & \tilde{D} \end{pmatrix} = \begin{pmatrix} 1 & b+c/2 \\ 0 & 1 \end{pmatrix} \begin{pmatrix} 1 & 0 \\ -2/\rho & 1 \end{pmatrix} \begin{pmatrix} 1 & a \\ 0 & 1 \end{pmatrix} \begin{pmatrix} 1 & 0 \\ -2/\rho & 1 \end{pmatrix} \begin{pmatrix} 1 & c/2+d \\ 0 & 1 \end{pmatrix} .$$

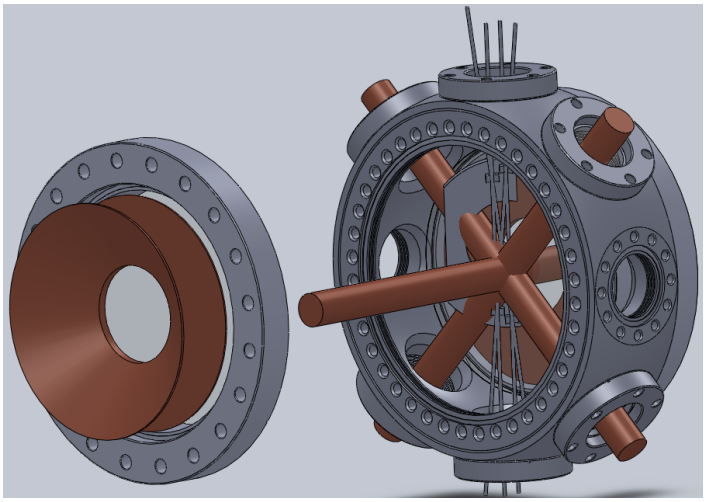

Figure 1.10: (code)

The waist at the atomic location follows as

$$\tilde{w}_0 = \left(\frac{\lambda}{\pi}\right)^{1/2} \frac{|\tilde{B}|^{1/2}}{\left[1 - \frac{1}{4}(\tilde{D} + \tilde{A})^2\right]^{1/4}} \ .$$

We find $w_{0s} = w_{0t} = 129\ \mu$m.

1.10.3 Construction of the cavity

Setting the location of the atomic cloud as origin, the coordinates where the intra-cavity laser beam hits the mirrors are given by

$$\vec{A} = \begin{pmatrix} -42.5 \\ 0 \end{pmatrix} \quad , \quad \vec{B} = \begin{pmatrix} 42.5 \\ 0 \end{pmatrix} \quad , \quad \vec{C} = \begin{pmatrix} -37.5 \\ 8 \end{pmatrix} \quad , \quad \vec{D} = \begin{pmatrix} 37.5 \\ 8 \end{pmatrix} \ .$$

Hence, the round trip of the laser beam is decribed by the vectors,

$$\vec{a} = \vec{B} - \vec{A} = \begin{pmatrix} 85 \\ 0 \end{pmatrix} \quad , \quad \vec{b} = \vec{C} - \vec{B} = \begin{pmatrix} -80 \\ 8 \end{pmatrix}$$
$$\vec{c} = \vec{D} - \vec{C} = \begin{pmatrix} 75 \\ 0 \end{pmatrix} \quad , \quad \vec{d} = \vec{A} - \vec{D} = \begin{pmatrix} -80 \\ -8 \end{pmatrix} \ .$$

The angle between incidence and reflection is

$$\alpha = \arccos \frac{-\vec{a} \cdot \vec{d}}{ad} = \frac{180^\circ}{\pi} \arccos \left(\frac{85 \cdot 80}{85 \cdot \sqrt{\left(\frac{1}{2}85 + \frac{1}{2}75\right)^2 + 8^2}} \right) = 5.7^\circ \ .$$

The vertical projection of the mirrors forms rectangles, the corners of which are given by

$$\vec{M} = \begin{pmatrix} d \\ \phi \end{pmatrix} = \begin{pmatrix} 4 \\ 7.75 \end{pmatrix} .$$

At their respective locations and rotations, the corners can be calculated via

$$\vec{A}_{corners} = \vec{A} + \begin{pmatrix} \cos\frac{\alpha}{2} & \sin\frac{\alpha}{2} \\ -\sin\frac{\alpha}{2} & \cos\frac{\alpha}{2} \end{pmatrix} \begin{pmatrix} \pm d \\ \pm\phi \end{pmatrix} .$$

The round trip length and the free spectral range are

$$L = a{+}b{+}c{+}d = 85{+}75{+}\sqrt{\left(\tfrac{1}{2}85 + \tfrac{1}{2}75\right)^2 + 8^2} = 320.8\,\text{mm} \quad , \quad \delta_{fsr} = \frac{c}{L} = 0.9351\,\text{GHz}\,.$$

All units are in mm.

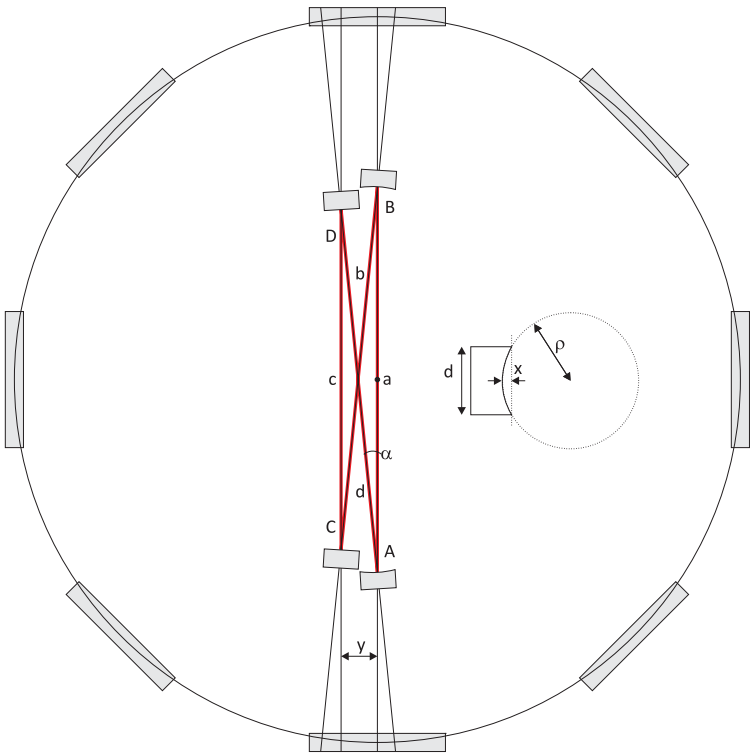

Figure 1.11: (code)

Note that due to the curved surface of the mirrors, the distance is slightly larger by $x = \rho - \sqrt{\rho^2 - \left(\frac{d}{2}\right)^2} = 0.15$ mm.

1.10.4 Mode structure

Some notes on the ring cavity mode structure.

1.10.5 Characteristic parameters for $F = 625$

Knowing the waists and the cavity length we can now calculate other parameters, such as the mode volume,

$$V = \int_0^L \int_0^{2\pi} \int_0^{w(z)} r dr d\phi dz = \pi \int_0^L w(z)^2 dz = \pi w_s w_t \int_0^L \left[1 + \left(\frac{\lambda z}{\pi w_s w_t}\right)^2\right] dz = \pi w_s w_t L \left[1 + \frac{1}{3}\right.$$

Sinced our cavity has two waists, we obtain

$$V = 2\pi w_s w_t \frac{a}{2}\left[1 + \frac{1}{3}\left(\frac{\lambda \frac{a}{2}}{\pi w_s w_t}\right)^2\right] + 2\pi \tilde{w}_s \tilde{w}_t \frac{b+c+d}{2}\left[1 + \frac{1}{3}\left(\frac{\lambda \frac{b+c+d}{2}}{\pi \tilde{w}_s \tilde{w}_t}\right)^2\right] = 9.1 \text{ mm}^3 .$$

Using $\omega_{rec} \equiv \frac{\hbar^2 k^2}{2m}$, the cavity field decay width is

$$\kappa = \frac{\delta_{fsr}}{2F} = 24.9\omega_{rec} \simeq (2\pi)\ 100 \text{ kHz} .$$

The coupling strength is

$$g_1 = \sqrt{\frac{3\pi\Gamma\omega}{k^3 V}} = 0.24\omega_{rec} = 0.01\kappa \simeq (2\pi)\ 1 \text{ kHz} .$$

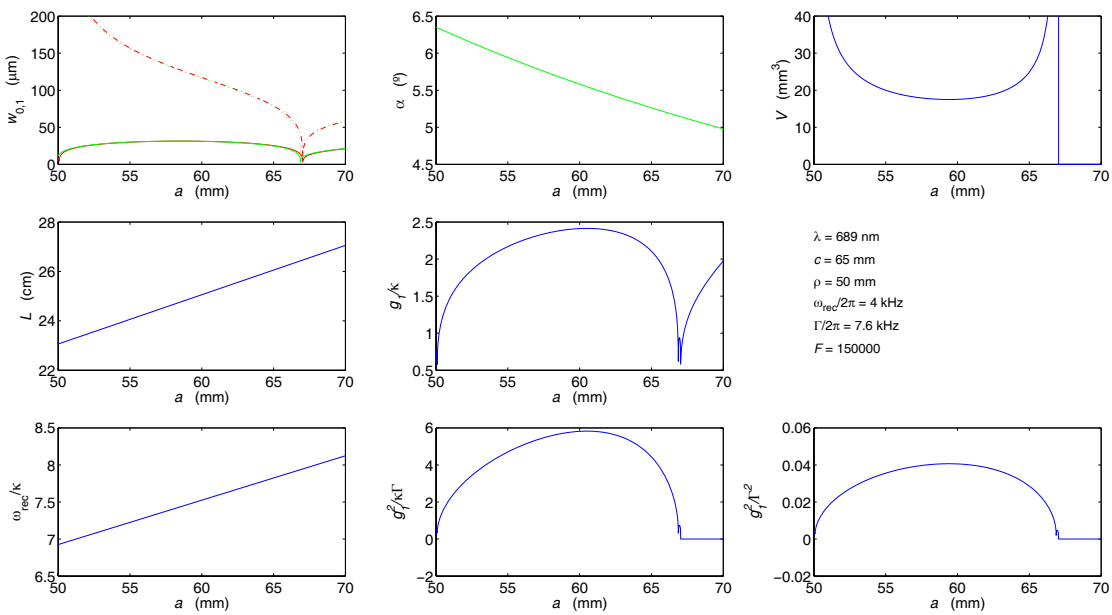

Figure 1.12: (code) Figures of merit of a long cavity in zigzag configuration with 2 curved and 2 plane mirrors.

1.10.6 Characteristic parameters for $F = 150000$

The cavity field decay width is

$$\kappa = \frac{\delta_{fsr}}{2F} = 0.1\omega_{rec} \simeq (2\pi)\ 500\ \text{Hz}\ .$$

The coupling strength is

$$g_1 = \sqrt{\frac{3\pi\Gamma\omega}{k^3 V}} = 0.24\omega_{rec} = 2.3\kappa \simeq (2\pi)\ 1\ \text{kHz}\ .$$

This shows that, while we are safely in the resolved photonic recoil regime, we are pretty far from the strong coupling regime. If we want to reach the strong coupling regime on the 7.6 kHz line, we'll have to reduce the size of our ring cavity to the limit of what is practically viable (or chose a mHz linewidth).

1.11 29.04.2013 Meeting with Celso and James

James presented preliminary calculations for an optical transistor with cascadibity option. He assumes a two-level atom coupled to a bad cavity and finds bistable behavior in the parameter regime: $N = 1000$, $n_{ph} = 1000$, $g_1 = 0.01\kappa$, $\Gamma = (2\pi)\ 7.6$ kHz. This is close to what is planned experimentally with a low finesse cavity.

Philippe presented the above considerations of how to design the ring cavity.

With the goal of getting closer to the strong coupling regime, we try other ring cavity geometries. The approach of using 3 or 4 curved mirror does not seem to pay off, neither in 3 nor in 4-mirror configurations. On the other hand, a small 3-mirror cavity seems to work. We get barely into the strong coupling regime at the price of

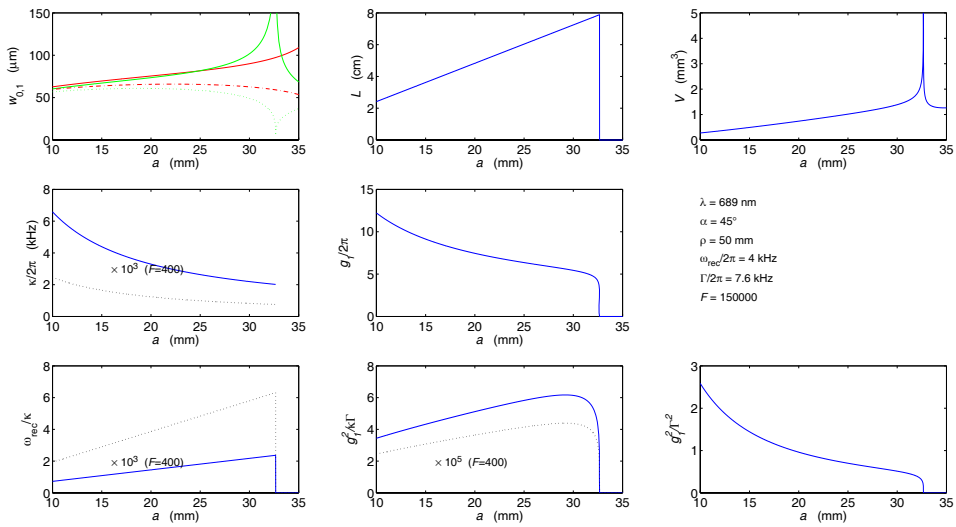

Figure 1.13: (code) Figures of merit of a short cavity in triangular configuration with 2 curved and 1 plane mirrors.

leaving the resolved photonic recoil regime, which however, could be recovered with better mirrors. So we decide to construct two cavities, a small triangular ring cavity, which is optimized for strong coupling and a long zigzag-shaped ring cavity, which is optimized for high resolution.

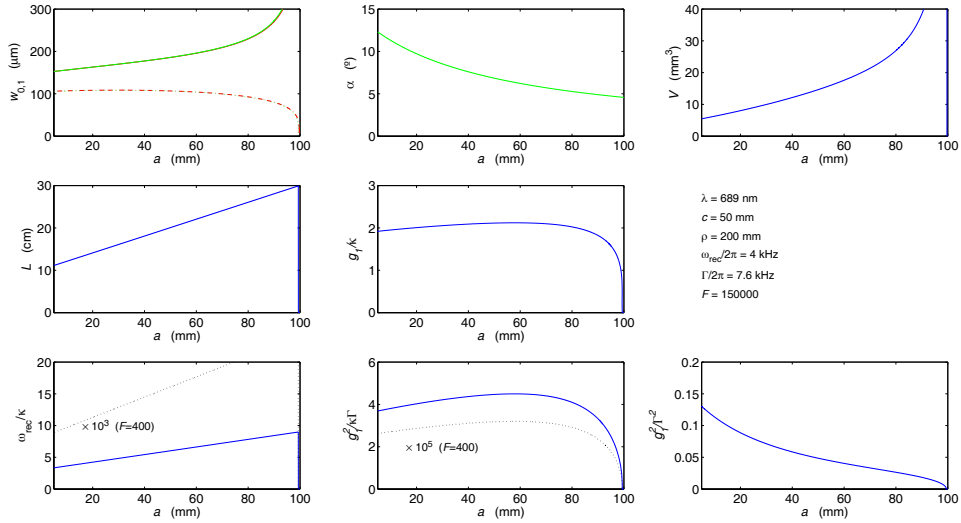

Figure 1.14: (code) Figures of merit of a short cavity in zigzag configuration with 2 curved and 2 plane mirrors.

1.12 22.07.2013 Simplified locking scheme

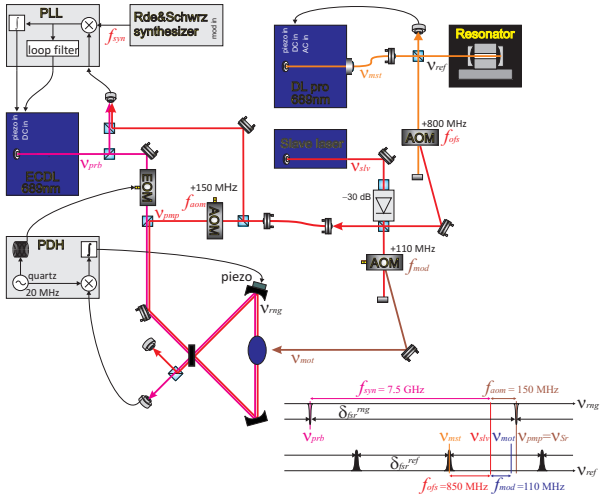

Figure 1.15: (code)

1.13 25.07.2013 Magnetic fields of the MOTs

Characterization of the main MOT coils: With the planned vacuum chamber we will be able to realize rectangular MOT coil shapes with inner radii $R_x = 34$ mm and $R_y = 38$ mm and distance from the MOT center $A_z = 13$ mm. Assuming that the current-carrying cross section is 26×26 mm^2, the mean radii and distances are: $R_x = 47$ mm, $R_y = 51$ mm, and $A_z = 26$ mm. From this, integration of the Biot-Savart law yields:

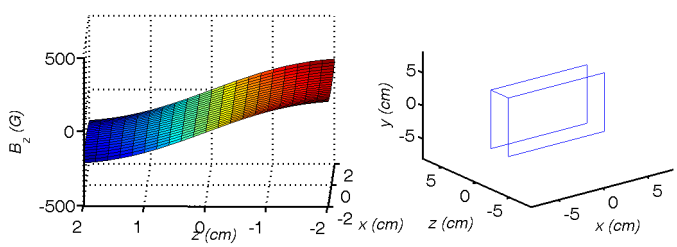

Figure 1.16: (code)

The 2D-MOT will be operated with permanent magnets: "Kyle's calculations".

1.14 20.08.2013 Final test cavity design

We will realize a rectangular three mirror ring cavity with the following data:

transition wavelength	λ	=689 nm
base length of the triangle	a	=1.6 cm
cavity round trip length	$L = a(1+\sqrt{2})$	=3.8 cm
cavity mode volume	V	=0.5 mm
free spectral range	$\delta_{fsr} = \frac{c}{L}$	=7.7611 GHz
radius of curvature of the high reflectors	ρ	=50 mm
reflection of the high reflector	R_{hr}	=99.9 %
reflection of the in coupler	R_{ic}	=99.7 %
finesse	$F = \frac{\pi(R_{hr}^2 R_{ic})^{1/6}}{1-(R_{hr}^2 R_{ic})^{1/3}}$	=1882
transition linewidth	Γ	=(2π)7.6 kHz
cavity linewidth	$\kappa = \frac{\delta_{fsr}}{F}$	=(2π)328 kHz
recoil shift	$\omega_{rec} = \frac{\hbar k^2}{2m}$	=(2π)4 kHz
coupling strength	$g_1 = \sqrt{\frac{3\pi\Gamma\omega_0}{k^3 V}} s_0 s_2$	=(2π)8.7 kHz

We will load the cavity mode with $N = 10^4$ to 10^5 strontium atoms at a temperature of about $T = 1$ μK. The cavity mode waist at the atomic location will be $w_0 = 70$ μm. The size of the thermal atomic cloud depends on the temperature, but can be made to fit into the waist.

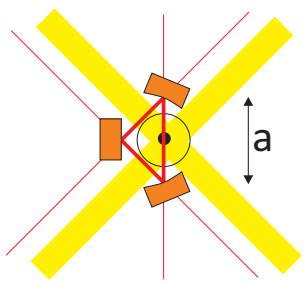

Figure 1.17: (code)

What effects can we study in this parameter regime? 1. Bistability and all-optical switching?
2. Bloch oscillations?

1.15 21.10.2013 Current PDH setup

Current setup as realized by Faizah:

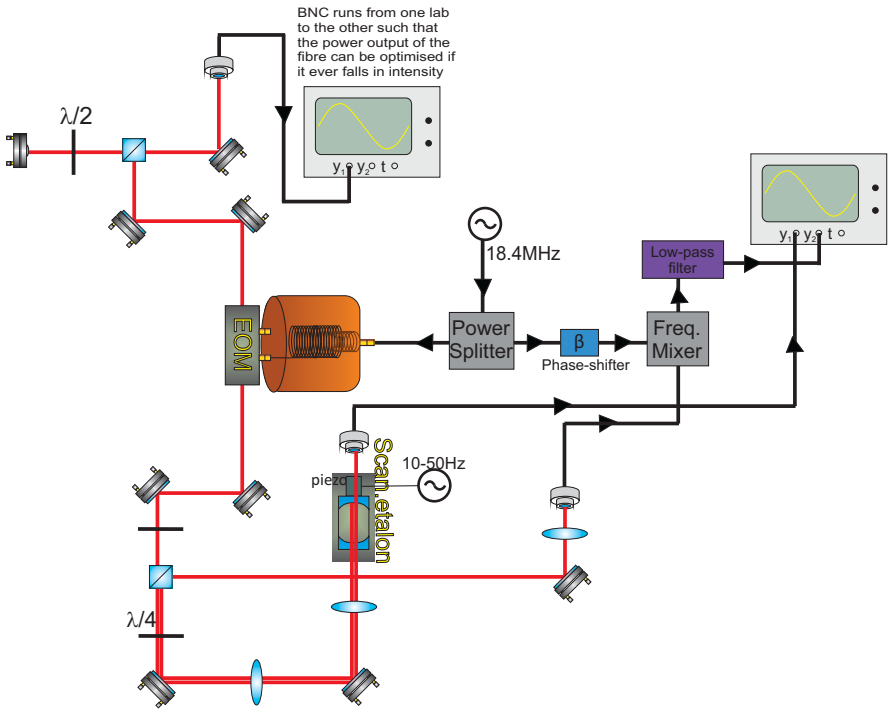

Figure 1.18: (code)

Needed urgently, work is held up by not having them:
- 20MHz photodetector
- Current driver for ECDL

Needed by end of next week, otherwise work will be held up:
- 20MHz amplifier with low gain or the possibility of attenuating
- PID servo-lock - start by testing the one we have in the lab

- Temperature driver for ECDL

Won't be needed for at least 2 weeks:
- Piezo driver for ECDL
- 1GHz photodetector, Ruben to test his laser (could be the 8GHz below)
- 8GHz photodetector, for PLL lock
- Mixer for 8GHz

1.16 06.01.2014 Progress on the PDH servo

In the last few days I tried to lock the Steck laser #2 to a test cavity using the EOM. The helical resonator and the EOM work nicely. A clear PDH signal is visible. The

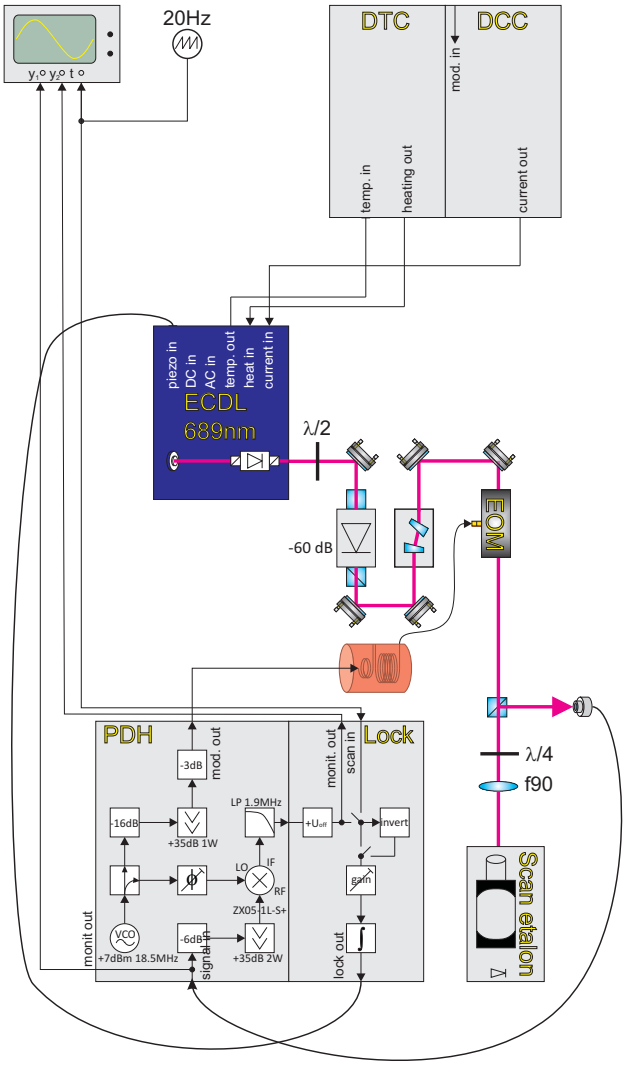

Figure 1.19: (code)

piezo is working fine.

I tried to close the PDH feedback loop. It worked, but not very nicely. Likely reasons are

1. transverse modes of the confocal cavity distorting the PDH signal;
2. the lack of a phase shifter allowing to adjust the PDH signal shape;
3. the very low bandwidth limited by the cavity piezo.

To remedy we now have to design a fast locking circuit controlling the laser current

via a loop filter and the piezo of the cavity (or the one of the ECDL) via a PID lock box.

I designed such an electronics including the a layout for a printed board (frontside, backside, and components, see LaborElectronics). But as I am no expert, I would appreciate if a real expert could check and eventually improve. I ordered the components from MiniCircuits, but it will take 2 months before they arrive. Anyway, it would be good if LIEPO could already prepare the boards, so that we can start testing some things.

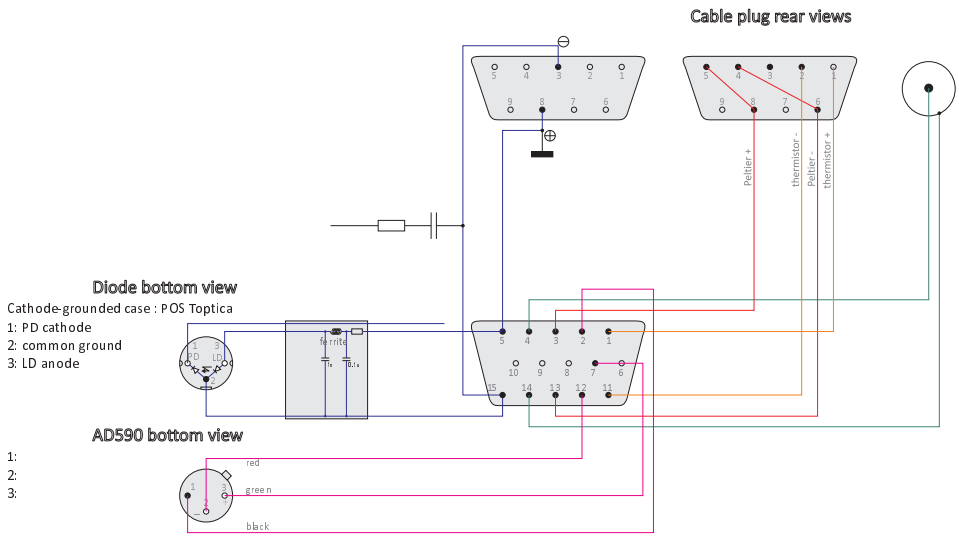

Figure 1.20: (code)

1.17 12.01.2014 Progress on the PDH servo 2

I aligned the second Steck laser such as to prepare for a beat frequency measurement. I also set up a loop filter trying for the PDH servo. But without success, yet.

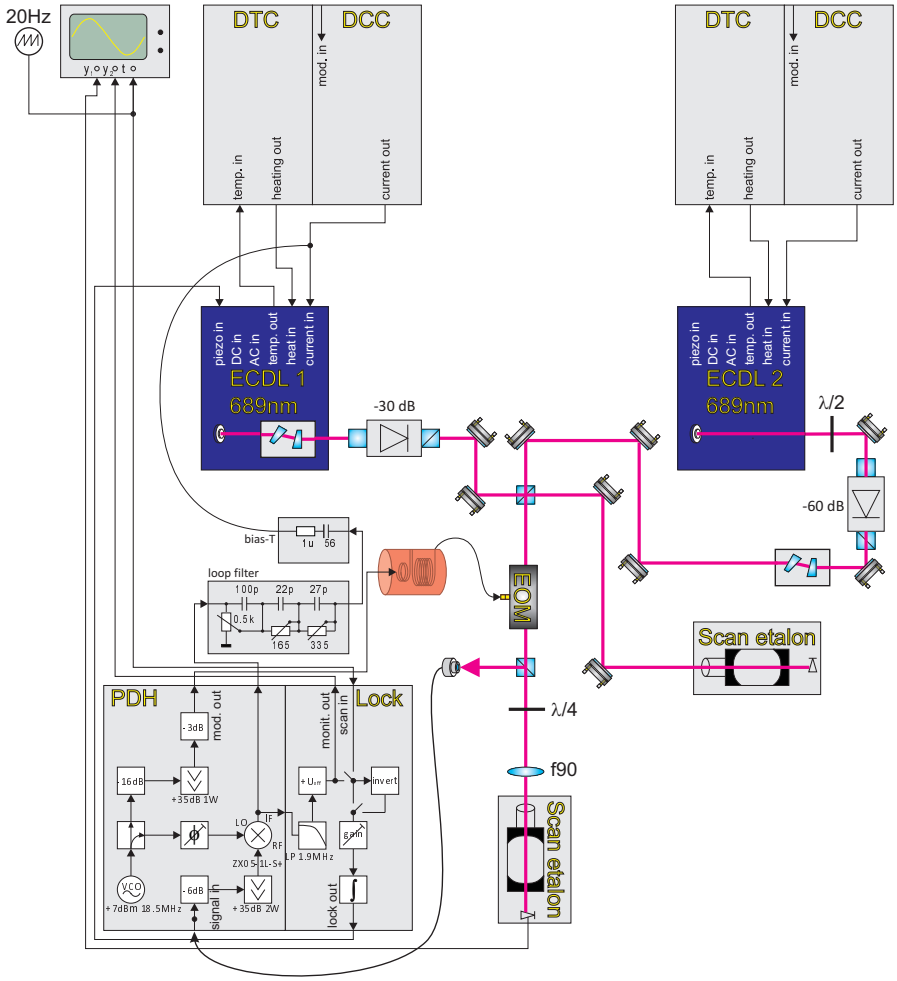

Figure 1.21: (code)

Actual problems:

1. Steck laser #2 threshold is poorly aligned;
2. Steck laser #1 collimation is bad;
3. Steck laser #2 piezo may have problem;

Things urgently needed:

1. 1x current drive for the Steck laser #2;
2. 1x temperature control for Steck laser #1;
3. 1x 8GHz photodetector;

4. MiniCircuits parts for the PDH and the PLL (e.g. phase shifter).

1.18 13.01.2014 Fast photodetector

I assembled a detector with the Thorlabs diode FDS02. Junction capacitance $C_J = 1$ pF, sensitivity $\eta = 0.5$ A/W, load resistance $R_L = 50\ \Omega$. With these parameters a $P = 100\ \mu$W light power fluctuation should give a $V_0 = P\eta R_L = 2.5$ mV signal. The bandwidth is $f_B = \frac{1}{2\pi R_L C_J} = 3\,\text{GHz}$. Using a bias voltage it might be possible to reduce the junction capacitance and increase the bandwidth.

Check detector:

1. DC signal;
2. modulated laser current.

Check laser current modulation:

1. couple AC signal and look for sidebands;
2. check protection circuit.

Design PI-servo for piezo.

1.19 21.02.2014 Steck protection circuit

Steck's protection circuit is composed of a low pass filter with two capacitors and a ferrite, and a Schottky diode. The low pass filter cuts off frequency components above 160 kHz. After Sharaf took out the 100 nF capacitor, the transfer function becomes much flatter until 20 MHz.

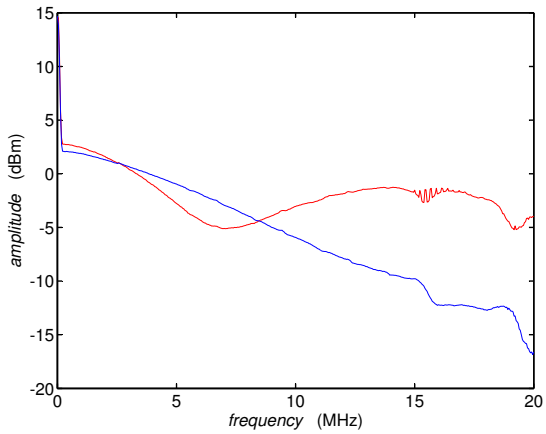

Figure 1.22: (code)

The AD590 produces a current. At a load of 1 kHz is shows the absolute temperature in K/mV.

1.20 21.02.2014 Thorlabs protection circuit

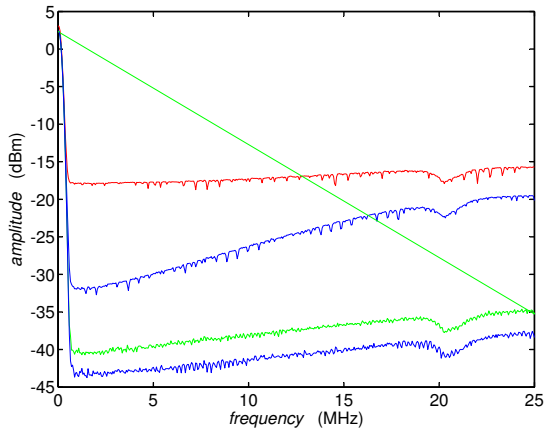

Figure 1.23: (code)

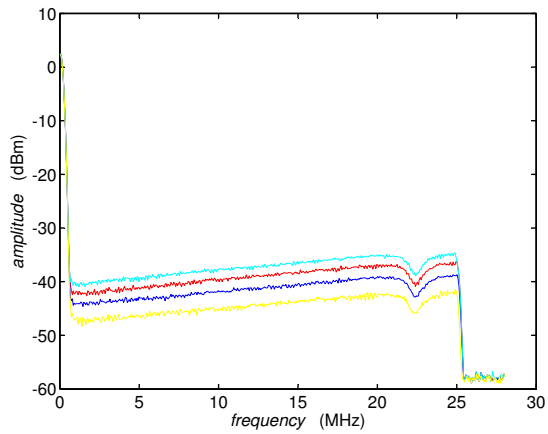

Figure 1.24: (code)

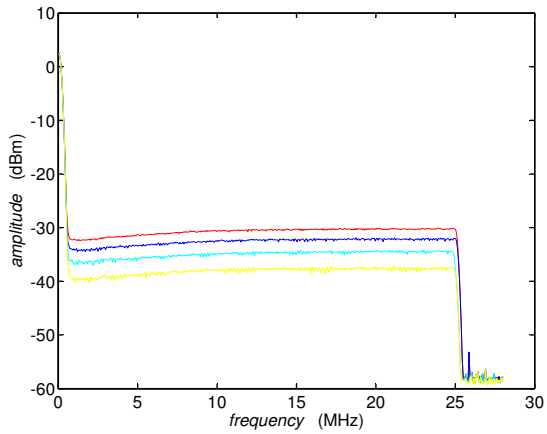

Figure 1.25: (code)

1.21 01.04.2014 Organizing our ring cavity collaborations

- Nice: cooperative scattering in free space (disorder, Anderson localization, subradiance,...)

- Milano / Strathclyde: emphasis on atomic motion, classical light, good & bad cavities (Bloch oscillations, CARL, subrecoil resolution,...)

- Birmingham / Nottingham: emphasis on technical aspects, bad cavities (Bloch oscillations, gravimetry, metrology,...)

- UFSCAR: emphasis on internal degrees of freedom & CQED (strontium intercombination line, three-level systems, EIT, entanglement, subradiance...)

1.22 12.06.2014 AlvaSource dispensers

We've got 2 AlvaTec dispensers type AS-5-Sr-500-F, meaning that the recipient of the dispenser has $d = 5$ mm diameter, $m = 500$ mg of Sr-mass, and $c = m/160$ mg/cm = 3.1 cm of length.

Later, we purchased AS-3-Sr-500-F, meaning that the recipient of the dispenser has $d = 3$ mm diameter, $m = 50$ mg of Sr-mass, and $c = m/60$ mg/cm = .83 cm of length.

1.23 25.06.2014 Laser diode connections

Using the homebuilt current and temperature control together with the Thorlabs bias-T we realize the following connection cdable:

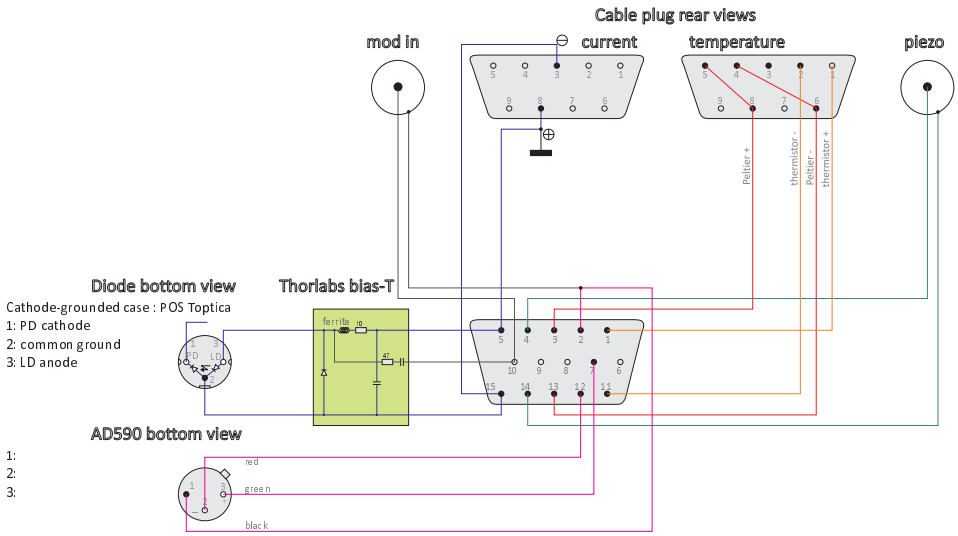

Figure 1.26: (code)

1.24 04.11.2014 Strategical planning

What experiment should we start constructing? Element, lasers, chamber? Construct rubidium cell or rubidium surface MOT experiment.

The mirror of the surface MOT would be nanostructured, metamaterial with thin alternating Ag and TiO_2 layers and nanoslits.

What are our questions? Strong coupling or high cooperativity? What to sense? Where exactly can atoms do the difference?

1.25 04.11.2014 Natal meeting

1.25.1 Peter's offer

We set up Rb experiment, he gives us his chip.

1.25.2 Carlos Farina

Levin 2010

Eberlein 2011, atoms between two layers evanescent waves may reduce atom-atom interaction, is this Feshbach tuning? or dipole force tuning?

Kort-Kamp 2013, cloaking microsphere for atoms

1.25.3 Maxim

PRA 84, 043802 (2011) PRA 91, 043835 (2015)

1.25.4 Francisco Intravaia

consider doped ZnO_2 for lowering plasmonic losses

other wavelengths (blue) for Au

holes in layers for getting repulsive forces, in water, control Casimir-Polder?

are surfaces good anyway (To strongly interacting with atoms)

1.25.5 Christian Koller

design of their science chamber? 2D MOT?

Membranes?

1.25.6 Yeshpal

Strontium

1.26 25.01.2015 Wastl's visit

1.26.1 People exchange and research proposals to DFG-FAPESP and PVE CNPq/CAPES

Wastl will send his old DFG proposal: Shall we use it or make a new one?

- Send David to São Carlos with a DAAD grant in autumn for writing his thesis. We help him to interprete his data on spatially resolved light intensity measurements using a nano tip in optical lattices or MOTs. Will it be possible to perform lifetime measurements (sub- or superradiance?) and compare them with coupled-dipoles model (CDM) simulations?
- Compare Philip's master thesis (radiation trapping in the saturate limit) with CDM simulations.

1.26.2 Subradiant CARL

Can we interprete the red and blue CARL threshold measurements in terms of sub- or superradiance. Hannah's 2-atom model looks similar to the DeVoe and Brewer two-ion experiment. Is it possible to reshape the classical CARL equation into a decay equation containing Γ or $\Gamma_{Rayleigh}$, which then could be explained as sub- oder superradiant?

1.26.3 Si chip cell

Construct glas cells with bonded Si chip supporting a metamaterial to the cell wall.

- Can we include João's detectors at the bottom side oft the metamaterial? Or rather use a translational APD?
- Which element to use? Rb at 780nm or 420nm? Yb, Iodine or what?

1.26.4 Optical cooling in evanescent waves

Is it possible to cool atoms in quasi-resonant evanescent waves near surfaces? One could imagine a scheme like in figure 1 with far-blue detuned evanescent waves and near-red detuned evanescent light. What is the capture velocity, the cooling rate?

1.26.5 Relationship between coupling strength and density of states

We need to understand better the relationship between coupling strength and density of states (numbers of modes, Purcell factor)? An acceleration of the decay is NOT the same as Purcell enhancement! There are 2 paradigms:

- Is a cooperativity enhancement by mode number enhancement possible? Or does it rather rely on phase matching and stronger coupling (CQED)?

- A mode number enhancement à la Ben Hur reduces Γ, but does not increase cooperativity.

While (b) does not favor backaction, (a) does! What we are aiming at is rather a reduction in the transverse density of states in order to create 2D photonic waveguide.

1.26.6 Model to describe backaction

Which model to use to describe backaction: 1. Finite elements simulation of the light fields (Ben Hur): Is the inclusion of backaction possible or already inherent? How to quantify the amount of backaction? 2. FDTD (John): similar to Ben Hur 3. CDM (Romain): Is it possible to simulate metamaterials ($\epsilon < 0$, $\mu < 0$) in gases? 4. Coupled Maxwell and Bloch equation (Sukharev)

1.26.7 Realizing a 2D light scattering geometry

How to realize a 2D light scattering geometry? First one needs to create 2D atomic clouds, f.ex. using bichromatic evanescent waves. Second one needs to impede the emission of light in transverse directions. This could be done in various ways:

- plasmonic (or evanescent) fields
- closely stacked mirrors
- closely stacked dielectrics with evanescent fields (in glas cells or BEC?)

1.26.8 Sebastian's proposal

Shall we recycle part of Sebastian's proposal?

Motivation

- study of disorder, Bose glass, quasi crystals for matter wave propagation
- BEC in subwavelength disordered potentials

Innovation:

- evanescent waves optical lattice for BEC with plasmonic structuring of disorder potentials
- localization of matter waves in a photonic bandgap cavity
- Bloch oscillations in an evanescent waves optical lattice:
-
  - if we can make small lattice constants, can we afford higher temperatures
  - how to read out the oscillations?

1.27 14.11.2015 Laser sword project

Cooperation with Leonardo (EESC) and xx (UNICAMP) on continuous Bessel beam superpositions. Propose to adapt Rb apparatus to fit their atomic guiding ideas.

I offer: lab space, equipment, post-doc and PhD grants. They have to provide man power, otherwise the project is not viable.

Questions:

- literature: who has already worked on atoms in Bessel beams? Verkerk
- what is the advantage? rigid walls versus Gaussian beams? non-harmonic potentials?
- wavelength, intensity, spectral purity, close or far from resonance, red or blue-detuned, choice of atom, typical dimensions?
- necessary equipment: lasers, lenses, polarization optics, CCD camera?

Equipment needed:

- Optical table & infrastructure (rack, electricity)
- $>$ 200 mW laser at 780nm (TA PRO from Toptica) and $>$ 20 mW laser as repumper (DL 100 L DFB)
- NIR optics
- Rb cell
- Agilent power supply for MOT and CCD camera & computer control

1.28 29.07.2014 Progress on the PDH servo 3

Frontpanel layout for the Pound-Drever-Hall servo:

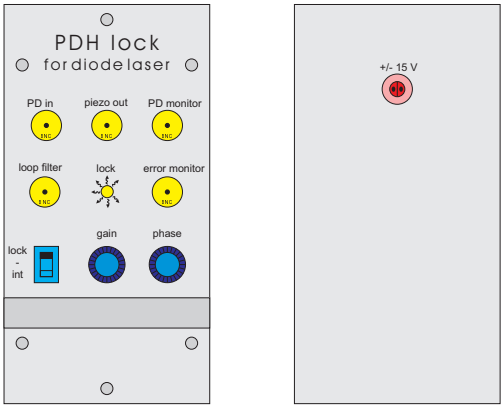

Figure 1.27: (code)

Circuit diagram. The optical layout is shown at 06.01.2014:
Board layout:

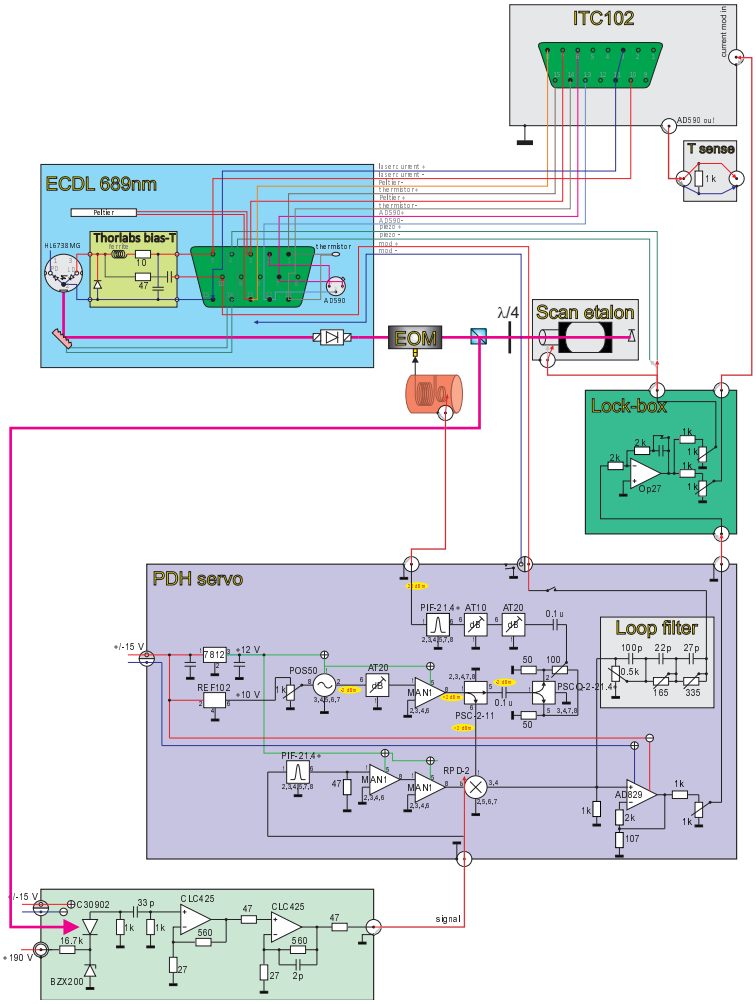

Figure 1.28: (code)

1.29 11.12.2014 Ring cavity coupling

Reflectivities of the DoroTek ring cavity mirrors at 690 nm:

- $R_{hr,s} = 0.9997$
- $R_{hr,p} = 0.9992$
- $R_{ic,s} = 0.9974$
- $R_{ic,p} = 0.9974$

This gives the finesses: $F_s = 2942$ and $F_p = 2242$.

Comparison of calculated and measured ring cavity modes.

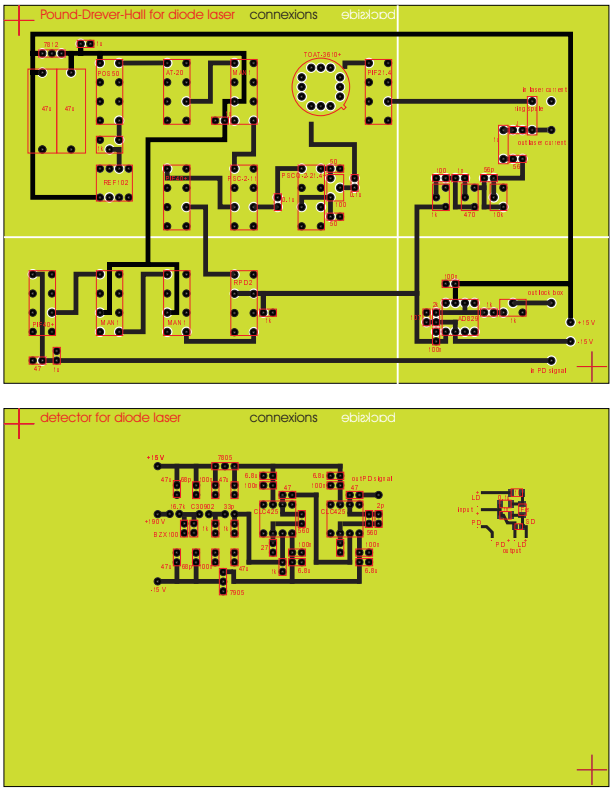

Figure 1.29: (code)

1.30 04.04.2015 Relevant data for the patent application

1.30.1 Ring cavity dimensions

We will realize a rectangular three mirror ring cavity with the following data:

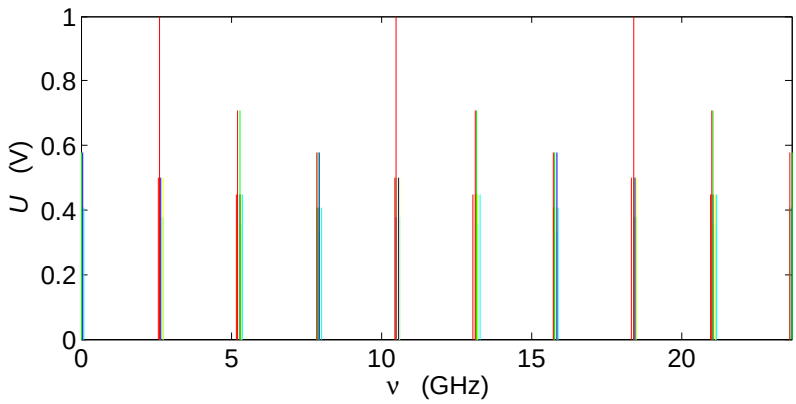

Figure 1.30: (code)

transition wavelength	λ	= 689 nm
cavity round trip length	L	= 3.8 cm
cavity mode volume	V	= 0.5 mm
free spectral range	$\delta_{fsr} = \frac{c}{L}$	= 7.7611 GHz
radius of curvature of the high reflectors	ρ	= 50 mm
reflection of the high reflector	$R_{hr,s}$	= 99.97 %
reflection of the high reflector	$R_{hr,p}$	= 99.92 %
reflection of the in coupler	R_{ic}	= 99.74 %
finesse	$F = \frac{\pi(R_{hr}^2 R_{ic})^{1/6}}{1-(R_{hr}^2 R_{ic})^{1/3}}$	= 1882
transition linewidth	Γ	= (2π)7.6 kHz
cavity linewidth	$\kappa = \frac{\delta_{fsr}}{F}$	= (2π)328 kHz
coupling strength	$g_1 = \sqrt{\frac{3\pi\Gamma\omega_0}{k^3 V}} s_0 s_2$	= (2π)8.7 kHz
cavity mode waist at the atomic location	w_0	= 70 μm

We will load the cavity mode with $N = 10^4$ to 10^5 strontium atoms at a temperature of about $T = 1$ μK.

1.30.2 Laser power for the vertical optical lattice

We want the vertical optical lattice with two laser beams at $\lambda_d = 532$ nm intersecting under an angle of $\alpha = 101°$. Under this angle the periodicity of the optical lattice is half the wavelength of the intercombination transition $\lambda_{689}/2 = 344.5$ nm whose recoil shift is,

$$\omega_{rec} = \frac{\hbar k^2}{2m} = (2\pi)\ 4.8\ kHz\ .$$

The dominating resonance for the dipole force is at $\lambda_{461} = 461$ nm. In order to observe the predicted mode-locking effect [94] we assume a depth of the optical lattice potential of $W_d(0) \simeq 3.2\hbar\omega_r$. Using [47], we calculate the dipole potential via,

$$W_d(\mathbf{r}) = \frac{3\pi c^2 \Gamma_{461}}{2\omega_{461}^3} \frac{1}{\omega_d - \omega_{461}} I(\mathbf{r})\ ,$$

with the maximum intensity,

$$I(0) = \frac{2P}{\pi w_d^2} \ .$$

Hence, shooting for a waist of $w_d = 500\ \mu$m,

$$\frac{3\pi c^2 \Gamma_{461}}{2\omega_{461}^3} \frac{1}{\omega_d - \omega_{461}} \frac{2P}{\pi w_d^2} \equiv 3.2\hbar\omega_{rec} \ .$$

Resolving for power,

$$P = 3.2\hbar\omega_{rec} \frac{\omega_{461}^3 w_d^2}{3c^2\Gamma_{461}} (\omega_d - \omega_{461}) \approx 1.7 \text{ W} \ .$$

1.30.3 Laser power for cavity pump laser

In order to observe the predicted mode-locking effect [94] we assume a depth of the optical lattice potential of $U_0 \simeq 0.04\hbar\omega_r$,

$$U_0 = \frac{g\Omega_p}{4\Delta} = \frac{1}{4\Delta} \frac{\wp \mathcal{E}_1}{\hbar} \sqrt{\frac{3\lambda_{689}^2}{2\pi} \frac{\Gamma_{689} I}{\hbar\omega_{689}}} \ .$$

Resolving for intensity,

$$I = U_0^2 \frac{2\pi}{3\lambda_{689}^2} \frac{\hbar\omega_{689}}{\Gamma_{689}} \left(\frac{4\Delta}{g}\right)^2 \ .$$

The waist of the cavity is $w_0 = 70\ \mu$m. Hence, the power is,

$$P_{cav} = \frac{\pi w_0^2}{2} I \ .$$

To achieve this power, the cavity must be pumped with,

$$P_{pmp} = \frac{P_{cav}}{1 - R} \approx 0.11 \text{ nW} \ .$$

We have about 30 photons,

$$P_{cav} = |\alpha|^2 \hbar\omega_{689} * \delta_{fsr} \approx 0.17 \text{ nW} \ .$$

1.31 05.05.2015 Questions to the Menlo system

1.31.1 Direct PDH locking of a ring cavity to the frequency comb

The Photonic crystal fiber delivers $P = 80$ mW in the range between $\lambda_1 = 600$ nm and $\lambda_2 = 900$ nm with $\Delta\nu = 250$ MHz mode spacing. Assuming a homogeneous power distribution, we expect per mode

$$P_{mode} = \frac{P\Delta\nu}{\frac{c_0}{\lambda_1} - \frac{c_0}{\lambda_2}} \simeq 120 \text{ nW} .$$

- fiber from/to DL pro
- use Falk to stabilize Steck laser

1.32 05.06.2015 Operating the fs-comb 1

I got the fs-comb to work locking the CEO and the RRE to the 10 MHz reference. The optical beats yield 20 dB using the Agilent spectrum analyzer.

I found that all the electronics needs to be turned on before the comb-control software be started. Otherwise, there are error messages and the software won't start.

Probably the linewidth of the lasers is not sufficient for a locking to the comb: Daniel's laser's beat with the comb has $\Delta\nu = 5$ MHz. Hence, the comb is narrower and hence the beat's linewidth with the optical lasers is due to the lasers: DL-pro free-running $\Delta\nu \approx 10$ MHz, DL-pro locked to cavity $\Delta\nu \approx 10$ MHz, Steck's ECDL free-running DL $\Delta\nu \approx 20$ MHz.

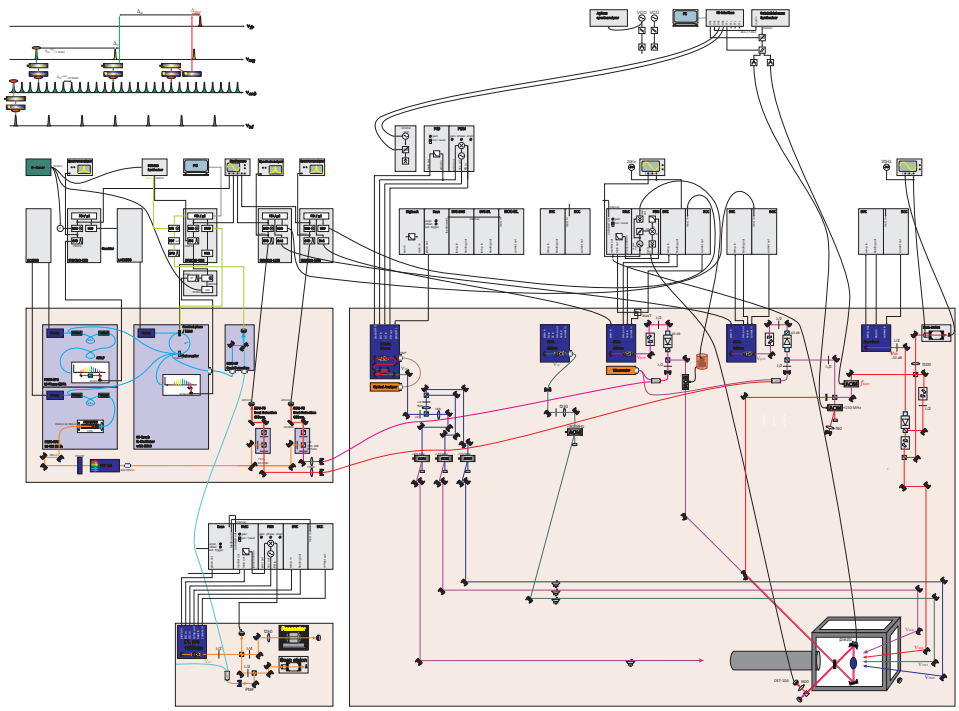

Figure 1.31: (code)

1.32.1 CEO

Mix

$$\Delta\omega = 2n\omega_r + 2\omega_0 - m\omega_r - \omega_0 = (2n - m)\omega_r + \omega_0 \ .$$

Now we filter the lowest component. If $\omega_0 \ll 250$ MHz then $2n = m$ gives the lowest frequency component.

1.32.2 Update from 11.06.2015

The comb electronics made a strange noise, like an exploding capacitor. The CEO was totally noisy for some time, and then worked again normally. However, there is a strange smell coming from the rack (like a burned capacitor).

1.33 02.07.2015 Operating the fs-comb 2

Found nice Comb-DLpro beat signal (25 dB, 1 MHz width probably due to acoustic noise). It is necessary to reduce the sideband modulation as much as possible. The DLpro settings were sideband mod ×3, gain ×5, cavity transmission 3.5 V @ 10 kΩ. It might be a problem that the sideband modulation frequency of 20 MHz is equal to the offset beat frequency.

1.33.1 Measuring a laser frequency

The repetition rate is

$$f_{rep} = \tfrac{1}{4}(980\text{ MHz} + f_{dds}) = 245\text{ MHz} + \tfrac{1}{4}f_{dds}\ .$$

The frequency of a laser is

$$\begin{aligned} f_{cw} &= nf_{rep} + 2f_{ceo} + f_{beat} \\ f_{ceo} &= \pm 20\text{ MHz} \\ f_{cw} &< 0 \quad \text{or} \quad > 0\ , \end{aligned}$$

i.e. the signs of f_{ceo} and f_{beat} can be positive or negative. The sign of f_{beat} can be determined as follows: We lock f_{rep} and f_{ceo} and watch f_{beat} on the spectrum analyzer. If, when increasing the repetition rate via f_{dds}, the beat frequency f_{beat} rises (diminishes), then $f_{cw} < f_{comb}$ ($f_{cw} > f_{comb}$), so that we have to use $f_{beat} = -|f_{beat}|$ ($f_{beat} = |f_{beat}|$) in the above equation.

To determine the sign of the carrier envelope offset f_{ceo}, we consider the case $f_{cw} < f_{comb}$. We unlock f_{ceo} and watch f_{ceo} and f_{beat} on the spectrum analyzer. If now, when increasing f_{ceo} via the output voltage of the SYNCRO-CEO or the computer control increases (reduces) the beat frequency f_{beat}, the comb moves toward higher (lower) frequencies, so that we have to use $f_{ceo} = 20$ MHz ($f_{ceo} = -20$ MHz) in the above equation. In the case $f_{cw} > f_{comb}$ the behavior in inverted.

1.33.2 Calculating the cavity fsr

The idea of making an absolute measurement of a continuous laser frequency f_{cw} using the comb is based on the equation

$$f_{cw} = \tilde{n}f_{rep} + 2f_{ceo} + f_{beat} \qquad \text{with} \qquad \Delta f_{cw} = \Delta f_{beat}\ ,$$

where $\tilde{n} = int(n + 0.5)$ is an integer number and

$$n = \frac{f_{wm} - 2f_{ceo} - f_{beat}}{f_{rep}} \qquad \text{with} \qquad \Delta n = \frac{\Delta f_{wm}}{f_{rep}} + \frac{\Delta f_{beat}}{f_{rep}}$$

is estimated from a wavemeter measurement,

$$f_{wm} \pm \Delta f_{wm}\ .$$

However, for this to hold, we need a reasonably precise wavemeter, $\Delta f_{wm} < f_{rep}$, capable of resolving the comb frequency spacing,

$$f_{cw} = \tilde{n} f_{rep} + 2f_{ceo} + f_{beat} = round\left(\frac{f_{wm} - 2f_{ceo} - f_{beat}}{f_{rep}}\right) f_{rep} + 2f_{ceo} + f_{beat}$$

$$\Delta f_{cw} > f_{rep} \quad \text{if} \quad \Delta n > 1 \quad \text{and} \quad \Delta f_{cw} = \Delta f_{beat} \quad \text{if} \quad \Delta n < 1 \ .$$

If this is not at hand, we may measure the beat signal between the DLpro and the comb for two sufficiently different settings $k = 1, 2$ of the repetition rate,

$$f_{wm} = n_k f_{rep,k} + 2f_{ceo,k} + f_{beat,k} \ .$$

1.33.3 Reducing the mode number uncertainty

How can we reduce the uncertainty for $\tilde{n}_k$? One way could be, to measure n_k for two different repetion rates, since we know that for $m \equiv n_2 - n_1$ holds $\Delta m \ll 1$, so that we can assume $\tilde{n}_2 - \tilde{n}_1$

$$n_2 - n_1 = \tilde{n}_2 - \tilde{n}_1 = \frac{f_{cw} - 2f_{ceo,2} - f_{beat,2}}{f_{rep,2}} - \frac{f_{cw} - 2f_{ceo,1} - f_{beat,1}}{f_{rep,1}} \ ,$$

from which we derive

$$f_{cw} = \frac{(\tilde{n}_2 - \tilde{n}_1) f_{rep,1} f_{rep,2} + f_{rep,1}(2f_{ceo,2} + f_{beat,2}) - f_{rep,2}(2f_{ceo,1} + f_{beat,1})}{f_{rep,1} - f_{rep,2}}$$

with $$\Delta f_{cw} = \left|\frac{-f_{rep,2}}{f_{rep,1} - f_{rep,2}}\right| \Delta f_{beat} + \left|\frac{f_{rep,1}}{f_{rep,1} - f_{rep,2}}\right| \Delta f_{beat} \simeq \frac{2f_{rep,2}}{|f_{rep,1} - f_{rep,2}|} \Delta f_{beat} \simeq 20000$$

which is too large.

However, we can determine the difference

$$m \equiv n_2 - n_1 = \frac{f_{cw} - 2f_{ceo,2} - f_{beat,2}}{f_{rep,2}} - n_1 = \frac{n_1 f_{rep,1} + 2f_{ceo,1} + f_{beat,1} - 2f_{ceo,2} - f_{beat,2}}{f_{rep,2}} - n_1$$
$$= n_1 \left(\frac{f_{rep,1}}{f_{rep,2}} - 1\right) + \frac{+2f_{ceo,1} + f_{beat,1} - 2f_{ceo,2} - f_{beat,2}}{f_{rep,2}}$$

between the mode numbers with negligible error,

$$\Delta m = \left(\frac{f_{rep,1}}{f_{rep,2}} - 1\right) \Delta n_1 \ll 1 \ .$$

This allows us to minimize the difference

$$\delta f_{cw} \equiv |f_{cw,1} - f_{cw,2}| = (\tilde{n}_1 + \delta\tilde{n}) f_{rep,1} + 2f_{ceo,1} + f_{beat,1} - (\tilde{n}_2 + \delta\tilde{n}) f_{rep,2} - 2f_{ceo,2} - f_{beat,2} = (f_{rep,1} - f_r$$

with respect to variation of an integer number $\delta\tilde{n}$. Obviously, for this to work we need that the resolution be larger than the uncertainty, $\delta f_{cw} > \Delta f_{cw}$, i.e.

$$(f_{rep,1} - f_{rep,2})\delta\tilde{n} > \Delta f_{beat}$$

for all $\delta\tilde{n} = 1, 2, ...$ Hence,

$$f_{rep,1} - f_{rep,2} > \Delta f_{beat} \ .$$

Note, that for the actual linewidth of the DLpro, $\Delta f_{beat} \approx 1$ MHz, implying $|f_{dds,1} - f_{dds,2}| > 4$ MHz.

1.33.4 The right procedure

1. Lock DLpro to cavity and measure its wavelength with a wavemeter,

$$f_{wm} \qquad \text{with} \qquad \Delta f_{wm} = 100 \text{ MHz} \ .$$

2. Watch the beat signal between DLpro and comb for two sufficiently different settings $k = 1, 2$ of the repetition rate, determine the signs of $f_{ceo,k}$ and $f_{beat,k}$, and calculate,

$$\tilde{n}_k \equiv round\left(\frac{f_{wm} - 2f_{ceo} - f_{beat}}{f_{rep}}\right) f_{rep} + 2f_{ceo} + f_{beat} \ .$$

3. Calculate the laser frequency differences,

$$\delta f_{cw} = |(\tilde{n}_1 + \delta\tilde{n})f_{rep,1} + 2f_{ceo,1} + f_{beat,1} - (\tilde{n}_2 + \delta\tilde{n})f_{rep,2} - 2f_{ceo,2} - f_{beat,2}|$$

for a set of $\delta\tilde{n} = .., -2, -1, 0, +1, +2, ..$, pick the minimum $\delta f_{cw}(\delta n_0) \simeq 0$, obtain,

$$f_{cw} = (\tilde{n}_1 + \delta\tilde{n})f_{rep,1} + 2f_{ceo,1} + f_{beat,1} \ .$$

4. Lock the DLpro to the next mode and repeat the procedures (1-4) finding f'_{cw}. The reference cavity fsr is

$$\delta_{fsr} = f'_{cw} - f_{cw} = \nu_{cw}/\tilde{N} \ ,$$

where $\tilde{N} = int(N + 0.5)$ is an integer number.
5. We compare to the strontium line, which is at $f_{wm} = 434.829121311$ THz.

1.33.5 Procedure

1.	Lock DLpro to ref. cavity (a) & read wavemeter	$f_{wm} = 434$..... THz
2.	Set $f_{dds,1a} = 20$ MHz and read beat frequency	$\lvert f_{beat,1}\rvert =$ ..... MHz
3.	Vary $f_{dds,1a} \nearrow$ via the DDS	if $\lvert f_{beat,1}\rvert \nearrow$ then $f_{beat} = -\lvert f_{beat}\rvert$
		else $\lvert f_{beat,1}\rvert \searrow$ then $f_{beat} = +\lvert f_{beat}\rvert$
4.	Unlock CEO and vary $\lvert f_{ceo}\rvert \nearrow$ via the SYNCRO	if $f_{beat} < 0$ and $\lvert f_{beat,1}\rvert \nearrow$ then f_{ceo}
		if $f_{beat} < 0$ and $\lvert f_{beat,1}\rvert \searrow$ then f_{ceo}
		if $f_{beat} > 0$ and $\lvert f_{beat,1}\rvert \nearrow$ then f_{ceo}
		if $f_{beat} > 0$ and $\lvert f_{beat,1}\rvert \searrow$ then f_{ceo}
5.	Set $f_{dds,1a} = 20.4$ MHz and read beat frequency	$\lvert f_{beat,2}\rvert =$ ..... MHz
6.	Vary $f_{dds,1a} \nearrow$ via the DDS	if $\lvert f_{beat,2}\rvert \nearrow$ then $f_{beat} = -\lvert f_{beat}\rvert$
		else $\lvert f_{beat,2}\rvert \searrow$ then $f_{beat} = +\lvert f_{beat}\rvert$
7.	Unlock CEO and vary $f_{ceo}\rvert \nearrow$ via the SYNCRO	if $f_{beat} < 0$ and $\lvert f_{beat,2}\rvert \nearrow$ then f_{ceo}
		if $f_{beat} < 0$ and $\lvert f_{beat,2}\rvert \searrow$ then f_{ceo}
		if $f_{beat} > 0$ and $\lvert f_{beat,2}\rvert \nearrow$ then f_{ceo}
		if $f_{beat} > 0$ and $\lvert f_{beat,2}\rvert \searrow$ then f_{ceo}
8.	Lock DLpro to ref. cavity mode (b) & repeat (1-7)	
15.	Run MATLAB routine	

1.33.6 First measurement

		(a)	(b)	(c)
	ν_{wm}	434.7848 THz	434.7788 THz	434.7833 THz
(1)	$f_{dds,1}$	20 MHz	20 MHz	20 MHz
	$f_{ceo,1}$	+20 MHz	+20 MHz	+20 MHz
	$f_{beat,1}$	−3.087 MHz	+13.826 MHz	−7.522 MHz
	n_1	1739139	1739114	1739130
	$\nu_{cw,1}$	434784786.913 MHz	434778803.826 MHz	434782532.478 MHz
(2)	$f_{dds,2}$	20.1 MHz	20.1 MHz	20.1 MHz
	$f_{ceo,2}$	+20 MHz	+20 MHz	+20 MHz
	$f_{beat,2}$	+22.848 MHz	+40.239 MHz	+27.261 MHz
	n_2	1738965	1738940	1738940
	$f_{cw,2}$	434784786.973 MHz	434778803.764 MHz	434782541.161 MHz
	$\nu_{wm,2} - \nu_{wm,1}$	1495787000 Hz		
	N	290672.928 Hz	290668.928 Hz	
	δ_{fsr}	1495786629.453 Hz	1495786629.448 Hz	
	ν_{Sr}	434829121.311 MHz		
	$290703\delta_{fsr} - \nu_{Sr}$	539.2300033750 MHz		
	$290702\delta_{fsr} - \nu_{Sr}$	−956.5566260625 MHz		

1.33.7 Error estimation

The largest error arises from the width of the beat signal, $\Delta f_{beat} \simeq 1$ MHz.

1.34 12.07.2015 List of projects

1.34.1 Sr1

1. Half cone on blue MOT
2. Reference cavity calibration with comb
3. Green MOT
4. Blue ray repumping
5. Atomic lighthouse
6. Sub-shot-noise spectroscopy
7. Lamb shift detection on the blue line in a red MOT (lock 922nm to comb)
8. (CBS in a hot Sr vapor, not prioritary)
9. (Mie resonances, not possible with Gaussian clouds)

1.34.2 Sr2

- BAL injection
- Vacuum chamber with indium-sealed windows

1.35 24.07.2015 Measuring the telecom laser with the comb

Rainer Blatt recommends FALC and DLpro. We should buy supercavity for 698 nm.

Why is the DLPro linewidth beat with comb so large? Check 1550 nm beat linewidth! Put DLpro beat signal to Sr1 lab and try enhancing stability!

	ν_{wm}	1550 THz
(1)	f_{dds}	19 MHz
	f_{ceo}	+20 MHz
	f_{beat}	+76 MHz
	n	6206209
	ν_{cw}	1550000813.75 MHz
(2)	f_{dds}	20 MHz
	f_{ceo}	+20 MHz
	f_{beat}	+103 MHz
	n	6200002
	f_{cw}	1550000643 MHz
(3)	f_{dds}	21 MHz
	f_{ceo}	+20 MHz
	f_{beat}	+25 MHz
	n	6193809
	f_{cw}	1550000767.25 MHz

1.36 26.07.2016 Side-of-filter locking project 1

The goal of this project is to frequency-lock two lasers with a 7.76 GHz offset [87, 27]. See also LabOptics script for phase-locking of two lasers. The side-of-filter locking

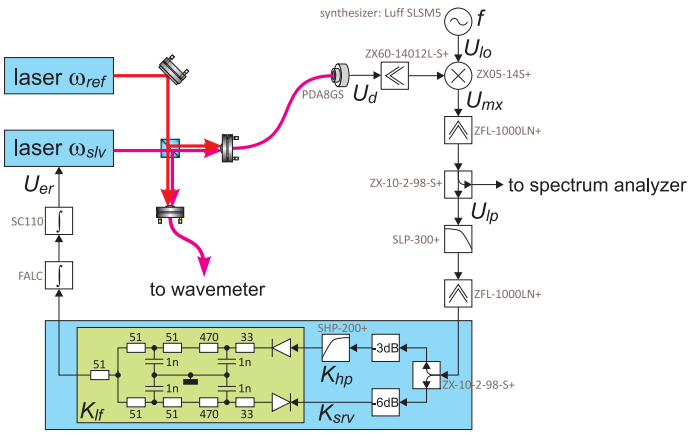

Figure 1.32: (code)

scheme basically consists locking the frequency of a slave laser to a master, while regulating the phase slip to a constant value. It is thus very different from a phase-lock.

The slave laser, which is characterized by its time-dependent frequency $\omega_{slv}(t)$, is to be stabilized to a reference laser with frequency ω_{ref}. Neglecting the phase for now, the beat frequency on the photodetector can thus be written,

$$U_d(t) = \cos[(\omega_{slv} - \omega_{ref})t] \ .$$

When demodulated with the local oscillator Ω_{lo}, the signal becomes,

$$\begin{aligned} U_{mx}(t) &= \cos[(\omega_{slv} - \omega_{ref})t] \cos(\Omega_{lo}t + 90^\circ) \\ &= \tfrac{1}{2} \sin[(\omega_{slv} - \omega_{rf})t - \Omega_{lo}t] - \tfrac{1}{2} \sin[(\omega_{slv} - \omega_{rf})t + \Omega_{lo}t] \ . \end{aligned}$$

Let us now assume that the frequency difference $\omega_{slv}(t) - \omega_{rf}$ be positive and not very far from Ω_{lo}, so that a low pass filter will block the second sine term,

$$U_{lp}(t) \simeq \tfrac{1}{2} \sin[\omega_{slv}(t) - \omega_{ref} - \Omega_{lo}]t \ ,$$

It seems clear, that when closing the feedback loop, a stationary situation can only be reached, when $U_{mx}(t) = 0$ for all times, which implies $\Delta\omega = \Omega_{lo}$.

In order to simulate the feedback loop in the time domain, we must convolute the time signal $U_{lp}(t)$ with the transfer function of the servo K_{srv},

$$\omega_{slv}(t) \propto U_{er}(t) = (K_{srv} \star U_{lp})(t) \ .$$

To do this, in the following, we first find the transfer function K_{srv} in the frequency domain for the case of the "side-of-filter locking technique" with a high-pass filtered

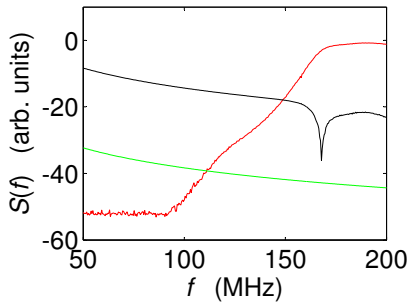

Figure 1.33: (code) Transfer functions converted from Watts to dB using $\tilde{P}[\mathrm{db}] = 10\,\lg \frac{P[\mathrm{W}]}{1\,\mathrm{mW}}$ and $P[\mathrm{W}] = 10^{\tilde{P}[\mathrm{db}]/10} \cdot 1\,\mathrm{mW}$.

branch of $f_g = 160\,\mathrm{MHz}$. The lowest order high-pass filter would be $K_{hp} = \frac{1}{1+f_g/f}$, but the MiniCircuit filter (SHP-200+) has, in fact, a much steeper cut-off slope and need to be characterized by measurement (as done in Fig. 1.33). The transfer function is obtained as the difference between two branches, one with the other without high-pass filter. Both branches are rectified separately by means of fast diodes with opposite polarities, smoothed to DC by identical low-pass filters K_{lf}, and subtracted. This is how the error signal is obtained.

1.37 28.07.2016 Birefringence of the ring cavity

The resonance frequencies of the s-polarized and the p-polarized modes of our ring cavity are very close, as calculated on 11.12.2014 for a finesse of $F = 2000$. In fact they are actually overlapping.

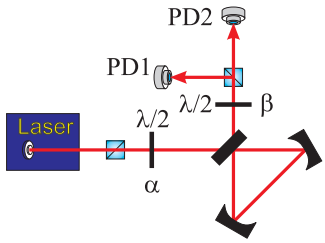

Figure 1.34: (code)

This leads to a birefringence used in the famous Hänsch-Couillaud locking scheme. The detector signal in the scheme shown in the figure may calculated via a concatenation of the Jones matrices for a $\lambda/2$-plate, the reflective response of the ring cavity, another $\lambda/2$-plate, and finally a polarizing beam splitter,

$$\begin{pmatrix} E_s \\ E_p \end{pmatrix} = \begin{pmatrix} 1 & 0 \\ 0 & 0 \end{pmatrix} \begin{pmatrix} \cos\beta & -\sin\beta \\ -\sin\beta & \cos\beta \end{pmatrix} \begin{pmatrix} \frac{1-e^{-2\pi i\omega/\delta_{fsr}+i\phi_s}}{1-R_s e^{-2\pi i\omega/\delta+i\phi_s}} & 0 \\ 0 & \frac{1-e^{-2\pi i\omega/\delta_{fsr}+i\phi_p}}{1-R_p e^{-2\pi i\omega/\delta+i\phi_p}} \end{pmatrix} \begin{pmatrix} \cos\alpha & -\sin\alpha \\ -\sin\alpha & \cos\alpha \end{pmatrix} \Bigg($$

$$= \begin{pmatrix} \frac{1-e^{-2i\pi\frac{\omega}{\delta_{fsr}}+i\phi_s}}{1-R_s e^{-2i\pi\frac{\omega}{\delta}+i\phi_s}} \cos\alpha\cos\beta + \frac{1-e^{-2i\pi\frac{\omega}{\delta_{fsr}}+i\phi_p}}{1-R_p e^{-2i\pi\frac{\omega}{\delta}+i\phi_p}} \sin\alpha\sin\beta \\ 0 \end{pmatrix} E_0 \ .$$

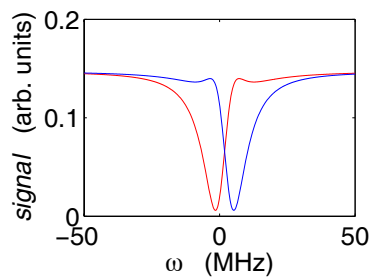

Figure 1.35: (code)

Calculating $|E_s|^2$ as a function of the laser frequency ω reproduces the observed curves.

1.38 02.08.2016 Ring cavity caracterization 1

Raul measured the free spectral range to be: $\delta_{fsr} = (8.23 \pm 0.02)\,\mathrm{GHz}$.

1.38.1 New theoretical project

We want to use an adjacent ring cavity mode as a nearly commensurate optical lattice for Bloch oscillations. Evaluate the impact on the coupled Bloch-CARL dynamics!

For a cavity mode waist at the atomic location of $w_0 = 70\,\mu\mathrm{m}$, an input power of $P_{in} = 10\,\mu\mathrm{W}$, and a finesse of $\mathcal{F} = 2000$, we expect an intracavity intensity of $I = \frac{2\mathcal{F}P_{in}}{\pi w_h w_v^2} = 2600\,\mathrm{W/cm^2}$, and,

dipole trap depth @ 689 nm	$U_{dip} = \frac{\pi c^2 \Gamma_{689} I}{2\omega_{689}^3} \frac{1}{2\pi\delta_{fsr}}$	$= 24\,\mathrm{kHz} = 1.1\ \mu\mathrm{K}$
Raleigh scattering rate	$\Gamma_{dip} = \frac{\pi c^2 \Gamma_{689}^2 I}{2\omega_{689}^3} \frac{1}{(2\pi\delta_{fsr})^2}$	$= 0.02\,\mathrm{s}^{-1}$
commensurability length	$l_{com} = \frac{c}{\delta fsr}$	$= 3.6$ cm
CARL depth for Bloch oscillations	$U_{blh} = 0.04\omega_{rec}$	$= 0.1$ kHz
lattice depth for Bloch oscillations	$W_{dip} = 3.2\omega_{rec}$	$= 15.1$ kHz
dipole trap depth @ 461 nm	$U_{dip} = \frac{\pi c^2 \Gamma_{461} I}{2\omega_{461}^3} \frac{1}{\omega_{461} - \omega_{689}}$	$= 1.1\,\mathrm{kHz} = 0.05\ \mu\mathrm{K}$

1.39 30.08.2016 MOT coils design

While having a good optical access the designed chamber does not easily permit accommodating the MOT coils along an optical axis of the MOT. Various simulations of the MOT fields have shown that a weird angle has to be chosen for the axis of the MOT coils, so that they cannot be close to the chamber requiring higher currents and water cooling.

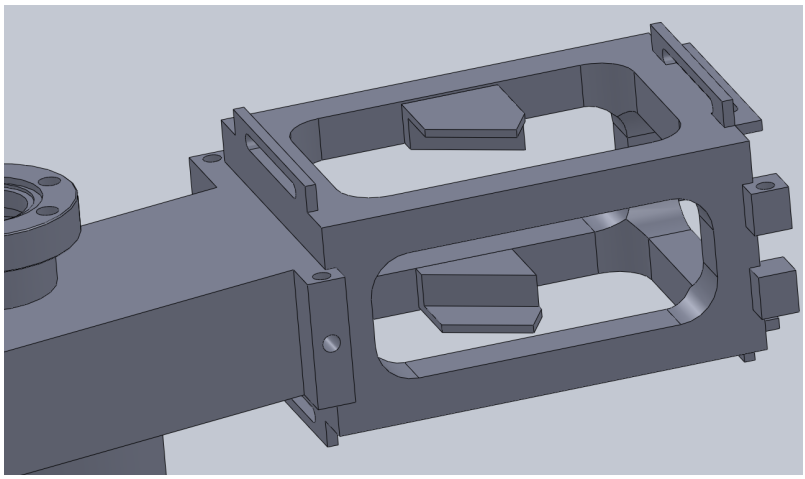

Figure 1.36: (code)

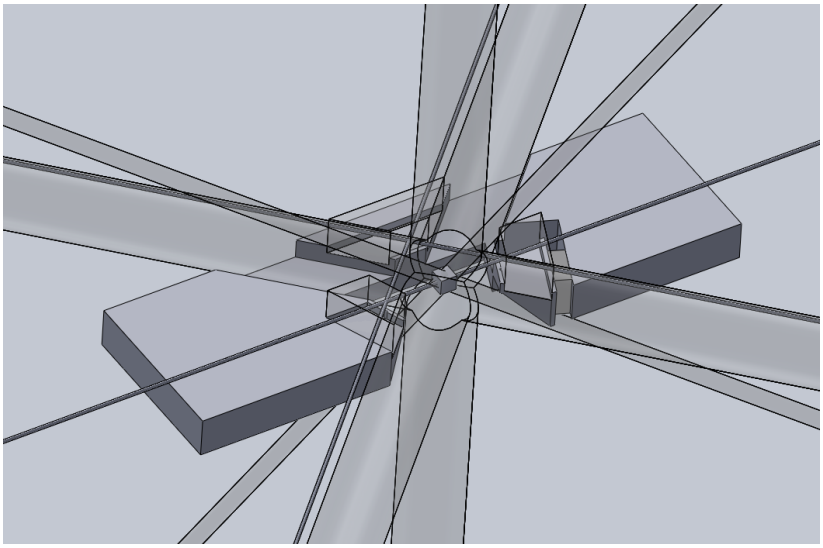

Figure 1.37: (code)

1.40 31.08.2016 New chamber design

In order to solve the MOT problem we consider redesigning the chamber. The goal is to use HighFinesse power supplies or at least minimize the switch-off problems due to excessive inductance. The objective must be to limit the inductance to $L = 100\ \mu$H. We need to buy new vacuum components for about US$10000.

Feasability of optical dipole trap: In order to match the cavity mode periodicity $\lambda_{sr} = 689$ nm, the optical standing wave created by two beams intersecting under an angle β need to have the wavelength

$$\lambda_{dip} = \lambda_{Sr} \sin(\beta/2) \ .$$

Furthermore, it must be red-detuned to the strong transition at 461 nm.

constraint	$\beta/2$	λ_{dip} [nm]
optical access given	17°	201
optical access given	25°	291
stable trapping	42°	461
stable trapping	45.1°	488
stable trapping	50.6°	532
2nd order	20.7°	488
2nd order	22.2°	520
2nd order	22.7°	532

The table shows, that standard Bloch-CARL is NOT feasible with the new setup. However, 2nd order Bragg scattering may be possible, i.e. the lattice for the Bloch oscillations has twice the lattice constant of the CARL resonant wavelength λ_{sr}.

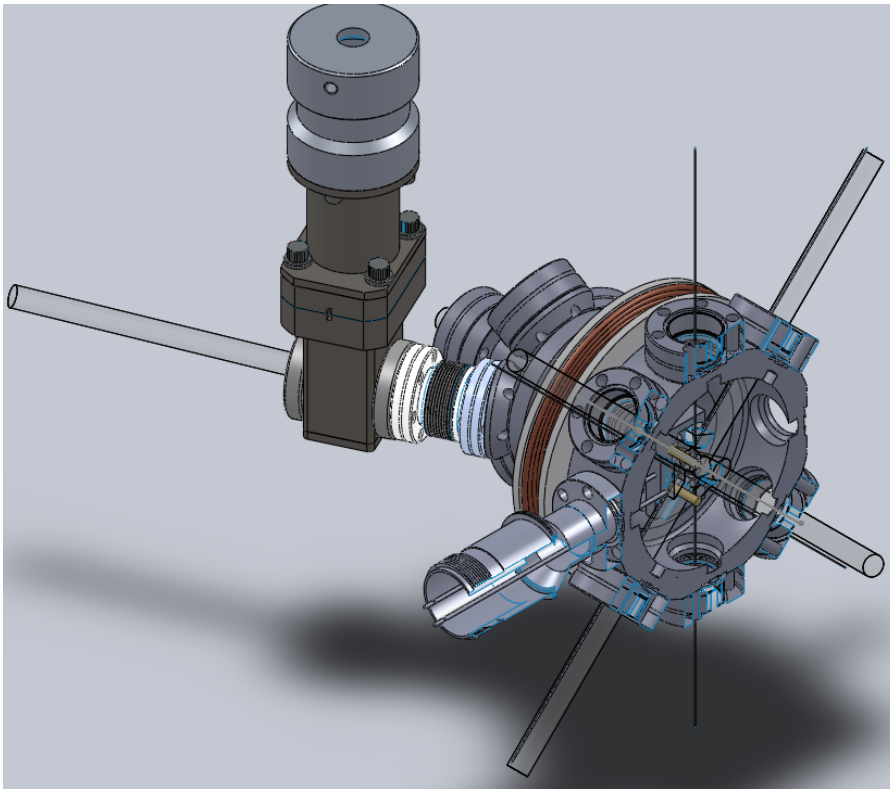

Figure 1.38: (code)

1.41 01.09.2016 New MOT coils design

Choosing $N = 28$ and for the design shown in the figure we estimate an inductance of $L = 72\ \mu$H not taking into account eddy currents. Using $\rho_{Cu} = 2 \cdot 10^{-8}\ \Omega$ we estimate a total resistance of $R = 0.04\ \Omega$. The required gradient of 70 G/cm is reached with 40 A.

We still need to estimate the heat production and dissipation...

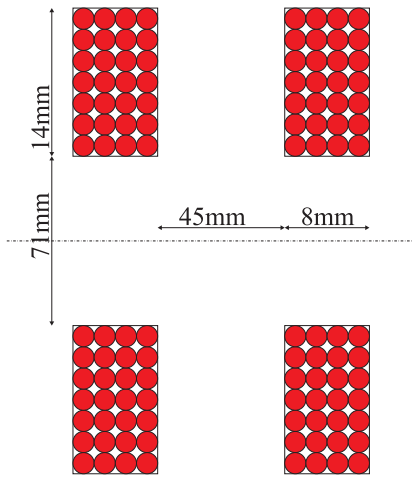

Figure 1.39: (code)

1.42 06.09.2016 Bloch-CARL on a higher harmonic?

The standard Bloch-CARL equations were,

$$i\hbar\frac{\partial\psi(x,t)}{\partial t} = -\frac{\hbar^2}{2m}\frac{\partial^2\psi(x,t)}{\partial x^2} - i\hbar U_0\left[\alpha(t)e^{2ik_0x} - \alpha^*(t)e^{-2ik_0x}\right]\psi(x,t) - mgx\psi(x,t) + \hbar\frac{W_0}{2}\sin(bk_0$$

$$\frac{\partial\partial\alpha(t)}{\partial t} = NU_0\int|\psi(x,t)|^2e^{-2ik_0x}d(2k_0x) + (i\delta-\kappa)\alpha(t)\ ,$$

or in the moving frame,

$$\frac{\partial\tilde{\psi}}{\partial t} = \frac{i\hbar}{2m}\left(\frac{\partial}{\partial x} + \frac{2imgt}{\hbar}\right)^2\tilde{\psi} - U_0\left[\alpha e^{2ik_0x} - \alpha^*e^{-2ik_0x}\right]\tilde{\psi} - \frac{W_0}{4}\left(e^{bik_0x} - e^{-bik_0x}\right)\tilde{\psi}$$

$$\frac{\partial\alpha}{\partial t} = NU_0\int|\tilde{\psi}|^2e^{-2ik_0x}d(2k_0x) + (i\delta-\kappa)\alpha\ .$$

The parameter $b = 1, 2$ stands for the periodicity of the applied standing wave potential. Inserting the expansion $\tilde{\psi} = \frac{1}{\sqrt{2\pi}}\sum_n C_n(t)e^{bink_0x}$, we obtain

$$\sum_n\frac{\partial C_n}{\partial t}e^{bink_0x} = -i\omega_r\sum_n e^{bink_0x}\left(bn + \frac{2mgt}{\hbar k_0}\right)^2C_n - U_0\sum_n\left(\alpha e^{(2+bn)ik_0x} - \alpha^*e^{(-2+bn)ik_0x}\right)C_n$$

$$\frac{\partial\alpha}{\partial t} = \frac{NU_0}{2\pi}\sum_{m,n}\int C_nC_m^*e^{i(bn-bm-2)k_0x}d(2k_0x) + (i\delta-\kappa)\alpha\ .$$

and

$$\frac{\partial C_n}{\partial t} = -i\omega_r\left(bn + \tfrac{2mgt}{\hbar k_0}\right)^2C_n - U_0(\alpha C_{n-2/b} - \alpha^*C_{n+2/b}) - \tfrac{W_0}{4}(C_{n-1/b} - C_{n+1/b})$$

$$\frac{\partial\alpha}{\partial t} = NU_0\sum_{m,n}C_nC^*_{(bn-2)/b} + (i\delta-\kappa)\alpha\ .$$

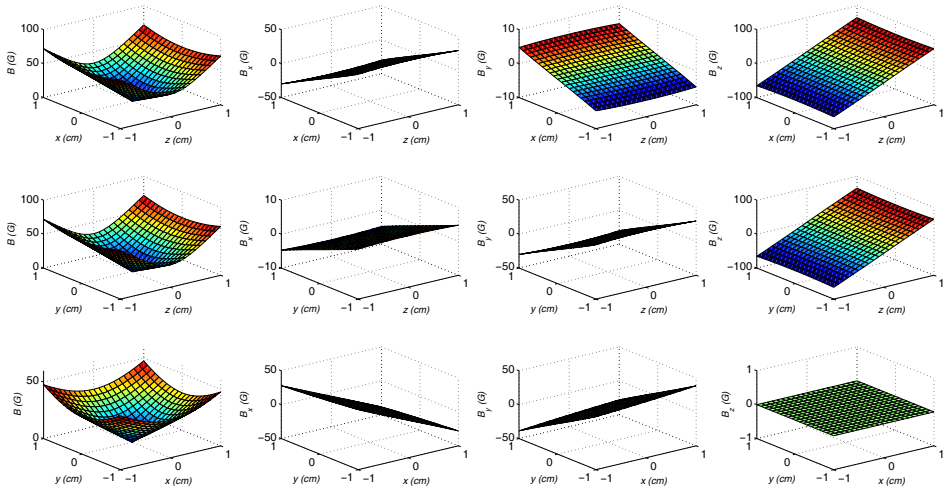

Figure 1.40: (code)

For $b = 2$ we recover the old Bloch-CARL equations, for $b = 1$ we obtain,

$$\frac{\partial C_n}{\partial t} = -i\omega_r \left(n + \tfrac{2mgt}{\hbar k_0}\right)^2 C_n - U_0(\alpha C_{n-2} - \alpha^* C_{n+2}) - \tfrac{W_0}{4}(C_{n-1} - C_{n+1})$$
$$\frac{\partial \alpha}{\partial t} = NU_0 \sum_{m,n} C_n C_{n-2}^* + (i\delta - \kappa)\alpha \ .$$

1.43 28.09.2016 Ring cavity alignement

The incidence angle seems to be 42° instead of 45°. We need to check carefully the optical access in the vacuum chamber!

I checked (substituting the reference cavity by a semitransparent mirror, that with the following setup we can stabilize two lasers simultaneously to the cavity by separating their polarizations in such a way that each PDH detector only receives the signal from one of the lasers.

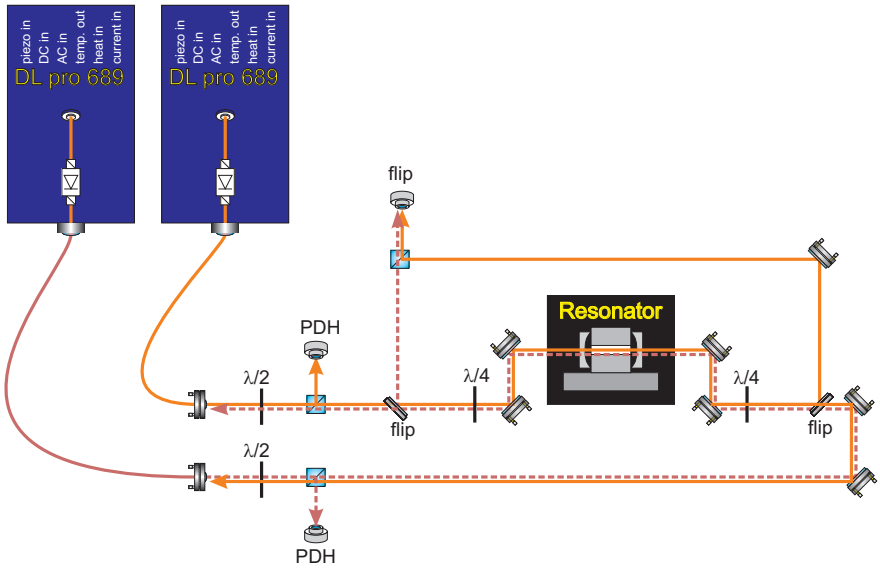

Figure 1.41: (code)

1.44 04.10.2016 Wavemeter readings

transition	frequency [THz]	WS30 readings	wavenumber vacuum [cm^{-1}]
461 nm	650.503 226	325.251 85	15 372.7139
497 nm	603.285 674	301.642 88	16 575.8950
689 nm (master)	434.828 994	434.828 15	22 997.5464
689 nm (slave)		434.828 95	
403 nm	743.252 960	743.	13 454.3695
679 nm	441.332 451	441.	22 658.6555

Toptica current drive settings. "pos" is chosen for cathode-grounded laser diodes (the − pin is connected to the case); "neg" is chosen for anode-grounded laser diodes (the + pin is connected to the case). Our homebuilt drives only work for "neg":

laser	diode	polarity
461 nm (Sr2)	?	pos
461 nm (slave)	Nichia NDBA116T	not grounded, pos chosen, needs up to 500 mA
461 nm (slave)	Nichia NDB7675	?
403 nm	Sanyo DL5146	pos
679 nm	Hitachi HL6738MG	?, pos chosen
689 nm (master Sr1)	?	neg
689 nm (slave Sr1)	Hitachi HL6738MG	?, pos chosen
689 nm (master Sr2)	?	pos
689 nm (master Sr2)	?	pos

1.45 10.10.2016 2D MOT alignement

Is it possible to run the 2D MOT with a single beam?

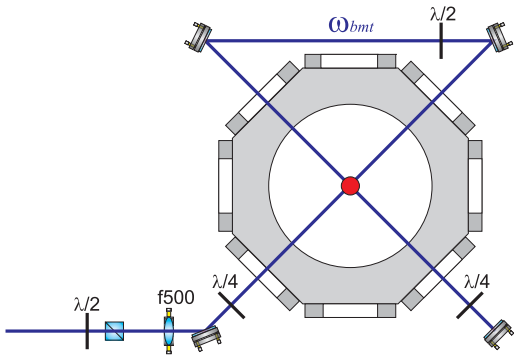

Figure 1.42: (code)

We evacuate the chamber and align the optics in double-pass retroreflection. Although we do not bake, the vacuum gauge and the 2l ion pump indicates pressures far below 10^{-8} mbar. It seems that the strontium acts like a getter. We observe strong fluorescence.

The operation of the Sr dispenser poses some problems, as they seems to coat the windows. A big blob (probably indium) has deposited inside the chamber. The dispenser should have been mounted upside down according to the Alvatec manual. We decide to vent the 2D-MOT chamber with Argon and to replace and clean the windows 1 by 1. It worked and we can see fluorescence again.

1.45.1 Blue laser locking

We have problems with the saturation spectroscopy on the strontium cell. After various tests with different AOM modulation parameters, lock-in amplifiers, DigiLock and LIR, we come to the conclusion that applying the modulation to the AOM is a BAD idea: Modulation amplitudes which are sufficient for the 33 MHz broad line necessarily result in huge AM modulation dramatically overwhelming the FM modulation and spoiling the error signal.

Either go back to directly modulate the laser or apply sidebands and do FM spectroscopy. Unfortunately, the sidebands generated by the Toptica SHG are not available in the blue (20 MHz modulation, ¡5 MHz linewidth). Changing the modulation frequency to its lower limit 12 MHz completely distorts the error signal.

1.45.2 22.11.2016 The 2D MOT works

Between 650.5027 THz and 650.5050 THz (measured with the WS6 wavemeter) we see fluorescence from atom ejected by the dispenser run at 4.0 A. Around 650.5039 THz we see a tiny very frequency-dependent spot close to the center of the chamber. Should be at 650.5032260 THz. Remember that all isotopes are within 300 MHz.

1.45.3 25.11.2016 Problem

The windows are coated again. We need to redesign the chamber to prevent this. Perhaps an oven would be better?

The necessary modifications are

- insert baffles or mount the windows on extensions
- place the dispenser upside down
- place an additional window (instead of the current blind flange) for monitoring fluorescence
- increase the size of the hole for differential vacuum

Possible modifications are

- use Ar buffer gas for the heatpipe
- 2D MOT with repumper?

1.46 14.11.2016 Round table with John, Tiago and Romain

Establish analogy between cavity and HMMs:

- Consider dispersion in ω (e.g., increasing the finesse of a cavity) and $\mathbf{k}$ (e.g., increasing the degeneracy of transverse modes in a cavity). What is the difference with respect to Ω, Γ and κ?

- What is the analogy of the resonant behavior of the cavity in an HMM, the layer thickness of the HMM stacks?

What are the conditions for backaction, limited sizes of the structures supporting the optical modes?

Anti-Casimir?

Anti-Purcell, cloaking

Using atoms to measure HMM rather than vice versa?

What is it that we want to measure? Forces, fields, presence of atoms?

PRL 117, 203003 (2016)

Topological structures?

1.47 18.11.2016 Round table with John, Tiago and Romain

We decide to define our research line in agreement with realistic experimental objectives. This means:

- We give up the idea of controlling the atomic position, as this requires ultracold atoms and the possibility to control strong Casimir-Polder forces at distances below 1 μm. Nevertheless, we will think about ways (evtl. in cooperation with Francois Impens from UFRJ) to control the Casimir-Polder forces (e.g., by special types of metamaterials or nanostructured surface geometries).

- This implies that we give up the idea of sensing the internal or the motional state of individual atoms. Instead, we will now aim sensing *density distributions*. Hence, we need spatial resolution. For example, we consider fiber nanotips sticked into MOTs or dipole-trapped atomic clouds or (nano-)fibers traversing atomic clouds.

- Apart from the atomic density distribution, we want to measure the *spatial light distribution* inside optically pumped clouds. A correlation between both, density and light intensity distributions, may allow to reconstruct the spatial distribution of optical modes and evtl. identify localization effects, local synchronization of atomic dipoles, photon bubbles, etc..

1.47.1 Strategy for measuring light modes:

1. Pump an atomic cloud resonantly (MOT) and stick the end of a fiber into the cloud at position $\mathbf{r}$ along the axis $\hat{\mathbf{e}}_z$ that collects the radiation $\hat{\mathbf{e}}_z \cdot \mathbf{E}(\mathbf{r}, \mathbf{k})$.

2. Use our coupled dipoles model to calculate the local light field distribution in a MOT, $\mathbf{E}(\mathbf{r}, \mathbf{k})$.

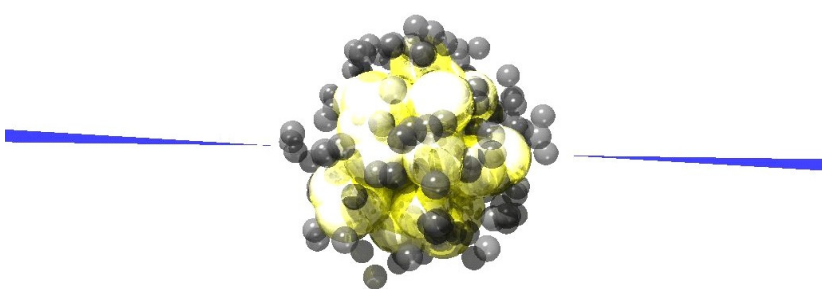

Figure 1.43: (code) Artist's view of a fiber nano tip sensing light modes within an atomic cloud.

1.47.2 Strategy 1 for measuring atomic density distributions:

1. Stick into the cloud at position **r** the end of a nanostructured fiber tip pumped with off-resonant light at 1064 nm.

2. Detect in the far field the light scattered off the fiber nanotip due to the presence of atoms with external detectors.

1.47.3 Strategy 2 for measuring atomic density distributions:

1. Fabricate nanostructured fiber tip (e.g., ring-shaped slit irradiated from behind with radially polarized light plus central cone and circular reflecting wall, the whole structure attached to the end of a fiber, check feasability!)

2. Excite the atoms resonantly and detect the light collected by the fiber.

3. Instead of using nanofabricated slits, we may think of applying HMM-like layers to the walls of the fiber (photonic crystal fiber) or to the walls of the cone formed by a fiber tip to manipulate the Purcell factor.

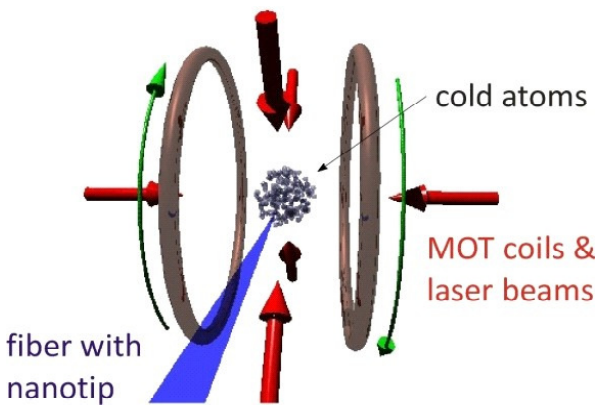

Figure 1.44: (code) Probing cold atoms with fiber nano tips.

1.47.4 Other comments:

In a MOT we have densities below $10^{11}/\mathrm{cm}^3$ corresponding to mean interatomic distances of 1 μm. In optical dipole traps one might reach [PRL81,69(1998)] $n < 10^{12}/cm^3$, in condensates $n < 10^{13}/cm^3$. Hence, there is no need to make very small tips. On the contrary, it is more interesting to increase the probing mode volume.

Work for Tiago:

- Extend his spherical calculations to cylindrical geometries?

- Can he calculate the impact of an atom on a (coated) sphere excited by an evanescent wave (or plasmon) at 1064 nm? Will the mode volume be deformed? Will the sphere radiate at 1064 nm?
- How to involve Ben-Hur? Can we define a common (theoretical) project with Ben-Hur, John, Romain and Tiago?

1.48 07.12.2016 Vacuum considerations

The 2 mm diameter aperture for differential pumping seems quite small for ajusting the 2D-MOT atomic beam. In order to decide whether we can increase it, we estimate the reachable vacuum based on our calculations for the Sr1 experiment from 28.1.2011:

Outgasing of the science chamber : Estimating the volume of the science chamber to $V_{chb} \approx 0.2$ l and the surface to $F_{chb} \approx 200$ cm^2, we estimate an outgassing rate of,

$$Q_{out} = R_{stl} F_{chb} = 7 \times 10^{-11} \text{ mbar l/s} ,$$

where $R_{stl} = 0.3 \times 10^{-12}$ mbar l/(s cm^2) is the outgassing rate of 316 steel after 2 weeks bake out at 250°.

Flow rate through the connecting tube : The differential pumping tube has a diameter of $D_a = 2$ mm and a length of $L_t = 3.5$ cm. Hence, the impedance is,

$$S_{tub} = \left(\frac{1}{S_A} + \frac{1}{S_T} \right)^{-1} = \left(\frac{4}{\bar{v}\pi D_a^2} + \frac{L_t}{\bar{v}\pi D_a^3} \right)^{-1} = 7 \cdot 10^{-2} \text{ l/s},$$

where $\bar{v} = 120$ m/s is the mean velocity of room temperature atoms. Assuming a background pressure in the 2D-MOT chamber of $P_{2d} = 10^{-8}$ mbar, the flow rate now becomes,

$$Q_{tub} = P_{2d} S_{tub} = 7 \cdot 10^{-10} \text{ mbar l/s} .$$

Quintessence: This is an order of magnitude larger than the outgassing rate. Hence, increasing the aperture diameter is a risk! Or we have to improve the 2D-MOT vacuum by an order of magnitude.

Pressure in the chamber : The pressure in the chamber P_{chb} results from an equilibrium between the feeding and the pumping,

$$Q_{pmp} = Q_{out} + Q_{tub} . \tag{1.1}$$

Let us assume that the full pumping speed of a $S_{pmp} = 40$ l/s ion pump is available. Then,

$$P_{chb} = \frac{Q_{out} + Q_{tub}}{S_{pmp}} \simeq 0.8 \cdot 10^{-10} \text{ mbar} . \tag{1.2}$$

Quintessence: We need to improve the pumping rate by one order of magnitude. Note, however, that titanium sublimation pumps or nonevaporable getter pumps can yield pumping rates of 1000 l/s!

1.49 03.01.2017 Project light localization in a glass surface

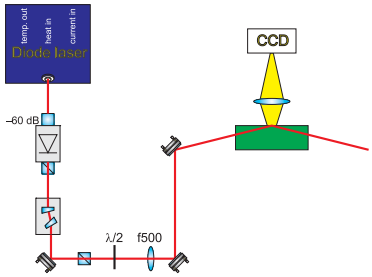

Figure 1.45: (code) Scheme for the experiment.

1.50 02.03.2017 Laser-controlled SrO desorption

An important advantage of 2D-MOTs over Zeeman slowers is their feature to preselect the desired Sr isotope. But both share the inconvenience of being fed from hot atom sources, i.e., oven or dispensers.

The Birmingham group seems to have found an alternative way of putting *cold* Sr atoms into the vacuum. We plan to test their proposal [57] to check whether it might be suitable for heatpipes or even to feed the 2D-MOT of Sr2.

Typical flux for ^{40}K is $5 \cdot 10^8$ s^{-1}.

1.51 10.03.2017 Side-of-filter locking project 2

The locking circuit works for the first time using the FALC slow branch (correction signal going via the backbone to the SC110 unit). It is very easy and stays locked at 172 MHz, but the beat frequency fluctuates within 10 MHz. Certainly the PID need some adjustments.

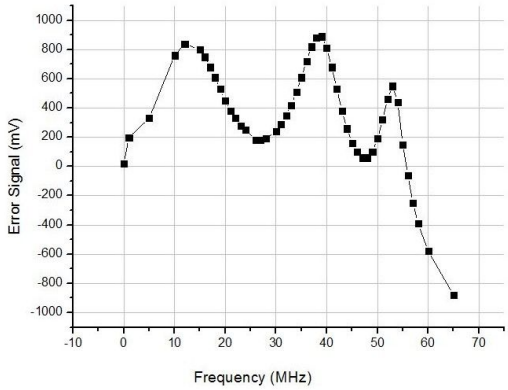

Figure 1.46: (code)

A direct PLL, connecting the mixer output to the FALC did not work, although the error signal was visible. Is the laser noise too strong? Do we need a loop filter?

To fine-tune the filter we plan to make a PLL locking a VCO to the Luff synthesizer, simplifying the scheme of day 26.07.2016. The PID could be designed in a similar way as for the intensity stabilization.

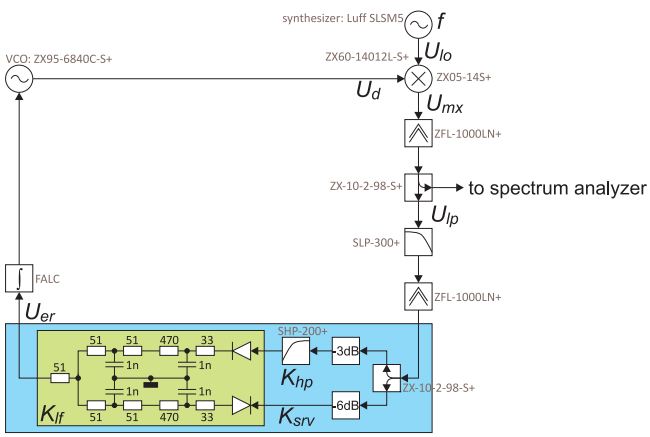

Figure 1.47: (code)

1.51.1 Update from 10.04.2017

The Luff synthesizer does not work! In fact it never worked reliably, but only sporadically. Can we send it back? Buy a Rohde&Schwarz at 8 GHz? For Camila we have to downgrade using a 4 GHz VCO and a 5 GHz synthesizer borrowed from the BECs.

1.52 16.03.2017 Cat eye laser project

1.52.1 Alignment

The alignment is done with a pair of $\alpha = 2°$ wedged, 2mm thick, AR-coated substrates. With the refraction index $n_{BK7} = 1.5243$ at 461 nm and $n_{BK7} = 1.5134$ at 689 nm, we expect a deviation angle of $\arcsin(n_{BK7} \sin\alpha) \simeq 3°$ after the first wedge and between 0° and 6° after the second wedge. If the laser beam is originally aligned to the z-axis, $\mathbf{n}_{in} = \hat{\mathbf{e}}_z$, and $\theta_{1,2}$ are the rotation angles of the wedges, then

$$\mathbf{n}_{out} = \begin{pmatrix} \arcsin(n_{BK7}\sin\alpha)(\cos\theta_1 - \cos\theta_2) \\ \arcsin(n_{BK7}\sin\alpha)(\sin\theta_1 + \sin\theta_2) \\ 1 \end{pmatrix} .$$

1.52.2 Tuning

Wavelength tuneability of the interference filter:

$$\lambda = \lambda_{max}\sqrt{1 - \frac{\sin^2\theta}{n_{eff}^2}} .$$

With $n_{eff} \simeq 2$ and $\theta = 6°$ for $\lambda_{max} = 706$ nm, we expect the following tuning curve.

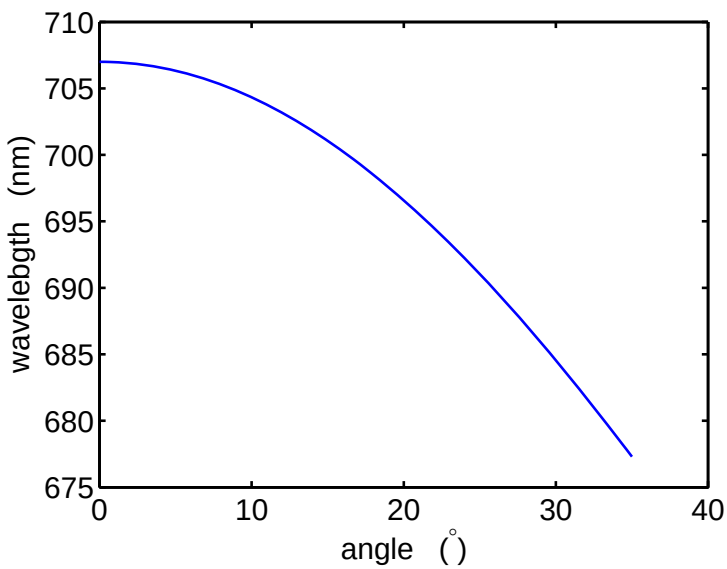

Figure 1.48: (code)

Typical dimensions for the interference filter are $L = 0.5$ mm, $n_{refr} = 1.45$,

$T_{total} = 90\%$, $\Delta\lambda = 0.3$ nm. With this

$$\delta_{fsr} = \frac{c}{2Ln_{refr}} = 200\,\text{GHz} \quad , \quad \kappa/2\pi = \frac{c\Delta\lambda}{\lambda^2} = 190\,\text{GHz} \quad , \quad F = \frac{2\pi\delta_{fsr}}{\kappa} = 1 = \frac{\pi\sqrt{R}}{1-R}$$

1.53 28.03.2017 Sr2 reference cavity

I mounted the ATFilms supercavity and evacuated it to $2.3 \cdot 10^{-7}$ mbar using the 10 l ion getter pump.

The supercavity is specified for a finesse of at least $F = 250000$. The transmission of the cavity mirrors has been measured to be $T = 0.0005\%$. Using $F = \frac{\pi\sqrt{R}}{1-R}$ we can estimate the reflection of the mirrors $R \simeq 1 - \frac{\pi}{F} = 0.999988$ and an absorption of $S = 1 - R - T = 0.0007\%$.

Using the Airy formula

$$E_{refl}(\delta) = E_{in}\left(\sqrt{R}\frac{1-(R+T)e^{-i\omega/\delta_{fsr}}}{1-Re^{-i\omega/\delta_{fsr}}}\right)$$

We may estimate the reflected intensity on resonance

$$I_{refl}(0) = |E_{refl}(0)|^2 = E_{in}^2\frac{RS^2}{(1-R)^2}$$

and the contrast of the reflection dip

$$\frac{I_{in} - I_{refl}(0)}{I_{in}(0)} = 1 - \frac{RS^2}{(1-R)^2} \simeq 0.66 \ .$$

This is the best constrast that we may expect. In fact, I measured a contrast of only 0.4. The reason for this is probably imperfect mode matching of the injected beam.

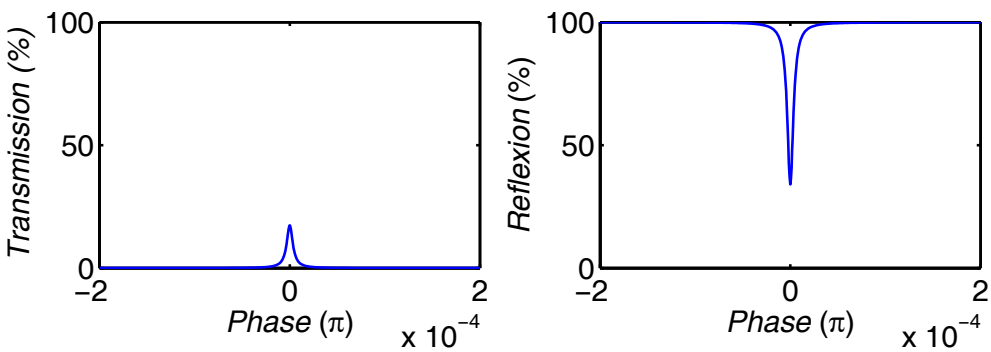

Figure 1.49: (code)

The supercavity is $d = 10$ cm long, has one flat mirror ($\rho_1 = \infty$) and a curved one with $\rho_2 = 500$ mm radius of curvature,

$$w_1^4 = \frac{\lambda^2\rho_1^2}{\pi^2}\frac{\rho_2 - d}{\rho_1 - d}\frac{d}{\rho_1 + \rho_2 - d} \longrightarrow \frac{\lambda^2}{\pi^2}(\rho_2 - d)d$$

$$\Longrightarrow w_1 = \left[\left(\frac{689 \cdot 10^{-9}}{\pi}\right)^2 (0.5 - 0.1) \cdot 0.1\right]^{1/4} = 209.44 \ \mu\text{m} \ .$$

Also,

$$w_2^4 = \frac{\lambda^2 \rho_2^2}{\pi^2} \frac{\rho_1 - d}{\rho_2 - d} \frac{d}{\rho_1 + \rho_2 - d} \longrightarrow \frac{\lambda^2}{\pi^2} \frac{\rho_2^2 d}{\rho_2 - d}$$

$$\Longrightarrow w_2 = \left[\left(\frac{689 \cdot 10^{-9}}{\pi} \right)^2 \frac{0.5^2 \cdot 0.1}{0.5 - 0.1} \right]^{1/4} = 234.16 \ \mu\text{m} \ .$$

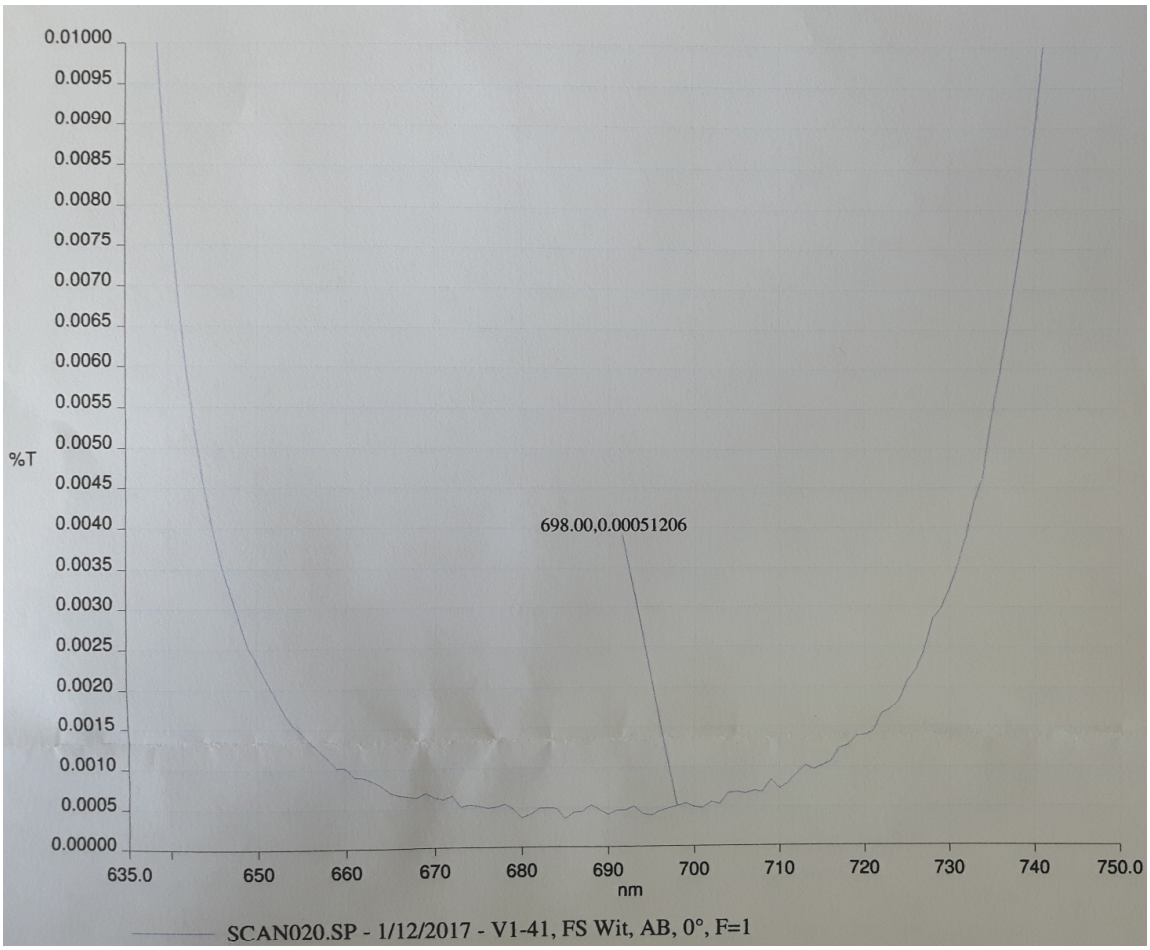

Figure 1.50: (code)

Locking the laser to the supercavity I observe fluctuations in the transmission well below $K = 10\%$. From this we can give a course estimation of the laser linewidth. Using the lorentzian approximation of the Airy formula near resonance,

$$I_{tr}(\Delta) \simeq I_{in} \frac{(\kappa/2)^2}{(\kappa/2)^2 + \Delta^2} \ ,$$

we get from,

$$\frac{I_{in} - I_{tr}}{I_{in}} \ll K$$

that

$$\frac{\Delta}{\kappa/2} \ll \sqrt{K} \ ,$$

where κ is the FWHM of the intensity transmission profile and related to the finesse via,

$$\kappa = \frac{2\pi\delta_{fsr}}{F} \simeq (2\pi)\ 6 \text{ kHz} \ .$$

Hence, laser linewidth is $\Delta\omega \ll 950$ Hz.

1.54 28.03.2017 Point grey camera

Type: Chameleon CMLN-13S2M
SN: 11445230
Pixelnumber: 1296×964 Pixelsize: 3.75 μm

Software: FlyCap2

1.55 04.04.2017 Reference cavity finesse

I measured a cavity decay time of 20 μs. This corresponds to a finesse of $F = 2\pi\delta_{fsr}\tau = 188000$. The finesse being lower than the guaranteed specification, we also expect a larger FWHM transmission linewidth,

$$\kappa/(2\pi) = \frac{\delta_{fsr}}{F} = 7961.6 \text{ kHz} ,$$

corresponding to a reflection of $R = 1 - \frac{\pi}{F} = 0.999983$. Given a transmission of $T = 0.000005$, the losses are

$$S = 1 - T - R = 11.7 \text{ ppm} .$$

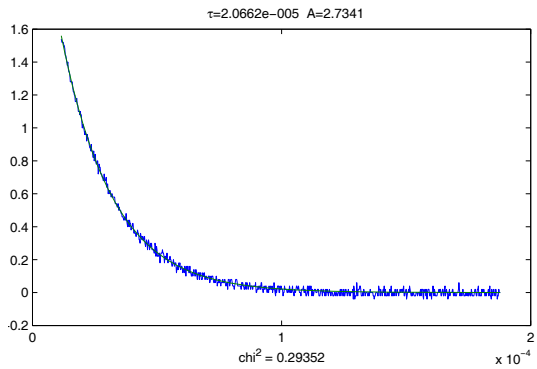

Figure 1.51: (code)

The pressure in the reference cavity chamber is now at $1.3 \cdot 10^{-7}$ mbar.

1.56 05.04.2017 Reference cavity locking

Valentin and me did a beat frequency measurement between the Sr1 injection locked red slave laser and the Sr2 laser. Both DLpro were PDH-locked to their respective reference cavities. The Sr1 slave laser was tuned via the synthesizer (+832 MHz) and the +110 MHz AOM to the Sr line. The beat frequency was found at 382 MHz, increasing the Sr2 laser frequency would reduce the beat frequency.

Hence, the resonance frequency of the supercavity at room temperature around 689 nm has to be (832 − 382) MHz above the Sr1 reference cavity. It also has to be (382 + 110) MHz below the Sr line.

The width of the beat signal, found to be below 1 kHz, is due to 1) the emission band with of the Sr1 and the Sr2 laser, 2) the tightness of the injection lock, 3) the noise of the synthesizer driving the 832 MHz AOM, and 4) acoustic noise coupling to the optical fiber.

Setting the modulation frequency of the PDH of both lasers to different values (17.1 and 19.6 MHz) I was able to lock both lasers simultaneously to the same (or different) supercavity modes. The beat frequency of both lasers was found at 1.496 772 5 GHz and exhibited < 1 kHz linewidth. This is a summary of the reference frequencies available at the Sr labs:

$$
\begin{aligned}
\nu_{Sr} &= 434.829121311 \text{ THz} \\
\nu_{cav,Sr1} &= 434.828164739 \text{ THz} \\
\delta_{fsr,Sr1} &= 1.495796921 \text{ GHz} \\
\nu_{cav,Sr2} &= \nu_{cav,Sr1} - (832 + 110) \text{ MHz} = 434.828614\ (10) \text{ THz} \\
\nu_{cav,Sr2} &= \nu_{Sr} - (382 + 110) \text{ MHz} = 434.828629\ (10) \text{ THz} \\
\delta_{fsr,Sr2} &= 1.4967725\ (10) \text{ GHz} .
\end{aligned}
$$

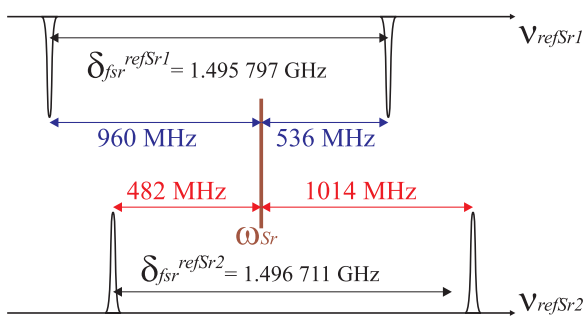

Figure 1.52: (code)

From these data we may estimate the mode number of the cavity,

$$N = \frac{\nu_{cav,Sr2}}{\delta_{fsr,Sr2}} \approx 290510.8 .$$

The uncertainty is,

$$\Delta N = \left|\frac{\partial N}{\partial \delta_{fsr,Sr2}}\right| \Delta\delta_{fsr,Sr2} + \left|\frac{\partial N}{\partial \nu_{cav,Sr2}}\right| \Delta\nu_{cav,Sr2} \simeq \frac{N}{\delta_{fsr,Sr2}} \Delta\delta_{fsr,Sr2} \approx 0.2 \ .$$

The fsr uncertainty is in the 7-th digit and therefore dominates the light frequency uncertainty which is in the 8-th digit.

Actually, the cavity is a room temperature $T_{room} = 22°\text{C}$. The thermal expansion coefficient of ULE between 5 and 35°C is $\alpha = \frac{\Delta L}{L\Delta T} \approx 10^{-8}$ K^{-1}. Hence, the cavity can vary up to

$$\frac{\Delta\nu_{cav}}{\Delta T} = \alpha\nu_{cav} \simeq 4.3 \text{ MHz K}^{-1} \ .$$

The cavity will be heated to about $T_{zero} = 37°\text{C}$, where α is expected to cross zero. Hence, the resonance frequency may shift up to,

$$\Delta\nu_{cav} = 4.3 \text{ MHz K}^{-1}(T_{room} - T_{zero}) \simeq 64.5 \text{ MHz} \ .$$

1.57 11.04.2017 Stabilizing the phase of a standing wave in a ring cavity

Shaking atoms around in a standing wave can heat them up. Here is a scheme to prevent phase and intensity fluctuations:

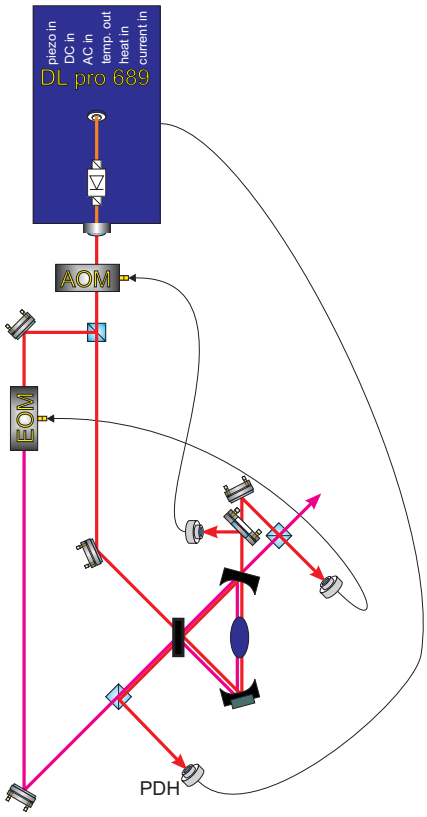

Figure 1.53: (code)

1.58 12.04.2017 Operating the frequency comb 3

1.58.1 Using the SYNCRO to phase-lock the two DLpros.

I installed the LLE3 SYNCRO device to try to phase-lock the two red lasers. The comb electronics made a strange noise, like an exploding capacitor. Same thing as on 11.06.2015. The strange smell seems to be coming from the piezo unit (like a burned capacitor).

The phase locking idea seems to work more or less: the lasers are locked at 20 MHz, but the beat signal looks 10 MHz broad! Try PDH-locking one laser to the supercavity. Try mixing up the difference signal 8 GHz!

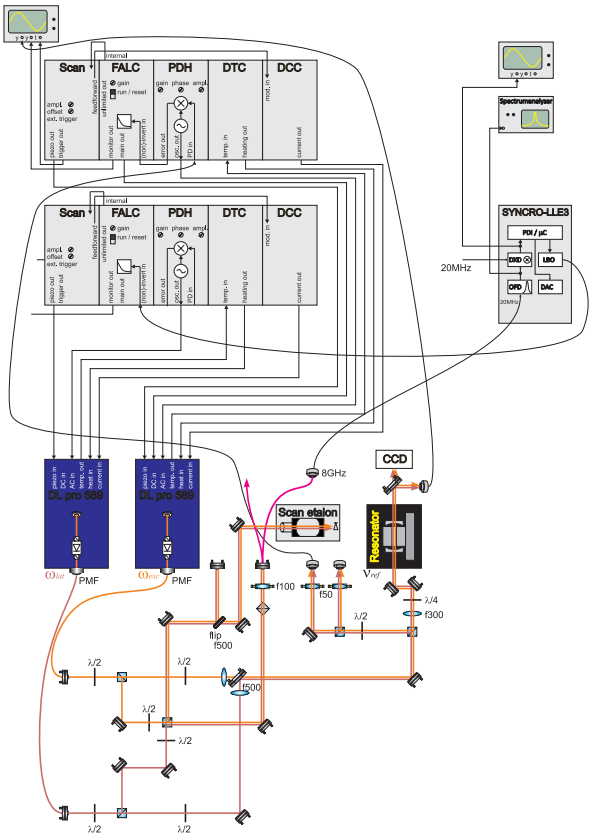

Figure 1.54: (code)

1.58.2 Switching on the comb

I did not manage to lock the RRE, while CEO lock work nicely. Is it configured to be locked by a laser.

There is a high voltage between the grounds of the comb and the 10 MHz reference signal. Ask Daniel whether this is normal.

1. Switch on computer, oscillator, amplifiers, DDS and everything else, start comb control software.
2. Adjust CEO phase plate looking at the analyzer (peak needs to be close to 20 MHz) and the scope (the ramps should be flat), lock the CEO.
3. Adjust RRE.

1.59 20.10.2017 Supercavity modes 1

Heating the supercavity with 1 A for about 3 h I reach the final temperature of 33°C. The thermistor has a resistance of 7.097 kHz at this temperature. Resistance variations of $\Delta R = 0.01\ \Omega$ correspond to temperature shifts of $\Delta T = 0.035$°C. According to the SLS specsheet a temperature variation of $\Delta T = 3$°C causes a beat frequency variation of 1 MHz.

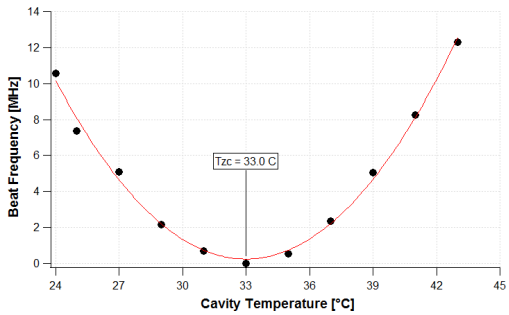

Figure 1.55: (code) Temperature calibration curve of the ULE spacer.

At $T = 33$°C the chamber pressure rises to $2.4 \cdot 10^7$ mbar. I use $I = 0.7$ A to maintain the cavity at this temperature.

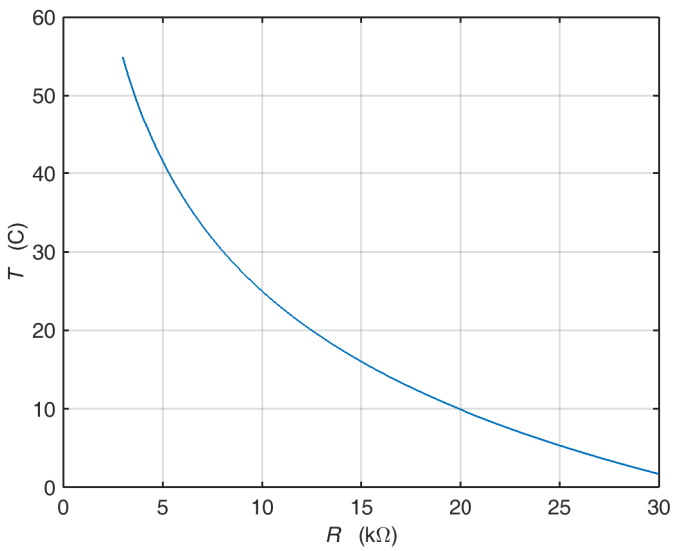

Figure 1.56: (code) Temperature calibration curve of the thermistors.

Measuring the cavity modes with the wavemeter I get at $I_{heating} = 0.63$ A and

$R = 7.07$ kΩ and $p = 1.4 \cdot 10^{-7}$ mbar,

$$\nu_{Sr2,refcav} = \begin{array}{r} 434.82555 \text{ THz} \\ 434.82705 \text{ THz} \\ 434.82854 \text{ THz} \\ 434.83004 \text{ THz} \\ 434.83154 \text{ THz} \\ 434.83303 \text{ THz} \\ 434.83453 \text{ THz} \\ 434.83603 \text{ THz} \end{array}$$

Hence, the fsr is 1.5 GHz and the nearest mode to the Sr resonance at $\nu_{atom} = 434.829\ 121\ 311$ THz is at $\nu_{Sr2,refcav} = 434.828\ 52$ THz, which is about 600 MHz below.

heating voltage	3.83 V	
heating current	0.63 A	
temperature	7.18 Ω	
pressure	$1.3 \cdot 10^{-7}$ mbar	
wavemeter	$\nu_{Sr1,refcav}$	= 434.82889 THz
wavemeter	$\nu_{Sr2,refcav}$	= 434.82854 THz
beat	$\nu_{Sr1,refcav} - \nu_{Sr2,refcav}$	= 345.6 MHz
red MOT	$\nu_{atom} - \nu_{Sr1,refcav}$	= +150 THz
Hence	$\nu_{atom} - \nu_{Sr2,refcav}$	= +495 MHz

We already did the measurement on 05.04.2017 and found:

beat	$\nu_{Sr1,refcav} - \nu_{Sr2,refcav}$	= 478 MHz
Hence	$\nu_{atom} - \nu_{Sr2,refcav}$	= +482 MHz

We repeated the measurement on 22.08.2018 and found:

heating voltage	4 V	
heating current	0.7 A	
temperature	7.01 Ω	
pressure	$1.7 \cdot 10^{-7}$ mbar	
beat	$\nu_{Sr1,refcav} - \nu_{Sr2,refcav}$	= 339.1 MHz
Hence	$\nu_{atom} - \nu_{Sr2,refcav}$	= +490 MHz

Note that only the last measurement is reliable, because the red laser has been calibrated to the red MOT. We repeated the measurement on 19.09.2018 and found:

heating voltage	4 V	
heating current	0.7 A	
temperature	7.01 Ω	
pressure	$1.9 \cdot 10^{-7}$ mbar	
wavemeter	$\nu_{Sr2,refcav}$	= 434.82857 MHz
Sr1-AOMs	$\nu_{atom} - \nu_{Sr1,refcav}$	= 2 × 399.8 MHz + 150 MHz
beat	$\nu_{Sr2,refcav} - \nu_{Sr1,refcav}$	= ±464 MHz
Hence	$\nu_{atom} - \nu_{Sr2,refcav}$	= +484.8 MHz

1.60 22.11.2017 Digital temperature stabilization of the supercavity

LIEPO has built a current drive. Using the NI USB6001 board I set up the following temperature stabilization scheme and tested it with a heating resistance and a thermistor: The servo signal U_{serv} is calculated from the error signal U_{err} as:

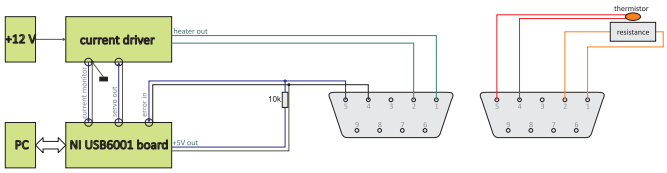

Figure 1.57: (code) Block diagram of the digital temperature stabilization of the supercavity.

$$U_{serv}(t) = U_{off} + A_{prop}U_{err}(t) + A_{intg}\sum_{k=1}^{100} e^{-(t-kt_i/100)}U_{err}(t-kt_i/100) \ ,$$

where U_{off} is a possible offset voltage, A_{prop} the proportional gain, A_{intg} the integrator gain, and t_i the integrator time constant.

Possible next step: check whether it is possible to use an Arduino to do the same job.

1.61 23.11.2017 Ruben's thesis

Is the coherence time during Bloch oscillations dramatically increased by the cavity ?

- smart: traveling retroreflected wave, how come?

merit of cavity as filter for off-resonant photons

We have optical access under $\beta/2 = 18..25°$: To obtain a commensurate lattice, we would need a UV laser: $291nm = 689nm \sin(25°)$. $532nm = 689nm \sin(50.6°)$ is not accessible.

The capability of making Bragg pulses is advantageous, e.g. for velocity purification. But such pulses can be made with arbitrary lattice periods. E.g., using lasers 10 GHz away from 461nm collinear to the cavity's vertical axis provided the power is strong.

Check our gravimeter for (low frequency) gravitational wave detection capability!

1.62 01.12.2017 Red laser system

In order to reproduce the Bloch-CARL dynamics simulated in LPL and Opt Exp, we have to provide,

$$U_0 = \frac{\Omega_1 \Omega_p}{\Delta} \approx 0.04\omega_r$$
$$\kappa = ?$$
$$\delta =$$

Where to operate the Bloch lattice, and where the CARL?

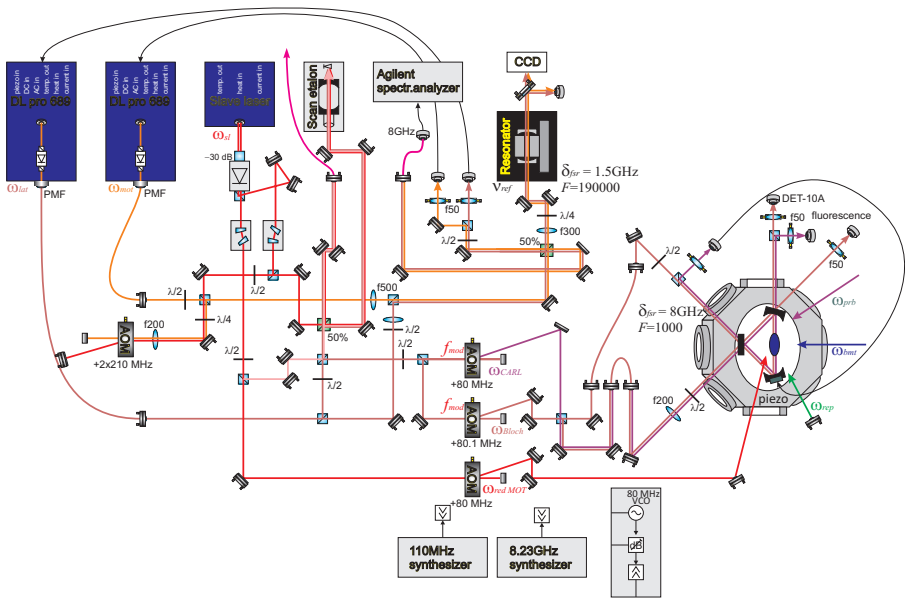

Figure 1.58: (code) Red laser system.

1.63 02.01.2018 Cat-eye and Littrow ECDL & role of AR-coating

Narrowband filters turn out to be very expensive (see SemRock, Laseroptik, Newport for 632.8nm, etc.). On the other hand, gratings are cheap, and we have a lot of them. For this reason I designed a Littrow-type ECDL laser partially compatible with the cat-eye design.

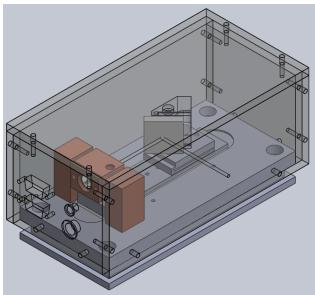

Figure 1.59: (code)

We have a problem with increasing the red MOT laser light: Tapered amplifiers at 689 nm have a limited lifetime and are expensive (Toptica BoosTApro 20000Eur, Eagleyard 2000Eur). AR-coated laserdiodes (Eagleyard, Ondax) also cost 1000EUR and have low emission powers (15 mW). Thorlabs laserdiodes have no AR-coating and spread over ±10 nm. Maybe we can AR-coat them at home.

I gave a HL6738MG laser diode to Marcos from the Optics Workshop to apply an AR-coating. I characterize the I-P curve with/out coating. Without AR-coating I find a threshold of $I = 47$ mA, a slope efficiency of 0.75 mW/mA, and a maximum power at 97 mA of 35.1 mW in agreement with the datasheet. Optical feedback from a 500 lines grating reduces the threshold to 39 mA.

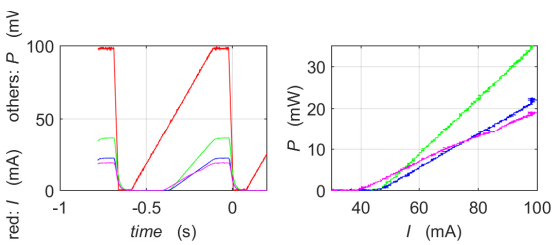

Figure 1.60: (code)

I was able to pull a 685.1 nm laser diode at 25 C and 90 mA to 689.26 nm. This will be more difficult injecting another laser beam, because mode matching will be not as good. Redo the same tests with an AR-diode.

1.64 17.01.2018 Red-MOT modulation

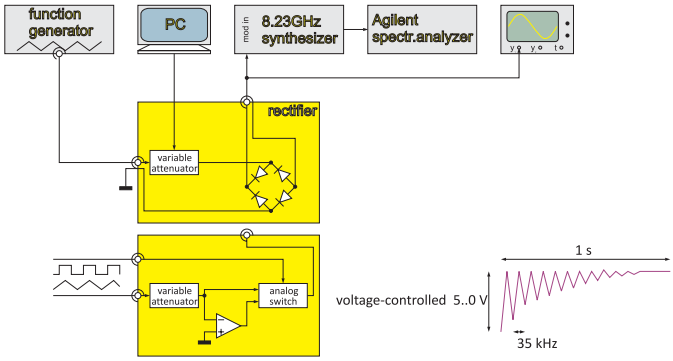

Figure 1.61: (code)

1.65 25.01.2018 Digital PLL for laser offset locking

Works just great! I measured an upper limit of 10 Hz uncertainty at a beat frequency of 2.97 GHz. The lock is extremely stable. Consult Meas.Sci.Technol. 20, 055302 (2009).

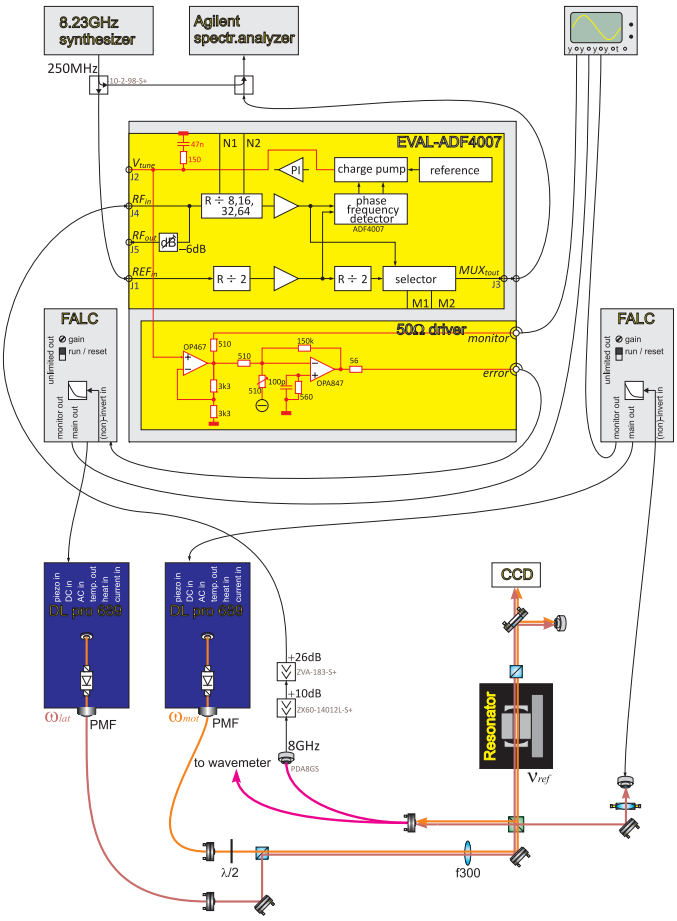

Figure 1.62: (code)

Characterization measurements:

1. Record beat spectrum at various resolution bandwidths & spans; 40 dB above noise, but there are sidebands at 90 kHz and 200 kHz and broad wings around 300 kHz;

2. Impact of modulation sidebands: no discernible impact;

3. Watch error signal on scope and spectrum analyzer; applying to the R&S a 5 kHz square frequency modulation with $f_{dev} = 100$ kHz deviation, we observe a 6.4 MHz $= 64 \cdot f_{dev}$ frequency excursion of the spectrum analyzer. The error signal

monitor shows 30 μs long impulse response after optimizing the FALC. This means that the servo is able to handle a 6.4 MHz jump within 30 μs.

4. Lock 1 laser to supercavity and use the second to resolve the cavity bandwidth.
5. Tuning range tested between 1..3 GHz.

I found the next TEM_{00} mode at 45.15829 MHz corresponding to 1.445065 GHz fsr. This value agrees with the measurement from 5.4.2017. The width of the spectrum is 4 kHz corresponding to a finesse of $F = \pi\delta_{fsr}/(2\pi\ 5\ \text{kHz}) = 185000$.

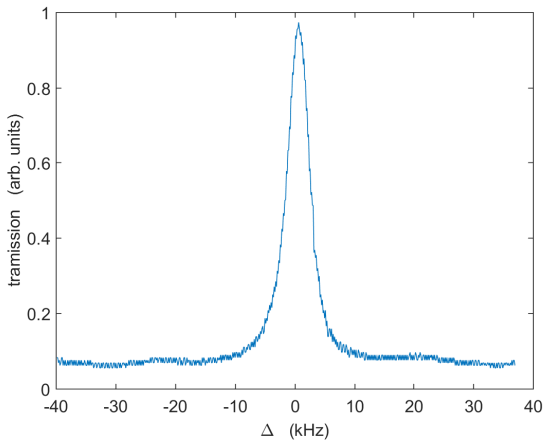

Figure 1.63: (code)

1.66 25.05.2018 Relative trap depth with respect to 461 and 689nm

Consider the Sr atom with the cooling transition at $\lambda_{461} = 461$ nm with the linewidth $\Gamma_{461}/2\pi = 30.5$ MHz and the clock transition at $\lambda_{689} = 689$ nm with the linewidth $\Gamma_{689}/2\pi = 7.6$ kHz. At what frequency does the dipolar force induced by the clock transition overrule that of cooling transition? At what frequency does the Rayleigh scattering rate at the clock transition overrule that of cooling transition?

The dipolar force and the scattering rate are proportional to

$$U_0 = \frac{g_1^2}{\Delta_a} \qquad \text{respectively} \qquad \gamma_0 = \Gamma \frac{g_1^2}{\Delta_a^2} \ ,$$

where the coupling strength is given by,

$$g_1 = \frac{dE_1}{\hbar} \qquad \text{with} \qquad d = \sqrt{\frac{3\pi\varepsilon_0\hbar\Gamma}{k_a^3}} \qquad \text{and} \qquad E_1 = \sqrt{\frac{\hbar\omega}{2\varepsilon_0 V}} \ .$$

With this, the dipolar forces behave like,

$$\frac{U_{0,689}}{U_{0,461}} = \frac{g_{1,689}^2}{g_{1,461}^2}\frac{\Delta_{a,461}}{\Delta_{a,689}} = \frac{\Gamma_{689}\omega_{a,461}^3}{\Gamma_{461}\omega_{a,689}^3}\frac{\omega_{a,689} + \Delta_{a,689} - \omega_{a,461}}{\Delta_{a,689}} > 1 \ ,$$

yielding $\Delta_{a,689} < (2\pi)\ 179\,\text{GHz}$. The scattering rates behave like,

$$\frac{\gamma_{0,689}}{\gamma_{0,461}} = \frac{\Gamma_{689}}{\Gamma_{461}}\frac{g_{1,689}^2}{g_{1,461}^2}\frac{\Delta_{a,461}^2}{\Delta_{a,689}^2} = \frac{\Gamma_{689}^2\omega_{a,461}^3}{\Gamma_{461}^2\omega_{a,689}^3}\frac{(\omega_{a,689} + \Delta_{a,689} - \omega_{a,461})^2}{\Delta_{a,689}^2} > 1 \ ,$$

yielding $\Delta_{a,689} < (2\pi)\ 98\,\text{GHz}$.

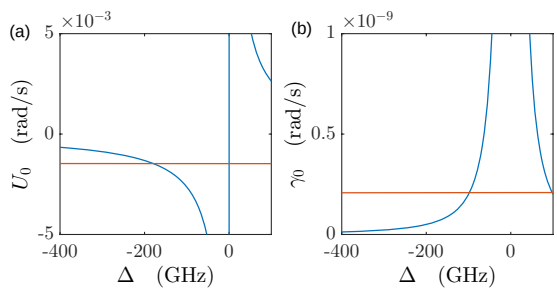

Figure 1.64: (code) (a) Single-photon light shifts and (b) Rayleigh scattering rates for (red) the cooling and (blue) the clock transition.

1.67 01.06.2018 Purifying Bragg pulses

The atomic cloud can be 'cooled' by velocity-selective π-Bragg pulses. The Bragg condition requests $K_{brg} \sin \frac{\beta}{2} = k_{dip}$, or $\lambda_{dip} = \frac{\lambda_{brg}}{\sin \frac{\beta}{2}}$. In practive, we have boundary conditions:

- limited optical access: $\beta = 0...28°$
- stay within first Brillouin zone? $q = 0...2\hbar k_{689}$
- stay close to atomic resonances? $\lambda_{brg} \simeq 689$ nm or even 461 nm

1.68 13.06.2018 Bessel beam project

Based on [105] we could make a 1 mK deep hollow beam:

$$U = \frac{3\pi c^2}{2\omega^3}\frac{\Gamma}{\Delta}\frac{I}{k_B} \ .$$

And the scattering rate,

$$\gamma = \frac{3\pi c^2}{2\omega^3}\frac{\Gamma^2}{\Delta^2}\frac{\omega I}{m} \ .$$

With $\Gamma = (2\pi)$ 30.5 MHz, $I = 1$ W/cm^2, and $\Delta = (2\pi)$ 1.5 GHz.

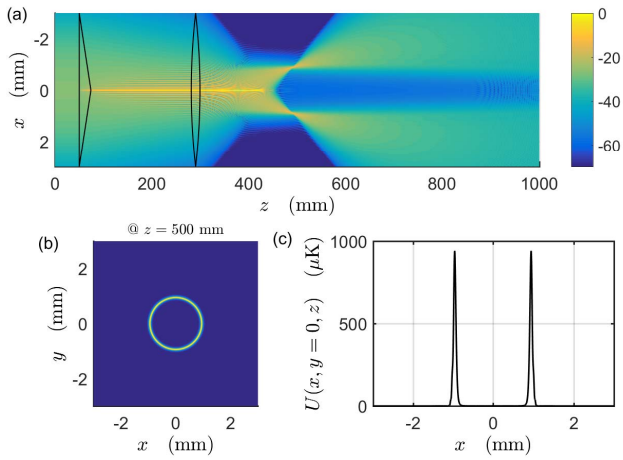

Figure 1.65: (code) Simulation of a Bessel beam with one axicon (base angle $\alpha = 0.5°$, refraction index $n_{rf} = 1.51$) located at $z = 50$ mm and one lens (focal length $f = 200$ mm) located at $z = 290$ mm. Figure (a) shows the intensity distribution $I(x, y = 0, z)$ in dB in the $y = 0$ plane; (b) is a radial cut of the intensity distribution $I(x, y, z = 500$ mm); and (c) shows the optical potential $U(x, y = 0, z = 500$ mm) along the $y = 0$ and $z = 500$ mm line.

1.69 03.09.2018 Ring cavity characterization 2

Parameters of the São Carlos ring cavity interacting with ^{88}Sr on its 7.6 kHz intercombination line:

transition wavelength	λ	$= 689$ nm
cavity round trip length	L	$= 3.6$ cm
cavity mode volume	V	$= 0.5$ mm
mode waist at location of atoms	w	$= 70$ μm
free spectral range	$\delta_{fsr} = \frac{c}{L}$	$= (8.2 \pm 0.02)$ GHz
radius of curvature of the high reflectors	ρ	$= 50$ mm
reflection of the high reflectors	R_{hr}	$= 99.9$ %
reflection of the (plane) incoupler	R_{ic}	$= 99.7$ %
finesse under s-polarization	$F = \frac{\pi(R_{hr}^2 R_{ic})^{1/6}}{1-(R_{hr}^2 R_{ic})^{1/3}}$	$= 1900$
measured finesse under p-polarization	F	≈ 500
transition linewidth	Γ	$=(2\pi)7.6$ kHz
cavity linewidth	$\kappa = \frac{\delta_{fsr}}{F}$	$=(2\pi)690$ kHz
recoil shift	$\omega_{rec} = \frac{\hbar k^2}{2m}$	$=(2\pi)4$ kHz
coupling strength	$g_1 = \sqrt{\frac{3\pi\Gamma\omega_0}{k^3 V}} s_0 s_2$	$=(2\pi)8.7$ kHz
current number of atoms	N	$= 10^5$
current temperature	T	$= 10$ mK
current size of atomic cloud	$\bar{r}$	$= 1$ mm
aimed temperature	T	$= 1$ μK
size of atomic cloud @ 1 μK	$\bar{r}$	$= 100$ μm

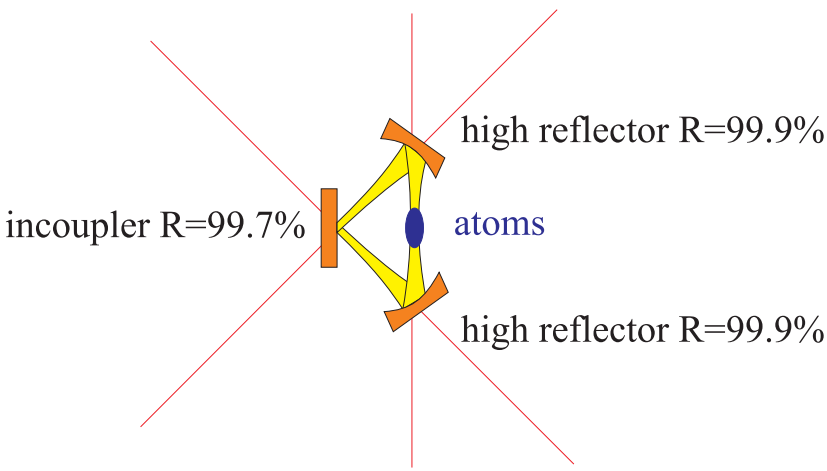

Figure 1.66: (code)

1.70 30.10.2018 Red MOT frequency comparison

In Sr1 they found the red MOT at:

$$\nu_{Sr1,slv} = \nu_{atom} - 150 \text{ MHz} - 2.8 \text{ MHz} \ .$$

When the Sr2 master laser is locked to its supercavity, we observe a beat between it and the Sr1 laser at,

$$\nu_{Sr2,mst} - \nu_{Sr1,slv} = -334.04 \text{ MHz} \ .$$

We shine into the Sr2 red MOT the frequency,

$$\nu_{Sr2,redMOT} = \nu_{Sr2,mst} + 2 \cdot 200 \text{ MHz} + 80 \text{ MHz} = \nu_{atom} - 150 \text{ MHz} - 2.8 \text{ MHz} - 334.04 \text{ MHz} + 2 \cdot 200 \text{ MH}$$

1.71 21.01.2019 Operation of the Sr2 experiment

1. Ti:Sapphire:
   - switch on Sprout by turning the key and pushing the button;
   - turn on Notebook, open html://192.168.1.222, user:main password:main;
   - power should be ~ 0.7, press 'start';
   - adjust etalon to right frequency, press etalon 'Lock' (TiSa is locked);
   - press 'OneShot', wait for 'Manual';
   - ECD lock (doublingcavity)
2. Spectroscopy:
   - switch on Agilent power supply (output should be set to 15.5 A);
   - turn on CameraComputer, run Toptica Digilock software;
   - open & connect TiSa module, scan on, modulation on, lock to extremum
3. Magnetic trap coils:
   - turn on ControlComputer, open and run LabView routine, update values
   - turn chiller in Sr1 Lab;
   - turn on Delta power supply, press 'unlock' then 'output on' (output should be 9.08 A)
4. turn on dispensers at 6.6 A
5. check and readjust fiber couplings
6. turn on power supply for shutters
7. Repumpers:
   - switch on Toptica upper power supply channel No1 for the 707 nm;
   - tune to resonance (wavemeter channel No4) using piezo;
   - switch on Toptica lower power supply channel No2 for the 679 nm;
   - tune to resonance using piezo
8. optimize 2D-MOT alignment with blocked Zeeman beams
9. run ActiveXChameleon (write file pics to directory)
10. activate Python camera program: run Cam shortcut (reads file pics to directory)
11. activate SrControl program

1.72 21.01.2019 Gaseous metamaterials?

Is it possible to design gases with hyperbolic dispersion relation in analogy to hyperbolic metamaterials?

We know it's possible to have $\varepsilon_r < 0$ and $\mu_r < 0$, even simultaneously. We also know that hyperbolic metamaterials do not need to be inhomogeneous on large scales, e.g. a disordered ensemble of tiny metal rods (or disks) all aligned to an axis can be hyperbolic. If we can break symmetry on the atomic level, e.g. via strong magnetic fields, can we arrange for non-isotropic ε?

Lattices can enhance cooperativity within photonic band edges, just like cavities? Can lattices break isotropy of $n(r)$?

$$
\begin{aligned}
n^2(r) &= 1 - \frac{4\pi\rho(r)}{k_0^3(2\Delta/\Gamma + i)} = 1 + \tfrac{2}{3}\alpha_{pol}\rho(r) \\
\frac{\alpha_{pol}}{\varepsilon_0} &= \frac{6\pi}{k_0^3}\frac{-1}{2\Delta/\Gamma + i} \\
\varepsilon_r - 1 = \chi_\varepsilon &= \frac{\frac{N}{V}\frac{\alpha_{pol}}{\varepsilon_0}}{1 - \frac{N}{V}\frac{\alpha_{pol}}{3\varepsilon_0}} \simeq \frac{N}{V}\frac{\alpha_{pol}}{\varepsilon_0} \\
\frac{\alpha_{pol}}{\varepsilon_0} &= \frac{\chi_\varepsilon}{\frac{N}{V}\left(1 + \frac{\chi_\varepsilon}{3}\right)} = \frac{3V}{N}\frac{\varepsilon_r - 1}{\varepsilon_r + 2} \,.
\end{aligned}
$$

Questions:

1. Simulation via coupled dipoles?
2. Negative refraction link to birefringence?
3. Link to light house effect?
4. Imagine we could make a 1D-lattice with alternating sign of ε. What would be its properties?
5. What are the properties of a material with an imaginary refractive index $n = \sqrt{\varepsilon\mu}$ with $\mu = 1$ and $\varepsilon = -1$.

The goal of the following paragraph is to estimate the maximum susceptibility variation on the strong blue transition in strontium. We assume the two-level system drawn in Fig. 1.67, the resonance condition could be modulated, e.g. via the light-shift induced by a far red-detuned optical lattice.

The stationary Bloch equations for a two-level system are solved by,

$$
\begin{aligned}
\begin{pmatrix} \rho_{22}(\infty) \\ \rho_{12}(\infty) \\ \rho_{21}(\infty) \end{pmatrix} &= -\begin{pmatrix} -\Gamma_{12} & -\frac{i}{2}\Omega_{12} & \frac{i}{2}\Omega_{12} \\ -\frac{i}{2}\Omega_{12} & -\frac{1}{2}\Gamma_{12} + i\Delta_{12} & 0 \\ \frac{i}{2}\Omega_{12} & 0 & -\frac{1}{2}\Gamma_{12} - i\Delta_{12} \end{pmatrix}^{-1} \begin{pmatrix} 0 \\ \frac{i}{2}\Omega_{12} \\ -\frac{i}{2}\Omega_{12} \end{pmatrix} \\
&= \frac{\Omega_{12}}{4\Delta_{12}^2 + 2\Omega_{12}^2 + \Gamma_{12}^2} \begin{pmatrix} -\Omega_{12} \\ -i\Gamma_{12} + 2\Delta_{12} \\ i\Gamma_{12} + 2\Delta_{12} \end{pmatrix} \,.
\end{aligned}
$$

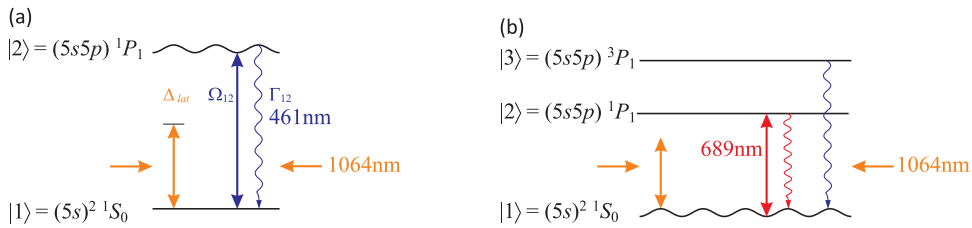

Figure 1.67: (code)

The susceptibility is,

$$\chi = \frac{N d_{12}}{V \varepsilon_0 E_{12}} \rho_{21} = \frac{N |d_{12}|^2}{V \varepsilon_0 \hbar \Omega} \rho_{21} = \frac{N |d_{12}|^2}{V \varepsilon_0 \hbar \Omega} \frac{\Omega_{12}(-i\Gamma_{12} + 2\Delta_{12})}{4\Delta_{12}^2 + 2\Omega_{12}^2 + \Gamma_{12}^2} \ .$$

With the dipole moment of the strong blue transition, $d_{12} = \sqrt{3\pi\varepsilon_0 \hbar \Gamma_{461}/k_{461}^3} \approx 2.5 \cdot 10^{-29}$ and densities of about $N/V = 10^{18}$, we estimate,

$$C \equiv \frac{N |d_{12}|^2}{V \varepsilon_0 \hbar} \approx 7.1 \cdot 10^5 \ .$$

With the dipole moment of the intercombination line $d_{12} = \sqrt{3\pi\varepsilon_0 \hbar \Gamma_{689}/k_{689}^3} \approx 7.4 \cdot 10^{-31}$ and densities of about $N/V = 10^{18}$, we estimate,

$$C \equiv \frac{N |d_{12}|^2}{V \varepsilon_0 \hbar} \approx 593 \ .$$

Now,

$$\chi = \frac{C}{\Omega_{12}} \rho_{21} \ .$$

The IR-laser can easily induce Stark shifts of $U = \frac{\Omega^2}{4\Delta} = -(2\pi)30$ MHz, which we take into account via a modulation of the ground-state energy:

$$\mathrm{Re}\ \chi = C \frac{2(\Delta_{12} - U_0 \sin^2 kz)}{4(\Delta_{12} - U_0 \sin^2 kz)^2 + 2\Omega_{12}^2 + \Gamma_{12}^2} < \frac{C}{2} \ .$$

1.73 22.01.2019 EIT Susceptibility?

The following estimations aim at verifying, whether high susceptibility modulations may be achieved in EIT systems, and whether it may be enhanced by collective interaction with light fields.

We consider the strontium level system drawn in Fig. **??**.

The stationary Bloch equations for a three-level system are solved by,

$$\begin{pmatrix}\rho_{22}\\ \rho_{33}\\ \rho_{12}\\ \rho_{21}\\ \rho_{13}\\ \rho_{31}\\ \rho_{23}\\ \rho_{32}\end{pmatrix} = -\begin{pmatrix} -\Gamma_{12}-\Gamma_{23} & 0 & -\frac{i}{2}\Omega_{12} & \frac{i}{2}\Omega_{12} & 0 & 0 & \frac{i}{2}\Omega_{23} & -\frac{i}{2}\Omega_{23}\\ \Gamma_{23} & -\Gamma_{13} & 0 & 0 & 0 & 0 & -\frac{i}{2}\Omega_{23} & \frac{i}{2}\Omega_{23}\\ -i\Omega_{12} & -\frac{i}{2}\Omega_{12} & -\Lambda_{12} & 0 & \frac{i}{2}\Omega_{23} & 0 & 0 & 0\\ i\Omega_{12} & \frac{i}{2}\Omega_{12} & 0 & -\Lambda_{12}^* & 0 & -\frac{i}{2}\Omega_{23} & 0 & 0\\ 0 & 0 & \frac{i}{2}\Omega_{23} & 0 & -\Lambda_{13} & 0 & -\frac{i}{2}\Omega_{12} & 0\\ 0 & 0 & 0 & -\frac{i}{2}\Omega_{23} & 0 & -\Lambda_{13}^* & 0 & \frac{i}{2}\Omega_{12}\\ \frac{i}{2}\Omega_{23} & -\frac{i}{2}\Omega_{23} & 0 & 0 & -\frac{i}{2}\Omega_{12} & 0 & -\Lambda_{23} & 0\\ -\frac{i}{2}\Omega_{23} & \frac{i}{2}\Omega_{23} & 0 & 0 & 0 & \frac{i}{2}\Omega_{12} & 0 & -\Lambda_{23}^* \end{pmatrix}^{-1} \begin{pmatrix} 0\\ 0\\ \frac{i}{2}\Omega_{12}\\ -\frac{i}{2}\Omega_{12}\\ 0\\ 0\\ 0\\ 0\end{pmatrix}$$

If we suppose very large detuning, $\Delta_{12} \gg 0$, the excited state populations will be small, $\rho_{22}, \rho_{33} \simeq 0$. The Bloch equations then simplify to,

$$\begin{aligned}\begin{pmatrix}\rho_{12}\\ \rho_{13}\\ \rho_{23}\end{pmatrix} &= -\begin{pmatrix} -\Lambda_{12} & \frac{i}{2}\Omega_{23} & 0\\ \frac{i}{2}\Omega_{23} & -\Lambda_{13} & -\frac{i}{2}\Omega_{12}\\ 0 & -\frac{i}{2}\Omega_{12} & -\Lambda_{23}\end{pmatrix}^{-1} \begin{pmatrix}\frac{i}{2}\Omega_{12}\\ 0\\ 0\end{pmatrix}\\ &= \frac{\Omega_{12}}{\Omega_{12}^2\Lambda_{12} + 4\Lambda_{12}\Lambda_{13}\Lambda_{23} + \Omega_{23}^2\Lambda_{23}} \begin{pmatrix}\frac{i}{2}(\Omega_{12}^2 + 4\Lambda_{13}\Lambda_{23})\\ -\Lambda_{23}\Omega_{23}\\ \frac{1}{2}i\Omega_{12}\Omega_{23}\end{pmatrix} .\end{aligned}$$

In the case of the strontium cascade system of Fig. **??**, we have $\Gamma_{13} \ll \Gamma_{12} \ll \Gamma_{23}$, such that $\Lambda_{12} = i\Delta_{12} + \frac{1}{2}\Gamma_{12}$, $\Lambda_{13} = i\Delta_{12} - i\Delta_{23} + \frac{1}{2}(\Gamma_{12}+\Gamma_{23}) \simeq i(\Delta_{12}-\Delta_{23}) + \frac{1}{2}\Gamma_{23}$, and $\Lambda_{23} = i\Delta_{23} + \frac{1}{2}(\Gamma_{12}+\Gamma_{13}+\Gamma_{23}) \simeq i\Delta_{23} + \frac{1}{2}\Gamma_{23}$. The susceptibility on the lower transition is,

$$\chi = \frac{Nd_{12}}{V\varepsilon_0 E_{12}}\rho_{21} = \frac{N|d_{12}|^2}{V\varepsilon_0\hbar\Omega}\rho_{21} .$$

With the dipole moment of the intercombination line $d_{12} = \sqrt{3\pi\varepsilon_0\hbar\Gamma_{689}/k_{689}^3} \approx 7.4\cdot 10^{-31}$ and densities of about $N/V = 10^{18}$, we estimate,

$$C \equiv \frac{N|d_{12}|^2}{V\varepsilon_0\hbar} \approx 593 .$$

Hence,

$$\chi = \frac{C}{\Omega}\rho_{21} .$$

Fig. **??** seems to show that high densities are necessary if one aims at $\chi \simeq \pm 1$.

In the strontium cascade system the upper level is not stable and can decay into very metastable states. While this will not impact the population decay rate Γ_{23}, it will increase the coherence decay rate, such that $\Lambda_{13} = i\Delta_{12} - i\Delta_{23} + \frac{1}{2}(\Gamma_{12}+\Gamma_{23}+\Gamma_{34})$ and $\Lambda_{23} = i\Delta_{23} + \frac{1}{2}(\Gamma_{12}+\Gamma_{13}+\Gamma_{23}+\Gamma_{34})$.

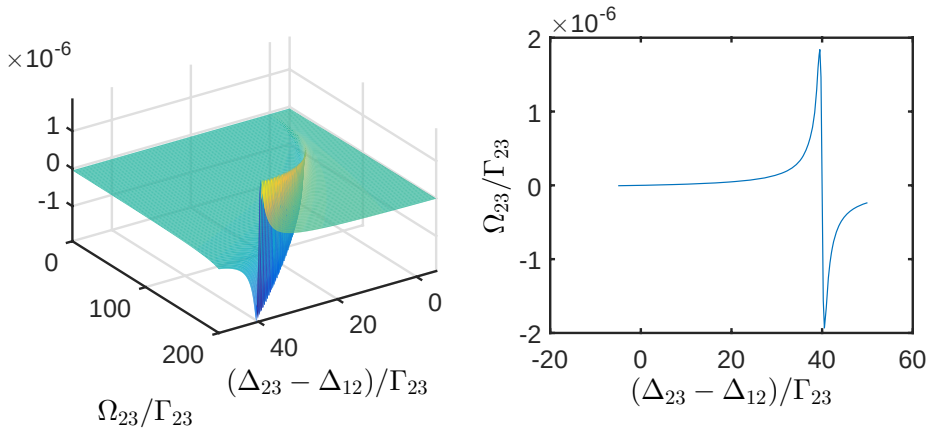

Figure 1.68: (code)

1.74 22.01.2019 CARL with EIT 1

An interesting question is now, what impact EIT would have on CARL? There is a number of open questions:

- The adiabatic elimination cannot be made as easily!
- CARL on a metastable ground state?
- Can the upper transition used to control the CARL dynamics or to induce *friction*? The upper transition induces a light-shift and simultaneously shifts the phase of the lower transition.

We assume the CARL with an additional field driving an upper (cascade EIT) transition. The Hamiltonian is given by Eq. (44.4) of the Quantummechanics script, with the following amendments,

$$\begin{aligned}
\hat{H} &= \hat{H}_{atom} + \hat{H}_{atom-eit} + \hat{H}_{cavity} + \hat{H}_{atom-cavity} + \hat{H}_{laser-cavity} \\
\hat{H}_{atom} &= -\omega_1 \hat{\sigma}^+ \hat{\sigma}^- - \omega_2 \hat{\varsigma}^+ \hat{\varsigma}^- + \tfrac{\hat{p}}{2m} \\
\hat{H}_{atom-eit} &= \Omega_\varsigma \hat{\varsigma}^+ + h.c \ ,
\end{aligned}$$

where $\hat{\sigma} = |1\rangle\langle 2|$ and $\hat{\varsigma} = |2\rangle\langle 3|$. The CARL equations follow from the Heisenberg equations for the quantum degrees of freedom $\hat{a}_\pm$, $\hat{x}$, $\hat{p}$, and the components of the atomic Bloch vector $\vec{\rho}$. As long as the internal dynamics is fast, we can still adiabatically eliminate it. However, if the lasers fulfill resonance conditions, such as $\Delta_{12} = \Delta_{23}$, there are other time constants entering the dynamics.

It is easy to see that, defining

$$\mathcal{L} \equiv \begin{pmatrix} 0 & \Gamma_{12} & 0 & -ig\Sigma^\dagger & ig\Sigma & 0 & 0 & 0 & 0 \\ 0 & -\Gamma_{12} & \Gamma_{23} & ig\Sigma^\dagger & -ig\Sigma & 0 & 0 & \frac{i}{2}\Omega_{23} & -\frac{i}{2}\Omega_{23} \\ 0 & 0 & -\Gamma_{23} & 0 & 0 & 0 & 0 & -\frac{i}{2}\Omega_{23} & \frac{i}{2}\Omega_{23} \\ -ig\Sigma^\dagger & ig\Sigma^\dagger & 0 & -\Lambda_{12} & 0 & \frac{i}{2}\Omega_{23} & 0 & 0 & 0 \\ ig\Sigma & -ig\Sigma & 0 & 0 & -\Lambda_{12}^* & 0 & -\frac{i}{2}\Omega_{23} & 0 & 0 \\ 0 & 0 & 0 & \frac{i}{2}\Omega_{23} & 0 & -\Lambda_{13} & 0 & -ig\Sigma^\dagger & 0 \\ 0 & 0 & 0 & 0 & -\frac{i}{2}\Omega_{23} & 0 & -\Lambda_{13}^* & 0 & ig\Sigma \\ 0 & \frac{i}{2}\Omega_{23} & -\frac{i}{2}\Omega_{23} & 0 & 0 & -ig\Sigma^\dagger & 0 & -\Lambda_{23} & 0 \\ 0 & -\frac{i}{2}\Omega_{23} & \frac{i}{2}\Omega_{23} & 0 & 0 & 0 & ig\Sigma & 0 & -\Lambda_{23}^* \end{pmatrix},$$

with

$$\begin{aligned} \Sigma &\equiv e^{ik\hat{z}}\hat{a}_+ + e^{-ik\hat{z}}\hat{a}_- \\ \Lambda_{12} &\equiv i\Delta_{12} + \tfrac{1}{2}\Gamma_{12} \\ \Lambda_{13} &\equiv i\Delta_{13} + \tfrac{1}{2}(\Gamma_{23} + \Gamma_{34}) \\ \Lambda_{23} &\equiv i\Delta_{23} + \tfrac{1}{2}(\Gamma_{12} + \Gamma_{23} + \Gamma_{34}) \ . \end{aligned} \tag{1.3}$$

the new equations of motion are:

$$\begin{aligned} \dot{\hat{a}}_\pm &= (-\kappa + i\Delta_c)\hat{a}_\pm - ig\hat{\rho}_{12}e^{\mp ik\hat{z}} + \eta_\pm \\ \dot{\vec{\rho}} &= \mathcal{L}\vec{\rho} \\ \dot{\hat{z}} &= \hat{p}/m \\ \dot{\hat{p}} &= ig\hbar k\hat{\sigma}(\hat{a}_+^\dagger e^{-ik\hat{z}} - a_-^\dagger e^{ik\hat{z}}) + c.c. \ . \end{aligned} \tag{1.4}$$

1.75 25.01.2019 Probe sequence

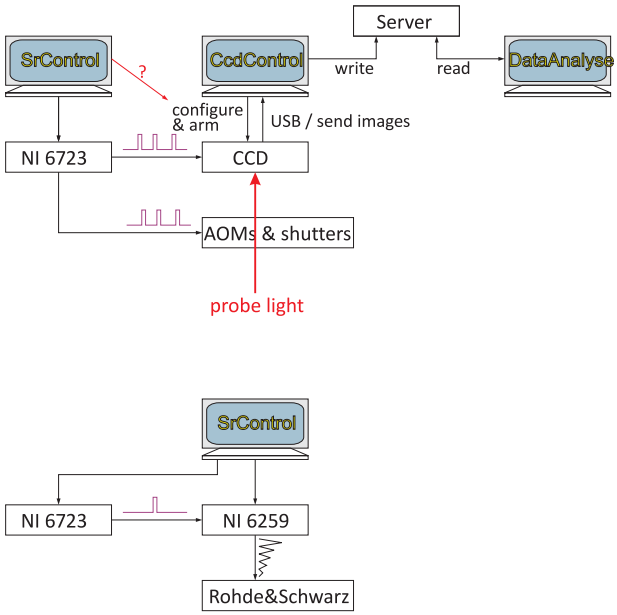

Figure 1.69: (code)

1.76 06.11.2019 Red MOT modulation

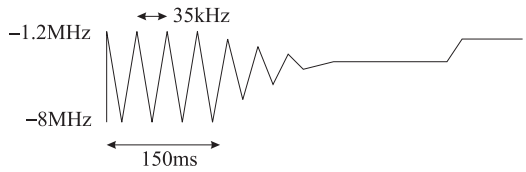

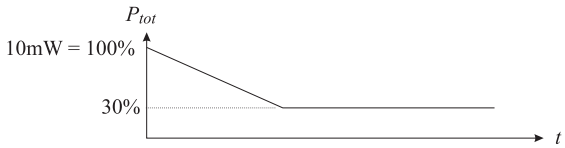

Figure 1.70: (code)

1.77 07.11.2019 Blue to red MOT switching circuit

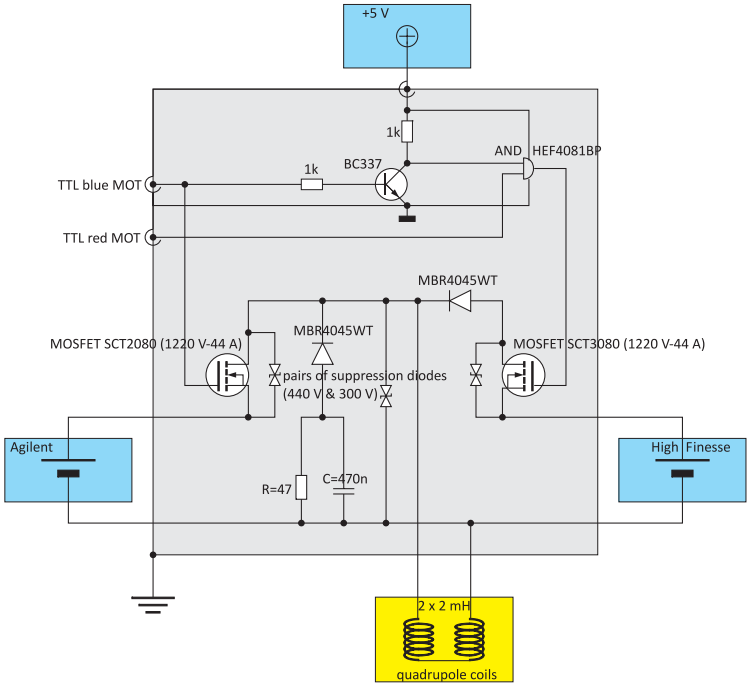

Figure 1.71: (code)

1.78 06.01.2020 Push beam acceleration

The force exerted by the push beam is given by,

$$F = \hbar k \Gamma_{psh} \ , \tag{1.5}$$

where the scattering rate is,

$$\Gamma_{psh} = \frac{6\pi}{k^2} \frac{\Gamma^2}{4\Delta^2 + 2\Omega^2 + \Gamma^2} \frac{I_{psh}}{\hbar\omega} \ . \tag{1.6}$$

If the push beam is on resonance, but the atom is moving with velocity v, then $\Delta = kv$. If the push beam is week, $\Omega \approx 0$. We obtain a differential equation,

$$F(v) = m\dot{v} = \hbar k \frac{6\pi}{k^2} \frac{\Gamma^2}{4k^2v^2 + \Gamma^2} \frac{I_{psh}}{\hbar\omega} = \frac{6\pi I_{psh}}{ck^2} \frac{\Gamma^2}{4k^2v^2 + \Gamma^2} \ . \tag{1.7}$$

It can be solved by,

$$\int_0^{v_0} (4k^2v^2 + \Gamma^2) dv = \int_0^{t_0} \frac{6\pi I_{psh}\Gamma^2}{cmk^2} dt \ , \tag{1.8}$$

that is,

$$v_0^3 + \frac{3\Gamma^2}{4k^2} v_0 = \frac{9\pi I_{psh}\Gamma^2}{2cmk^4} t_0 \ . \tag{1.9}$$

Setting $P_{psh} = 0.1(0.01)$ mW and $w_0 = 1$ mm, we get with $I_{psh} = \frac{2P_{psh}}{\pi w_0^2}$ the following curves for the position s of the atoms and their velocity v as a function of time. For comparison the figures also show the transfer due to thermal motion of the atoms along the horizontal axis:

$$v_{thrm} = \sqrt{\frac{k_B T}{m}} \ . \tag{1.10}$$

During the transfer time the atom will suffer a gravitational sag,

$$z_{sag} = \frac{g}{2} t^2 \ . \tag{1.11}$$

Fig. 1.72(d) demonstrates that, without push beam, the gravitational sag is way too large to allow for transfer.

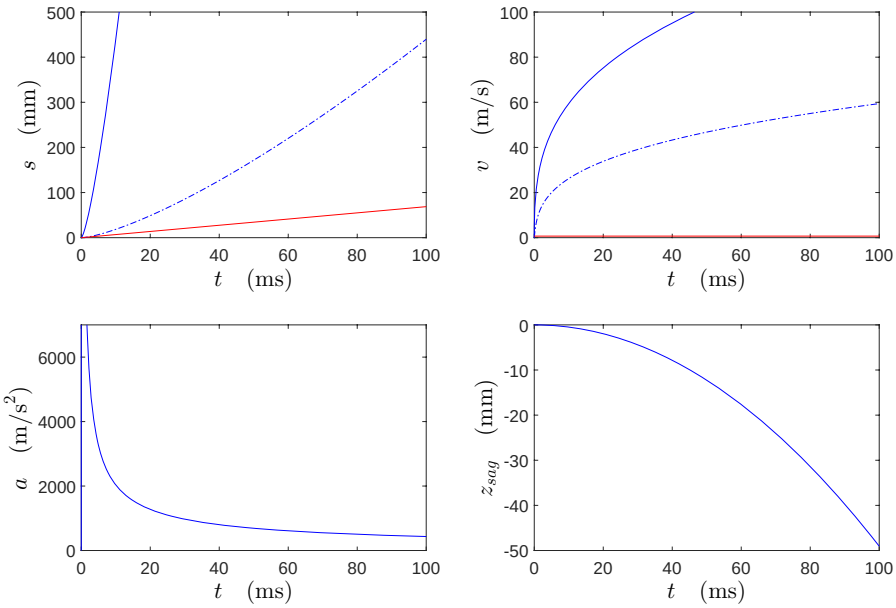

Figure 1.72: (code) (a-c) Position, instantaneous velocity, and acceleration along the optical axis. Blue solid curves: push beam transfer with $P_{psh} = 0.1$ mW. Blue dash-dotted curves: push beam transfer with $P_{psh} = 0.01$ mW. Red solid curves: thermal atoms transfer with $P_{psh} = 0$ mW. (d) Gravitational sag perpendicular to the optical axis.

1.79 27.02.2020 Maxwell-Boltzmann distribution in blue MOT

Calculated for $\omega_{tr} = (2\pi)$ 100 Hz, $N = 2 \cdot 10^6$, and $T = 3$ mK and 10 mK using the formula,

$$n(E) = Ze^{-E/k_BT} \frac{E^2}{(\hbar\omega)^3} \ , \tag{1.12}$$

where $Z = N \left(\frac{\hbar\omega_{tr}}{k_BT}\right)^3$.

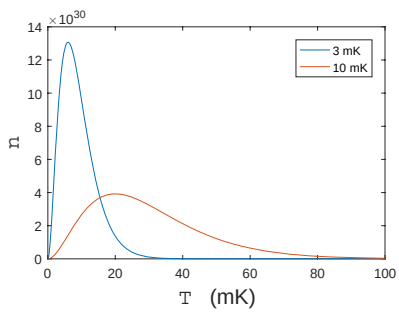

Figure 1.73: (code) Maxwell-Boltzmann distribution in blue MOT.

The curves demonstrate the importance of pre-cooling the blue MOT.

1.80 13.03.2020 Adjusting the beam diameter for the Bessel beam

Imaging by a lens in Gaussian optics is described by the following equations,

$$\left(\frac{d_2}{f}-1\right)\frac{w_1}{w_2}=\left(\frac{d_1}{f}-1\right)\frac{w_2}{w_1}=\sqrt{1-\left(\frac{kw_1w_2}{4f}\right)^2}\ . \tag{1.13}$$

Note, that the ray optics results are recovered for $k \to 0$. Spatial filtering by an $a = 100\ \mu$m pinhole generates a Gaussian beam with waist,

$$w_1=\frac{2a}{1.38}\approx 145\ \mu\text{m}\ , \tag{1.14}$$

which we want to transform into a beam with $w_2 = 500\ \mu$m. Using a $f = 500$ mm lens, we have to choose the distances according to $d_1 = 523$ mm and $d_2 = 770$ mm.

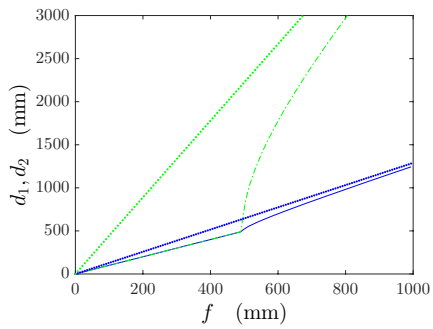

Figure 1.74: (code) Adjusting the beam diameter for the Bessel beam.

1.81 19.08.2020 CARL with EIT 2

Continuing on Sec. ??: How to calculate the CARL and radiation pressure forces from the coupled Bloch-CARL equations?

1.82 31.08.2020 Gravimeters

Common units for measuring gravity are: 1 μGal $= 10^{-6}$ cm/s^2 $= 10^{-9}$ g. Current gravimeters are distinguished as *absolute* and *relative gravimeters*. While absolute gravimeters tend to measure the attractive force exerted by a heavy body with the highest possible accuracy, relative gravimeters only aim at detecting variations of this force.

Gravimeters can also be classified by the underlying technique. Classical gravimeters are based on Newton's mechanics, quantum gravimeters exploit quantum effects (superconductivity, atomic matter waves).

gravimeter	type	sensitivity g/$\sqrt{\text{Hz}}$	drift g/day	accuracy g	cycles s
0-length mech. spring (Lacoste-Romberg)	rel.	10^{-10}	$3 \cdot 10^{-8}$	bad	15
liquid He superconducting ideal-spring	rel.	$< 10^{-12}$	$2 \cdot 10^{-10}$	bad	15
opt. interferom. free-falling corner-cube	abs.	$5 \cdot 10^{-8}$	0	$2 \cdot 10^{-9}$	10
commercial atom interferometer [71]	abs.	$5 \cdot 10^{-8}$	0	$1 \cdot 10^{-9}$	2
cold atom interferometer	abs.	$4 \cdot 10^{-9}$	0	$3 \cdot 10^{-9}$	1.3
Bloch oscillations [39]	abs.	$5 \cdot 10^{-6}$/10 s	0	good	
Bloch oscillations [20]	abs.	$2 \cdot 10^{-7}$/300 s	0	10^{-7}	

As an example: a mass of 10 t at a distance of 1 m generates a gravitational acceleration of,

$$a_d = \frac{\gamma_N m_{sphere}}{d^2} = 6.67 \cdot 10^{-7} \text{ m/s}^2 = 6.8 \cdot 10^{-8}\ g = 6.67 \text{ nGal} .$$

[39] measured 4000 oscillations with frequency $\nu_{bl} = 574$ Hz in 7 s.

[84] achieved 50 to 100 measurement per second with sensitivities below 1 $\mu g/\sqrt{Hz}$ aiming at 10 $ng/\sqrt{Hz}$.

1.83 26.02.2021 Heterodyne probing of Bloch-CARL oscillations

The recoil shift and the Bloch oscillation frequency are, respectively,

$$\omega_{rec} = \frac{\hbar k^2}{2m} \quad , \quad \nu_{blo} = \frac{mg}{2\hbar k} \ .$$

With this we calculate for the gravitation-induced Bloch oscillations in a strontium gravimeter a Lamb-Dicke parameter of

$$\eta_{blo} = \sqrt{\frac{\omega_{rec}}{2\pi\nu_{ho}}} = \sqrt{\frac{\hbar k^2}{2m}\frac{\hbar k}{\pi m g}} \approx 2.4 \ .$$

The modulation index is,

$$kz_0 = \frac{kv}{2\pi\nu_{ho}} = \frac{2\omega_{rec}}{2\pi\nu_{ho}} = 2\eta_{blo}^2 \approx 12.5 \ .$$

Hence, the continued fractions method is NOT applicable. In contrast, the cavity linewidth does not matter.

The CARL equations of motion modified to account for the periodic vibration of the atom, are,

$$\dot{\alpha}_\pm = (-\kappa + \imath\Delta_c - \imath U_0)\alpha_\pm - \imath U_0 e^{\mp 2\imath k z_0 \sin 2\pi\nu_{ho} t}\alpha_\mp + \eta_\pm \ ,$$

ω being the vibration frequency and kz_0 the modulation excursion. The results of the simulation are exhibited in Fig. 1.75.

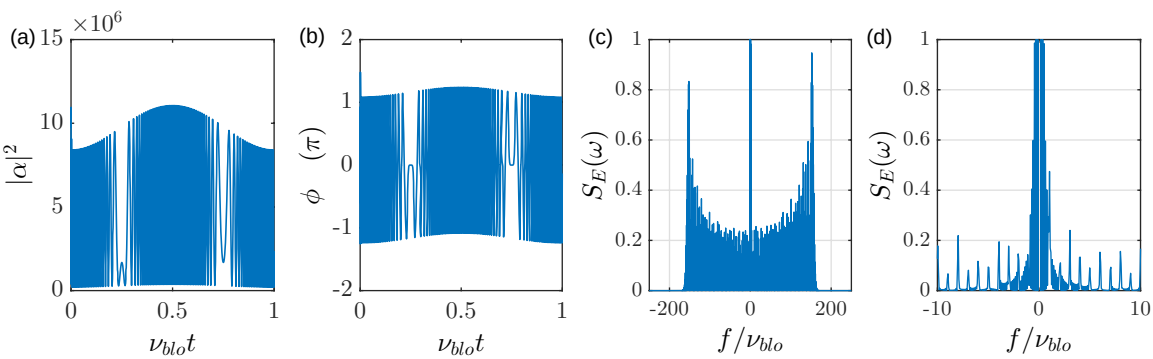

Figure 1.75: (code) (a) Photon number and (b) phase shift of the cavity in response to a modulated atomic position. The chosen parameters are $kz_0 = 12.5$, $\kappa = (2\pi)\ 440\,\text{kHz}$, $\nu_{blo} = 745\,\text{Hz}$, $\eta_\pm = 2900\kappa$, $U_0 = -\kappa$. The initial photon number is $|\alpha|^2 = |\eta/\kappa|^2$. (c) Spectrum recorded behind a cavity mirror with the transmittivity t_{hr}. The spectrum is obtained as the Fourier transform of the $g^{(1)}(\tau)$ correlation function of the transmitted field $E_{out} = t_{hr}e^{\imath ka}E_{cav}$, where $e^{\imath ka}$ is a fixed phase factor depending on the mirror position a.

Here, we want to calculate the heterodyne signal of the transmitted signal with a local oscillator frequency-shifted by an amount ω_{md}.

Mixing the transmitted signal with a local oscillator $E_{lo}e^{\imath(\omega+\omega_{md})t}$, we obtain the heterodyned signal,

$$\begin{aligned} S &= |E_{carl}e^{\imath\omega t} + E_{lo}e^{\imath(\omega+\omega_{md})t}|^2 \\ &= |E_{carl}|^2 + |E_{lo}|^2 + (E_{carl}E_{lo}^* e^{-\imath\omega_{md}t} + E_{carl}^* E_{lo}e^{\imath\omega_{md}t}) \\ &= |E_{carl}|^2 + |E_{lo}|^2 + 2|E_{lo}||E_{carl}|\cos(\omega_{md} - \Delta\omega)t \ . \end{aligned}$$

Now, demodulating this signal simultaneously with the modulation signals $\cos(\omega_{md}t + \phi)$ and $\sin(\omega_{md}t + \phi)$, we get,

$$\begin{aligned} U_c &= S\cos\omega_{md}t = |E_{lo}||E_{carl}|\cos\Delta\omega t + \text{oscillating terms} \\ U_s &= S\sin\omega_{md}t = |E_{lo}||E_{carl}|\sin\Delta\omega t + \text{oscillating terms} \ , \end{aligned}$$

where the oscillating terms can be filtered by a low-pass. Finally,

$$|E_{carl}| = \frac{\sqrt{U_c^2 + U_s^2}}{|E_{lo}|} \qquad , \qquad \tan\Delta\omega t = \frac{U_s}{U_c} \ .$$

That is,

$$E_{carl} = |E_{carl}|e^{\imath\Delta\omega t} = \frac{\sqrt{U_c^2 + U_s^2}}{|E_{lo}|}e^{\imath\arctan\frac{U_s}{U_c}} \ .$$

Therefore, we can monitor the complex CARL amplitude in real time. This allows us to calculate the $g^{(1)}(\tau)$ correlation function and the emission spectrum.

Until now we did not take into account the backaction of atomic motion on the Bloch beams. Find a regime where Bloch is strong while CARL is weak. We take the equations of [94], remove the external potential, but consider the dynamics of both counterpropagating modes,

$$\begin{aligned} \imath\hbar\frac{d}{dt}\psi &= -\frac{\hbar^2}{2m}\frac{d^2}{dz^2}\psi - \imath U_0(\alpha_+^*\alpha_- e^{2\imath kz} - \alpha_+\alpha_-^* e^{-2\imath kz})\psi - maz\psi \\ \dot{\alpha}_\pm &= -(\kappa + \imath\Delta_c - \imath U_0)\alpha_\pm + NU_0\alpha_\mp \int |\psi|^2 e^{-2\imath kz} d(2kz) + \eta_\pm \ . \end{aligned}$$

With the unitary transformation $\psi = \tilde{\psi}e^{\imath maz t/\hbar}$, we derive,

$$\begin{aligned} \imath\hbar\frac{d}{dt}\tilde{\psi} &= -\frac{\hbar^2}{2m}\left(\frac{d}{dz} + \frac{\imath mat}{\hbar}\right)^2\tilde{\psi} - \imath U_0(\alpha_+^*\alpha_- e^{2\imath kz} - \alpha_+\alpha_-^* e^{-2\imath kz})\tilde{\psi} \\ \dot{\alpha}_\pm &= -(\kappa + \imath\Delta_c - \imath U_0)\alpha_\pm + NU_0\alpha_\mp \int |\tilde{\psi}|^2 e^{-2\imath kz} d(2kz) + \eta_\pm \ , \end{aligned}$$

and with the mode expansion $\tilde{\psi} = \frac{1}{\sqrt{2\pi}}\sum_n c_n(t)e^{2\imath nkz}$, we obtain,

$$\begin{aligned} \dot{c}_n &= -4\imath\omega_{rec}(n + \nu_{blo}t)^2 c_n + U_0(\alpha_+\alpha_-^* c_{n+1} - \alpha_+^*\alpha_- c_{n-1}) \\ \dot{\alpha}_\pm &= -(\kappa + \imath\Delta_c - \imath U_0)\alpha_\pm + NU_0\alpha_\mp \sum_n c_{n-1}^* c_n + \eta_\pm \ . \end{aligned}$$

1.84 02.03.2021 Parameter regimes for Bloch oscillations and CARL 1

In this section we will investigate in which regimes of experimental parameters signatures Bloch oscillations and CARL dynamics may be expected. We distinguish between, on one hand, parameters that are fixed, such as atomic constants (atomic mass m, transition wavelengths λ, and decay rates Γ) or invariable parameters determined by the geometry of the ring cavity (free spectral range δ_{fsr}, mode volume V, finesse F, and mirror reflectivities R). Other parameters are tunable (frequency detuning Δ_a and powers of the lasers $P_\pm$ pumping the two counterpropagating modes of the ring cavity) or fluctuate from shot to shot with an experimental run (atom number N and temperature T of the cloud interacting with the cavity).

input parameters			
atomic constants	cavity constants	tunable parameters	fluctuating parameters
$m = 88u$	δ_{fsr}	Δ_a	N
ω_{689}	w_0	$P_\pm$	T
Γ_{689}	F_s, F_p		
	R_{hr}		

These parameters are the 'input' for the derivation of other quantities which are characteristic for the atom-cavity interaction and which follow from the following relationships:

derived parameters			
atomic parameters	cavity parameters	cavity fields	atom cavity interactions
$\omega_{rec} = \frac{\hbar^2 k^2}{2m}$	$V = \pi L w_0^2$	$I_\pm = \frac{2P_\pm}{\pi w_0^2}$	$g_1 = \sqrt{\frac{3\pi\Gamma\omega}{k^3 V}}$
$T_{Doppler} = \frac{\hbar\Gamma}{2}$	$\kappa_{s,p} = \frac{\delta_{fsr}}{2F_{s,p}}$	$P_\pm = \hbar\omega\delta_{fsr}\alpha_\pm^2$	$U_0 = \frac{g_1^2}{\Delta_a}$, $\gamma_0 = \frac{\Gamma g_1^2}{\Delta_a^2}$
$I_{sat} = \frac{2\pi^2 c\hbar\Gamma}{3\lambda^3}$		$C_{dip} = \frac{\sqrt{P_+P_-}}{(\sqrt{P_+}+\sqrt{P_-})^2}$	$\Upsilon = \frac{g_1^2}{\kappa\Gamma}$
$\nu_{blo} = \frac{mg}{2\hbar k}$		$\eta_\pm = \kappa\alpha_\pm$	$s = \frac{g_1^2}{\Gamma^2}$
		$P_{cav,\pm} = \frac{P_{trns,\pm}}{1-R_{hr}}$	$r = \frac{\omega_{rec}}{\kappa}$
			$\Omega_{cav} = \Gamma\sqrt{\frac{I}{I_{sat}}}$
			$V_{dip} = \frac{3\pi c^2\Gamma}{2\omega^3\Delta} I$
			$\omega_{ax}, \omega_{rad}, \omega_{lat}$

1.84.1 Conditions for Bloch oscillations

The adiabatic rapid passage (ARP) condition for the observability of Bloch oscillations is [79, 94],

$$\frac{16\nu_{blo}}{\omega_{rec}} \ll \left(\frac{V_{0,dip}}{\hbar\omega_{rec}}\right)^2 \ll 1 \ . \tag{1.15}$$

For the strontium line λ_{689} we have $16\nu_{blo}/\omega_{rec} = 0.398$, so that, defining a 'Bloch parameter',

$$\varepsilon_{blo} \equiv \frac{V_{0,dip}}{\hbar\omega_{rec}} \tag{1.16}$$

the dipole trap depth needs to satisfy,

$$0.631 < \varepsilon_{blo} < 1 \ . \tag{1.17}$$

For Bloch oscillations we consider equal field amplitudes, $\alpha_+ = \alpha_-$, so that the above condition can be rewritten,

$$\varepsilon_{blo} \equiv \frac{4nU_0}{\omega_{rec}} = \frac{4g_1^2}{\omega_{rec}} \frac{n}{\Delta_a} \approx 1 \ , \tag{1.18}$$

with $n \equiv |\alpha_+|^2$ the photon number.

1.84.2 CARL

On the other hand, CARL works best for a collective mode-mode coupling strength of [60] [2,3],

$$\varepsilon_{crl} \equiv \frac{NU_0}{\kappa} = \frac{Ng_1^2}{\kappa} \frac{1}{\Delta_a} \lesssim 1 \ .$$

1.84.3 Experimental schemes

We may think of different experimental configurations for studying Bloch-CARL interplay, three of them will be discussed in the following:

(I) In the simulations [94] the light beams destined to generate the standing wave, in which the atoms should undergo Bloch oscillations, were irradiated from the side crossing the ring cavity mode. When the light beams intersect under an angle β, in order to fulfill the Bragg condition for a given lattice constant, the frequency of light beams must be tuned accordingly,

$$\lambda_{light} = \lambda_{lat} \sin \tfrac{\beta}{2} \ . \tag{1.19}$$

For angles $\beta \ll 180°$ the Bragg condition implies $\lambda_{light} \ll \lambda_{lat}$. On the other hand, we want to probe the Bloch oscillations via CARL, which only works sufficiently close to an atomic resonance, $\lambda_{lat} \simeq \lambda_{atom}$. Hence, for large angles β the frequency of the light beams must be tuned far into the blue side of the atomic resonance.

For strong atomic resonances, such as the D_2 line in rubidium or the 461 nm transition in strontium, this is certainly a viable solution [94]. However (for other reasons), we opted for the narrow 689 nm transition in strontium, for which this experimental configuration is not realistic. Indeed, the 689 nm transition is so weak, that as soon as we tune an exciting laser beam more than 200 GHz away from it, the 461 nm transition will complete dominate the atomic dynamics. Hence, in the Bragg condition (1.19),

$$\omega_{lat} = \omega_{light} \sin \tfrac{\beta}{2} \ , \tag{1.20}$$

[2] In practice, however, the atoms will not be perfectly bunched. That is, the effective atom number N may be much smaller. Also, the bunching depends on the depth of the dipole potential such that the CARL strength also depends on the temperature and on the number of photons $|\alpha|^2$, after all.

[3] The more correct formula would be,

$$U_0 = \frac{g_1^2 \Delta_a}{\Delta_a^2 + \Gamma^2} \ ,$$

but $|\Delta_a| \gg \Gamma$ is always well satisfied.

we need $\omega_{light} - \omega_{lat} \gg 200\,\mathrm{GHz}$, that is,

$$\beta = 2\arcsin\frac{\omega_{lat}}{\omega_{lat} + (2\pi)\ 200\,\mathrm{GHz}} = 180^\circ - 0.25^\circ\ . \tag{1.21}$$

In other words, no Bloch oscillations can be observed via CARL on the narrow transition, unless $\beta \approx 180^\circ$. This led us to envisage another configuration, where the lattice beams would be anti-parallel and collinear with the CARL beams,

$$\omega_{lat} = \omega_{light} = \omega_{689}\ . \tag{1.22}$$

(II) If all beams are collinear, they must we supported by cavity modes, i.e. they must be resonant. Let us now, based on the relationships (1.15) to (1.18) evaluation the best set of parameters for combined Boch and CARL dynamics. Assuming an atom number of $N = 100000$, we want to express both parameters ε_{blo} and ε_{crl} as a function of the experimentally tunable parameters Δ_a and $P = n\hbar\omega\delta_{fsr}$ and plot them in a two-dimensional graph, as done in Fig. 1.76.

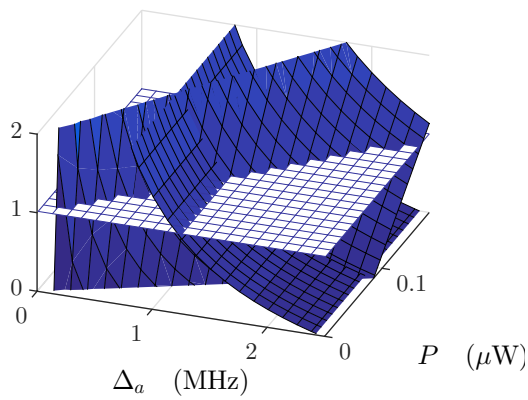

Figure 1.76: (code) CARL and Bloch parameters as a function of photon number and detuning. The fixed parameters are: $\kappa = (2\pi)\ 440\,\mathrm{kHz}$, $\omega_{rec} = (2\pi)\ 4.8\,\mathrm{kHz}$, and $g_1 = (2\pi)\ 9.1\,\mathrm{kHz}$.

The optimum condition is reached for $\varepsilon_{crl} = 1 = \varepsilon_{blo}$. The first condition which implies,

$$\Delta_a = \frac{Ng_1^2}{\kappa} \approx (2\pi)2.4\,\mathrm{MHz}\ . \tag{1.23}$$

The second condition implies, inserting the first condition,

$$n = \frac{\omega_{rec}}{4g_1^2}\Delta_a = \frac{N\omega_{rec}}{4\kappa} \approx 35\ , \tag{1.24}$$

meaning that Bloch oscillations should be observed when 35 photons, or equivalently $P = 160\,\mathrm{nW}$ of power circulate in the ring cavity.

Both conditions are difficult to realize, because Δ_a is extremely small (within the cavity linewidth) and so low powers are difficult to control in view of the large

cavity enhancement factor. With the present cavity it seems impossible to drive Bloch oscillations and CARL simultaneously. Nevertheless, we still may study the two dynamics separately:

(IIa) For CARL, we note that it can be observed for $\epsilon_{crl} \simeq 0.1$ relaxing somewhat the condition (1.22). However, care must be take to avoid strong intracavity powers, as these would induce considerable power broadening, which could easily exceed the detuning.

(IIb) For Bloch, instead of using extremely weak intracavity powers, we could tune the lasers far from resonance, i.e. at least several 4 GHz.

(IIc) Note also, that both of the above equations scale with κ^{-1}, so that higher finesses of the cavity would considerably ease the situation. Anyhow, the goal has always been to replace the ring cavity mirrors by supermirrors.

(III) Another strategy may consist in operating CARL and Bloch at different frequencies, $\Delta_{a,blo} \gg \delta_{a,crl}$, violating weakly the Bragg condition (1.22). We could run the Bloch laser with low but reasonable intracavity power on a cavity mode at $\nu_a - 4.2\,\text{GHz}$ and the CARL laser (phase-locked to the Bloch laser) on another cavity mode at $\nu_a - 200\,\text{MHz}$. In this case, we need to evaluate the consequences of the Bragg condition violation!

1.84.4 Parameters for simulations

The simulations performed by [94] assumed Rb atoms driven on their D_2-line with the following set of parameters ($W_0 \equiv V_{0,dip}$),

$$N = 40000 \tag{1.25}$$

$$\begin{aligned} \alpha_0 &\equiv \frac{W_0}{4U_0} = 20 \\ \nu_{blo} &= 0.035 \\ \kappa &= 160\omega_{rec} \\ U_0 &= 0.04\omega_{rec} \ . \end{aligned} \tag{1.26}$$

Translated into our figures of merit, we deduce,

$$\varepsilon_{blo} = \frac{V_{0,dip}}{\omega_{rec}} = 0.32 \qquad \text{and} \qquad \varepsilon_{crl} = \frac{NU_0}{\kappa} = 10 \ . \tag{1.27}$$

1.85 30.05.2021 Phosphoretic traps

Zhiyong Gong et al., *Optical configurations for photophoretic trap of single particles in air* [DOI]

B. Redding et al., *Optical trap for both transparent and absorbing particles in air using a single shaped laser beam* [DOI]

1.86 01.06.2021 Supernarrow clock transitions

While the $^1S_0$-$^3P_0$ transition is weakly allowed in ^{87}Sr, it seems to be strictly forbidden in ^{88}Sr. Nevertheless, it can be driven when a magnetic field is applied [96, 109, 52]. The magnetic field admixes the $^3P_1$ level, whose decay is weakly allowed. According to [109], the Rabi frequency is,

$$\Omega_{698} = \alpha_{Sr}\sqrt{I}|B|\cos\theta \ ,$$

where θ is the angle between the $\mathcal{B}$-field and the laser polarization and $\alpha_{Sr} = 2\pi \cdot 198\,\mathrm{Hz/T}\sqrt{\mathrm{mW\ cm^{-2}}}$. I checked that we can readily make $B = 200\,\mathrm{G}$ with our MOT coils in Helmholtz configuration with 9 A, and intracavity we easily get intensities higher than $2\,\mathrm{kW/cm^2}$, yielding,

$$\Omega_{698} \approx (2\pi)\ 1\,\mathrm{kHz} \ .$$

This Rabi frequency is still small [52], the problem being that the saturation broadening is generally well below the Doppler width. At this intensity, we have on the $^1S_0$-$^3P_1$ transition a Rabi frequency of,

$$\Omega_{689} = \sqrt{\frac{3\lambda^2}{2\pi}\frac{I}{\hbar\omega}\Gamma_{689}} \approx 2\pi \cdot 140\,\mathrm{MHz} = 1.6 \cdot 10^4\gamma_{689} \ .$$

With the fine structure splitting,

$$\Delta_{fs} = \omega_{689} - \omega_{698} \approx (2\pi)5.6\,\mathrm{THz} \ ,$$

we can calculate the coupling matrix element,

$$\Omega_B = \frac{\Omega_{698}\Delta_{fs}}{\Omega_{689}} \approx 2\pi \cdot 40\,\mathrm{MHz} \ ,$$

and finally, the decay width,

$$\gamma_{698} = \gamma_{689}\frac{\Omega_{689}^2/4 + \Omega_B^2}{\Delta_{fs}^2} \approx 2\pi 1.5\,\mu\mathrm{Hz} = \Omega_{698}/67 \cdot 10^8 \ .$$

1.86.1 Single-photon matter wave interferometry

The possibility of Rabi cycling (absorption and stimulated emission) on an optical transition without spontaneous emission opens possibilities for gravitational wave detection [122, 46] and gravity gradient measurements. While two-photon transitions are always afflicted by laser phase noise. One-photon transitions are immune.

Questions:

- Is it possible to have Bloch oscillations with a single laser? Does the absence of spontaneous emission allows us to do CARL on resonance?
- The occurrence of gravitational waves generated by supernovae seems not predictable. So a matter wave detector would have to run continuously!
- Higher-order Bragg interferometers are not possible with single-photon processes!

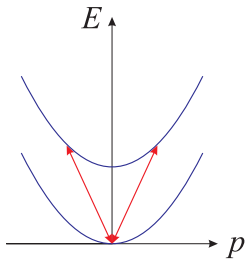

Figure 1.77: (code) .

1.86.2 Superradiant enhancement

Supernarrow *clock transitions* might be *superradiantly* excited in high finesse cavities.

Questions:

- working in ring cavity? would expect some mode competition between counterpropagating modes, each one fighting for who may use the inversion for gain! - working on 7.6 kHz line? - how to pump? via blue transition? making a reservoir in the $^3P_2$?

For $T = 2\mu\text{K}$,

$$k\bar{v} = k\sqrt{\frac{k_B T}{m}}$$
$$\delta\nu_{Dpl} = \frac{k\bar{v}}{\ln 2} \approx 180000\,\text{s}^{-1}$$
$$\frac{\delta\nu_{Dpl}}{\Gamma} \approx \frac{180}{2\pi \cdot 7600} = 3.8\ .$$

We are safely in the Markovian regime $\Gamma\tau_{rt} \ll 1$. Low-Q regime of CQED. How about if we superradiantly enhance Γ?

1.87 15.07.2021 Sr in a ring cavity near resonance

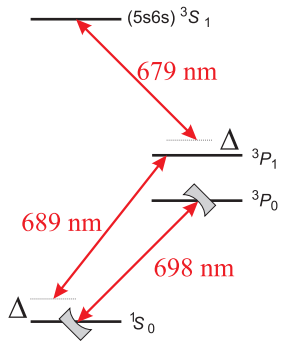

Figure 1.78: (code) .

Consider Sr 689 nm and 679 nm cascade system with $\Gamma_{689}/2\pi = 7.6\,\text{kHz}$ and $\Gamma_{679}/2\pi = 2\,\text{MHz}$. The repumper transition is driven off resonance. Assuming $\Delta_{679} = 100\Gamma_{679}$ and $\Omega_{679} = \Gamma_{679}$, the time required for a π-pulse is,

$$t = \frac{4\pi\Delta}{\Omega^2} = 100\,\mu\text{s} \ .$$

For the Sr 689 nm and 698 nm V system, we have actually,

$\kappa/2\pi = 440\text{kHz}$	
$\Gamma_{689}/2\pi = 7.6\text{kHz}$	$\Gamma_{698}/2\pi = 0.1\text{mHz}$
$g_{689}/2\pi = 9.1\text{kHz}$	$g_{698}/2\pi = 1.1\text{Hz}$
$s_{689} = 1.4$	$s_{698} = 11000$
$\Upsilon_{689} = 0.02$	$\Upsilon_{698} = 1.1$
$\kappa \gg g_{689} \simeq \Gamma_{689}$	$\kappa \gg g_{698} \gg \Gamma_{698}$

1.88 21.08.2021 Bragg spectroscopy on Sr 1

Momentum state squeezing is predicted to allow for sub-standard quantum limit resolution in Ramsey-Bordé interferometers [92]. Salvi et al. propose to generate coherent momentum state superpositions whose population imbalance is then determined by a ring cavity-assisted quantum non-demolition measurement based on a Pound-Drever-Hall type scheme (see Physics, Exc. 44.3.8.6).

1.88.1 Realization of Bragg pulses

We have at our disposal the main ingredients to implement this proposal: ultracold strontium atoms and a ring cavity. Only missing is a pair of Raman beams allowing for controlled Bragg diffraction. Unlike proposed in [92] we will not (easily) be able to use counterpropagating Raman beams, but our chambers has two unused ports proving a 30° have access to the ring cavity mode (see Kimball Flange Multiplexer MCF275-FlgMplxr-Cr1A5). Hence, we can realize 60° Bragg angles. Considering the blue MOT transition for Bragg diffraction, the momentum transfer will be,

$$\frac{\Delta p}{\hbar k_{689}} = \frac{2\hbar k_{461} \sin \frac{60^\circ}{2}}{\hbar k_{689}} = \frac{2\lambda_{689}}{\lambda_{461}} \sin \frac{\pi}{12} = 1.5 \ ,$$

which is above the recoil limit, but we could also do multi-photon higher-order Bragg diffraction. Note also, that using the red MOT transition we would have $\frac{\Delta p}{\hbar k_{689}} = 1$.

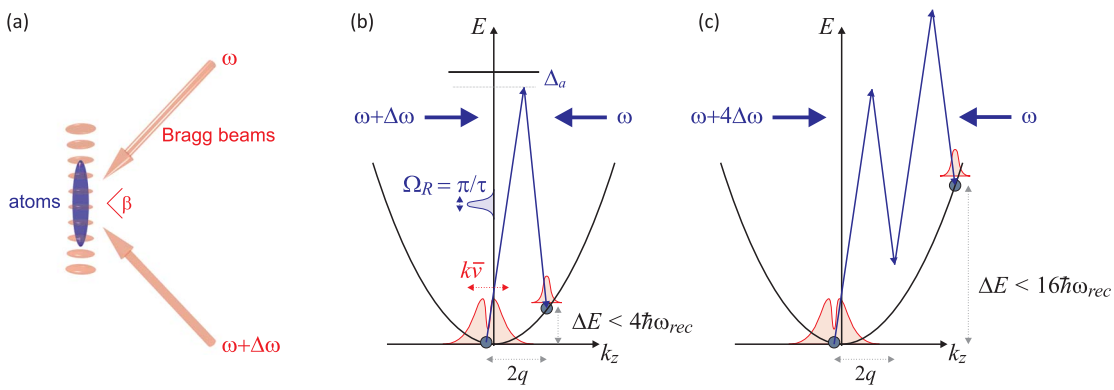

Figure 1.79: (code) Bragg scattering scheme.

What do we need? We would need a Toptica DLproHP and an AOM shifting the frequencies of the Bragg beams by,

$$\Delta\omega \simeq 0 ... \omega_{rec} \ .$$

I propose to have Henrique set up Bragg lasers.

Some estimations: At $T = 800$nK the Doppler broadening of the thermal cloud at 689nm is,

$$k_{689}\bar{v} = k_{689}\sqrt{\frac{k_B T}{m}} \simeq k_{689} 8.7\,\mathrm{mm/s} = (2\pi)\ 12.6\,\mathrm{kHz} \ .$$

The recoil velocity is,

$$v_{rec} = \frac{\hbar k_{689}}{m} = 6.6\,\mathrm{mm/s} \ .$$

Hence, $v_{rec} < \bar{v}$. The recoil shift is,

$$\omega_{rec,689} = \frac{\hbar k_{689}^2}{2m} \simeq (2\pi)\ 4.8\,\mathrm{kHz} \ .$$

Assuming a Bragg angle of θ, the momentum transfer is,

$$\Delta p = 2\hbar q = 2\hbar k_{461} \sin\tfrac{\theta}{2} \ .$$

and the energy transfer,

$$\Delta E = \frac{(2\hbar q)^2}{2m} < \frac{(2\hbar k_{689})^2}{2m} = 4\hbar\omega_{rec,689} \ .$$

The power broadening of the Raman transition is,

$$\Omega_R = \frac{\Omega_1\Omega_2}{\Delta_a} \ .$$

If we limit the pulse length to $\tau = 50\mu$s, the Raman Rabi frequency for a π-pulse must be,

$$\Omega_R = \frac{\pi}{\tau} \simeq (2\pi)\ 10\,\mathrm{kHz} \ .$$

1.88.2 Simulation of Bragg scattering for ultracold thermal clouds

As a proof of principle we could start repeating some of the experiments of [11, 32, 68]. The optimum parameters for strontium (detuning, pulse length, power) can be estimated from simulations as done in [32] (see Physics, Sec. 51.2.2).

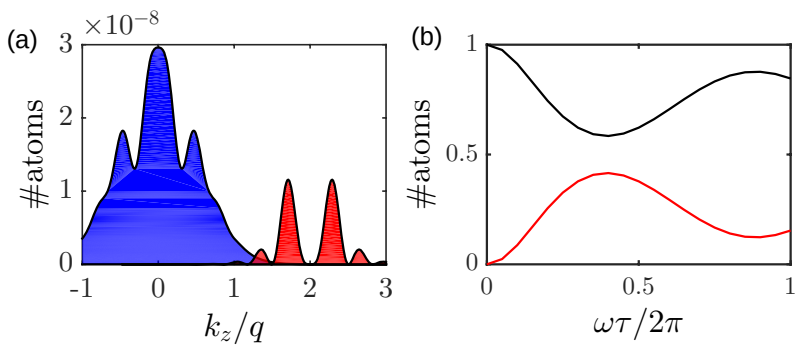

Figure 1.80: (code) (a) Distribution of momentum classes in the direction of k_z after irradiation of a 2π Bragg pulse. The width of the structure is determined by the power broadening of the Raman transition. (b) Temporal evolution of the populations of the momentum states 0 and $2q$.

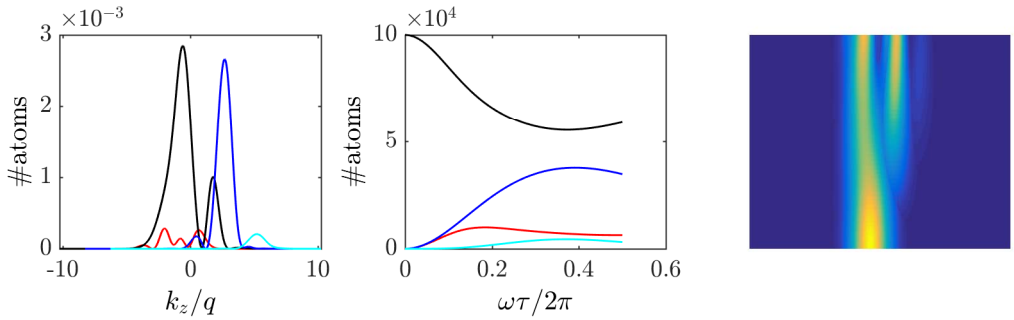

Figure 1.81: (code) Same as above in the Raman-Nath regime with 4 momentum states.

1.88.3 Cooling by velocity-selection

There are various ways of reducing the width of the velocity distribution [79]. E.g. we could apply a Bragg pulse long enough to diffract a narrow velocity distribution, but short enough to prevent thermal expansion. The diffracted atoms could be shelved on a metastable level, while the non-diffracted atoms could be removed by a resonant laser pulse.

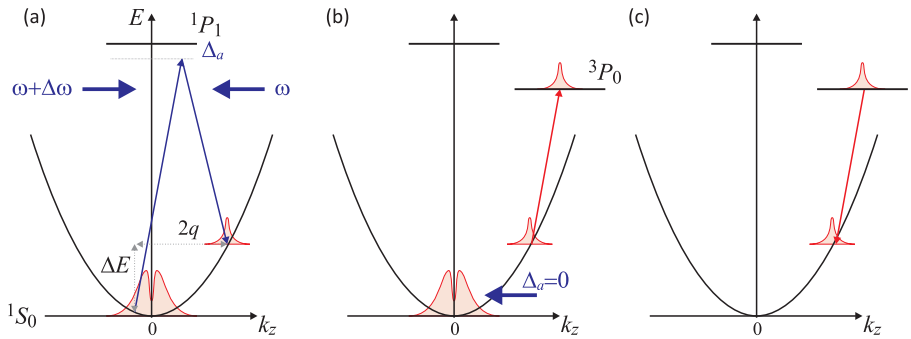

Figure 1.82: (code) (a) Distribution of momentum classes in the direction of k_z after irradiation of a 2π Bragg pulse. The width of the structure is determined by the power broadening of the Raman transition. (b) Temporal evolution of the populations of the momentum states 0 and $2q$.

1.88.4 Raman sideband cooling

Resolved sideband cooling requires to confine the atoms in a tight potential, e.g. a 1D lattice [Bishof, thesis, University of Colorado at Boulder (2014)]. This lattice must, however be operated at the magic wavelength. Perhaps, Raman sideband cooling?

In contrast, Bragg diffraction velocity selection could be done on free atoms.

1.89 22.08.2021 Ring cavity frequency-shift between s and p-polarization

How to represent the Bloch oscillation dynamics on a Bloch sphere?

What happens with uniformly propagating standing waves? Asymmetric Brioullin zone?

1.90 26.08.2021 Ring cavity frequency-shift between s and p-polarization

Dalila observes 4 GHz frequency shift between the TEM_{00} of s and p-polarization. This would mean that the p-polarization penetrates by half a wavelength into the mirrors, which seems quite a lot.

1.91 22.11.2021 Mirror backscattering in the ring cavity

Dalila measured the light power leaking through both ring cavity modes when only one direction is pumped (input power: 2 mW and coupling efficiency 50%). When pumped from below the transmission of the pumped mode through a HR mirror is roughly $P_+^\uparrow = 20\,\mu$W. When pumped from above the transmission of the backscattered light through the same HR mirror is roughly $P_+^\downarrow 2\,$nW, that is,

$$\frac{P_+^\downarrow}{P_+^\uparrow} \simeq 0.0001 \ ,$$

and hence,

$$\left|\frac{\alpha_+^\downarrow}{\alpha_+^\uparrow}\right| =\simeq 0.01 \ .$$

As expected (because of the lower finesse of our cavity), the values are a bit lower than what we found in Tübingen [58]. There we got $U_s \leq 0.034\kappa$ and the value depended strongly on the cavity length.

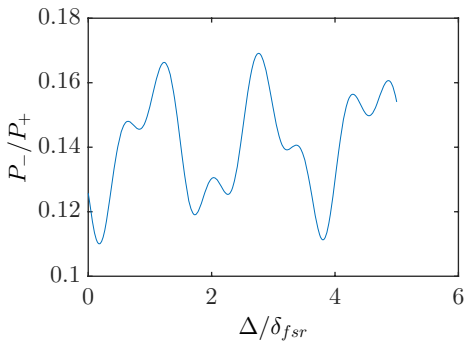

Figure 1.83: (code) Typical expected frequency-dependence of the power ratio.

The CARL equations for symmetric pumping are,

$$\begin{aligned}\dot{\alpha}_+ &= -\kappa\alpha_+ - \imath(U_1 e^{-2\imath kz_1} + U_2 e^{-2\imath kz_2} + U_3 e^{-2\imath kz_3}\alpha_- + \eta_+ \\ \dot{\alpha}_- &= -\kappa\alpha_- - \imath(U_1 e^{2\imath kz_1} + U_2 e^{2\imath kz_2} + U_3 e^{2\imath kz_3})\alpha_+ + \eta_- \ .\end{aligned}$$

In steady-state and pumping from below the mode $\alpha_+^\uparrow = \frac{\eta_+}{\kappa}$, we get,

$$\frac{\alpha_-^\uparrow}{\alpha_+^\uparrow} = -\frac{\imath(U_1 e^{2\imath kz_1} + U_2 e^{2\imath kz_2} + U_3 e^{2\imath kz_3})}{\kappa} \ .$$

Alternatively, we may pump from above the other mode $\alpha_-^\downarrow = \frac{\eta_-}{\kappa}$. Then we get,

$$\frac{\alpha_+^\downarrow}{\alpha_-^\downarrow} = -\frac{\imath(U_1 e^{-2\imath kz_1} + U_2 e^{-2\imath kz_2} + U_3 e^{-2\imath kz_3})}{\kappa} = -\frac{(\alpha_-^\uparrow)^*}{(\alpha_+^\uparrow)^*} \ ,$$

and consequently,

$$\frac{P_-^\uparrow}{P_+^\uparrow} = \left| \frac{U_1 e^{2\imath k z_1} + U_2 e^{2\imath k z_2} + U_3 e^{2\imath k z_3}}{\kappa} \right|^2 = \frac{P_+^\downarrow}{P_-^\downarrow} \ .$$

So, we should expect exactly the same ratio.

1.92 12.12.2021 Heating in the ring cavity

Dalila found that resonant light, $\Delta_a = 0 = \Delta_c$, coupled into the cavity heats up the red MOT. When she blocked the cavity light, no heating is observed. Is this heating really caused by the cavity mode? Or could it be caused by stray light coming from reflections at some interface (which we observed earlier)?

Let us first remember the saturation intensity of the red transition, $I_s = 3\,\mu\mathrm{W/cm}^2$, and the recoil energy, $\hbar\omega_{rec} = h^2/2m\lambda^2 \approx k_B 230\,\mathrm{nK}$. Assuming a stray light intensity of $I_{stray} = 10\,\mathrm{nW/cm}^2 \ll I_{sat}$, a course estimation of the resonant heating rate gives,

$$\frac{dE_{stray}}{dt} = \hbar\omega_{rec}\,\frac{3\lambda^2}{2\pi}\frac{\Gamma^2}{4\Delta^2+2\Omega^2+\Gamma^2}\,\frac{I_{stray}}{\hbar\omega_{las}}\Gamma \simeq \frac{3h\lambda}{2mc}\frac{\Gamma}{2\pi}I_{stray} \approx 1.3\,\mathrm{K/s}\ ,$$

which could well explain Dalila's observation.

On the other hand, pumping the ring cavity with $P_{in} = 1\,\mathrm{mW}$ power with $\eta = 50\%$ coupling efficiency and assuming a finesse of $F = 1000$ we generate an intracavity power of,

$$P_{cav} = \eta F P_{in} \approx 500\,\mathrm{W}\ .$$

We found earlier that this yields a transmitted power of $P_{trans} = t_{in}P_{cav} \approx 20\,\mathrm{mW}$, from which we determine $t_{in} \approx 0.00004$. The intensity at the waist is then $I_{cav} = 2P_{cav}/\pi w_0^2 \approx 6.5\,\mathrm{kW/cm}^2$. Assuming non-resonant light, $\Delta_a = \Delta_c = 400000\Gamma \approx (2\pi)\,3\,\mathrm{GHz}$, using the same formula for the heating rate, I estimate,

$$\frac{dE_{cav}}{dt} \simeq \frac{3h\lambda}{2mc}\frac{\Gamma^2}{4\Delta^2}I_{cav}\frac{\Gamma}{2\pi} \approx 1.3\,\mathrm{K/s}\ ,$$

or,

$$\frac{dE_{stray}/dt}{dE_{cav}/dt} = \frac{4\Delta^2 I_{stray}}{\Gamma^2 I_{cav}} \approx 1\ .$$

We learn two things from these estimations: (1) stray light will generate huge heating on resonance: STAY AWAY FROM RESONANCE; (2) at large detunings the cavity-induced heating rate is still many orders of magnitude larger than the on-resonance heating rate caused by stray light. For CARL we will need to tune further away and reduce the intracavity power.

For the above values, the saturation parameter is,

$$s = \frac{\frac{1}{2}\Omega^2}{\Delta^2+\frac{1}{4}\Gamma^2}\quad,\qquad s_0 = \frac{2\Omega^2}{\Gamma^2} = \frac{I}{I_{sat}} \approx \frac{6.5\cdot 10^3}{3\cdot 10^{-6}} = 2.2\cdot 10^9\ ,$$

and the power broadening,

$$\Omega = \Gamma\sqrt{\frac{s_0}{2}} = \Gamma\sqrt{\frac{I}{2I_{sat}}} \approx (2\pi)\ 7.6\,\mathrm{kHz}\sqrt{\frac{2.2\cdot 10^9}{2}} = (2\pi)\ 250\,\mathrm{MHz}\ .$$

Hence, in order to avoid heating, we need to tune further away than $|\Delta| \gg \Omega$.

The following tests could be done:

- tune laser to resonance, $\Delta_a = 0$, and compare the heatings for the cavity on and off resonance $\Delta_c \binom{=}{\neq} 0$;
- tune the laser away from resonance, $|\Delta_a| > 100000\Gamma$, and search for the cavity mode volume.

1.93 21.12.2021 Vacuum Rabi splitting

According to [27] we expect (see Physics Script, Exc. 42.2.6.8),

$$T = \frac{\kappa^2}{|\kappa - \imath\Delta_c + g_1\sqrt{N}/(\gamma - \imath\Delta_a)|^2}$$

for the transmission spectrum of the ring cavity. In our case, $\Delta_a = \Delta_c$, $g_1/2\pi = 9.1\,\mathrm{kHz}$, $\Gamma/2\pi = 7.6\,\mathrm{kHz}$, $\kappa/2\pi = 690\,\mathrm{kHz}$, and $N = 1..10^5$. Using the scheme of

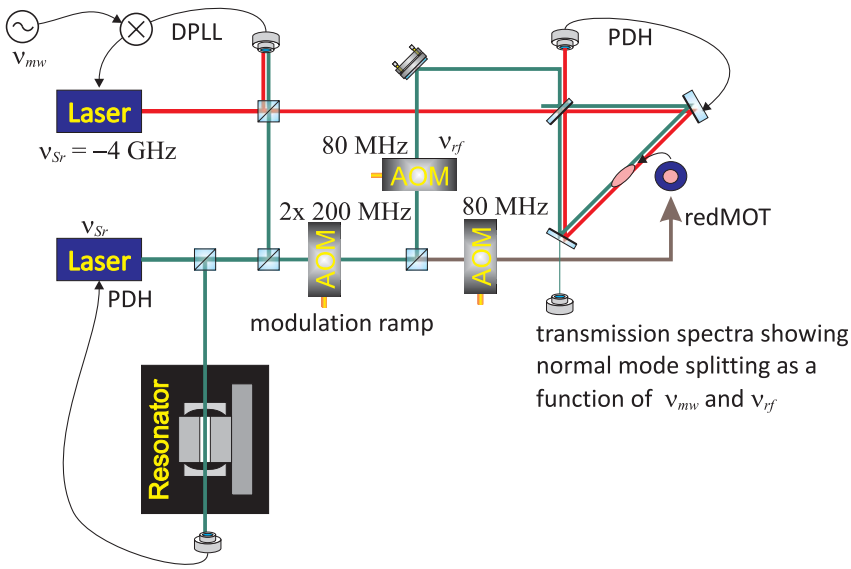

Figure 1.84: (code) .

Fig. 1.84 observe the transmitted intensity as a function of ν_{rf}, ν_{mw}, and N.

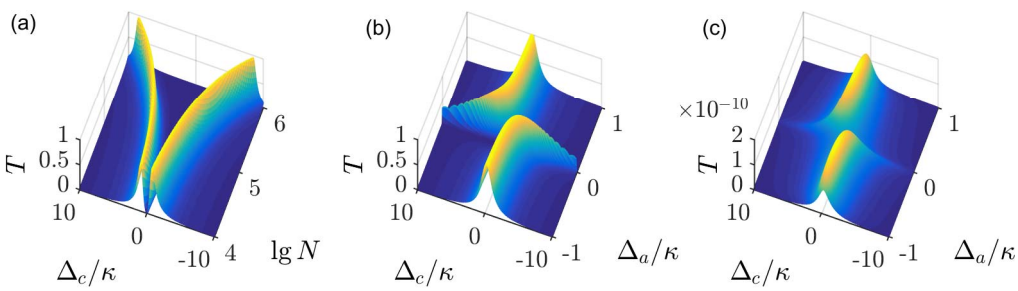

Figure 1.85: (code) .

1.94 13.01.2022 Parameter regimes for Bloch oscillations and CARL 2

Dalila managed to hold $N = 100000$ atoms in the ring cavity standing wave at temperatures of μK for times as long as 400 ms with the laser detuning $\Delta_a = (2\pi)\,4\,\mathrm{GHz}$ and the intracavity laser powers $P_{cav,+} = P_{cav,-} = 1\,\mathrm{W}$.

We can now envisage searching for Bloch oscillations, at first concentrating on signatures in absorption images. However, the dipole trap depth is currently way to deep, as revealed by the above estimations. Logical next steps would be:

1. Measure the trap lifetime, i.e. take curves of N, T_{hor}, T_{vrt} as a function of t_{hold} for various detunings Δ_a and intracavity powers $P_\pm$. Note that oscillations that may appear in the curves could result from ω_r and ω_{lat}. In this case their frequency should depend on Δ_a and $P_\pm$.

2. Optimization: Evtl. rotate the camera in order to represent gravity along the vertical axis of the screen.

3. Observe the stability of the cavity lattice potential: Fluctuations of the transmitted light of each mode, as well as their interference. If stability turns out to be an issue we will need to design a new monolithic coupling mount for both cavity directions.

4. Calibrate the intracavity powers via the light transmitted through the HR-mirrors, find also alternative (complementary) ways. One possible way may be to send a short red MOT pulse with blue-tuned frequency into the dipole trap. Note that full red MOT power corresponds to $2700 I_{sat}$, that is, $\Omega = \Gamma\sqrt{2700/2} \approx (2\pi)\ 0.28$ MHz.

5. Reduce the intracavity powers as much as possible and check out the limit for stable PDH-locking.

6. At the lowest possible power increase the detuning until the potential depth is on the order of the recoil frequency, $nU_0 \simeq \omega_{rec}$. Here, we may search for Bloch oscillations.

7. CARL comes later! It will probably turn out necessary to lock the cavity far away and drive Bloch + CARL weakly near resonance. How to separate the beams? By heterodyning?

1.95 19.01.2022 Summary of ring cavity estimations

1.95.1 Cavity finesse

The cavity consists of two highly reflecting mirrors with the measured reflectivities $R_{hr,s} = 99.85\%$ and $R_{hr,p} = 99.71\%$ for the two polarizations under an angle of incidence of $\alpha = 22.5°$ and one incoupler with the measured reflectivities $R_{ic,s} = 99.69\%$ and $R_{ic,p} = 96.72\%$ for the two polarizations under an angle of incidence of $\beta = 45°$ [4]. With this, we expect a finesse of

$$F_n = \frac{\pi(R_{hr,n}^2 R_{ic,n})^{1/6}}{1 - (R_{hr,n}^2 R_{ic,n})^{1/3}} \tag{1.28}$$

with $n = s, p$, yielding $F_s = 1546$ and $F_p = 241$. We measured, however, the finesses $F_s = 1200$ and $F_p = 500$. The mean reflectivities,

$$\bar{R}_n \equiv (R_{hr,n}^2 R_{ic,n})^{1/3} \simeq 1 - \frac{\pi}{F} \tag{1.29}$$

corresponding to these finesses are $\bar{R}_s = 99.738\%$ and $\bar{R}_p = 99.374\%$. As the finesse measurements are more precise than the reflectivity measurements, we will use them in the following to recalibrate the input coupler reflectivities according to $R_{ic,n} = \bar{R}_n^3 / R_{hr,n}^2$, yielding $R_{ic,s} = 99.51\%$ and $R_{ic,s} = 98.71\%$. The cavity linewidth is now obtained as,

$$\kappa_n = \frac{\delta_{fsr}}{2F_n} \ , \tag{1.30}$$

giving $\kappa_s/2\pi = 3.43\,\mathrm{MHz}$ and $\kappa_p/2\pi = 8.23\,\mathrm{MHz}$.

1.95.2 Cavity geometry

We measured a free spectral range of $\delta_{fsr} = 8.23\,\mathrm{GHz}$, which corresponds to a round trip length of the cavity of

$$L = \frac{c}{\delta_{fsr}} \ , \tag{1.31}$$

yielding $L = 3.64\,\mathrm{cm}$. The radii of curvature of the spherical highly reflecting cavity mirrors are $\rho = 50\,\mathrm{mm}$, while the incoupler mirror is plane. Under the angle of incidence α, the mirror effective radius of curvature perpendicular to the ring cavity plane, $\rho_\perp$, and the effective radius of curvature parallel to the plane, $\rho_\parallel$, modify to,

$$\rho_\perp = \frac{\rho}{\cos\alpha} \qquad \text{respectively} \qquad \rho_\parallel = \rho\cos\alpha \ . \tag{1.32}$$

With this we calculate the waists of the cavity mode. We denote by a the distance between the high reflecting mirrors and b the distance between each high reflecting mirror and the incoupler. For symmetry reasons, it is clear that there must be two

[4] Note that the reflectivities specified by the seller are much higher: $R_{hr,s} = 99.97\%$ and $R_{hr,p} = 99.92\%$ under an angle of incidence of $\alpha = 22.5°$ and $R_{ic,s} = 99.74\%$ and $R_{ic,p} = 99.74\%$ under an angle of incidence of $\beta = 45°$.

waists of the cavity mode. One waist, $w_{0,m}$ ($m = \perp, \|$) is in free space halfway between the high reflecting mirrors, and we calculate it with the help of the propagation matrix M for a round-trip beginning at the waist position,

$$M = \begin{pmatrix} 1 & a/2 \\ 0 & 1 \end{pmatrix} \begin{pmatrix} 1 & 0 \\ -2/\rho_m & 1 \end{pmatrix} \begin{pmatrix} 1 & 2b \\ 0 & 1 \end{pmatrix} \begin{pmatrix} 1 & 0 \\ -2/\rho_m & 1 \end{pmatrix} \begin{pmatrix} 1 & a/2 \\ 0 & 1 \end{pmatrix}$$
$$w_{0m}^2 = \left(\frac{\lambda_{689}}{\pi}\right) \frac{|M_{12}|}{\sqrt{1 - \frac{1}{4}(M_{22} + M_{11})}} , \tag{1.33}$$

yielding $w_{0\perp} = 70\,\mu\text{m}$ and $w_{0\|} = 67\,\mu\text{m}$, such that $w_0 = \sqrt{w_{0,\perp} w_{0,\|}} = 68.5\,\mu\text{m}$. The other waist w_{2m} is on the incoupler plane mirror, and we calculate it with the help of the propagation matrix N for a round-trip beginning at the plane mirror,

$$N = \begin{pmatrix} 1 & b \\ 0 & 1 \end{pmatrix} \begin{pmatrix} 1 & 0 \\ -2/\rho_m & 1 \end{pmatrix} \begin{pmatrix} 1 & a \\ 0 & 1 \end{pmatrix} \begin{pmatrix} 1 & 0 \\ -2/\rho_m & 1 \end{pmatrix} \begin{pmatrix} 1 & b \\ 0 & 1 \end{pmatrix}$$
$$w_{2m}^2 = \left(\frac{\lambda_{689}}{\pi}\right) \frac{|N_{12}|}{\sqrt{1 - \frac{1}{4}(N_{22} + N_{11})}} , \tag{1.34}$$

yielding $w_{2\perp} = 64\,\mu\text{m}$ and $w_{2\|} = 60\,\mu\text{m}$, such that $w_2 = \sqrt{w_{2,\perp} w_{2,\|}} = 62\,\mu\text{m}$.

The mode volume of the cavity is obtained by integrating over the entire mode via the condition, $I(0)V = \int I(\mathbf{r}) d^3r$,

$$V = \pi w_{0,\perp} w_{0,\|} a \left[1 + \left(\frac{\lambda_{689} a}{2\pi w_{0,\perp} w_{0,\|}}\right)^{2/3}\right] + \pi w_{2,\perp} w_{2,\|} 2b \left[1 + \left(\frac{\lambda_{689} b}{2\pi w_{2,\perp} w_{2,\|}}\right)^{2/3}\right] , \tag{1.35}$$

giving $V = 0.5\,\text{mm}^3$. In fact, this value is well approximated by,

$$V \simeq \pi w_0^2 L , \tag{1.36}$$

which is the expression we will use from now on.

1.95.3 Atom number and temperature

Important experimental parameters are the number of atoms trapped by the mode of the ring cavity and their temperature. These parameters vary from shot to shot, but typical values are $N = 10^5$ and $T = 1\,\mu\text{K}$.

1.95.4 Coupling strength

With $\lambda_{689} = 689\,\text{nm}$, we calculate,

$$\omega_{rec} = \frac{\hbar k^2}{2m} \tag{1.37}$$

giving $\omega_{rec}/2\pi = 4.78\,\text{kHz}$. With the linewidth, $\Gamma/2\pi = 7.6\,\text{kHz}$, we calculate the coupling strength,

$$g_1 = \sqrt{\frac{3\pi\Gamma\omega}{k^3 V}} \tag{1.38}$$

to be $g_1/2\pi = 8.8\,\mathrm{kHz}$. The cooperativity is,

$$\Upsilon_n = \frac{g_1^2}{\kappa_n \Gamma} \tag{1.39}$$

yielding in the high finesse case $\Upsilon_s = 0.02$. The single-photon saturation is,

$$s = \frac{g_1^2}{\Gamma^2} \tag{1.40}$$

yielding $s = 1.4$. The single-photon light-shift far from resonance is,

$$U_0 = \frac{g_1^2}{\Delta_a} \ . \tag{1.41}$$

For example, assuming a detuning of the laser from the strontium resonance of $\Delta_a \approx 2\pi\ 200\,\mathrm{MHz}$ and an atom number of $N = 10^5$, we expect $NU_0 \approx 0.076\kappa$. The Rayleigh scattering rate is,

$$\gamma_0 = \frac{g_1^2 \Gamma}{\Delta_a^2} \tag{1.42}$$

yielding for the same values $N\gamma_0 \approx 2.9 \cdot 10^{-6}\kappa$.

1.95.5 Gain by resonant enhancement of the intracavity field

The strength of the atom-field interaction depends on the intensities of the intracavity light fields, that is, the number of photons circulating in the cavity is an important parameter, which we must know with maximum precision. For example, the ratio between injected and circulating light powers will allow us to determine the pump rate η, which is an essential parameter for CARL. To measure the intracavity power P_{cav} we can (a) use the atoms themselves as a probe, (b) measure the light injected into the cavity by one mirror and transmitted through another mirror when the cavity is in resonance, or (c) measure the light reflected from the mirror through which the light is injected. In this section we will discuss the methods (b) and (c) using the Airy formulas as starting point.

(b) We call P_{in} the power provided to pump the cavity and begin calculating the cavity field amplitude assuming plane waves,

$$E_{cav} = E_{in} t_{ic} \sum_n (-r_{hr}^2 r_{ic})^n e^{\imath k(nL+x)} = \frac{E_{in} t_{ic} e^{\imath kx}}{1 + r_{hr}^2 r_{ic} e^{\imath kL}} \tag{1.43}$$

which is the well-known Airy formula. From this, in resonance, $kL = \pi(2n-1)$, the enhancement factor of the cavity becomes,

$$G \equiv \frac{I_{cav}}{I_{in}} = \frac{|E_{cav}|^2}{|E_{in}|^2} = \frac{t_{ic}^2}{(1 - r_{hr}^2 r_{ic})^2} = \frac{T_{ic}}{\left(1 - \bar{R}^{3/2}\right)^2} \ , \tag{1.44}$$

exploiting the abbreviation (1.29), that is $\bar{R}^3 = R_{hr}^2 R_{ir}$. Noting that for the given finesses (1.28) the mean reflection $\bar{R}$ is fixed, we may also express the gain as a function of R_{hr} only,

$$G = \frac{1 - \frac{\bar{R}^3}{R_{hr}^2}}{(1 - \bar{R}^{3/2})^2} \ . \tag{1.45}$$

Inserting the reflectivities given at the beginning, we obtain the gains $G_s = 318$ and $G_p = 147$.

Similarly,

$$E_{trns} = E_{in} t_{ic} t_{hr} e^{\imath ka} \sum_n (-r_{hr}^2 r_{ic})^n e^{\imath nkL} = E_{in} \frac{t_{ic} t_{hr} e^{\imath ka}}{1 + r_{hr}^2 r_{ic} e^{\imath kL}} \ , \tag{1.46}$$

yielding,

$$\frac{I_{trns}}{I_{in}} = \frac{|E_{trns}|^2}{|E_{in}|^2} = \frac{t_{ic}^2 t_{hr}^2}{(1 - r_{hr}^2 r_{ic})^2} = \frac{T_{ic} T_{hr}}{(1 - \bar{R}^{3/2})^2} = G T_{hr} \ , \tag{1.47}$$

such that,

$$\boxed{\frac{I_{trns}}{I_{cav}} = T_{hr}} \ . \tag{1.48}$$

Therefore, we may simply deduce the intracavity power from the light transmitted through a high-reflecting mirror. We just need to know the mirror transmission T_{hr}. Inserting the reflectivities given at the beginning, we obtain the power ratios, $T_{hr,s}^{-1} = 678$ and $T_{hr,p}^{-1} = 348$.

(c) An alternative way consists in measuring the light power missing in the light reflected from the input coupler. To estimate this, we again start from the Airy-formulas,

$$E_{refl} = E_{in} \left(r_{ic} + t_{ic}^2 r_{hr}^2 \sum_n (-r_{hr}^2 r_{ic})^n e^{\imath knL} \right) = E_{in} \left(r_{ic} + \frac{t_{ic}^2 r_{hr}^2 e^{\imath kL}}{1 + r_{hr}^2 r_{ic} e^{\imath kL}} \right) \ , \tag{1.49}$$

yielding,

$$\frac{I_{refl}}{I_{in}} = \frac{|E_{refl}|^2}{|E_{in}|^2} = \left(r_{ic} - \frac{t_{ic}^2 r_{hr}^2}{1 - r_{hr}^2 r_{ic}} \right)^2 = R_{ic} \left(1 - \frac{T_{ic} R_{hr}}{r_{ic} \left(1 - \bar{R}^{3/2}\right)} \right)^2 \ . \tag{1.50}$$

Energy conservation requires,

$$\boxed{\frac{I_{refl}}{I_{in}} = 1 - \frac{2 I_{trns}}{I_{in}} = 1 - 2 G T_{hr}} \ . \tag{1.51}$$

We can measure $\frac{I_{trns}}{I_{in}}$ and $\frac{I_{refl}}{I_{in}}$ and calculate their ratio which, once the finesse (and therefore $\bar{R}$) are known, only depends on R_{hr},

$$\frac{I_{refl}}{I_{trns}} = \frac{(R_{hr}^2 - R^{\frac{3}{2}})^2}{(R_{hr}^2 - R^3)(1 - R_{hr})} \ . \tag{1.52}$$

I.e. measuring this ratio, we should be able to calculate R_{hr} and all the other mirror quantities. The dependencies of G, T_{hr}, I_{trns}, I_{refl}, and I_{refl}/I_{trns} are exhibited in Fig. 1.86. Note, that for a certain reflection R_{hr} no light is reflected. This corresponds to perfect impedance-matching [5]

[5] In order to obtain a rough estimation of the gain in terms of the finesse, we approximate the

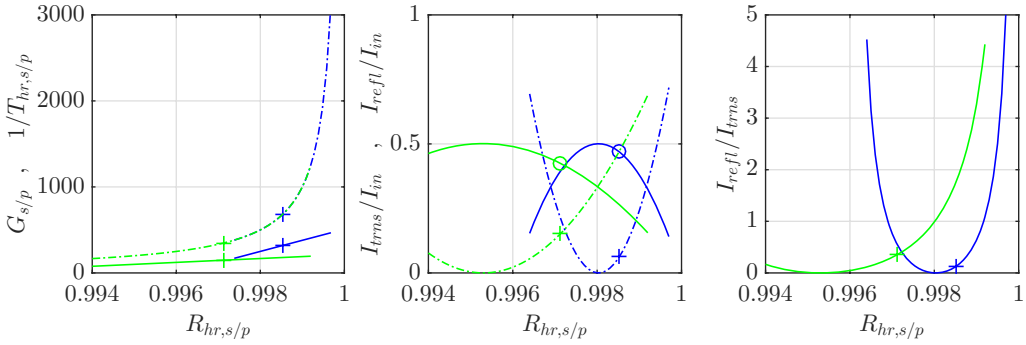

Figure 1.86: (code) (a) Gain G (solid lines) and output coupling $1/T_{hr}$ (dash-dotted lines) as a function of the HR mirror reflection R_{hr}. Blue curves refer to s-polarization and green curves to p-polarization. (b) Transmitted (solid lines) and reflected (dash-dotted lines) intensities. The sum of both yields the total injected intensity (dots) according to Eq. (1.51). (c) Ratio of transmitted and reflected intensities.

1.95.6 Photon number and pump rate

Once we have determined the gain, the intracavity photon number is easy to calculate from

$$|\alpha_+|^2 = \frac{P_{cav}}{\delta_{fsr}\hbar\omega} = G\frac{P_{in}}{\delta_{fsr}\hbar\omega} \ . \tag{1.53}$$

For the gain $G = 200$, assuming $P_{in} = 100\,\mu\text{W}$, we estimate, $|\alpha_+|^2 \approx 8.2\cdot 10^6$ photons.

In steady state, $\dot{\alpha}_\pm = 0$, we may derive the pump rate from,

$$\eta = \kappa|\alpha_+| \ . \tag{1.54}$$

finesse for high reflectivities (1.29) by,

$$\bar{R} \simeq 1 - \frac{\pi}{F} \ .$$

Inserting this into equation (1.52) and expanding in terms of π/F,

$$G \simeq \frac{T_{ic}}{\left(1-(1-\pi/F)^{3/2}\right)^2} = T_{ic}\left(\frac{2F}{3\pi}\right)^2 + ...$$

Now, we can make (at least) two hypothesis about the degradation of the mirrors:
(1) All mirrors degraded such as to yield the same reflectivity, $T_{ic} = 1 - R_{ic} \simeq 1 - \bar{R} \simeq \frac{\pi}{F}$. Then we calculate the gain due to resonant enhancement as,

$$G \simeq \frac{4F}{9\pi} \ ,$$

The gains obtained from this formula are not too different from the exact results obtained from the complete formula: $G_s \approx 200$ and $G_p \approx 70$.
(2) Alternatively, we could suppose that the high reflectors are still good and only the incoupler degraded, that is, $r'_{hr} = 1$. Then, to maintain the same (measured) finesse, we must have $T_{ic} = 1 - R_{ic} \simeq 1 - \bar{R}^3 \simeq 1 - \left(1 - \frac{\pi}{F}\right)^3 \simeq 3\frac{\pi}{F}$. Then we calculate the gain due to resonant enhancement as,

$$G' \simeq \frac{4F}{3\pi} \ .$$

The gains obtained from this formula are not too different from the exact results obtained from the complete formula: $G'_s \approx 500$ and $G'_p \approx 200$.

1.95.7 Intensity in the free space focus

The Airy formulas (1.47) were derived under the assumption of plane waves, but in fact the light field are Gaussian beams,

$$I_{cav}(\rho, z) = \frac{2P_{cav}}{\pi w^2(z)} e^{-2\rho^2/w^2(z)} \tag{1.55}$$

with

$$w(z) = w_0 \sqrt{1 + \left(\frac{\lambda z}{\pi w_0^2}\right)^2} \ . \tag{1.56}$$

In the case of perfect mode-matching, the beam diameters at $z = 0$ just in front and just behind the incoupler are the same, such that,

$$\frac{I_{cav}(\rho, 0)}{I_{in}(\rho, 0)} = \frac{P_{cav}}{P_{in}} = G \ , \tag{1.57}$$

such that we may simply replace $P_{cav} = GP_{in}$ in Eq. (1.55). Close to the free space focus w_0, we may approximate the intensity distribution by,

$$\boxed{I_{cav}(\rho, z) = \frac{2P_{cav}}{\pi w_0^2} e^{-2\rho^2/w_0^2 - z^2/z_R^2}} \ , \tag{1.58}$$

where $z_R \equiv \pi w_0^2/\lambda$ is the Rayleigh range.

1.95.8 Impact of blue transition

The depth of the optical potential caused by the clock transition dominates the one caused by the cooling transition for detunings from the clock transition inferior to $\Delta/2\pi < 200\,\text{GHz}$ (see Labbook, Strontium cavities, 25.05.2018). As we plan to work much closer to the clock transition, we may thus safely disregard the blue transition.

1.95.9 Dipole trap depth for one-sided pumping

With the intensity calculated in (1.58), we can now estimate the dipolar trap depth and the Rayleigh scattering rate for a given detuning [see script on Electrodynamics, Eq. (20.130) and Labbook, Strontium cavities, 02.08.2016],

$$V_{dip}(\rho, z) = \frac{3\pi c^2}{2\omega^3} \frac{\Gamma_{689}}{\Delta_a} I_{cav}(\rho, z) \qquad \text{and} \qquad \hbar\gamma_{sct}(\rho, z) = \frac{3\pi c^2}{2\omega^3} \frac{\Gamma_{689}^2}{\Delta_a^2} I_{cav}(\rho, z) \ . \tag{1.59}$$

We will now estimate the potential depth and the trap oscillation frequencies for the lowest bound state by a harmonic approximation for the spatial intensity distribution considering single-sided pumping of the ring cavity. The case of double-sided but asymmetric pumping of the two counterpropagating cavity modes will be treated in the next section.

We expect for the dipole potential in the case of one-sided pumping (see Physics Script: Sec. 46.3.2),

$$V_{dip}^{\uparrow}(\mathbf{r}) = V_{0,dip}^{\uparrow} e^{(-2x^2-2y^2)/w_0^2 - z^2/z_R^2} \qquad \text{with} \qquad \boxed{V_{0,dip}^{\uparrow} = \frac{3\pi c^2}{2\omega_0^3} \frac{\Gamma_{689}}{\Delta} \frac{2P_{cav}}{\pi w_0^2}} \ , \tag{1.60}$$

yielding,

$$\boxed{\omega_r^{\uparrow} = \frac{2}{w_0}\sqrt{\frac{V_{0,dip}^{\uparrow}}{m}} \quad \text{and} \quad \omega_z^{\uparrow} = \frac{\sqrt{2}}{z_R}\sqrt{\frac{V_{0,dip}^{\uparrow}}{m}}} \ . \tag{1.61}$$

With the detuning and intracavity laser powers used by Dalila, $\Delta_a/2\pi = -4\,\text{GHz}$ and $P_{\pm,cav} = 1\,\text{W}$, we find,

$$\begin{aligned} &V_{0,dip}^{\uparrow}/h \approx 8.3\,\text{MHz} = k_B\ 0.4\,\text{mK} \\ &\text{and} \quad \omega_z^{\uparrow}/2\pi \approx 2\,\text{Hz} \quad \text{and} \quad \omega_r^{\uparrow}/2\pi \approx 900\,\text{Hz} \ . \end{aligned} \tag{1.62}$$

1.95.10 Dipole trap depth for double-sided pumping

In the case of two-sided pumping the dipole potential in a ring cavity becomes,

$$V_{dip}^{\updownarrow}(\mathbf{r}) = \frac{3\pi c^2\Gamma_{689}}{2\omega^3\Delta_a}\left|e^{\imath kz}\sqrt{I_{+,cav}(\rho,z)} + e^{-\imath kz}\sqrt{I_{-,cav}(\rho,z)}\right|^2 \ , \tag{1.63}$$

where $\sqrt{I_{\pm}} \propto \mathcal{E}^{\pm}$ is the electric field amplitude. Exploiting the formulas (1.31), (1.36), (1.38), (1.41), and (1.53), we find,

$$\begin{aligned} V_{dip}^{\updownarrow}(\mathbf{r}) &= \frac{3\pi c^2\Gamma_{689}}{2\omega^3\Delta_a}\frac{2}{\pi w_0^2}e^{-2\rho^2/w_0^2}\left|e^{\imath kz}\sqrt{P_{+,cav}} + e^{-\imath kz}\sqrt{P_{-,cav}}\right|^2 \\ &= \hbar U_0 e^{-2\rho^2/w_0^2}|e^{\imath kz}\alpha_+ + e^{-\imath kz}\alpha_-|^2 \\ &= \hbar U_0 e^{-2\rho^2/w_0^2}(e^{-2\imath kz}\alpha_+^*\alpha_- + e^{2\imath kz}\alpha_+\alpha_-^* + |\alpha_+|^2 + |\alpha_-|^2) \ . \end{aligned} \tag{1.64}$$

Writing $\alpha_{\pm} = |\alpha_{\pm}|e^{\pm\imath\phi}$, we get,

$$\begin{aligned} V_{dip}^{\updownarrow}(\mathbf{r}) &= \hbar U_0 e^{-2\rho^2/w_0^2}(2|\alpha_+||\alpha_-|\cos(2kz+2\phi) + |\alpha_+|^2 + |\alpha_-|^2) \\ &\overset{\alpha_+=\alpha_-}{\longrightarrow} 4\hbar U_0 e^{-2\rho^2/w_0^2}\cos^2(kz+\phi) \ . \end{aligned} \tag{1.65}$$

Finally,

$$V_{dip}^{\updownarrow}(\mathbf{r}) = V_{0,dip}^{\updownarrow}e^{-2\rho^2/w_0^2}\cos^2\tfrac{kz}{2} \tag{1.66}$$

with

$$V_{0,dip}^{\updownarrow} = \frac{3\pi c^2}{2\omega_0^3}\frac{\Gamma_{689}}{\Delta}\frac{2(\sqrt{P_{cav,+}} + \sqrt{P_{cav,-}})^2}{\pi w_0^2} = \frac{3\pi c^2}{2\omega_0^3}\frac{\Gamma_{689}}{\Delta}\frac{8\sqrt{P_{cav,+}P_{cav,-}}}{\pi w_0^2 C_{sw}} \ , \tag{1.67}$$

where we introduced the standing wave contrast,

$$C_{sw} \equiv \frac{4\sqrt{P_+P_-}}{\sqrt{P_+} + \sqrt{P_-}} \ . \tag{1.68}$$

In the limit of symmetric pumping we can simply set $P_+ = P_-$ and $C_{sw} = 1$. The dipole trap depth is related to the single-photon light shift via, $V_{0,dip}^{\updownarrow} = 4|\alpha_+|^2U_0$.

Similarly to the one-sided pumping case, a harmonic approximation for the spatial intensity distribution yields the oscillation frequencies,

$$\boxed{\omega_r^{\updownarrow} = \frac{2}{w_0}\sqrt{\frac{V_{0,dip}^{\updownarrow}}{m}} \quad \text{and} \quad \omega_{lat}^{\updownarrow} = k\sqrt{\frac{V_{0,dip}^{\updownarrow}}{2m}}} \ . \tag{1.69}$$

With the detuning and intracavity laser powers used by Dalila,

$$\begin{aligned} &V_{0,dip}^{\updownarrow} \approx h\ 66.4\,\text{MHz} = k_B\ 3.2\,\text{mK} \\ &\text{and} \quad \omega_r^{\updownarrow}/2\pi \approx 2550\,\text{Hz} \quad \text{and} \quad \omega_{lat}/2\pi \approx 800\,\text{kHz} \ . \end{aligned} \tag{1.70}$$

1.95.11 Bloch force

The relative strength of the Bloch oscillations and the CARL dynamics is characterized by the depth of the respective potentials. Let us first analyze the potentials separately based on the above calculations for the dipole potentials $V_{dip}^{\updownarrow}$, which will now be renamed into V_{blo} respectively, V_{crl}. First Bloch.

The Bloch oscillation frequency is calculated via,

$$\boxed{\nu_{blo} = \frac{mg}{2\hbar k}} \ , \tag{1.71}$$

yielding $\nu_{blo} = 745\,\text{Hz}$.

The figure of merit for the occurrence of Bloch oscillations is the adiabatic rapid passage (ARP) condition (see LabBook 2.3.2021), according to which the dipolar standing wave potential should only support a single bound state [79, 94],

$$\frac{16\nu_{blo}}{\omega_{rec}} \ll \left(\frac{V_{0,dip}^{\updownarrow}}{\hbar\omega_{rec}}\right)^2 \ll 1 \ . \tag{1.72}$$

For the strontium line λ_{689} we have $16\nu_{blo}/\omega_{rec} = 0.398$, so that, defining a 'Bloch parameter',

$$\boxed{\varepsilon_{blo} \equiv \frac{V_{0,dip}^{\updownarrow}}{\hbar\omega_{lat}} = \sqrt{\frac{V_{0,dip}^{\updownarrow}}{\hbar\omega_{rec}}} = \sqrt{4|\alpha_+||\alpha_-|\frac{U_0}{\omega_{rec}}}} \ , \tag{1.73}$$

the dipole trap depth needs to satisfy $0.631 < \varepsilon_{blo} < 1$.

The simulations carried out in [94] assumed [6],

$$\begin{aligned} \nu_{blo} &= 0.035\omega_{rec} && (= \ 0.025\omega_{rec}) \\ \kappa &= 160\omega_{rec} && (= \ 110\omega_{rec}) \\ \alpha_0 &= 20 && (= \ ?) \\ V_{0,dip}^{\updownarrow} &= 3.2\omega_{rec} && (= \ ?) \\ U_0 &= 0.008\omega_{rec} = 5\cdot 10^{-5}\kappa && (= \ ?) \\ NU_0 &= 2\kappa && (= \ ?) \ . \end{aligned} \tag{1.74}$$

[6] Note that the parameter $U_{Marina} = \frac{g_1^2\alpha_p}{4\Delta_s} = \frac{\alpha_p}{4}U_0$ is defined differently in [94].

The values in brackets are realized in our experiment, those with question mark can be tuned via Δ_a and $P_{\pm,cav}$.

For the detuning and intracavity laser powers currently used by Dalila we expect $\varepsilon_{blo} \approx 42$, meaning that the pump power generating the Bloch lattice is orders of magnitude to high. Actually, at $\Delta_a/2\pi = -4\,\mathrm{GHz}$ a detuning $P_{\pm,cav} \approx 150\,\mu\mathrm{W}$ would be required in order to reach $\varepsilon_{blo} \approx 1$ and $P_{\pm,cav} \approx 450\,\mu\mathrm{W}$ in order to reach the value used in Marina's simulations.

1.95.12 Heating

Heating is due to spontaneous emission, i.e.,

$$\hbar\gamma_{sct} = \hbar\gamma_0|\alpha_+|^2 \ . \tag{1.75}$$

1.95.13 CARL force and saturation broadening

The CARL coupling strength is given by the collectively enhanced single-photon light shift,

$$\boxed{\varepsilon_{crl} \equiv \frac{NU_0}{\kappa}} \ . \tag{1.76}$$

With the atom number estimated to $N = 100000$, in order to reach $\varepsilon_{crl} \approx 1$, we need to tune the laser to $\Delta_a/2\pi \approx 2.3\,\mathrm{MHz}$. This detuning is within the cavity linewidth.

The saturation power in the ring cavity is,

$$P_{sat} = \frac{\pi w_0^2}{2} I_{sat} \approx 22\,\mathrm{nW} \ . \tag{1.77}$$

If we request saturation broadening not to exceed the cavity linewidth, we need,

$$\Omega = \frac{\Gamma_{689}}{2}\sqrt{\frac{I_{cav}}{I_{sat}}} < \kappa \ . \tag{1.78}$$

Hence,

$$P_{cav} < \left(\frac{2\kappa}{\Gamma_{689}}\right)^2 P_{sat} \approx 17.6\,\mathrm{mW} \ . \tag{1.79}$$

1.95.14 Measured CARL signals

As already derived in (1.48), the portion of the intracavity light power leaking through a high-reflecting mirror is,

$$P_{trns} = T_{hr} P_{cav} \ . \tag{1.80}$$

To estimate the amplitude of the CARL signal, we have a look at the classical CARL equations,

$$\dot{\alpha}_\pm = -\kappa\alpha_\pm - \imath U_0 \alpha_\mp \sum_j e^{-2\imath k x_j} + \eta_\pm \tag{1.81}$$

$$m\ddot{x}_j = 2\imath\hbar k U_0 (\alpha_+\alpha_-^* e^{\imath k x_j} - \alpha_+^*\alpha_- e^{-\imath k x_j}) \ .$$

When the pump laser is locked to the ring cavity (or vice versa), we have $\alpha_+ = \eta_+/\kappa$. An upper bound for the probe beam power generated by CARL can be estimated assuming steady state, $\dot{\alpha}_- = 0$, and perfect bunching, $\sum_j e^{-2\imath k x_j} = N$. Then,

$$\alpha_- = -\frac{\imath N U_0}{\kappa}\alpha_+ \ . \tag{1.82}$$

Hence, the intracavity probe beam power is,

$$\boxed{P_{-,cav} = |\alpha_-|^2 \hbar\omega\delta_{fsr} = \left(\frac{NU_0}{\kappa}\right)^2 P_{+,cav} = \varepsilon_{crl}^2 P_{+,cav}} \ . \tag{1.83}$$

Of course, the real signal will be lower. For example, using the power (1.79) and the mirror reflection $R = 99.97\%$, we expect $P_{trns} < 5.3\,\mu\mathrm{W}$.

The CARL parameter is defined as,

$$\rho^3 = \frac{nNU_0^2}{8\omega_{rec}^2} \ . \tag{1.84}$$

For Marina's simulations we used, $\rho^3_{Marina} = 3200$. For Dalila's parameters, $\rho^3_{Dalila} =$ ....

1.95.15 Laser locking

Also interesting is the optical density

$$OD = \frac{-N(\gamma_0 + \imath U_0)}{\delta_{fsr}} \ , \tag{1.85}$$

giving rise to a small phase shift (imaginary part) and an even smaller absorption (real part). Note, however, that these values are to be multiplied with the cavity gain G.

At $\Delta_a = -(2\pi)\ 200\,\mathrm{MHz}$, the cavity resonance is shifted due to the refraction index generated by the atomic cloud by an amount (see Labbook, Strontium cavities, 30.10.2018),

$$NU_0 = -N(2\pi)\ 0.42\,\mathrm{Hz} = -8.2\,\mathrm{kHz} \ , \tag{1.86}$$

Hence, when the pump laser is locked to a ring cavity resonance, its frequency will be $\omega = NU_0 + \omega_c$.

1.95.16 Quantum CARL simulations

The quantum CARL simulations are done with the following set of equations,

$$\dot{\alpha}_- = -\kappa\alpha_- + \imath U_0 \frac{\eta_+}{\kappa}\sum_m c_m^* c_{m\pm1} + \eta_- \tag{1.87}$$

$$\dot{c}_\nu = -4\imath\omega_{rec}(\nu + \nu_{blo}t)^2 c_\nu - \imath U_0 \frac{\eta_+}{\kappa}(\tilde{\alpha}_- c_{\nu+1} + \tilde{\alpha}_-^* c_{\nu-1}) \ ,$$

where the ratio between the Bloch and CARL coupling strength is given by,

$$\frac{W_0}{U_0} = \frac{\eta_- e^{-2\imath\phi}}{\kappa} \ . \tag{1.88}$$

1.95.17 Normal mode splitting

Normal mode splitting is observed when a resonance of the ring cavity is tuned to the atomic transition, $\omega_c = \omega_a$, by varying the laser frequency. To calculate the transmission spectrum observed by ramping the pump laser while monitoring the light power leaking through one of the high reflectors, we solve the CARL equation (1.66)(i) in steady-state assuming perfect bunching, $\sum_j e^{-2\imath k x_j} = N$, and one-sided pumping, $\eta_- = 0$ [27],

$$\alpha_+ = \frac{\eta_+}{\kappa - \imath\Delta_c + \frac{g_N^2}{\Gamma - \imath\Delta_a}} \ . \tag{1.89}$$

The transmission is given by,

$$T_+ = \left|\frac{\kappa\alpha_+}{\eta_+}\right|^2 = \frac{\kappa^2(\Gamma^2 + \Delta_a^2)}{(\kappa\Gamma + g_N^2 - \Delta_c\Delta_a)^2 + (\Gamma\Delta_c + \kappa\Delta_a)^2} \tag{1.90}$$

Fig. **??** shows cavity transmission spectra. Defining $\tilde{\Delta}_c \equiv \Delta_c/\kappa$ and $\tilde{\Delta}_a \equiv \Delta_a/\Gamma$ and using the definition (1.40) of the cooperativity, we can also write,

$$T_+ = \frac{1 + \tilde{\Delta}_a^2}{\left(1 + N\frac{\Upsilon}{2} - \tilde{\Delta}_c\tilde{\Delta}_a\right)^2 + (\tilde{\Delta}_c + \tilde{\Delta}_a)^2} \ . \tag{1.91}$$

Keeping the laser at a fixed frequency ω (so that Δ_a is constant) and varying the cavity length Δ_c, we obtain from (1.90),

$$\begin{aligned} 0 = \frac{\partial T_+}{\partial \Delta_a} &= \frac{\partial \Delta_a^2}{\partial \Delta_a}\frac{\partial T_+}{\partial \Delta_a^2} \\ &= 2\Delta_a \frac{\partial}{\partial \Delta_a^2}\frac{\kappa^2\Delta_a^2 + \kappa^2\Gamma^2}{\Delta_a^4 + (\kappa^2 + \Gamma^2 - 2g_N^2)\Delta_a^2 + (\kappa\Gamma + g^2)^2} \ . \end{aligned} \tag{1.92}$$

The solution of this equation,

$$\Delta_a^2 = -\Gamma^2 \pm g_N\sqrt{2\Gamma^2 + g_N^2 + 2\kappa\Gamma} \ , \tag{1.93}$$

is plotted in Fig. **??**(c) as a black line. For cases of very narrow atomic resonances, $\kappa \gg \Gamma$, we may simplify,

$$\Delta_a^2 \simeq \pm g_N^2\sqrt{1 + \frac{4\kappa\Gamma}{2g_N^2}} = \pm N g^2\sqrt{1 + \frac{N_{crt}}{N}} \ , \tag{1.94}$$

where $N_{crt} = 4/\Upsilon$ is the critical atom number and Υ the cooperativity (1.40).

The following table summarizes the invariable experimental constants:

transition wavelength	$\lambda = 689\,\mathrm{nm}$
cavity round trip length	$L = 3.64\,\mathrm{cm}$
cavity mode volume	$V = 0.50\,\mathrm{mm}^3$
cavity mode free space waist	$w_0 = 68.5\,\mu\mathrm{m}$
free spectral range	$\delta_{fsr} = 8.23\,\mathrm{GHz}$
curvature of high reflectors	$\rho = 50\,\mathrm{mm}$
reflection of high reflector	$R_{hr,s} = 99.85\%$, $R_{hr,p} = 99.71\%$
reflection of in coupler	$R_{ic,s} = 99.51\%$, $R_{ic,p} = 98.71\%$
finesse	$F_s = 1200$, $F_p = 500$
supposed resonant gains	$G_s = 318$, $G_p = 147$
transmission at HR mirror	$T_{hr,s}^{-1} = 678$, $T_{hr,p}^{-1} = 348$
transition linewidth	$\Gamma/2\pi = 7.6\,\mathrm{kHz}$
cavity linewidth	$\kappa_s/2\pi = 3.43\,\mathrm{MHz}$, $\kappa_p/2\pi = 8.23\,\mathrm{MHz}$
recoil shift	$\omega_{rec}/2\pi = 4.78\,\mathrm{kHz}$
1-photon coupling strength	$g_1/2\pi = 8.9\,\mathrm{kHz}$
cooperativity	$\Upsilon = 0.02$
1-photon saturation	$s = 1.4$
resolvability of recoil shift	$\kappa_s/\omega_{rec} = 110$ (160)
Bloch frequency	$\nu_{blo} = 745\,\mathrm{Hz}$
Bloch ratio	$\nu_{blo}/\omega_{rec} = 0.025$ (0.035)

The following table summarizes the ranges for experimental input parameters:

atoms trapped	$N = 0...100000$
laser detuning from atom	$\Delta_a/2\pi = 0...6\,\mathrm{GHz}$
intracavity powers	$P_{\pm,cav} = 0...1\,\mathrm{W}$

The following table summarizes characteristic parameters for particular choices of the experimental input parameters ($N = 100000$, $\Delta_a/2\pi = -200\,\mathrm{GHz}$, $P_{\pm,cav} = 1\,\mathrm{W}$):

1-photon light shift	$U_0 = -(2\pi)0.42\,\mathrm{Hz}$
1-photon scattering per atom	$\gamma_0 = (2\pi)0.016\,\mathrm{mHz}$
collective coupling	$NU_0/\kappa_s = -0.011$
CARL pump power	$P_{in} = 100\,\mu\mathrm{W}$
intracavity photon number	$\lvert\alpha_+\rvert^2 = 7\ 200\ 000$
pump rate	$\eta = 3 \cdot 10^9 \kappa_s$
dipole trap depth	$V_{dip} = h3.5\,\mathrm{MHz} = k_B 167\,\mu\mathrm{K}$
scattering rate	$\gamma_{sct} = 830\,\mathrm{s}^{-1}$
leaking pump beam power	$P_{+,leak} = 6\,\mu\mathrm{W}$
leaking probe beam power	$P_{-,leak} = 1.35\,\mathrm{nW}$
CARL ratio	$V_{crl}/\omega_{rec} = 0.025$ (0.04)
Bloch lattice depth	$W_0/\omega_{rec} = 0.007$ (0.007)
Bloch beam pump power	$P_{in,blo} = 1\,\mathrm{nW}$
normal mode splitting	$\Delta_{a,n}/\kappa_s = 2.4$

The values in parenthesis are those assumed in [94].

1.96 21.01.2022 Phase-modulation of the cavity standing wave

In order to measure the dipole trap depth we could phase modulate the standing wave in the ring cavity, e.g. by passing the probe beam through an EOM. The atom-cavity system should respond to this by parametric heating, which can be simulated using the CARL equations,

$$\dot{\alpha}_- = -\kappa\alpha_+ - \imath U_0 \sum_j e^{-2\imath k z_j}\alpha_+ + \eta e^{\imath\phi_0 \sin\omega_{mod} t} \tag{1.95}$$
$$\dot{p}_j = 2\hbar k U_0 \alpha_+ (\alpha_- e^{-2\imath k z_j} - \alpha_-^* e^{2\imath k z_j}) \ .$$

For the strontium intercombination line, using the parameters of 13.1.2022, that Dalila can provide experimentally, $N = 10^5$, $T = 1\,\mu$K, $\Delta_a/2\pi = -200\,$MHz, and $P_\pm = 1\,$W, we estimate the lattice secular frequency and the center-of-mass frequency,

$$\omega_{lat} = \sqrt{4\omega_{rec}|\alpha_+|^2 U_0} \quad \text{and} \quad \omega_{cm} = \omega_{lat}\sqrt{1-\mu_N} \quad \text{with} \quad \mu_N = \frac{2NU_0(\Delta_c - 2NU_0)}{\kappa^2 + (\Delta_c - 2NU_0)^2} \ , \tag{1.96}$$

yielding $\omega_{lat}/2\pi = 1.7559\,$MHz and $\omega_{cm}/2\pi = 1.7555\,$MHz.

The simulation is done by iterating the CARL equations for some time (κt) and then evaluating (i) the maximum oscillation amplitude of the center-of-mass position of the atomic and (ii) the oscillation amplitude of the difference of the field amplitudes ($|\alpha_+|^2 - |\alpha_-|^2$).

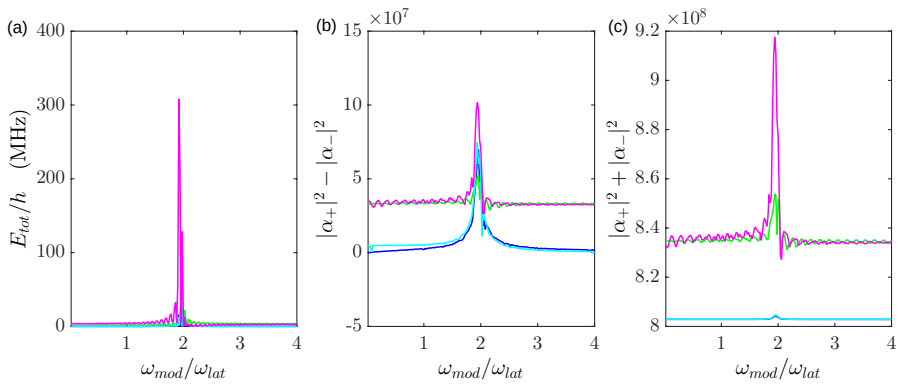

Figure 1.87: (code) .

The peak observed in $|\alpha_+|^2 + |\alpha_-|^2$ comes from the fact that the pump laser is locked to the cavity. It is not observed for symmetric pumping of $\alpha_\pm$ and low NU_0.

The phase does show a dispersive frequency-dependence $\theta(\omega)$ if $\eta \simeq \kappa$. If the pumping is too strong, $\eta \gg \kappa$, the phase does not exhibit any resonant enhancement. Even though the phase-oscillations are suppressed as ω_ϕ is increased beyond κ, the atomic center-of-mass motion is excited, when the secular resonance, $\omega_\phi = \omega_{cm}$, is met. The other modes ω_0 are not excited. Also the power-imbalance of the beams $|\alpha_+|^2 - |\alpha_-|^2$ always has a strong resonant enhancement.

The simulations have been done for the two situations that 1. the laser not being locked to the cavity resonance, but fixed to $\Delta_c = 0$, and 2. the laser being locked to the cavity resonance, which means $\Delta_c = (1 + N^{-1}|\sum_j e^{-\imath k z_j}|)NU_0 \simeq 2NU_0$. This second case is shown in the blue curves in Figs. 1.87(a) to (d). The simulation exactly reproduces the expected deviation of the resonance frequency ω_{cm} from the secular frequency ω_0 (??). Obviously, at $\Delta_c \simeq 2NU_0$ the shift of the CoM mode can not be observed via its resonant enhancement. We can excite the CoM, but at the unshifted frequency ω_0. At $\Delta_c \simeq 0$ where the shift occurs, we can not lock the laser [7].

[7] It would also be interesting to calculate the resonance maxima as a function of ω to see if the finite cavity bandwidth has an influence on atomic response!

1.97 15.02.2022 Excitation blockade and spin-squeezing using a cavity

Spin-squeezing of atomic ensembles is a way of overcoming the standard quantum limit and approaching the Heisenberg limit in ultrahigh resolution spectroscopy [35, 119, 14, 7, 43, 62, 98, 92, 44, 55, 21, 12, 26].

Here, we study spin-squeezing of a collection of three-level atoms $|1\rangle$-$|2\rangle$-$|3\rangle$ in cascade configuration, as illustrated in Fig. 1.88(a). The atoms interact with a linear cavity tuned quasi-resonant to the upper $|2\rangle$-$|3\rangle$ transition. In certain regimes controlled by parameters of the upper transitions, we observe excitation blockade on the lower transition, similar to what is observed in dense clouds of Rydberg atoms. With respect to Rydberg blockade systems our proposal has the advantage of generating uniform coupling between all atoms located in the mode volume of the cavity. This is particularly true, when ring cavities are used.

For the sake of concreteness we may have in mind the strontium level scheme $|1\rangle \equiv {}^1S_0$, $|2\rangle \equiv (5s5p)^3P_1$, and $|3\rangle \equiv (5s6s)^3S_1$ with the respective transition wavelength $\lambda_{12} = 689\,\mathrm{nm}$ and $\lambda_{23} = 688\,\mathrm{nm}$ and the decay widths $\Gamma_{12}/2\pi = 7.6\,\mathrm{kHz}$ and $\Gamma_{23}/2\pi = 4\,\mathrm{MHz}$.

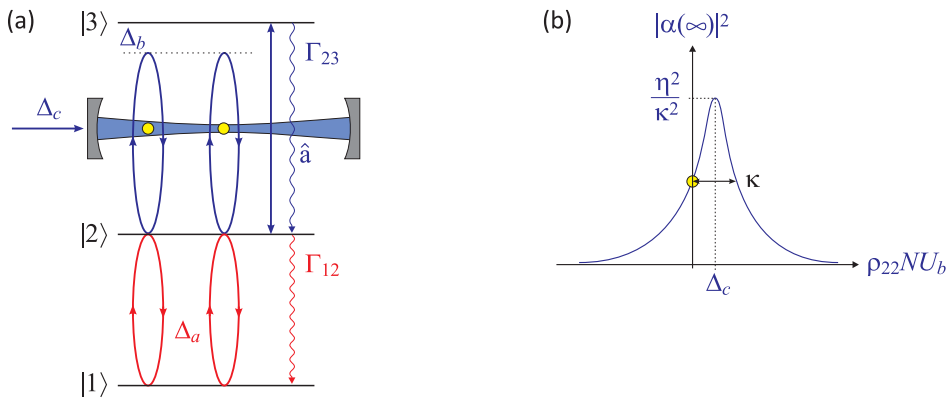

Figure 1.88: (code) (a) Level scheme and driven transitions. (b) Stationary cavity field intensity as a function of the population $\sum_j \mathrm{Tr}\,\hat{\rho}\sigma_j^{22}$ of level $|2\rangle$.

1.98 16.03.2022 Bloch oscillations in a tilted waveguide

Within the Rayleigh length, the potential generated by the cavity fields is,

$$U_{lat}(\mathbf{r}) \simeq U_0 e^{(-2x^2-2y^2)/w_0^2} e^{-z^2/z_R^2} \frac{P_+ + P_- + 2\sqrt{P_+P_-}\cos kz}{P_+ + P_- + 2\sqrt{P_+P_-}} \tag{1.97}$$

$$\simeq U_0 \left(1 - \frac{2x^2}{w_0^2} - \frac{2y^2}{w_0^2} - \frac{z^2}{z_R^2} - \frac{\sqrt{P_+P_-}}{(\sqrt{P_+}+\sqrt{P_-})^2} k^2 z^2 + ...\right) . \tag{1.98}$$

We see that the dimensions become separable only near the bottom of the potential, where the harmonic expansion works. In this case, a tilted gravity force,

$$U_{grv}(\mathbf{r}) = mgz\cos\alpha + mgx\sin\alpha \ , \tag{1.99}$$

maintains separability.

Obviously, the harmonic expansion is not possible for the description of Bloch oscillations. Maybe an expansion into Wannier functions would help.

1.99 29.03.2022 Water resonances perturbing the lock of doubling cavity

$\nu_{461}/2/c = 10849.226\,\mathrm{cm}^{-1}$
$\nu_{H_2O}/c = 10849.303\,\mathrm{cm}^{-1}$
$\nu_{461}/2 - \nu_{H_2O} = 2.3\,\mathrm{GHz}$ plus Doppler broadening

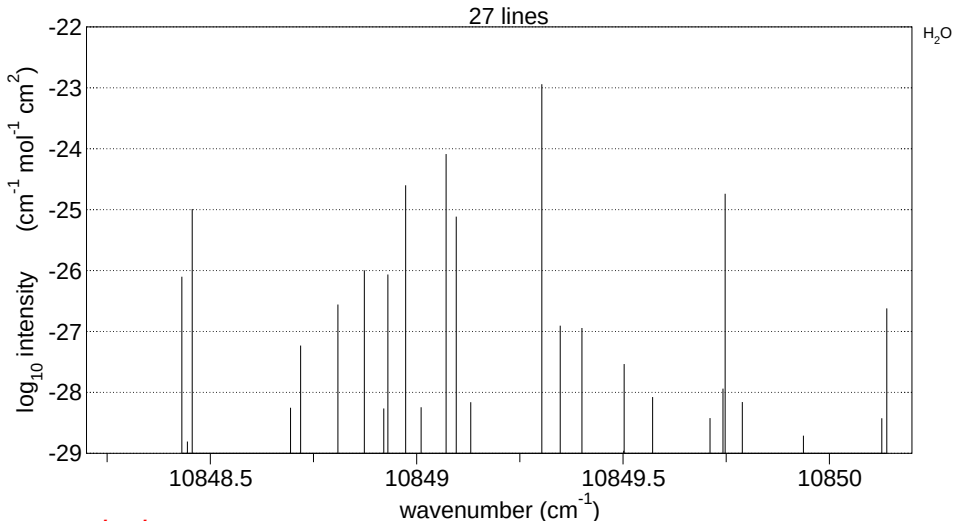

Figure 1.89: (code) Water resonances.

1.100 12.04.2022 Cavity-driven double resonance in Sr

We consider the strontium level scheme $|1\rangle \equiv {}^1S_0$, $|2\rangle \equiv (5s5p)^3P_1$, and $|3\rangle \equiv (5s6s)^3S_1$ with the respective transition wavelength $\lambda_{12} = 689\,\mathrm{nm}$ and $\lambda_{21} = 688\,\mathrm{nm}$ and the decay widths $\gamma_{12}/2\pi = 7.6\,\mathrm{kHz}$ and $\gamma_{23}/2\pi = 4\,\mathrm{MHz}$.

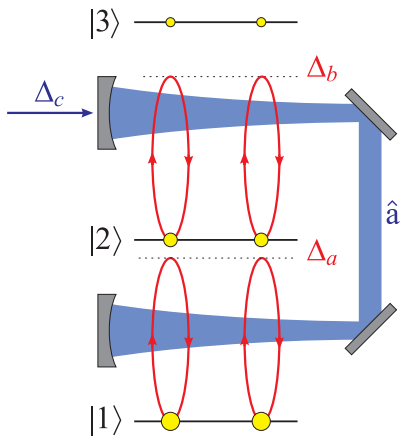

Figure 1.90: (code) Double resonance in Sr.

In the quest for Bloch oscillations Dalila uses a detuning of $\Delta_{12}/2\pi = 4\,\mathrm{GHz}$. Interestingly, the dipole potential generated on the two transitions are the similar,

$$\frac{V_{0,dip,689}}{V_{0,dip,688}} = \frac{\Gamma_{689}}{\Gamma_{688}}\frac{\Delta_{688}}{\Delta_{689}} = \frac{7.6\,\mathrm{kHz}}{4\,\mathrm{MHz}}\frac{920\,\mathrm{GHz}}{4\,\mathrm{GHz}} \simeq 0.44\ . \tag{1.100}$$

The question is now, what are possible consequences and/or opportunities!

1. Keep in mind that, at large detunings, excited state population are really small, $\rho_{33} \ll \rho_{22} \ll \rho_{11}$!

2. Is it a way to overcome light-shift? Disregarding degeneracies of the levels and neglecting all other energy levels, we might set the detuning to,

$$\Delta_{689} = \Delta_{688}\frac{\Gamma_{689}}{\Gamma_{689}} \simeq -1.7\,\mathrm{GHz}\ . \tag{1.101}$$

   However, the periodicities of the light-shift potentials are not exactly commensurate.

3. Discuss the relationship to the magical wavelength (Raul and Pablo already did some calculations).

4. Discuss possible impacts for Bloch oscillations and/or CARL.

5. Verify that, without atomic motion, the Hamiltonian for the three-level system is,

$$\hat{H} = -\imath\eta(\hat{a}-\hat{a}^\dagger)-\Delta_c\hat{a}^\dagger\hat{a}-\Delta_a\hat{S}_{22}+g_a(\hat{a}^\dagger\hat{S}_{12}+\hat{S}_{21}\hat{a})-\Delta_b\hat{S}_{33}+g_b(\hat{a}^\dagger\hat{S}_{23}+\hat{S}_{32}\hat{a})\ . \tag{1.102}$$

1.101 14.04.2022 Tasks for Bruno, Claudio and Gustavo

Claudio:

1. First priority learn from Dalila everything you can!!!
2. Calculate stability of new cavity with bow-tie design taking account of all boundary conditions (see 24.4.2013).

Design new cavity for alternative use as linear or ring cavity!
Verifications: Consider a bow-tie cavity with 2 spherical mirrors. Is it possible to use it simultaneously as a (non-confocal, non-concentrical) linear cavity?

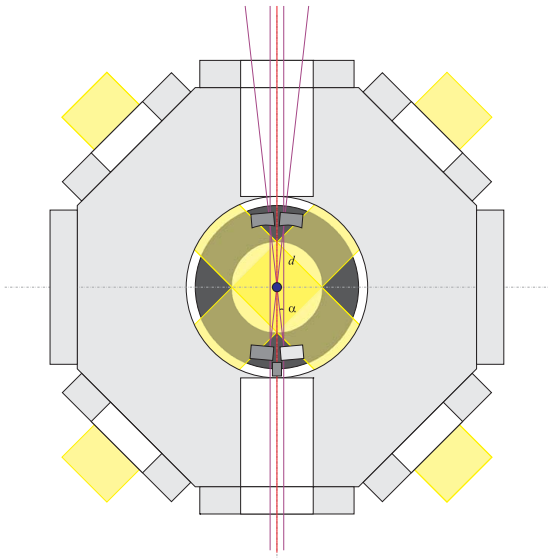

Figure 1.91: (code) New cavity design.

Sections to study in the Labbook/Cavity:

- Labbook 26.4.2013
- Labbook 14.4.2022
- Matlab-file: LB_Cavity_20220414_RingcavityStability.m
- Tex-file: LB_Cavity_20220414_RingcavityStability.tex

Sections to study in the Electrodynamics script:

- Sec. 7.4.1.2

- Exc. 7.4.4.4

Sections to study in the Quantummechanics script:

- Sec. 3.5-8: Harmonic oscillator,
- Sec. 5.2: Bloch oscillations,
- Sec. 14: Bloch equations,
- Sec. 15.1-2: Jaynes-Cummings model,
- Sec. 18.2: Optical forces,
- Sec. 20: Cavities & atoms,
- Sec. 21.1-3: Correlated atoms & Dicke model,
- Sec. 22.1-2: CARL,
- Sec. 22.4: Quantized CARL.

Bruno & Gustavo:

1. Find out whether Bloch oscillation interferometry may benefit from spin-squeezing.
2. Find out the impact of CARL probing at a wavelength differing from λ_{blo}. Influence on accuracy of inertial force measurement? Heating or cooling?

$$\begin{aligned}
\Delta_{a,blo} &= (2\pi)\delta_{fsr} + \Delta_{a,carl} \\
\frac{\Delta_{a,blo} - \Delta_{a,carl}}{\Delta_{a,blo}} &= \frac{(2\pi)\delta_{fsr}}{\omega_{689}} \approx 1.9 \times 10^{-5} \\
\Delta q_{blo} &= \frac{\omega_{blo}}{c} \\
\Delta E_{kin} &= \frac{\hbar^2(\Delta q_{blo} - \Delta q_{carl})^2}{2m} \approx (2\pi\hbar)1.7 \times 10^{-6}\,\mathrm{Hz}\ .
\end{aligned}$$

3. Long term: Set up Bragg lasers and implement them in the experiment.

1.102 15.05.2022 Stability of a bow-tie ring cavity

Stability of a bow-tie ring cavity with $d = 18\,\mathrm{mm}$ length and two flat and two curved mirrors as a function of the mirror curvature.

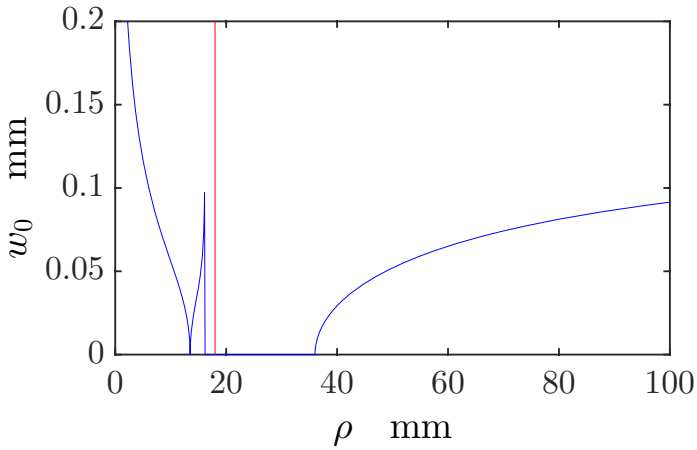

Figure 1.92: (code) Stability of a bow-tie ring cavity.

1.103 20.04.2022 Bloch signal simulation

The limits of the first Brillouin zone are given by,

$$\frac{p_{bri}}{\hbar k} = \pm 1 \qquad \text{or} \qquad y_{bri} = \pm \frac{\hbar k}{m t_{tof}} \ . \tag{1.103}$$

The atomic velocities are distributed according to a Maxwell-Boltzmann distribution,

$$\Delta y_k = \zeta_k t_{tof} \sqrt{\frac{k_B T}{m}} \ , \tag{1.104}$$

where ζ_k is a random number. The center of the Maxwell-Boltzmann distribution is,

$$\bar{y} = \tfrac{1}{N} \sum_k \Delta y_k \ . \tag{1.105}$$

We fake a Bloch oscillation signal via,

$$y = y_{bri} \cdot [\tfrac{1}{\pi} mod(\nu_{blo} t, 1) - 1] \ . \tag{1.106}$$

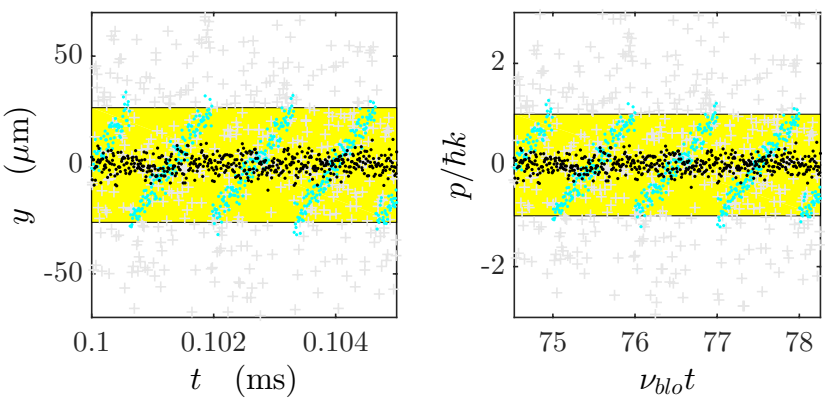

Figure 1.93: (code) Type of signal expected in SI-units (left) and scaled units (right). The yellow area denotes the first Brillouin zone, the gray crosses are randomly chosen individual atoms moving at velocities within a Maxwell-Boltzmann distribution at $T = 1\,\mu$K, the blue dots are expected Bloch oscillations, and the black dots for no Bloch oscillations.

1.104 21.04.2022 Impact of phase noise on Bragg reflection

Phase noise can inhibit transitions. This can be checked with simple two-level Bloch equations,

$$\dot{\hat{\rho}}(t) = e^{\mathcal{M}t}\hat{\rho}(0) \qquad \text{with} \qquad \mathcal{M} = \begin{pmatrix} 0 & 0 & -\frac{\imath}{2}\Omega & \frac{\imath}{2}\Omega \\ 0 & 0 & \frac{\imath}{2}\Omega & -\frac{\imath}{2}\Omega \\ -\frac{\imath}{2}\Omega & \frac{\imath}{2}\Omega & -\frac{1}{2}\Gamma + \beta & 0 \\ \frac{\imath}{2}\Omega & -\frac{\imath}{2}\Omega & 0 & -\frac{1}{2}\Gamma + \beta \end{pmatrix} . \tag{1.107}$$

The Rabi frequency is just the coupling strength $\Omega = U_0$. We assume a finite fluctuation bandwidth β, which introduces a decay of the coherence. As seen in the figure, the transition is not complete in the presence of phase noise.

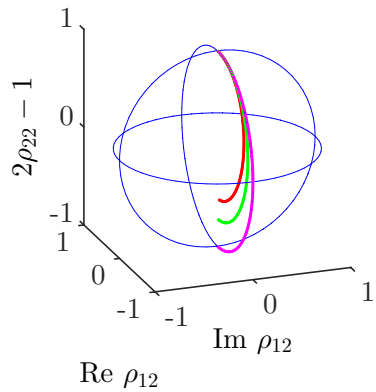

Figure 1.94: (code) The parameters chosen are $\Omega = \omega_{rec}$ and $\beta/2\pi = 0, 1, 2\,\text{kHz}$.

1.105 09.06.2022 Normal-mode splitting reloaded

The stationary solution of the Maxwell-Bloch equations yields, without any approximation, the following transmission of the cavity,

$$T = \left|\frac{\kappa\alpha}{\eta}\right|^2 = \frac{\kappa^2(\Gamma^2+\Delta_a^2)}{(\kappa\Gamma + g_N^2 - \Delta_c\Delta_a)^2 + (\Gamma\Delta_c + \kappa\Delta_a)^2} \ . \tag{1.108}$$

The same formula can be derived from the coupled atom-cavity equations under adiabatic elimination of the excited state and empirical reintroduction of spontaneous emission (see script QuantumMechanics, Excs. 19.2.6.9 and 19.2.6.10),

$$\dot{\alpha}_\pm = [-\kappa - \gamma_0 + \imath(\Delta_c - U_0)]\alpha_\pm - (\gamma_0 + \imath U_0)e^{\pm 2\imath kz}\alpha_\mp + \eta_\pm \ , \tag{1.109}$$

with

$$U_0 = \frac{g_1^2\Delta_a}{\Delta_a^2+\Gamma^2} \qquad \text{and} \qquad \gamma_0 = \frac{g_1^2\Gamma}{\Delta_a^2+\Gamma^2} \ . \tag{1.110}$$

These are exactly the CARL equations except for the fact that here we assume fixed atomic positions and consider the stationary solution. For $\Gamma \ll \kappa, g_N$, we can simplify,

$$|\alpha|^2 = \frac{\eta^2\Delta_a^2}{(g_N^2 - \Delta_c\Delta_a)^2 + \kappa^2\Delta_a^2} \ . \tag{1.111}$$

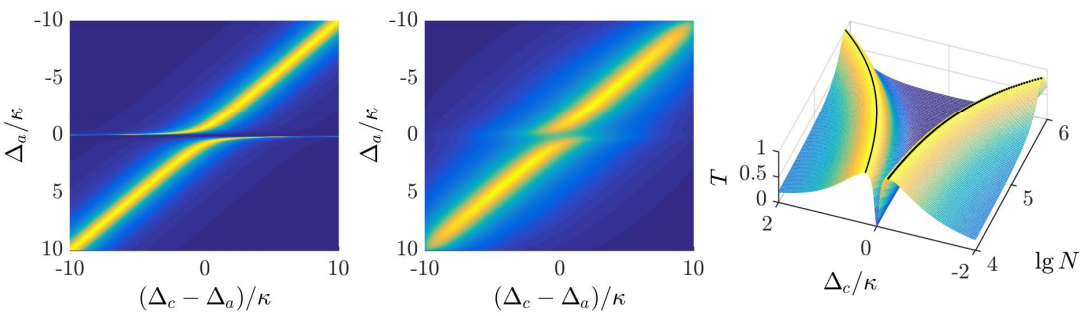

Figure 1.95: (code) The parameters chosen are $\kappa/2/\pi = 3.9\,\text{MHz}$ and $N = 10^4...10^6$.

Formula (1.111) holds for a motionless cloud of atoms not subject to perturbations leading to line shifts, such as light-shifts experienced by atoms trapped in a dipole potential or to Doppler shifts due to atomic motion. In reality, however, the atoms are subject to inhomogeneous broadenings, because they can be heated due to spontaneous emission during the scan and because the are trapped in a standing light wave. At low temperatures around $T = 2\,\mu\text{K}$ the Doppler broadening is on the order of $k\bar{v}/2\pi = \lambda^{-1}\sqrt{k_BT/m} \approx 20\,\text{kHz}$, and thus negligible. On the other hand, the Stark shift may be considerable, so that we need to discuss the effect.

Let us call ω_{Sr} the frequency of the unperturbed strontium line. Trapped atoms are subject to Stark shift, which means, $\omega_a = \omega_{Sr} + \Delta_{stark}$, or $\Delta_a = \Delta_{Sr} - \Delta_{stark}$. In the experiment, the cavity frequency is maintained fixed at $\omega_c = \omega_{Sr} + \Delta_{dpll}$, where

Δ_{dpll} can be fixed via the DPLL. Hence, $\Delta_c = \Delta_{Sr} - \Delta_{dpll}$, and therefore Eq. (1.111) becomes,

$$\boxed{T_r(\Delta_{Sr}) \equiv |\alpha|^2 = \frac{\eta^2(\Delta_{Sr} - \Delta_{stark})^2}{[g_N^2 - (\Delta_{Sr} - \Delta_{dpll})(\Delta_{Sr} - \Delta_{stark})]^2 + \kappa^2(\Delta_{Sr} - \Delta_{stark})^2}} \ . \tag{1.112}$$

Assuming that $\Delta_{dpll} = 0$ and κ and g_1 are known, and supposing that all atoms are exposed to the same Stark shift, the formula (1.112) would allows us to fit the atom number N and the pump rate η.

However, the atoms could be distributed in the trapping potential, which would lead to an inhomogeneous broadening. Let us assume a Boltzmann distribution,

$$\varrho(\Delta_{stark}) = \frac{\hbar N}{k_B T(1-e^{-U_{dip}/k_B T})} e^{-(U_{dip} - \hbar\Delta_{stark})/k_B T} \ , \tag{1.113}$$

normalized such that,

$$N = \int_0^{U_{dip}/\hbar} \varrho(\Delta_{stark}) d\Delta_{stark} \ . \tag{1.114}$$

The signal now is,

$$\boxed{T_r(\Delta_{Sr}) = \int_0^{U_{dip}/\hbar} |\alpha|^2 \varrho(\Delta_{stark}) d\Delta_{stark}} \ . \tag{1.115}$$

Now, U_{dip} and T are additional fit parameters.

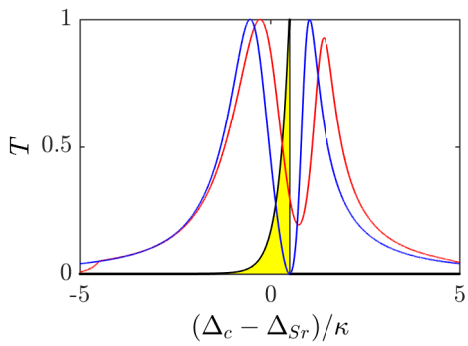

Figure 1.96: (code) (blue) Normal-mode spectrum with uniform Stark shift. (black) Boltzmann distribution of the atoms trapped inside the cavity standing wave. (red) Normal-mode spectrum with inhomogeneous Stark shift of Boltzmann-distributed atoms. The parameters chosen are $\kappa/2/\pi = 3.9\,\mathrm{MHz}$, $g_1/2\pi = 9.1\,\mathrm{kHz}$, $T = 50\,\mu\mathrm{K}$, $U_{dip} = h \cdot 2\,\mathrm{MHz}$, $N = 10^5$, and $\Delta_{dpll} = 0$.

Note, that the fact that the potential is truncated does not allow for thermal equilibrium. However, if $U_{dip} \gg \kappa_B T$ and the atoms are deep at the bottom of the potential, we can set $E \equiv U_{dip} - \hbar\Delta_{stark}$ and approximate,

$$\varrho(\Delta_{stark}) \simeq \hbar\tilde{\varrho}(E) \equiv \frac{N}{k_B T} e^{-E/k_B T} \tag{1.116}$$

and

$$T_r(\Delta_{Sr}) = \int_0^\infty |\alpha|^2 \tilde{\varrho}(E) dE = (|\alpha|^2 \star \varrho)(\Delta_{Sr}) \ . \tag{1.117}$$

If the curve is asymmetric, use the formula (1.109) and additionally fit Δ_a. The detuning Δ_a will be a function of the intracavity light power because of the Stark shift. Thus, measuring $\Delta_a = \Delta_a(\eta)$ we should be able to calibrate the intracavity power.

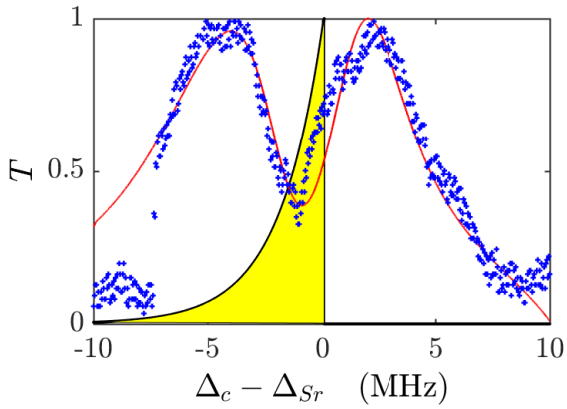

Figure 1.97: (code) (blue) .

1.106 18.06.2022 CARL reloaded

The CARL coupling parameter is,

$$\frac{NU_0}{\kappa} = \frac{N}{\kappa}\frac{g_1^2\Delta_a}{\Delta_a^2+\Gamma^2} \simeq \frac{g_N^2}{\kappa\Delta_a} = 0.01...0.1 \ .$$

With $g_N^2/\kappa \approx (2\pi)2\,\mathrm{MHz}$ obtained from the normal-mode splitting we need to tune $\Delta_a = (2\pi)20...200\,\mathrm{MHz}$.

1.107 23.08.2022 Normal-mode splitting in a ring cavity

In the quantum mechanics script we show that for $|\alpha_\pm|^2 \ll 1$ the stationary solution of the equations of motion for an atom interacting with the counterpropagating modes of a ring cavity is given by,

$$\alpha_+ = \frac{\eta_+[\kappa + \gamma_0 - \imath(\Delta_c - U_0)] - \eta_-(\gamma_0 + \imath U_0)e^{-2\imath kz}}{[\kappa + \gamma_0 - \imath(\Delta_c - U_0)]^2 - (\gamma_0 + \imath U_0)^2} \ ,$$

where $U_0 = g^2\Delta_a/(\Delta_a^2 + \Gamma^2) \simeq g^2/\Delta_a$.

Now, assuming $\gamma_0 = 0$, we get for anti-symmetric pumping, $\eta_- = \eta_+$ and $kz = \pi/2$,

$$\begin{aligned} \alpha_+ &= \eta_+ \frac{\kappa - \imath(\Delta_c - 2U_0)}{[\kappa - \imath(\Delta_c - U_0)]^2 + U_0^2} \\ \left|\frac{\alpha_+}{\eta_+}\right|^2 &= \frac{1}{\kappa^2 + \Delta_c^2} \ . \end{aligned}$$

That is, the transmission profile is a Lorentzian.

For symmetric pumping, $\eta_- = \eta_+$ and $kz = 0$,

$$\begin{aligned} \alpha_+ &= \eta_+ \frac{\kappa - \imath\Delta_c}{[\kappa - \imath(\Delta_c - U_0)]^2 + U_0^2} \\ \left|\frac{\alpha_+}{\eta_+}\right|^2 &= \frac{1}{\kappa^2 + (\Delta_c - 2U_0)^2} \ . \end{aligned}$$

Setting $\Delta_c = \Delta_a$ we find from $0 \equiv \frac{d}{d\Delta_c}\left|\frac{\alpha_+}{\eta_+}\right|^2$ a minimum at $\Delta_c = 0$ and two maxima at $\Delta_c = \sqrt{2}g$. This is the usual normal mode splitting for a ring cavity.

For uni-directional pumping, $\eta_- = 0$,

$$\begin{aligned} \alpha_+ &= \eta_+ \frac{\kappa - \imath(\Delta_c - U_0)}{[\kappa - \imath(\Delta_c - U_0)]^2 + U_0^2} \\ \left|\frac{\alpha_+}{\eta_+}\right|^2 &= \frac{\kappa^2 + (\Delta_c - U_0)^2}{[\kappa^2 - \Delta_c(\Delta_c - 2U)]^2 + 4\kappa^2(\Delta_c - U)^2} \ . \end{aligned}$$

That is, the transmission profile is a more complicated and may exhibit up to three peaks.

1.108 28.02.2023 Bragg spectroscopy on Sr 2

See also 21.8.2021. The saturation intensity observed in the normal-mode spectra seems lower than expected. Could this be due to Doppler broadening? The estimated Doppler width at $T = 1\,\mu\text{K}$ is,

$$\frac{k\bar{v}}{2\pi} = \frac{1}{\lambda}\sqrt{\frac{k_B T}{m}} \approx 14\,\text{kHz} \ .$$

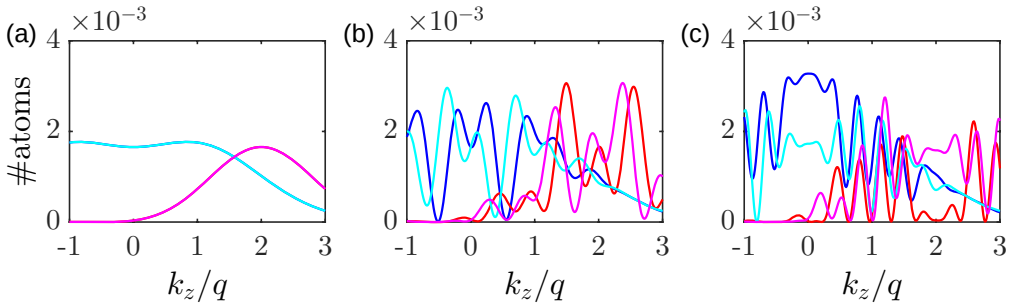

Figure 1.98: (code) Ramsey-Bordé pulse sequence.

In order to realize $\frac{\pi}{2}$ Ramsey pulses, we have,

$$\frac{\pi}{2} = \Omega_R \tau \qquad \text{and} \qquad \Omega_R = \frac{\Omega_1 \Omega_2}{4\Delta_R} \qquad \text{and} \qquad s = \frac{2\Omega_1\Omega_2}{\Gamma_{689}^2} \ .$$

Setting $\Delta_R = 500\Gamma_{689} \simeq (2\pi)\ 3.75\,\text{MHz}$,

$$\tau = \frac{\pi}{2\Omega_R} = \frac{2\pi\Delta_R}{\Omega_1\Omega_2} = \frac{2}{s}\frac{2\pi\Delta_R}{\Gamma_{689}^2} = \frac{2}{s}\cdot 67\,\text{ms} \ .$$

Assuming $\Omega_{1,2} = 100\Gamma_{689}$, we find $s = 20000$, so that $\tau = 6.7\,\mu\text{s}$.

1.108.1 Questions

Criticality on the duration of the pulses and the free intervals.

1.108.2 Step-by-step procedure

- Bragg spectroscopy without gravity. Tune the cavity to $\Delta_a = -1000\Gamma$.
- Provide two laser beams with frequency separations $\nu_+ - \nu_- = \frac{2\hbar k^2}{m} \approx (2\pi)\ 19\,\text{kHz}$.
- Trap $< 1\,\mu\text{K}$ cold atoms in a standing wave potential (or not).
- Pump counterpropagating cavity modes with the lasers $\nu_\pm$ making π-pulses.
- Distinguish velocity classes $\pm\hbar k$.

1.109 29.07.2024 Next measurements for Sr 2

1.109.1 Study inhomogeneous broadening mechanisms

Inhomogeneous broadening mechanisms, such as the Stark shift of atoms trapped in the dipole potential or Doppler-broadening may affect the normal mode spectra.

Asymmetries in the spectra can have various origins. (a) Heating of the atoms during the scan can remove atoms from the cavity mode volume thus changing the number of atoms interacting with the cavity. (b) The thermal cloud trapped in the dipolar potential occupies a finite region of space which leads to an inhomogeneous Stark shift which, in the spectrum, can be accounted for via a convolution with a Boltzmann distribution. (c) If the magnetic field at the atomic location is not completely compensated the spectrum is additionally split by the Zeeman effect. A way around this can be to apply a magnetic field sufficient strong that the Zeeman splitting exceeds the NMS by far, or oriented in a direction parallel to the polarization of the probe light, so that only $\Delta m_J = 0$ transition are driven.

1.109.2 Hysteresis in the bistable regime

The bistability causes a hysteresis upon ramping experimental parameters. Obviously, the hysteresis depends on the ramping speed and disappears below saturation as seen in Fig. 1.99.

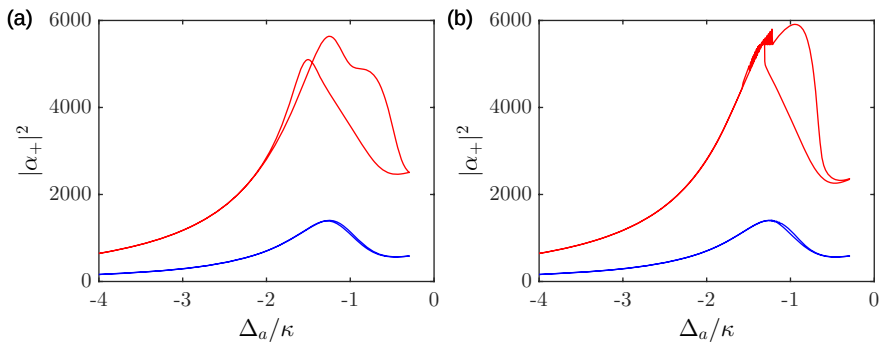

Figure 1.99: (code) Time-evolution of the intracavity photon number upon ramping the pump laser back and forth with total scan durations (a) 1 ms and (b) 100 ms. The red curves are for $\eta_+ = 50\kappa$ and the blue curves for $\eta_+ = 100\kappa$. The parameters are those specified in the text.

1.109.3 Theoretical tasks

- Check and discuss frustrated ladder excitation picture, destructive interference of excitation paths? Redraw the complete level scheme [43] emphasizing that, without cavity, all levels are resolved in principal, since $\Gamma < g$.
- Simulate emission spectrum using the code of [16, 81] for superradiant lasers.

- Once expanded on a basis, the classically non-linear equations of motion linearize (otherwise linear algebra wouldn't work for quantum mechanics). That means, that the non-linear bistability must correspond to a quantum picture of transitions and coherences between discrete quantum or photon number states. Find out whether the non-linear dynamics leads to some non-trivial quantum correlations. E.g. check whether the spectra can be understood in terms of collective two-photon absorption by the cloud followed by emission of photons at both of the normal-mode frequencies.

1.109.4 To dos

- Homodyne detection, Daniel: PLL
- State of 688 nm laser? Insist on 403 nm and 679 nm lasers!
- Pulse sequences?
- Fridays for studies?
- Sr2 purchases from Temático and BraQIT: Bragg laser, supermirrors, amplifiers, ...
- Short-term projects: Ramsey pulse sequence instead Bloch, quenching of bistability, heterodyne cavity signal, new cavity holder, ...
- Long term projects / Research lines: Metrological gain via quantum correlations $\longrightarrow$ quantum sensing; Matter wave interferometry; Superradiant lasing
- Raul on magic wavelength calculation
- Power broadening on the strontium clock transition: Assuming $\lambda_{698} = 698\,\mathrm{nm}$, $\Gamma_{698} = (2\pi)1\,\mathrm{mHz}$, $P = 1\,\mathrm{mW}$, and $w_0 = 100\,\mu\mathrm{m}$, we expect,

$$\Omega = \sqrt{\sigma(\omega_0)\frac{\bar{I}}{\hbar\omega_0}\Gamma} \approx (2\pi)\,2\,\mathrm{kHz}$$

1.110 31.07.2024 Spin-squeezing witnesses

In the bad cavity limit ($\hat{a} \propto \hat{S}_-$) the light mode might be photon-squeezed. How to measure, how to calculate?

1.111 05.08.2024 Bistability quenching via coupling to a third level

Coupling the upper level of the 7.6 kHz transition via a 4 MHz broad resonance to an excited state can reduce saturation.

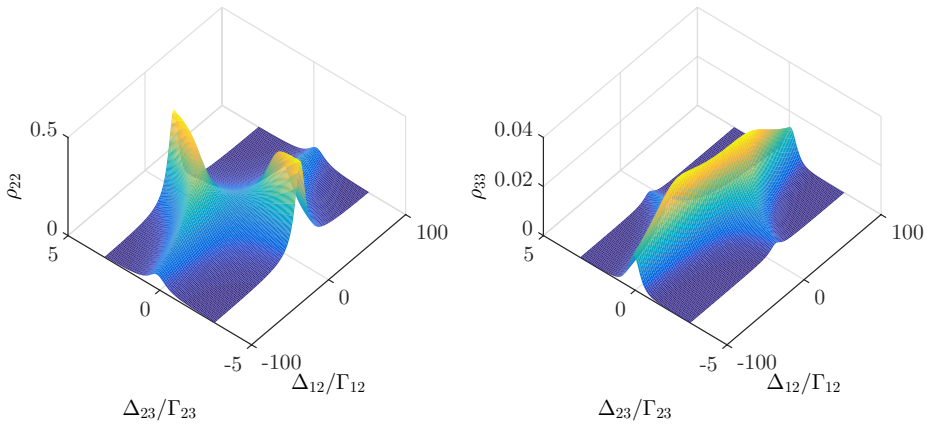

Figure 1.100: (code) Populations ρ_{22} and ρ_{33} as a function of detunings for the Rabi frequencies $\Omega_{12}/\Gamma_{12} = 5$ and $\Omega_{23}/\Gamma_{23} = 0.5$.

The bistability is induced by saturation, but it also depends on the collective cooperativity. That means, we manipulate the onset of bistability via N.

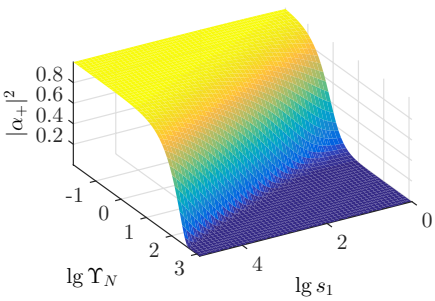

Figure 1.101: (code) See Fig. 8 of [88].

1.112 13.08.2024 Finding the 698 nm transition using the supercavity

From data tables we know,

$$\nu_{689} = 434.829121311\,\mathrm{THz}$$
$$\nu_{698} = 429.2280664180083\,\mathrm{THz}\ .$$

From the beat between adjacent reference cavity modes, we can determine a first guess for the free spectral range with a precision limited by the cavity line width $\kappa = (2\pi)\ 7.5\,\mathrm{kHz}$,

$$\delta_{fsr} = 1.445065(7.5)\,\mathrm{GHz}\ .$$

The cavity mode which is closest to the ν_{689} line is at,

$$\nu_{cav,689} = \nu_{689} - \Delta\nu_{AOM,689} = N_{689}\delta_{fsr}\ ,$$

where

$$\Delta\nu_{AOM,689} = 495\,\mathrm{MHz}$$

determined by measurement on a red MOT. Hence,

$$N_{689} = \frac{\nu_{cav,689}}{\delta_{fsr}} = \frac{\nu_{689} - \Delta\nu_{AOM,689}}{\delta_{fsr}} = 300905.93\ ,$$

which is close to

$$\bar{N}_{689} \approx 300906\ .$$

An error of 1 in the counting of N_{689} would correspond to $\Delta\delta_{fsr} = \frac{\delta_{fsr}}{N_{689}} \approx 5\,\mathrm{kHz}$, which is on the same order as κ confirming that the beat frequency determination of δ_{fsr} is insufficient. Now, recalibrating the free spectral range,

$$\bar{\delta}_{fsr} \equiv \frac{\nu_{cav,689}}{\bar{N}_{689}} = 1.445066304\,\mathrm{GHz}\ .$$

Trusting this free spectral range, at the clock transition,

$$N_{698} = \frac{\nu_{698}}{\bar{\delta}_{fsr}} = 297030.28\ ,$$

which is close to

$$\bar{N}_{698} \approx 297030\ .$$

Thus

$$\Delta\nu_{AOM,698} = \nu_{698} - \bar{\delta}_{fsr}\bar{N}_{698} = 409.4\,\mathrm{MHz}\ .$$

To double-check it would be good to verify at other wavelengths $679\,\mathrm{nm} < \lambda < 707\,\mathrm{nm}$, that the corresponding wavemeter reading ν_λ, when the laser is resonant with a supercavity mode, satisfies approximately,

$$\frac{\nu_\lambda}{\bar{\delta}_{fsr}} \approx integer\ .$$

1.113 14.08.2024 Phase shifts of the supercavity

Dielectric mirrors have frequency-dependent phase shifts [63], which can be quite large.

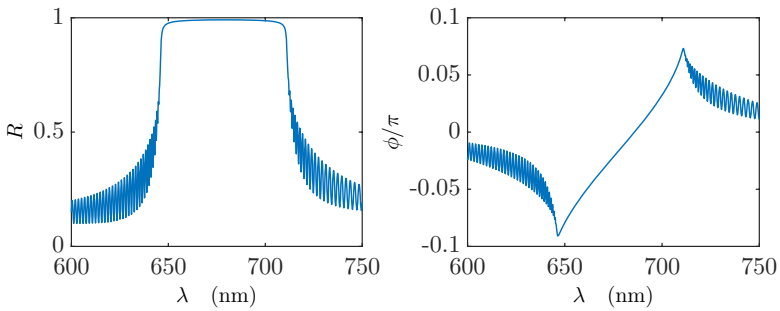

Figure 1.102: (code) Reflection and phase shift of a supercavity.

The question is, whether these phase shifts will lead to a frequency-dependent value of the free spectral range once the mirrors are used in a cavity. To get a feeling for the importance of this effect, we make a simple model of our supercavity ($\delta_{\mathrm{fsr}}^{(0)} = 1.5\,\mathrm{GHz}$), treating the supermirrors as stacks of dielectric layers ($N_{\mathrm{layers}} = 15$, $n_1 = 2.4$, $n_2 = 1.5$, $d_1 = d_2 = 353\,\mathrm{nm}$). The overall absorption losses are assumed to sum up to 10^{-6}. Fig. 1.103(left) shows a zoom on a cavity reflection spectrum close to a resonance. The width is about 8 kHz.

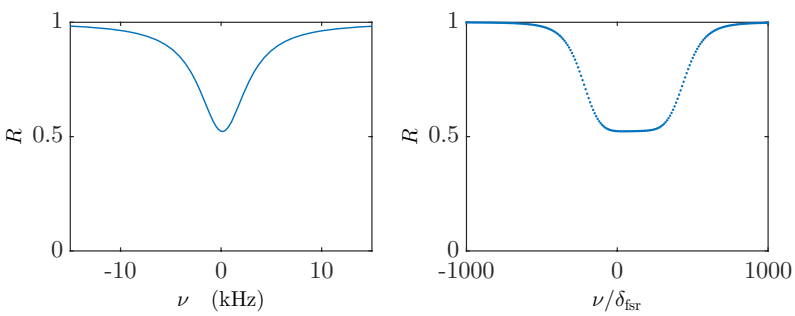

Figure 1.103: (code) Reflection and phase shift of a supercavity.

Fig. 1.103(right) shows cavity reflections evaluated at frequencies $\nu = N(\delta_{\mathrm{fsr}}^{(0)} + \delta_{\mathrm{fsr}}^{(1)})$, where the correction term accounting for phase shifts in the dielectric mirrors was adjusted to $\delta_{\mathrm{fsr}}^{(1)} = 30.395\,\mathrm{kHz}$. With the corrected value the stays constant over more than 500 modes with a precision well below the cavity linewidth. Nevertheless, it may not be possible to transfer the precision of δ_{fsr} to far away frequencies, such as from 689 nm to 698 nm.

1.114 03.09.2024 Sub- and superradiance in a cavity

When the atoms trapped in an are excited from the side by a coherent laser pulse, their emission into the cavity mode is suppressed by destructive interference between light emitted from atoms trapped in adjacent antinodes [51, 13]. A first idea for theoretical modeling can be to generalize the Hamiltonian (12) of [88] for $N/2$ atoms being located at $z_j = 0$ and $N/2$ atoms located at $z_j = \lambda_{\mathrm{lat}}/2$. Furthermore, the atoms must be driven be a classical laser field independently on their location,

$$\hat{H}_{\mathrm{atom:laser}} = \tfrac{\Omega}{2}(\hat{\sigma}_j^+ + \hat{\sigma}_j^-) \ .$$

The equations of motion (14) for the atoms to not change, but Eq. (15) for the field gets an extra term,

$$\dot{\hat{a}}_\pm = (\imath\Delta_{\mathrm{c}} - \kappa)\hat{a}_\pm - \imath g \sum_i \sigma_i^- + \imath g \sum_j \sigma_j^- \ .$$

In this perfectly ordered case, the sums cancel each other, and the counter-propagating modes decouple.

1.115 05.10.2024 Heterodyne signals from the bistability

Beat between local oscillator $\eta_+ e^{-\imath\theta}$ and cavity transmission on resonance,

$$\alpha_+ = \frac{\eta_+}{\kappa}\frac{1}{1+\frac{N\Upsilon}{2(1+s_1 n)}}$$
$$S = \frac{\eta_+^*}{\kappa}e^{\imath\theta}t\alpha_+ = e^{\imath\theta}t\frac{|\eta_+|^2/\kappa^2}{1+\frac{N\Upsilon}{2(1+s_1 n)}}$$

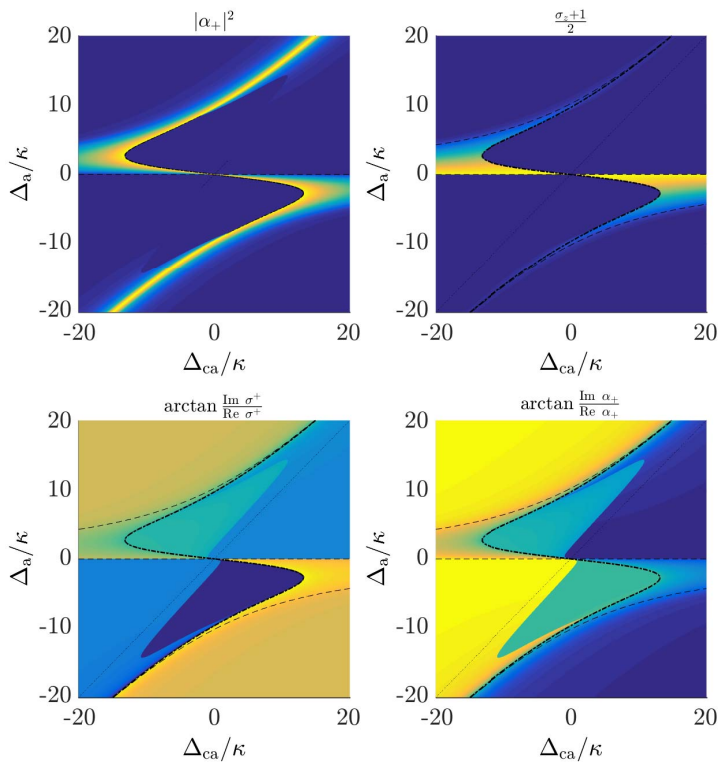

Figure 1.104: (code) Avoided crossing phase.

Apparently, the phase of the intracavity light is locked to the pump.

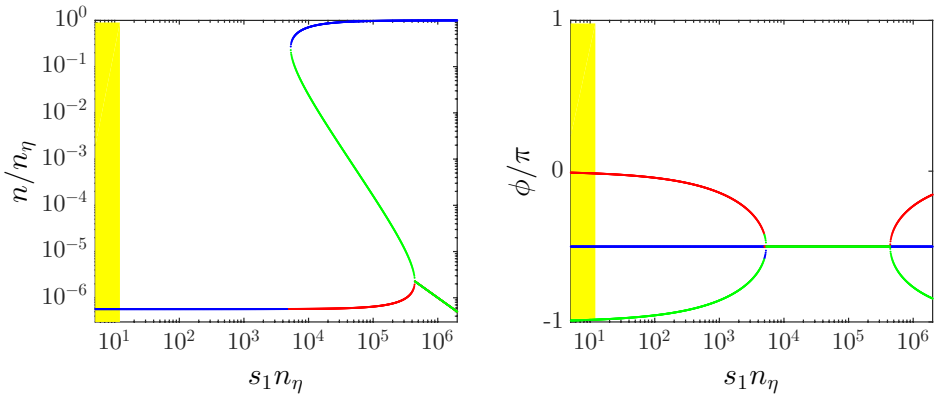

Figure 1.105: (code) Avoided crossing phase.

1.116 05.10.2024 Driven-dissipative spin-squeezing

The model shown in [88] does not eliminate the cavity, but if we do assuming $\dot{\hat{a}} = 0$, we derive exactly the equations of [61, 104]. Assuming additionally $\dot{\hat{S}} = 0$, the solutions and the bistability curves are identical! Hence, we believe that our experiment is well described by their theory! Unfortunately, the cavity light field does not provide spin-squeezing witnesses, since CRSS states emit coherent light [61, 104].

1.116.1 Discussion with Efi Shahmoon

Note that single atom decay via backscattering into the cavity can be larger than outside the cavity Γ_1.

What is the impact of timed Dicke state dynamics? Should be OK in forward direction.

1.117 05.11.2024 Coherent excitation of the 686 nm transition

The CRSS are squeezed in polar direction so their projection onto the equatorial plane is not squeezed. In contrast, squeezing in equatorial direction might result in light squeezing. So, how about switching off the cavity field, rotating the atoms, and measure squeezed light? So check whether this is viable, we need to estimate some experimental parameters, such as switch-off time, Rabi pulse power, and spontaneous and superradiant decay rate at $\Delta_c = 0 = \Delta_a$, i.e. between the normal modes.

1.117.1 Experimental implementation of rotations about arbitrary axes

Changing the phase of a driving field can be experimentally challenging in case of an optical transition. Changing ω for a given time causes a precession of the Bloch vector, while changing ω_0 rotates the coordinate system of the Bloch sphere. The bottom-line is that, if one can resolve Ramsey fringes, then one can try to rotate the Bloch vector in the equatorial plane about an arbitrary axes.

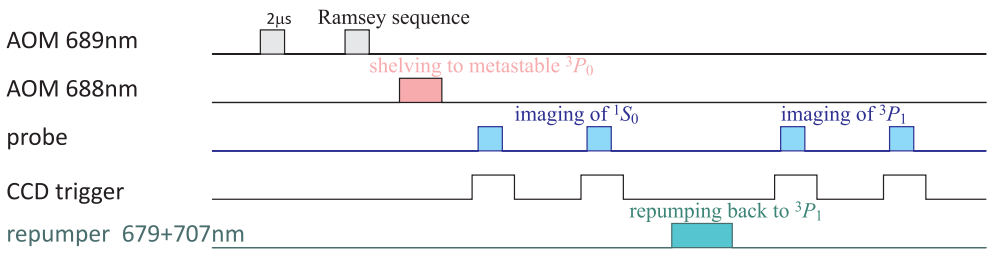

Figure 1.106: (code) Experimental sequence.

The question is then, whether we can do coherent manipulation of the 7.5 kHz transition. In other words, can we do Rabi pulses or resolve Ramsey fringes? And how to monitor them?

A possible technique for measuring population inversion is to shelve the atoms transferred to the $^3P_1$ state by optically pumping them into the $^3P_0$ state, using with Gustavo's laser at 688 nm. Then imaging the remaining atoms in the $^1S_0$. Then repumping the atoms back to the $^3P_1$, letting them decay to the $^3P_1$, and finally imaging them, as well.

In the lab we need first to try pulse sequences using the NI-board; first dry (without atoms) on an oscilloscope and checking the laser beams with photodetectors; then on the red MOT, then on cavity, then Rabi $\pi/2$ pulse followed by shelving.

Just to give an example, let us consider Ramsey pulses of duration $\tau_{\mathrm{R}} = 2\,\mu\mathrm{s}$, which is shorter than the spontaneous decay time,

$$\tau_{\mathrm{sp}} = \frac{1}{\Gamma_{689}} \approx 21\,\mu\mathrm{s} \ .$$

The Rabi frequency required for $\pi/2$ pulses is,

$$\Omega = \frac{\pi}{2\tau_{\mathrm{R}}} \approx 125\,\mathrm{kHz} \ .$$

Providing this Rabi frequency requires a saturation parameter of $s = 2\Omega^2/\Gamma^2 = 555$ and, hence, an intensity of,

$$I = sI_{\mathrm{sat}} \approx 6.7\,\mathrm{mW/cm^2}$$

with the saturation intensity $I_{\mathrm{sat}} \approx 1.6\,\mu\mathrm{W/cm^2}$.

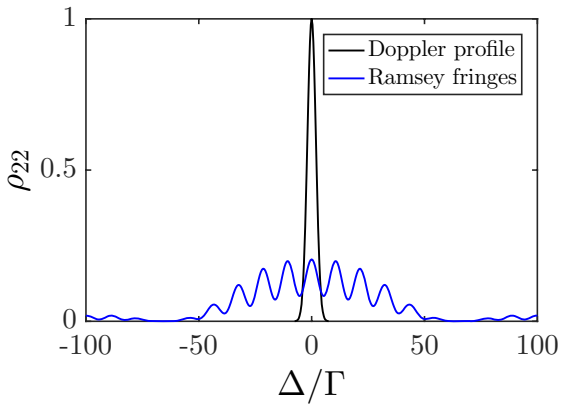

Figure 1.107: (code) Ramsey fringes with spontaneous emission ($\Gamma/2\pi = 7.5\,\mathrm{kHz}$) and Doppler broadening ($T = 1\,\mu\mathrm{K}$).

At a temperature of $T = 1\,\mu\mathrm{K}$ the atomic cloud is Doppler-broadened by an amount,

$$kv = \frac{2\pi}{689\,\mathrm{nm}}\sqrt{\frac{k_{\mathrm{B}}T}{m}} \approx 21\,\mathrm{kHz} \ .$$

Thus, in order to resolve Ramsey fringes, the precession time is limited to,

$$\tau_{\mathrm{P}} < \frac{\pi}{kv} \approx 23\,\mu\mathrm{s} \ .$$

Fig. 1.107 shows Ramsey fringes with spontaneous emission and Doppler broadening ($T = 1\,\mu\mathrm{K}$). Otherwise, one might try photon echo pulse sequences.

1.118 08.10.2024 Transfer of correlations between transitions

Optical pumping will certainly destroy quantum correlations, but StiRAP maybe not.

1.119 13.11.2024 Shelving laser 1

Hybrid Bloch and rate equation for 7 levels: $|1\rangle = {}^1S_0$, $|2\rangle = {}^1P_1$, $|3\rangle$, $|4\rangle = {}^3P_0$, $|5\rangle = {}^3P_1$, $|6\rangle = {}^3P_2$, and $|7\rangle$. The $|1\rangle - |2\rangle - |5\rangle$ system is treated as a three-level system separately from the $|4\rangle - |7\rangle$, $|5\rangle - |7\rangle$, and $|6\rangle - |7\rangle$ systems, which are treated as decoupled two-level systems.

This holds when Ω_{12}, Ω_{15}, Ω_{47}, Ω_{57}, and Ω_{67} are driven, but NOT simultaneously.

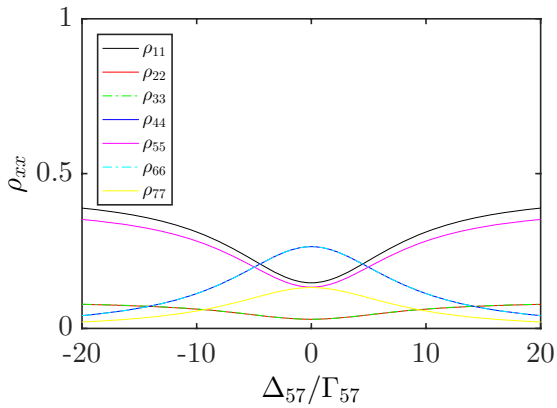

Figure 1.108: (code) Scanning the shelving laser.

1.120 16.12.2024 Shelving laser 2

Gustavo and Claudio aligned a probe beam of up to $P = 2\,\mathrm{mW}$ power and about $w = 470\,\mu\mathrm{m}$ waist to the red MOT. The maximum intensity is therefore,

$$I = \frac{2P}{\pi w^2} \approx 560\,\mathrm{mW/cm^2} \ .$$

The saturation parameter is,

$$s = \frac{2\Omega^2}{\Gamma^2} = \sigma \frac{2I}{\hbar\omega\Gamma} = \frac{3\lambda^3 I}{\pi h c \Gamma} \approx 1.89 \times 10^5$$

and the maximum pulse area for pulse durations of $\tau = 1\,\mu\mathrm{s}$,

$$\frac{\Omega\tau}{\pi} = \frac{\Gamma\tau}{\pi}\sqrt{\frac{s}{2}} \approx 4.6 \ ,$$

which should be sufficient, but without a lot of margin.

Hybrid Bloch and rate equation for 3 levels: $|1\rangle = {}^1S_0$, $|2\rangle = {}^1P_1$, and $|3\rangle = {}^3P_2$. The $|1\rangle - |2\rangle$ system is treated as a two-level system separately from the $|1\rangle - |2\rangle$ and $|2\rangle - |3\rangle$ systems, which are treated as decoupled two-level systems. Either Ω_{12} is coherently driven or R_{23} or R_{31} are incoherently pumped,

$$\frac{d}{dt}\begin{pmatrix}\rho_{11}\\ \rho_{22}\\ \rho_{33}\\ \rho_{12}\\ \rho_{21}\end{pmatrix} =$$

$$\begin{pmatrix} 0 & \Gamma_{12} & R_{31} & \frac{\imath}{2}\Omega_{12} & -\frac{\imath}{2}\Omega_{12} \\ 0 & -\Gamma_{12} - R_{23} & 0 & -\frac{\imath}{2}\Omega_{12} & \frac{\imath}{2}\Omega_{12} \\ 0 & R_{23} & -R_{31} & 0 & 0 \\ \frac{\imath}{2}\Omega_{12} & -\frac{\imath}{2}\Omega_{12} & 0 & \imath\Delta_{12} - \frac{1}{2}\Gamma_{12} - \frac{1}{2}R_{23} - \frac{1}{2}R_{31} & 0 \\ -\frac{\imath}{2}\Omega_{12} & \frac{\imath}{2}\Omega_{12} & 0 & 0 & -\imath\Delta_{12} - \frac{1}{2}R_{23} - \frac{1}{2}R_{31} \end{pmatrix} \begin{pmatrix}\rho_{11}\\ \rho_{22}\\ \rho_{33}\\ \rho_{12}\\ \rho_{21}\end{pmatrix} \ .$$

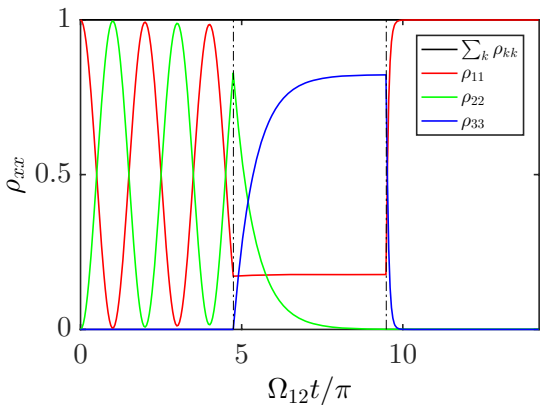

Figure 1.109: (code) Time sequence for a Rabi experiment with three pulses: (1) only the probe laser Ω_{12} is 'on', (2) only the shelving laser R_{23} is 'on', (3) only the repumping laser R_{31} is on.

1.121 13.1.2025 Rabi pulsing

After a Rabi pulse the population should oscillate. The subsequent two figures represent simulations of the ground state population after Rabi pulses on the 689 nm transition of variable Rabi frequency Ω, pulse duration τ, detuning Δ, and laser emission bandwidth β. The noise observed in experimental measurements of Rabi

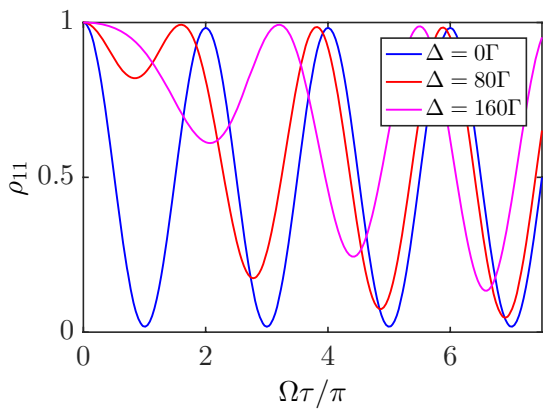

Figure 1.110: (code) Power-dependence of the ground state population with $\tau = 1\,\mu s$, $\beta_1 = (2\pi)\,10kHz$.

oscillations seems not to be due to laser phase noise, which should be negligible in comparison to power broadening. On the other hand, inhomogeneous broadening could be a reason.

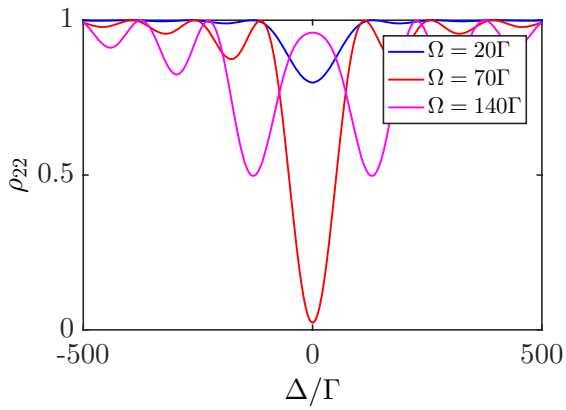

Figure 1.111: (code) Detuning-dependence of the ground state population with $\tau = 1\,\mu s$, $\beta_1 = (2\pi)\,10kHz$.

1.122 18.2.2025 Timing of the SrControl program 1

1.122.1 Problem

What is the benefit that one may expect from pseudo-clock triggering?

Rough estimation of the number of data points assuming a long MOT phase of $\sim 3\,s$ and mostly short time periods of $\sim 1\,s$ in total. This means that, assuming maximum resolution, we must transfer to the NI AO6723 board $(4\,s)/(20\,\mu s) \approx 200000$ data points in a non-clocked fashion. That is, by providing trigger pulses only when things are happening (either switches or ramps), we gain roughly a factor of 4.

For the NI MF6259 board the total duration of periods where devices are ramped is about $\sim 400\,ms$ requiring, together with the negligible number of pulses, $(0.4\,s)/(1\,\mu s) \approx 400000$ non-clocked data points.

We currently use two analog output channels of the fast board AO0 and AO1. The outputs AO1 and AO2 are not operational for unknown reasons. The problem with analog output channels, apart from their insufficient number, is that preloaded (analog or digital) waveforms cannot be triggered by a single trigger signal.

The Matlab command
`addTriggerConnection(s,'external','MF6259/PFI8','StartTrigger')` yields an error message when previously digital channels have been added via
`addDigitalChannel(s,'MF6259','Port0/Line1','OutputOnly')` but not when analog channels have been added via
`addAnalogOutputChannel(s,'MF6259',[0 1],'Voltage')`.

1.122.2 Solution

According to the NI-PCI6259 manual (page 6-2) a solution could be to trigger an analog input channel, which in turn triggers a digital output channel:

```
addClockConnection(s,'External','Dev1/PFI9','ScanClock')
```

1.122.3 Questions

Do we need separate pseudo-clock signals for both boards?

1.122.4 Quintessence

LabScript seems incompatible with Matlab, there are no drivers around generating pseudo-clock signals for Raspberry Pie or Arduino.

At Sr2 we have in the past been able to generate very nice curves (even nicer than Sr1). Hence, there is no pint in giving up the basic rule: 'Never change a winning team.' Any initiative to change the control program at the present stage is nothing else than a displacement activity.

1.123 26.2.2025 Timing of the SrControl program 2

The figure below quantifies the delay in experimental runs due to data processing by the computer. Note that we observe exactly same timing with the NI boards disconnected!

Total duration	3000 ms
MOT loading time	2400
Shutters open	20
Blue ramp 1	4
BR1	0.02
Blue ramp 2	2
Blue off	0.02
Magnetic field off	0.145
Red ramp1	175
RR1	0.02
Red ramp2	100
RR2	0.02
Red Ramp 3	40
RR3	0.02
Red Ramp 4	95
RR4	2
shelving	0.09
trap heat	0.02
scan	0
Tof	4.98
Cam 1	0.02
Probe 1	0.02
wait1	50
Cam 2	0.02
Probe 2	0.02
Wait 2	50
Cam 3	0.02
Probe 3	0.02
Wait 3	56.545

Figure 1.112: (code) Timing panel of the with SrControl software.

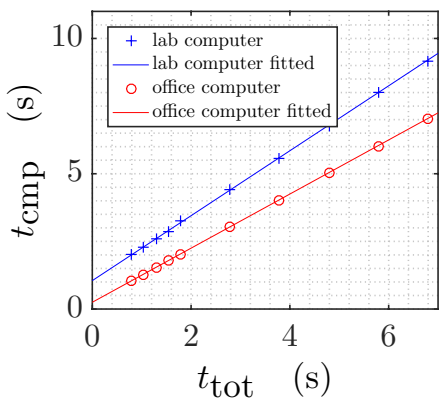

Figure 1.113: (code) Timing with SrControl software of various computers. The abscissa is the total time duration of the SrControl sequence. Varied is the MOT duration $t_{\rm mot}$, while the remaining sequences are kept constant at $t_{rst} = 790\,\rm ms$. The ordinate is the time delay $t_{\rm cmp}$ measured between two subsequent data points.

The fitted curves assumes an angular coefficient of 1.2 and an offset of 1.05 s. The conclusions are:

- the data transfer to the NI board take NO TIME;

- Matlab take very little time to compile big matrices (the 1.2 factor);
- 1.05 s are required to do the rest, such as read out pictures (no done in the tests) and write them with all data to the HardDisk;
- the timing seems not to depend on the size of matrix loaded to the MF6259 board.

1.124 28.2.2025 Problems with the Sr2 data acquisition system

In Sr1 the MF6259 board is connected via TWO cables to TWO buffer boards. In Sr2 the MF6259 board is connected only via ONE cables to ONE buffer board! No surprise that the analog channels 2 and 3 do not work!

At Sr2 we only have the MF6259 BNC-panels, the AO6723 panels are missing.

At Sr2 the AIx BNC-connections of the MF6259 ports are missing on the panel, and the AO connections of the AO6723 ports are wired to the existing MF6259 panel. At Sr1 many of the analog input ports MF6259 AI0..31 are used! What for?

AIx ports are probably needed for triggering digital waveforms. Can we configure PFI ports instead?

In Sr1 the channels `freqout`, `ctr0`, and `ctr1` of the AO6723 board are wired to the BNC panel, but not in Sr2! I provisionally connected them to unused BNC connectors of the MF6259 board.

Figure 1.114: Connectors panel at Sr1 and Sr2.

Different boards may be directly connected by RTSI (Real-Time System Integration) cables. This is not done in Sr1 nor Sr2! This serves, e.g. to synchronize triggers and clocks.

Figure 1.115: .

1.125 5.3.2025 Shelving laser 3

The Rabi laser has power up to $P_{\mathrm{Rb}} < 3\,\mathrm{mW}$ and waist $w = 500\,\mu\mathrm{m}$. Hence, its intensity is,

$$I = \frac{2P}{\pi w^2} \approx 7.6\,\mathrm{mW/cm^2}$$

corresponding at 689 nm and with $\sigma_0 = \frac{3\lambda^2}{2\pi}$ to a Rabi frequency of,

$$\Omega = \sqrt{\sigma(\Delta)\frac{I}{\hbar\omega}\Gamma} \approx (2\pi)\,2.7\,\mathrm{MHz}\ .$$

Note, that the Clebsch-Gordans are all,

$$\left(\begin{array}{cc|c} 0 & 1 & 1 \\ 0 & m & m \end{array}\right) = 1\ .$$

Hence, for pulse durations of $\Delta t = 1\,\mu\mathrm{s}$ we get,

$$\frac{\Omega\Delta t}{\pi} < 5.4\ .$$

Which is roughly what is observed in experiment.

1.125.1 3-level simulations

For modeling we use the Liouvillean (see also Sec. 5.11.2024),

$$\mathcal{M} = \begin{pmatrix} 0 & \Gamma & 0 & \frac{\imath}{2}\Omega & -\frac{\imath}{2}\Omega \\ 0 & -\Gamma - R_{\mathrm{shv}} & R_{\mathrm{rep}} & -\frac{\imath}{2}\Omega & \frac{\imath}{2}\Omega \\ 0 & R_{\mathrm{shv}} & -R_{\mathrm{rep}} & 0 & 0 \\ \frac{\imath}{2}\Omega & -\frac{\imath}{2}\Omega & 0 & -\frac{1}{2}(\Gamma + R_{\mathrm{rep}} + R_{\mathrm{shv}}) + \imath\Delta & 0 \\ -\frac{\imath}{2}\Omega & \frac{\imath}{2}\Omega & 0 & 0 & -\frac{1}{2}(\Gamma + R_{\mathrm{rep}} + R_{\mathrm{shv}}) - \imath\Delta \end{pmatrix},$$

and solve the reduced time-dependent hybrid Bloch-rate equations,

$$\rho(t) = e^{\mathcal{M}_0 t_{\mathrm{ToF}}} e^{\mathcal{M}_{\mathrm{shv}} t_{\mathrm{shv}}} e^{\mathcal{M}_0 t_{\mathrm{wai}}} e^{\mathcal{M}_{\mathrm{Rab}} t_{\mathrm{Rab}}} \rho(0)\ .$$

Here, we don't use repumpers, $R_{\mathrm{rep}} = 0$.

The simulation shows that:

- the Rabi pulse duration should not be too long, $t_{\mathrm{Rab}} < 5\,\mu\mathrm{s}$;
- detuning is critical on the few Γ level;
- shelving pulse durations $t_{\mathrm{shv}} > 1\,\mu\mathrm{s}$ are necessary.

The same simulation but for a Ramsey sequence, see Fig. 1.117.

$$\vec{\rho}(t) = e^{\mathcal{M}_0 t_{\mathrm{ToF}}} e^{\mathcal{M}_{\mathrm{shv}} t_{\mathrm{shv}}} e^{\mathcal{M}_0 t_{\mathrm{wai}}} e^{\mathcal{M}_{\mathrm{Rab}} t_{\mathrm{Rab}}} e^{\mathcal{M}_0 t_{\mathrm{Rmy}}} e^{\mathcal{M}_{\mathrm{Rab}} t_{\mathrm{Rab}}} \vec{\rho}(0)\ .$$

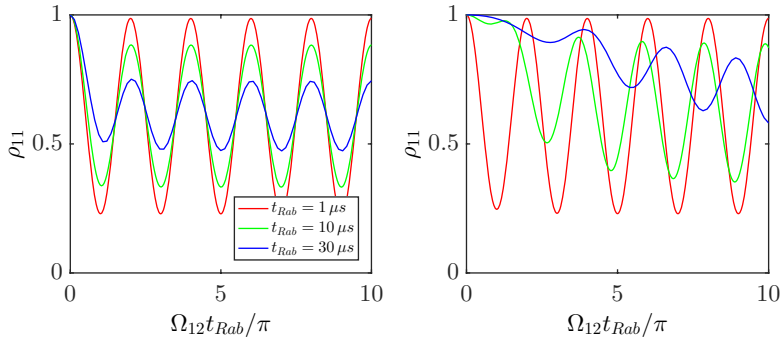

Figure 1.116: (code) Experimental sequence with Rabi, shelving, and probe pulse. The length of the Rabi pulse t_{Rab} is varied, after that come a delay time of $t_{\mathrm{dly}} = 5\,\mu\mathrm{s}$, a shelving pulse of $t_{\mathrm{shv}} = 1\,\mu\mathrm{s}$, and a time-of-flight delay $t_{\mathrm{ToF}} = 5\,\mathrm{ms}$. The Rabi laser is (left) on resonance, (right) detuned by 10Γ.

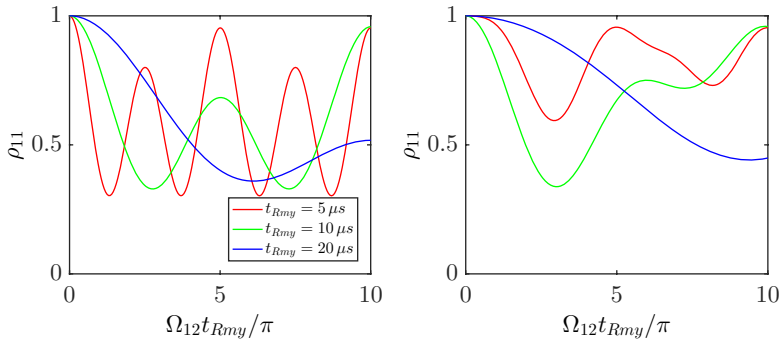

Figure 1.117: (code) Experimental sequence with two Ramsey pulses, shelving, and probe pulse. The time between the Ramsey pulses t_{Rab} is varied, the pulse lengths are $T_{\mathrm{Rab}} = 2\,\mu\mathrm{s}$, after that come a delay time of $t_{\mathrm{dly}} = 5\,\mu\mathrm{s}$, a shelving pulse of $t_{\mathrm{shv}} = 1\,\mu\mathrm{s}$, and a time-of-flight delay $t_{\mathrm{ToF}} = 5\,\mathrm{ms}$. The Rabi laser is (left) on resonance, (right) detuned by 10Γ.

Spectra are also interesting, see Fig. 1.118.

We experimentally observe an oscillation in the center-of-mass of the cloud of about $\Delta s = 35\,\mu\mathrm{m}$ after $t_{\mathrm{ToF}} 5\,\mathrm{ms}$ time-of-flight synchronous with the Rabi oscillations, which could be momentum states separated by 1 photon recoil:

$$v_{\mathrm{meas}} = \frac{\Delta s}{\sin \alpha t_{\mathrm{ToF}}} \approx 8.5\,\mathrm{mm/s} \qquad \text{and} \qquad v_{\mathrm{estm}} \approx \frac{\hbar k}{m} \approx 6.6\,\mathrm{mm/s}\ ,$$

where $\alpha = 55\,^{\circ}$ is the angle between the Rabi and the imaging beam.

The sequence is illustrated Fig. 1.119.

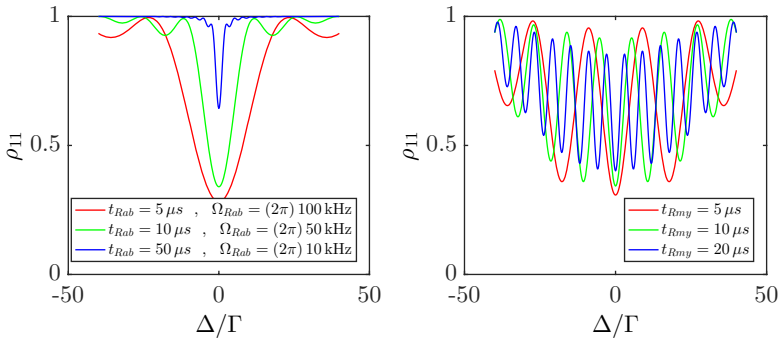

Figure 1.118: (code) (left) Rabi spectra and (right) Ramsey spectra.

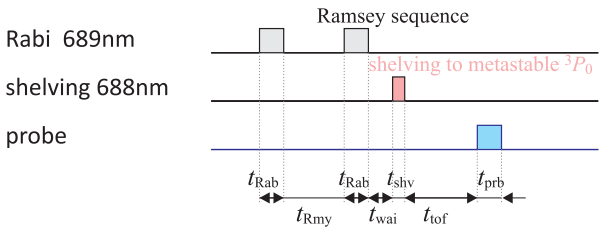

Figure 1.119: (code) Experimental sequence with Ramsey, shelving, and probe pulses.

1.125.2 5-level simulations

The simulation can be extended to include all three Zeeman levels of the $^3P_1$ state with the equation exhibited in Fig. 1.120. with the abbreviations,

$$
\frac{d}{dt}\begin{pmatrix}
\rho_{11}\\ \rho_{22}\\ \rho_{33}\\ \rho_{44}\\ \rho_{55}\\ \rho_{12}\\ \rho_{21}\\ \rho_{13}\\ \rho_{31}\\ \rho_{14}\\ \rho_{41}\\ \rho_{23}\\ \rho_{32}\\ \rho_{24}\\ \rho_{42}\\ \rho_{34}\\ \rho_{43}
\end{pmatrix}
=
\begin{pmatrix}
0 & \Gamma_e & \Gamma_e & \Gamma_e & \Gamma_m & \frac{\imath}{2}\Omega_{12} & -\frac{\imath}{2}\Omega_{12} & \frac{\imath}{2}\Omega_{13} & -\frac{\imath}{2}\Omega_{13} & \frac{\imath}{2}\Omega_{14} & -\frac{\imath}{2}\Omega_{14} & 0 & 0 & 0 & 0 & 0 & 0\\
0 & -\Gamma_e - S & 0 & 0 & R/3 & -\frac{\imath}{2}\Omega_{12} & \frac{\imath}{2}\Omega_{12} & 0 & 0 & 0 & 0 & 0 & 0 & 0 & 0 & 0 & 0\\
0 & 0 & -\Gamma_e - S & 0 & R/3 & 0 & 0 & -\frac{\imath}{2}\Omega_{13} & \frac{\imath}{2}\Omega_{13} & 0 & 0 & 0 & 0 & 0 & 0 & 0 & 0\\
0 & 0 & 0 & -\Gamma_e - S & R/3 & 0 & 0 & 0 & 0 & -\frac{\imath}{2}\Omega_{14} & \frac{\imath}{2}\Omega_{14} & 0 & 0 & 0 & 0 & 0 & 0\\
0 & S & S & S & -\Gamma_m - R & 0 & 0 & 0 & 0 & 0 & 0 & 0 & 0 & 0 & 0 & 0 & 0\\
\frac{\imath}{2}\Omega_{12} & -\frac{\imath}{2}\Omega_{12} & 0 & 0 & 0 & -\Lambda_{12} & 0 & 0 & 0 & 0 & 0 & 0 & -\frac{\imath}{2}\Omega_{13} & 0 & -\frac{\imath}{2}\Omega_{14} & 0 & 0\\
-\frac{\imath}{2}\Omega_{12} & \frac{\imath}{2}\Omega_{12} & 0 & 0 & 0 & 0 & -\Lambda_{12}^* & 0 & 0 & 0 & 0 & \frac{\imath}{2}\Omega_{13} & 0 & \frac{\imath}{2}\Omega_{14} & 0 & 0 & 0\\
\frac{\imath}{2}\Omega_{13} & 0 & -\frac{\imath}{2}\Omega_{13} & 0 & 0 & 0 & 0 & -\Lambda_{13} & 0 & 0 & 0 & -\frac{\imath}{2}\Omega_{12} & 0 & 0 & 0 & 0 & -\frac{\imath}{2}\Omega_{14}\\
-\frac{\imath}{2}\Omega_{13} & 0 & \frac{\imath}{2}\Omega_{13} & 0 & 0 & 0 & 0 & 0 & -\Lambda_{13}^* & 0 & 0 & 0 & \frac{\imath}{2}\Omega_{12} & 0 & 0 & \frac{\imath}{2}\Omega_{14} & 0\\
\frac{\imath}{2}\Omega_{14} & 0 & 0 & -\frac{\imath}{2}\Omega_{14} & 0 & 0 & 0 & 0 & 0 & -\Lambda_{14} & 0 & 0 & 0 & -\frac{\imath}{2}\Omega_{12} & 0 & -\frac{\imath}{2}\Omega_{14} & 0\\
-\frac{\imath}{2}\Omega_{14} & 0 & 0 & \frac{\imath}{2}\Omega_{14} & 0 & 0 & 0 & 0 & 0 & 0 & -\Lambda_{14}^* & 0 & 0 & 0 & \frac{\imath}{2}\Omega_{12} & 0 & \frac{\imath}{2}\Omega_{12}\\
0 & 0 & 0 & 0 & 0 & 0 & \frac{\imath}{2}\Omega_{13} & -\frac{\imath}{2}\Omega_{12} & 0 & 0 & 0 & -\Lambda_{23} & 0 & 0 & 0 & 0 & 0\\
0 & 0 & 0 & 0 & 0 & -\frac{\imath}{2}\Omega_{13} & 0 & 0 & \frac{\imath}{2}\Omega_{12} & 0 & 0 & 0 & -\Lambda_{23}^* & 0 & 0 & 0 & 0\\
0 & 0 & 0 & 0 & 0 & 0 & \frac{\imath}{2}\Omega_{14} & 0 & 0 & -\frac{\imath}{2}\Omega_{12} & 0 & 0 & 0 & -\Lambda_{24} & 0 & 0 & 0\\
0 & 0 & 0 & 0 & 0 & -\frac{\imath}{2}\Omega_{14} & 0 & 0 & 0 & 0 & \frac{\imath}{2}\Omega_{12} & 0 & 0 & 0 & -\Lambda_{24}^* & 0 & 0\\
0 & 0 & 0 & 0 & 0 & 0 & 0 & 0 & \frac{\imath}{2}\Omega_{13} & -\frac{\imath}{2}\Omega_{13} & 0 & 0 & 0 & 0 & 0 & -\Lambda_{34} & 0\\
0 & 0 & 0 & 0 & 0 & 0 & 0 & -\frac{\imath}{2}\Omega_{14} & 0 & 0 & \frac{\imath}{2}\Omega_{13} & 0 & 0 & 0 & 0 & 0 & -\Lambda_{34}^*
\end{pmatrix}
\begin{pmatrix}
\rho_{11}\\ \rho_{22}\\ \rho_{33}\\ \rho_{44}\\ \rho_{55}\\ \rho_{12}\\ \rho_{21}\\ \rho_{13}\\ \rho_{31}\\ \rho_{14}\\ \rho_{41}\\ \rho_{23}\\ \rho_{32}\\ \rho_{24}\\ \rho_{42}\\ \rho_{34}\\ \rho_{43}
\end{pmatrix}
$$

Figure 1.120: (code) 5 levels Bloch equations.

$$
\begin{aligned}
\Gamma_{\mathrm{ge}} &= \Gamma_{\mathrm{e}} \quad , \quad \Gamma_{\mathrm{em}} = \Gamma_{\mathrm{m}} \quad , \quad \text{for } \; g = 1, e = 2, .., 4, m = 5 \; ,\\
\gamma_{ij} &= 2\beta_{ij} + \sum\nolimits_{k=1..7} (\Gamma_{\mathrm{ik}} + \Gamma_{\mathrm{jk}})\\
\Delta_{\mathrm{ge}} &= \Delta_{\mathrm{ge}} + \Delta_{\mathrm{Zeeman}}\\
\Delta_{\mathrm{em}} &= \Delta_{\mathrm{em}} + \Delta_{\mathrm{Zeeman}}\\
\Delta_{\mathrm{gm}} &= \Delta_{\mathrm{em}} - \Delta_{\mathrm{ge}}\\
\Lambda_{ij} &= \frac{1}{2}\gamma_{ij} + \imath\Delta_{ij}\\
\frac{\imath}{2}\Omega_{12} &= \frac{1}{4}\sin^2\alpha \quad , \quad \frac{\imath}{2}\Omega_{13} = \frac{1}{3}\cos^2\alpha \quad , \quad \frac{\imath}{2}\Omega_{14} = \frac{1}{4}\sin^2\alpha \; .
\end{aligned}
$$

Fig. 1.120 shows calculated curves.

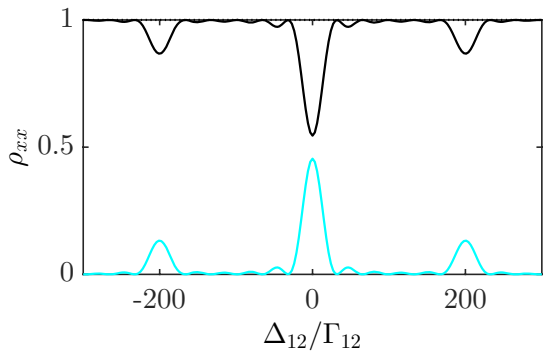

Figure 1.121: (code) Rabi spectra.

1.126 11.3.2025 Timing of the SrControl program 3

The problem is now resolved using a 1 MHz clock generated on the `CLK`-channel using the command `addCounterOutputChannel(s,'AO6723','ctr0','PulseGeneration')` switched by an analog output channel of the same AO6723 board. This gated pulse train then clocks the MF6259 board via the `PFI8`-channel using the `addClockConnection(s,'external','MF6259/PFI8','ScanClock')`. The advantage is that both boards are then perfectly gated, see Fig. 1.122.

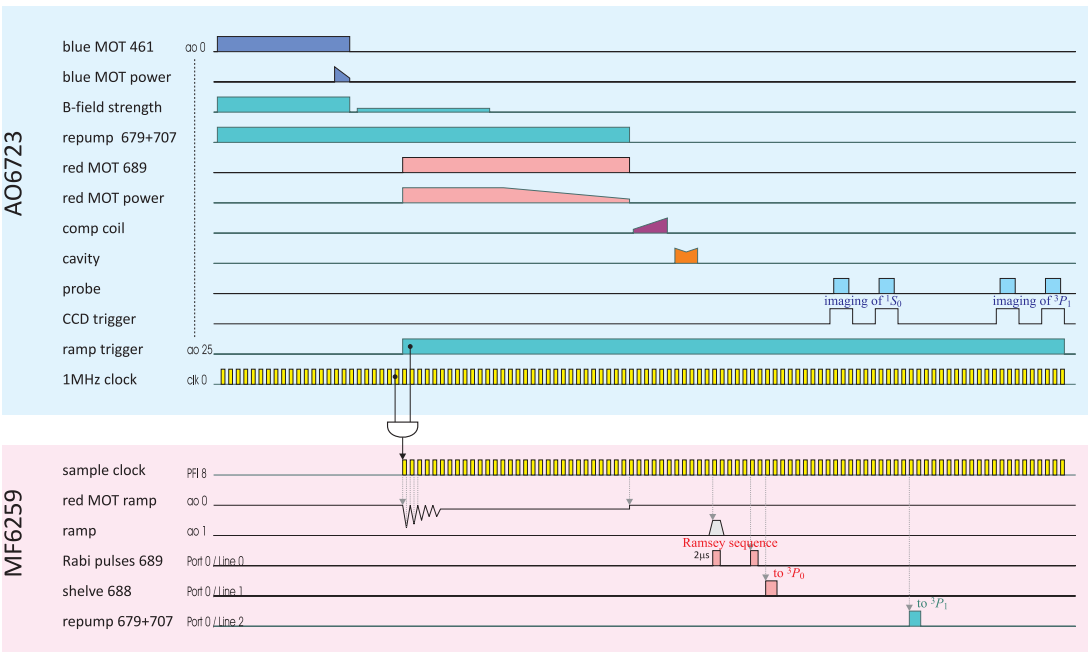

Figure 1.122: (code) Experimental sequence.

We currently use an rf-switch, which is an overkill. A logical `AND` would do perfectly.

I also tried to set an initial delay to the counter via `clk0.InitialDelay=2`, but the delay is limited on the AO6723 by the condition,

$$\texttt{InitialDelay} \leq \frac{\texttt{ctr.MaxCount}}{\texttt{ctr.TimeBase}} \ ,$$

yielding in our case,

$$\texttt{InitialDelay} \leq \frac{20\,\mathrm{MHz}}{16\,777\,215} < 0.8\,\mathrm{s} \ ,$$

which is insufficient as compared to the duration of the MOT.

1.127 11.8.2025 Dicke phase transition in free clouds

A Dicke phase transition may also be expected in free clouds if the saturation parameter exceeds a critical value, $s > s_{\rm c}$, where

$$
\begin{aligned}
& s_{\rm c} \equiv \frac{2\Omega_{\rm c}^2}{\Gamma^2} \\
\text{and} \qquad & \Omega_{\rm c} \equiv N\frac{g^2}{\kappa} \\
\text{and} \qquad & \Upsilon_N \equiv N\frac{F}{\pi}\frac{6}{k^2w^2} = N\frac{F}{\pi}\frac{\sigma_0}{\pi w^2} = Fb_0 \ .
\end{aligned}
$$

Hence,

$$
s_{\rm c} = F^2\frac{b_0^2}{8} \ ,
$$

where in free space space we may set the finesse to $F = 1$.

1.128 12.8.2025 Bragg scattering on lattice 1

Interesting effects may occur when every second site is populated [42, 24]. This can be achieved with two Bragg lasers intersecting at the location of the cloud under an angle of $\beta = 60°$,

$$d = \frac{\pi}{k_{\rm lat}} = \frac{\pi}{K \sin\frac{\beta}{2}} = \frac{\pi}{\frac{2\pi}{\lambda_{\rm brg}} \sin\frac{\beta}{2}} = \frac{\lambda_{\rm brg}}{2\sin\frac{\beta}{2}} = \frac{\lambda_{\rm brg}}{2\sin\frac{60°\pi}{2\cdot 180°}} = \lambda_{\rm brg}$$

For example, we may choose $\lambda_{\rm brg} = 689\,\text{nm}$. In this case the optical potential must be calculated from the detuning to the red of the intercombination line. Alternatively, we could use our new laser at $\lambda_{\rm brg} = 813\,\text{nm}$ intersecting at 72.3°. In this case the optical potential must be calculated from the detuning to the 461 nm transition.

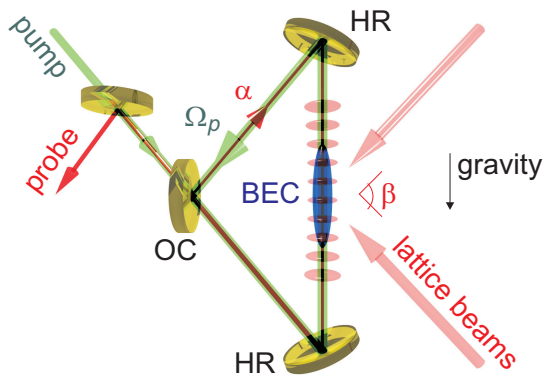

Figure 1.123: (code) Scheme of the setup.

The tolerance for the intersection angle for perfect commensurability of the lattice period with the strontium resonance is given by,

$$\Delta d = \left|\frac{\partial d}{\partial \beta}\right| \Delta\beta = \left|\frac{\lambda_{\rm brg}\cos\frac{1}{2}\beta}{4\sin^2\frac{1}{2}\beta}\right| \Delta\beta < \frac{d^2}{L} = \lambda_{\rm brg}\frac{\delta_{\rm fsr}}{\nu_{689}} \ .$$

For $\beta = 60°$ we expect,

$$\Delta\beta < \frac{\lambda_{\rm brg}\delta_{\rm fsr}}{\nu_{689}\left|\frac{\lambda_{\rm brg}\cos\frac{1}{2}\beta}{4\sin^2\frac{1}{2}\beta}\right|} = \frac{6\lambda_{689}\delta_{\rm fsr}}{c} = 1.1\times 10^{-4}\,\text{rad} \ .$$

The structure factor for the optical lattice has been derived,

$$S_{\mathbf{k}_0}(\mathbf{k}) = \frac{n_0}{N}\frac{1-e^{\imath N_s d\,(k_z-k_{0z})}}{e^{-\imath d\,(k_z-k_{0z})}-1} e^{(k_x-k_{0x})\sigma_r^2/2} e^{(k_y-k_{0y})\sigma_r^2/2} e^{(k_z-k_{0z})\sigma_z^2/2}$$

$$|S_{\mathbf{k}_0}(\mathbf{k})|^2 = \frac{n_0^2}{N^2}\frac{1-\cos N_s(k_z-k_{0z})d}{1-\cos(k_z-k_{0z})d} e^{(k_x-k_{0x})\sigma_r^2} e^{(k_y-k_{0y})\sigma_r^2} e^{(k_z-k_{0z})\sigma_z^2}$$

Here, we assume $d = 2\pi/k_0$ and

$$\mathbf{k}_0 = k_0\begin{pmatrix}\cos 60°\\ 0\\ \sin 60°\end{pmatrix} \qquad \text{and} \qquad \mathbf{k} = k_0\begin{pmatrix}\cos\alpha\\ 0\\ \sin\alpha\end{pmatrix}$$

Not surprisingly, we find that Bragg scattering into the axis of the optical lattice is NOT cooperatively enhanced, except for perpendicular incidence. However, for perpendicular incidence the large radial extend of the atomic clouds suppresses Bragg scattering even along the axis (see [102]).

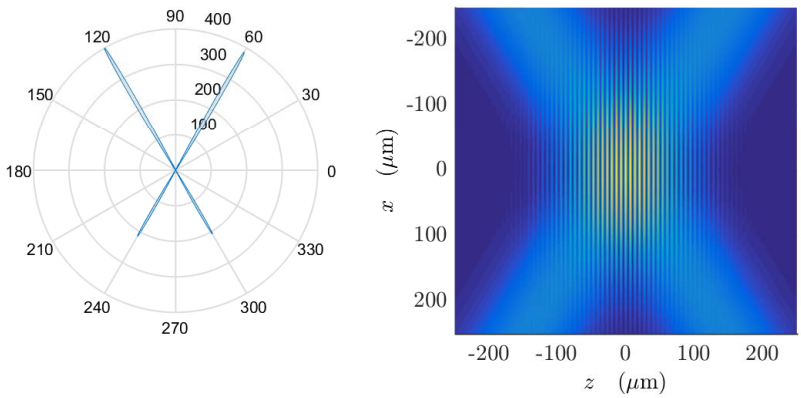

Figure 1.124: (code) (a) Structure factor for 60° incidence. (b) Optical lattice formed by the Bragg lasers.

Maybe we could study Bloch oscillations in the tight binding limit [24] looking at the reflection signal?

1.128.1 Optical potential shape

Let us now calculate the intensity distribution of two intersecting lasers with equal powers and waists. Generalizing the formula for one laser propagating along the z-axis,

$$I(\mathbf{r}) = \frac{2P}{\pi w_0^2} |e^{-(x^2+y^2)/w_0^2} e^{-z^2/2z_R^2} e^{\imath kz}|^2$$

to two arbitrary directions $\mathbf{k}_\pm$, we get,

$$I(\mathbf{r}) = \frac{2P}{\pi w_0^2} \left| \sum_\pm e^{-(\mathbf{k}_\pm \times \mathbf{r})^2/k^2 w_0^2} e^{-(\mathbf{k}_\pm \cdot \mathbf{r})^2/2k^2 z_R^2} e^{\imath \mathbf{k}_\pm \cdot \mathbf{r}} \right|^2 ,$$

where $z_R \equiv \pi w_0^2/\lambda$ is the Rayleigh range. For $\mathbf{k}_\pm = k\hat{\mathbf{e}}_z$ we recover old result. Now, set we choose $\mathbf{k}_\pm = k\begin{pmatrix}\cos\beta' \\ 0 \\ \pm\sin\beta'\end{pmatrix}$ with $\beta' \equiv \frac{\beta}{2}$, so that,

$$\begin{aligned}
\mathbf{k}_\pm \cdot \mathbf{r} &= kx\cos\beta' \pm kz\sin\beta' \\
(\mathbf{k}_\pm \cdot \mathbf{r})^2 &= k^2x^2\cos^2\beta' + k^2z^2\sin^2\beta' \pm k^2xz\sin\beta \\
\mathbf{k}_\pm \times \mathbf{r} &= \begin{pmatrix} \mp ky\sin\beta' \\ \pm kx\sin\beta' - kz\cos\beta' \\ ky\cos\beta' \end{pmatrix} \\
(\mathbf{k}_\pm \times \mathbf{r})^2 &= k^2y^2 + k^2x^2\sin^2\beta' + k^2z^2\cos^2\beta' \mp k^2xz\sin\beta \ .
\end{aligned}$$

Inserted into the intensity distribution, we get,

$$\begin{aligned}
I(\mathbf{r}) = \frac{2P}{\pi w_0^2} e^{-2(x\sin\beta'/w_0)^2 - (x\cos\beta'/z_R)^2} e^{-2(y/w_0)^2} e^{-2(z\cos\beta'/w_0)^2 - (z\sin\beta'/z_R)^2} \times \\
\times \left| \sum_\pm e^{\pm xz\sin\beta(1/w_0^2 - 1/2z_R^2)} e^{\imath k(x\cos\beta' \pm z\sin\beta')} \right|^2 \ .
\end{aligned}$$

Because typically $w_0 \ll z_R$, we may simplify to,

$$I(\mathbf{r}) \overset{w_0 \ll z_R}{=} \frac{2P}{\pi w_0^2} e^{-2(x\sin\beta'/w_0)^2} e^{-2(y/w_0)^2} e^{-2(z\cos\beta'/w_0)^2} \left| \sum_\pm e^{\pm xz\sin\beta/w_0^2} e^{\pm\imath kz\sin\beta'} \right|^2 \ .$$

On the optical axis $x = 0 = y$,

$$I(0,0,z) = \frac{4P}{\pi w_0^2} e^{-2(z\cos\beta'/w_0)^2} \cos kz \sin\beta' \ .$$

Setting $\beta' = 30°$,

$$I(\mathbf{r}) \overset{\beta'=30°}{\longrightarrow} \frac{4P}{\pi w_0^2} e^{-3z^2/2w_0^2} \cos\tfrac{kz}{2} \ .$$

1.128.2 Optical potential depth

The maximum intensity is always,

$$I_0 = \frac{4P}{\pi w_0^2}$$

and the optical potential depth is given by

$$U(\mathbf{r}) \simeq \frac{3\pi c^2}{2\omega_0^3}\frac{\Gamma}{\Delta} I(\mathbf{r}) \qquad , \qquad U_0 \simeq \frac{3\pi c^2}{2\omega_0^3}\frac{\Gamma}{\Delta}\frac{4P}{\pi w_0^2} \ .$$

For $\lambda_{\rm brg} = 689\,{\rm nm}$, $\Gamma = (2\pi)30\,{\rm MHz}$, $\Delta = \frac{2\pi c}{461\,{\rm nm}} - \frac{2\pi c}{689\,{\rm nm}} = (2\pi)215\,{\rm THz}$, $P = 10\,{\rm mW}$, and $w_0 = 100\,\mu{\rm m}$ we get,

$$U_0 \simeq k_{\rm B}\,0.2\,\mu{\rm K} = h\,5.6\,{\rm kHz} \ .$$

For $\lambda_{\rm brg} = 689\,{\rm nm}$, $\Gamma = (2\pi)7.4\,{\rm kHz}$, $\Delta = (2\pi)4\,{\rm GHz}$, $P = 10\,{\rm mW}$, and $w_0 = 100\,\mu{\rm m}$ we get,

$$U_0 \simeq k_{\rm B}\,3.5\,\mu{\rm K} = h\,74\,{\rm kHz}\ .$$

For $\lambda_{\rm brg} = 813\,{\rm nm}$, $\Gamma = (2\pi)30\,{\rm MHz}$, $\Delta = \frac{2\pi c}{461\,{\rm nm}} - \frac{2\pi c}{813\,{\rm nm}} = (2\pi)282\,{\rm THz}$, $P = 100\,{\rm mW}$, and $w_0 = 100\,\mu{\rm m}$ we get,

$$U_0 \simeq k_{\rm B}\,3.3\,\mu{\rm K} = h\,70\,{\rm kHz}\ .$$

1.129 21.8.2025 Bragg scattering on lattice 2

In the experiment we will superpose the Bragg optical lattice (BOL) with the optical dipole potential supported by the cavity mode. If the cavity is pumped from one side, we obtain additional lattices formed by interference with each of the Bragg laser beams. If the cavity is pumped from both sides, we obtain another optical lattice along the optical lattice (COL).

Whether the cavity beams and the Bragg beams interfere depends on their polarizations. Assuming that all beams propagate within the $y = 0$ plane, the polarizations of every laser can be parametrized by a single angle α_i between the polarization vector $\vec{\epsilon}$ and the y-axis. We then may use the previous formula generalized to more incident beams,

$$I(\mathbf{r}) = \left| \sum_i \sqrt{\frac{2P_i}{\pi w_i^2}} \begin{pmatrix} \mathbf{k}_i/k_0 \cdot \hat{\mathbf{e}}_z \sin\alpha_i \\ \cos\alpha_i \\ \mathbf{k}_i/k_0 \cdot \hat{\mathbf{e}}_x \sin\alpha_i \end{pmatrix} e^{-(\mathbf{k}_i \times \mathbf{r})^2/k^2 w_i^2 - (\mathbf{k}_i \cdot \mathbf{r})^2/2k^2 z_{Ri}^2 + \imath \mathbf{k}_i \cdot \mathbf{r} + \imath \varphi_i} \right|^2 ,$$

where the index i marks the individual beams with their respective powers P_i, waists w_i, wavevectors $\mathbf{k}_i$, polarization angles $\mathbf{k}_i$, and phase shifts φ_i.

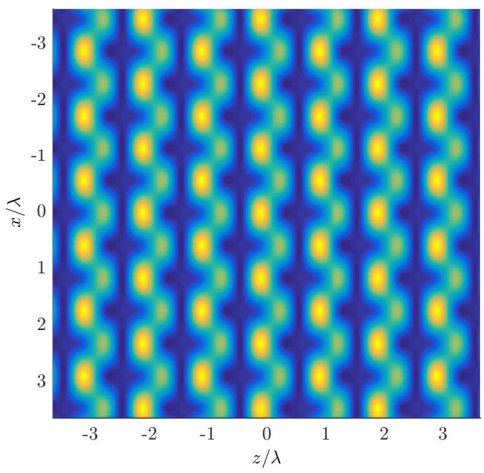

Figure 1.125: (code) Optical lattice formed by the Bragg lasers together with the cavity modes.

The result is a complicated array whose periodicity (λ_{brg} or $\lambda_{\text{brg}}/2$) depends on the relative phase shifts of the lasers. Note that this can be mitigated by proper choice of polarizations or detunings: When the polarizations of the lasers generating the BOL and the COL are perpendicular, they don not interfere and the total lattice is oriented along the cavity axis.

Bibliography

[1] A. André, L.-M. Duan, and M. D. Lukin, *Coherent atom interactions mediated by dark-state polaritons*, Phys. Rev. Lett. **88** (2002), 243602, .

[2] M. Antezza and Y. Castin, *Fano-hopfield model and photonic band gaps for an arbitrary atomic lattice*, Phys. Rev. A **80** (2009), 013816, DOI.

[3] _____, *Spectrum of light in a quantum fluctuating periodic structure*, ePrints (2009), 0903.0765, .

[4] A. S. Arnold, J. S. Wilson, and M. G. Boshier, *A simple extended-cavity diode laser*, Rev. Sci. Instr. **69** (1998), 1236, .

[5] M. Artoni and G. La Rocca, *Optically tunable photonic stop bands in homogeneous absorbing media*, Phys. Rev. Lett. **96** (2006), 073905, .

[6] M. Artoni, G. La Rocca, and F. Bassani, *Resonantly absorbing one-dimensional photonic crystals*, Phys. Rev. E **72** (2005), 046604, .

[7] K. Baumann, C. Guerlin, F. Brennecke, and T. Esslinger, *Dicke quantum phase transition with a superfluid gas in an optical cavity*, Nature **464** (2010), 1301, DOI.

[8] Y. Bidel, *Piégeage et refroidissement laser du strontium: Etude de l'effet des interférences en diffusion multiple*, Ph.D. thesis, Université de Nice - Sophia Antipolis, 2001.

[9] Y. Bidel, B. Klappauf, J. C. Bernard, D. Delande, G. Labeyrie, C. Miniatura, D. Wilkowski, and R. Kaiser, *Coherent light transport in a cold strontium cloud*, Phys. Rev. Lett. **88** (2002), 203902, DOI.

[10] G. Birkl, M. Gatzke, I. H. Deutsch, S. L. Rolston, and W. D. Phillips, *Bragg sccattering from atoms in optical lattices*, Phys. Rev. Lett. **75** (1995), 2823, .

[11] P. B. Blakie and R. J. Ballagh, *Mean-field treatment of Bragg scattering from a Bose-Einstein condensate*, J. Phys. B **33** (2000), 3961, .

[12] J. G. Bohnet, K. C. Cox, M. A. Norcia, J. M. Weiner, Z. Chen, and J. K. Thompson, *Reduced spin measurement back-action for a phase sensitivity ten times beyond the standard quantum limit*, Nature Phot. **8** (2014), 731, DOI.

[13] E. A. Bohr, S. L. Kristensen, C. Hotter, . A. Schäffer, J. Robinson-Tait, J. W. Thomsen, T. Zelevinsky, H. Ritsch, and J. H. Müller, *Collectively enhanced ramsey readout by cavity sub- to superradiant transition*, Nature Comms. **15** (2023), 1084, DOI.

[14] Ph. Bouyer and M. A. Kasevich, *Heisenberg-limited spectroscopy with degenerate Bose-Einstein gases*, Phys. Rev. A **56** (1997), R1083, DOI.

[15] F. Brennecke, T. Donner, S. Ritter, T. Bourdel, M. Köhl, and T. Esslinger, *Cavity QED with a Bose-Einstein condensate*, Nature **250** (2007), 268, .

[16] A. Bychek, Ch. Hotter, D. Plankensteiner, and H. Ritsch, *Superradiant lasing in inhomogeneously broadened ensembles with spatially varying coupling*, ePrints (2021), arXiv2105.11023, DOI.

[17] T. Chaneliere, *Diffusion multiple cohérente avec atomes froids de strontium*, Ph.D. thesis, Université de Nice - Sophia Antipolis, 2004.

[18] T. Chanelière, L. He, R. Kaiser, and D. Wilkowski, *Three dimensional cooling and trapping with a narrow line*, Eur. Phys. J. D **46** (2008), 507, DOI.

[19] T. Chanelière, J.-L. Meunier, R. Kaiser, C. Miniatura, and D. Wilkowski, *Extra-heating mechanism in doppler cooling experiments*, J. Opt. Soc. Am. B **22** (2005), 1819, DOI.

[20] R. Charrière, M. Cadoret, N. Zahzam, Y. Bidel, and A. Bresson, *Local gravity measurement with the combination of atom interferometry and Bloch oscillations*, Phys. Rev. A **85** (2012), 013639.

[21] Zilong Chen, Ju. G. Bohnet, S. R. Sankar, Jiayan Dai, and J. K. Thompson, *Conditional spin squeezing of a large ensemble via the vacuum Rabi splitting*, Phys. Rev. Lett. **106** (2011), 133601, DOI.

[22] N. V. Cohan, D. Pugh, and R. H. Tredgold, *Band structure of diamond*, Proc. Phys. Soc. **82** (1963), 65, .

[23] Y. Colombe, T. Steinmetz, G. Dubois, F. Linke, D. Hunger, and J. Reichel, *Strong atom field coupling for bose Einstein condensates in an optical cavity on a chip*, Nature **250** (2005), 272, .

[24] Ph. W. Courteille, D. Rivero, G. H. de FrançÃ§a, C. A. Pessoa Jr, A. Cipris, M. N´ unez Portela, R. C. Teixeira, and S. Slama, *Photonic bands and normal mode splitting in optical lattices interacting with cavities*, Phys. Rev. A **111** (2025), 013310, DOI.

[25] I. Courtillot, A. Quessada, R. P. Kovacich, J-J. Zondy, A. Landragin, A. Clairon, and P. Lemonde, *Efficient cooling and trapping of strontium atoms*, Opt. Lett. **28** (2003), 468, DOI.

[26] K. C. Cox, G. P. Greve, J. M. Weiner, and J. K. Thompson, *Deterministic squeezed states with collective measurements and feedback*, Phys. Rev. Lett. **116** (2016), 093602, DOI.

[27] R. Culver, A. Lampis, B. Megyeri, K. Pahwa, L. Mudarikwa, M. Holynski, Ph. W. Courteille, and J. Goldwin, *Collective strong coupling of cold potassium atoms in a ring cavity*, New J. Phys. **18** (2016), 113043.

[28] F. Dalfovo, S. Giorgini, L. P. Pitaevskii, and S. Stringari, *Theory of Bose-condensation in trapped gases*, Rev. Mod. Phys. **71** (1999), 463, cond-mat/9806038.

[29] Y. N. Martinez de Escobar, P. G. Mickelson, P. Pellegrini, S. B. Nagel, A. Traverso, M. Yan, R. Côté, and T. C. Killian, *Two-photon photoassociative spectroscopy of ultracold 88sr*, Phys. Rev. A **78** (2008), 062708, DOI.

[30] Y. N. Martinez de Escobar, P. G. Mickelson, M. Yan, R. Chakraborty, and T. C. Killian, *Modification of atom scattering using an intercombination-line optical Feshbach resonance at large detuning*, ePrints **0906.1837** (2009), .

[31] Y. N. Martinez de Escobar, P. G. Mickelson, M. Yan, B. J. DeSalvo, S. B. Nagel, and T. C. Killian, *Bose-Einstein condensation of 84sr resonance at large detuning*, Phys. Rev. Lett. **103** (2009), 200402, DOI.

[32] B. Deh, C. Marzok, S. Slama, C. Zimmermann, and Ph. W. Courteille, *Bragg spectroscopy and Ramsey interferometry with an ultracold Fermi gas*, Appl. Phys. B **97** (2009), 387, DOI.

[33] B. J. DeSalvo, M. Yan, P. G. Mickelson, Y. N. Martinez de Escobar, and T. C. Killian, *Degenerate Fermi gas of 87sr*, ePrints **arXiv:1005.0668** (2010), DOI.

[34] I. Deutsch, A. Barenco, and A. Ekert, Proc. Roy. Soc. Lond. **449** (1995), 669, DOI.

[35] R. H. Dicke, *Coherence in spontaneous radiation processes*, Phys. Rev. **93** (1954), 99, DOI.

[36] B. Edlén, *The refractive index of air*, Metrologia **2** (1966), 71, .

[37] Ph. T. Ernst, S. Götze, J. S. Krauser, K. Pyka, D.-S. Lühmann, D. Pfannkuche, and K. Sengstock, *Probing superfluids in optical lattices by momentum-resolved Bragg spectroscopy*, Nature Phys. **06** (2009), 56, DOI.

[38] G. Ferrari, P. Cancio, R. Drullinger, G. Giusfredi, N. Poli, M. Prevedelli, C. Toninelli, and G. M. Tino, *Precision frequency measurement of visible intercombination lines of strontium*, Phys. Rev. Lett. **91** (2003), 243002, DOI.

[39] G. Ferrari, N. Poli, F. Sorrentino, and G. M. Tino, *Long-lived Bloch oscillations with bosonic sr atoms and application to gravity measurement at the micrometer scale*, Phys. Rev. Lett. **97** (2006), 060402, DOI.

[40] T. Fukuhara, Y. Takasu, M. Kumakura, and Y. Takahashi, *Degenerate Fermi gases of ytterbium*, Phys. Rev. Lett. **98** (2007), 030401, DOI.

[41] H. Fukuyama, R. A. Barit, and H. C. Fogedby, *Tightly bound electrons in a uniform electric field*, Phys. Rev. B **8** (2009), 5579, DOI.

[42] B. Gábor, A. K. Varooli, D. Varga, B. Sárközi, Á. Kurkó, A. Dombi, T. W. Clark, F. I. B. Williams, D. Nagy, A. Vukics, and P. Domokos, *Demonstration of strong coupling of a subradiant atom array to a cavity vacuum*, Eur Phys J Quantum Technology **12** (2025), 93, DOI.

[43] B. M. Garraway, *The Dicke model in quantum optics: Dicke model revisited*, Phil. Trans. R. Soc. A **369** (2011), 1137, DOI.

[44] M. Gegg, A. Carmele, A. Knorr, and M. Richter, *Superradiant to subradiant phase transition in the open system Dicke model: dark state cascades*, New J. Phys. **20** (2018), 013006, DOI.

[45] A. Görlitz, M. Weidemüller, T. W. Hänsch, and A. Hemmerich, *Observing the position spread of atomic wave packets*, Phys. Rev. Lett. **78** (1997), 2096, DOI.

[46] P. W. R. Graham, J. M. Hogan, M. A. Kasevich, and S. Rajendran, *New method for gravitational wave detection with atomic sensors*, Phys. Rev. Lett. **110** (2013), 171102, DOI.

[47] R. Grimm, M. Weidemüller, and Y. B. Ovchinnikov, *Optical dipole traps for neutral atoms*, Adv. At. Mol. Opt. Phys. **42** (2000), 95, .

[48] C. J. Hawthorn, K. P. Weber, and R. E. Scholten), *Littrow configuration tunable external cavity diode laser with fixed direction output beam*, ePrints (2001), 4477, .

[49] S. M. Heider and G. O. Brink, *Hyperfine structure of* ^{87}*sr in the* $^3p_2$ *metastable state*, Phys. Rev. A **16** (1977), 1371, DOI.

[50] K. M. Ho, C. T. Chan, and C. M. Soukoulis, *Existence of a photonic gap in periodic dielectric structures*, Phys. Rev. Lett. **65** (1990), 3152, .

[51] Ch. Hotter, L. Ostermann, and H. Ritsch, *Cavity sub- and superradiance for transversely driven atomic ensembles*, Phys. Rev. Res. **5** (2023), 013056, DOI.

[52] Liang Hu, E. Wang, L. Salvi, J. N. Tinsley, G. M. Tino, and N. Poli, *Sr atom interferometry with the optical clock transition as a gravimeter and a gravity gradiometer*, Class. Quantum Grav. **37** (2020), 014001, DOI.

[53] H. Katori, T. Ido, Y. Isoya, and M. Kuwata-Gonokami, *Magneto-optical trapping and cooling of strontium atoms down to the photon recoil temperature*, Phys. Rev. Lett. **82** (1999), 1116, DOI.

[54] H. Katori, T. Ido, and M. Kuwata-Gonokami, *Optimal design of dipole potentials for efficient loading of sr atoms*, J. Phys. Soc. Japan **68** (1999), 2479, DOI.

[55] P. Kirton, M. M. Roses, J. Keeling, and E. G. Dalla Torre, *Introduction to the Dicke model: From equilibrium to nonequilibrium, and vice versa*, Adv. Quantum Technol. **2** (2019), 1800043, DOI.

[56] J. A. Klugkist, M. Mostovoy, and J. Knoester, *Mode softening, ferroelectric transition, and tunable photonic band structures in a point-dipole crystal*, Phys. Rev. Lett. **96** (2006), 163903, DOI.

[57] O. Kock, Wei He, D. Swierad, L. Smith, J. Hughes, K. Bongs, and Y. Singh, *Laser controlled atom source for optical clocks*, Sci. Rep. **6** (2016), 37321, .

[58] G. Krenz, S. Bux, S. Slama, C. Zimmermann, and Ph. W. Courteille, *Controlling mode locking in optical ring cavities*, Appl. Phys. B **87** (2007), 643.

[59] D. Kruse, *Selbstorganisation und laseremission in kalten atomaren ensembles*, Ph.D. thesis, Universität Tübingen, 2004, http://www.uni-tuebingen.de/ub/elib/tobias.htm.

[60] D. Kruse, M. Ruder, J. Benhelm, C. von Cube, C. Zimmermann, Ph. W. Courteille, B. Nagorny, Th. Elsässer, and A. Hemmerich, *Cold atoms in a high-q ring-cavity*, Phys. Rev. A **67** (2003), 051802(R).

[61] N. Leppenen and E. Shahmoon, *Quantum bistability at the interplay between collective and individual decay*, ePrints **arXiv2404.0213** (2024), DOI.

[62] I. D. Leroux, M. H. Schleier-Smith, and V. Vuletic, *Implementation of cavity squeezing of a collective atomic spin*, Phys. Rev. Lett. **104** (2010), 073602, DOI.

[63] W. Lichten, *Precise wavelength measurements and optical phase shifts: I. general theory*, J. Opt. Soc. Am. A **2** (1985), 1869, .

[64] T. Loftus, C. A. Regal, C. Ticknor, J. L. Bohn, and D. S. Jin, *Resonant control of elastic collisions in an optically trapped Fermi gas of atoms*, Phys. Rev. Lett. **88** (2002), 173201.

[65] Huanqian Loh, Yu-Ju Lin, I. Teper, M. Cetina, J. Simon, J. K. Thompson, and V. Vuletic, *Influence of grating parameters on the linewidths of external-cavity diode lasers*, Appl. Opt. **45** (2008), 9191, .

[66] A. D. Ludlow, *The strontium optical lattice clock: Optical spectroscopy with sub-hertz accuracy*, Dissertation (2008), .

[67] A. D. Ludlow, S. Blatt, T. Zelevinsky, G. K. Campbell, M. J. Martin, J. W. Thomsen, M. M. Boyd, and J. Ye, *Ultracold strontium clock: Applications to the measurement of fundamental constant variations*, Eur. Phys. J. Special Topics **163** (2008), 9, DOI.

[68] C. Marzok, B. Deh, C. Zimmermann, Ph. W. Courteille, E. Tiemann, Y. V. Vanne, and A. Saenz, *Feshbach resonances in an ultracold* ^{7}*li and* ^{87}*rb mixture*, Phys. Rev. A **79** (2009), 012717, DOI.

[69] C. E. Máximo, R. Kaiser, Ph. W. Courteille, and R. Bachelard, *The atomic lighthouse effect*, J. Opt. Soc. Am. A **31** (2014), 2511.

[70] D. Meiser, Jun Ye, D. R. Carlson, and M. J. Holland, *Prospects for a millihertz-linewidth laser*, Phys. Rev. Lett. **102** (2009), 163601, DOI.

[71] V. Ménoret, P. Vermeulen, N. Le Moigne, S. Bonvalot, Ph. Bouyer, A. Landragin, and B. Desruelles, *Gravity measurement below* $10^{-9}g$ *with a transportable absolute quantum gravimeter*, Scientific Reports **8** (2018), 12300.

[72] P. G. Mickelson, Y. N. Martinez de Escobar, M. Yan, B. J. DeSalvo, and T. C. Killian, *Bose-Einstein condensation of* ^{88}*sr through sympathetic cooling with* ^{87}*sr*, Phys. Rev. A **81** (2010), 051601(R), DOI.

[73] T. Mukaiyama, H. Katori, T. Ido, Ying Li, and M. Kuwata-Gonokami, *Recoil-limited laser cooling of ^{87}sr atoms near the Fermi temperature*, Phys. Rev. Lett. **90** (2003), 113002, DOI.

[74] J. A. Muniz, M. A. Norcia, J. R. K. Cline, and J. K. Thompson, *A robust narrow-line magneto-optical trap using adiabatic transfer*, ePrints: arXiv:1806.00838 (2018), .

[75] S. B. Nagel, C. E. Simien, S. Laha, P. Gupta, V. S. Ashoka, and T. C. Killian, *Magnetic trapping of metastable $^3p_2$ atomic strontium*, Phys. Rev. A **67** (2003), 011401(R), DOI.

[76] M. A. Norcia, J. R. K. Cline, J. P. Bartolotta, M. J. Holland, and J. K. Thompson, *Narrow-line laser cooling by adiabatic transfer*, New J. Phys. **20** (2018), 023021, DOI.

[77] Yu. B. Ovchinnikov, *A zeeman slower based on magnetic dipoles*, Opt. Comm. **276** (2007), 261, DOI.

[78] B. M. Peden, D. Meiser, M. L. Chiofalo, and M. J. Holland, *Nondestructive cavity QED probe of Bloch oscillations in a gas of ultracold atoms*, Phys. Rev. A **80** (2009), 043803, DOI.

[79] E. Peik, M. Ben Dahan, I. Bouchoule, Y. Castin, and C. Salomon, *Bloch oscillations of atoms, adiabatic rapid passage, and monokinetic atomic beams*, Phys. Rev. A **55** (1997), 2989, DOI.

[80] K. I. Petsas, A. B. Coates, and G. Grynberg, *Crystallography of optical lattices*, Phys. Rev. A **50** (1994), 5173, .

[81] D. Plankensteiner, Ch. Hotter, and H. Ritsch, *Quantumcumulants.jl: A julia framework for generalized mean-field equations in open quantum systems*, Quantum **6** (2021), 617, DOI.

[82] N. Poli, R. E. Drullinger, G. Ferrari, J. Léonard, F. Sorrentino, and G. M. Tino, *Cooling and trapping of ultracold strontium isotopic mixtures*, Phys. Rev. A **71** (2005), 061403(R), DOI.

[83] N. Poli, G. Ferrar, M. Prevedelli, F. Sorrentino, R. E. Drullinger, and G. M. Tino, *Laser sources for precision spectroscopy on atomic strontium*, Spectrochimica Acta A **63** (2006), 981, DOI.

[84] A. V. Rakholia, H. J. McGuinness, and G. W. Biedermann, *Dual-axis high-data-rate atom interferometer via cold ensemble exchange*, Phys. Rev. Appl. **02** (2014), 054012, .

[85] A. Rawankar, J. Urakawa, H. Shimizu, Yan You, N. Terunuma, A. Aryshev, and Y. Honda, *Design studies on compact four mirror laser resonator with mode-locked pulsed laser for 5 um laser wire*, Nucl. Instr. Meth. Phys. Res. A **700** (2013), 145, DOI.

[86] L. Ricci, M. Weidemüller, T. Esslinger, A. Hemmerich, C. Zimmermann, V. Vuletic, W. König, and T. W. Hänsch, *A compact grating-stabilized diode laser system for atomic physics*, Opt. Comm. **117** (1995), 541.

[87] G. Ritt, G. Cennini, C. Geckeler, and M. Weitz, *Laser frequency offset locking using a side of filter technique*, Appl. Phys. B **79** (2004), 363, .

[88] D. Rivero, C. A. Pessoa Jr., G. H. de França, R. C. Teixeira, S. Slama, and Ph. W. Courteille, *Quantum resonant optical bistability with a narrow atomic transition: bistability phase diagram in the bad cavity regime*, New J. Phys. **25** (2023), 093053, DOI.

[89] J. Ruostekoski, *Optical kagome lattice for ultracold atoms with nearest neighbor interactions*, Phys. Rev. Lett. **103** (2009), 080406, DOI.

[90] P. A. Ruprecht, M. J. Holland, K. Burnett, and M. Edwards, *Time-dependent solutions of the nonlinear schrödinger equation for Bose-condensed trapped neutral atoms*, Phys. Rev. A **51** (1995), 4704.

[91] A. Saenz, *461nm laser for studies in ultracold neutral strontium*, Ph.D. thesis, Rice University, 2004.

[92] L. Salvi, N. Poli, V. Vuletić, and G. M. Tino, *Squeezing on momentum states for atom interferometry*, Phys. Rev. Lett. **120** (2018), 033601, DOI.

[93] M. Samoylova, N. Piovella, R. Bachelard, and Ph. W. Courteille, *Microscopic theory of photonic bandgaps in optical lattices*, Opt. Comm. **312** (2014), 94.

[94] M. Samoylova, N. Piovella, M. Holynski, Ph.W. Courteille, and R. Bachelard, *One-dimensional photonic band gaps in optical lattices*, Annual Review of Cold Atoms and Molecules **2** (2014), 193.

[95] J. E. Sansonetti and G. Nave, *Wavelengths, transition probabilities, and energy levels for the spectrum of neutral strontium*, J. Phys. Chem. Ref. Data **39** (2010), 033103, DOI.

[96] R. Santra, E. Arimondo, T. Ido, Ch. H. Greene, and Jun Ye, *High-accuracy optical clock via three-level coherence in neutral bosonic* ^{88}sr, Phys. Rev. Lett. **94** (2005), 173002, DOI.

[97] W. Saslow, T. K. Bergstresser, and M. L. Cohen, *Band structure and optical properties of diamond*, Phys. Rev. Lett. **16** (1966), 0354, .

[98] M. H. Schleier-Smith, I. D. Leroux, and V. Vuletic, *Squeezing the collective spin of a dilute atomic ensemble by cavity feedback*, Phys. Rev. A **81** (2010), 021804(R), DOI.

[99] M. O. Scully, *Correlated spontaneous emission on the volga*, Laser Phys. **17** (2007), 635.

[100] E. Shahmoon, D. S. Wild, M. D. Lukin, and S. F. Yelin, *Cooperative resonances in light scattering from two-dimensional atomic arrays*, Phys. Rev. Lett. **118** (2017), 113601, DOI.

[101] S. Slama, S. Bux, G. Krenz, C. Zimmermann, and Ph. W. Courteille, *Superradiant Rayleigh scattering and collective atomic recoil lasing in a ring cavity*, Phys. Rev. Lett. **98** (2007), 053603.

[102] S. Slama, C. von Cube, A. Ludewig, M. Kohler, C. Zimmermann, and Ph. W. Courteille, *Dimensional crossover in Bragg scattering from optical lattices*, Phys. Rev. A **72** (2005), 031402(R).

[103] J. Söding, D. Guéry-Odelin, P. Desbiolles, F. Chevy, H. Inamori, and J. Dalibard, *Three-body decay of a rubidium Bose-Einstein condensate*, Appl. Phys. B **69** (1999), 257, .

[104] O. Somech and E. Shahmoon, *Quantum entangled states of a classically radiating macroscopic spin*, Phys. Rev. X Quantum **5** (2024), 010349, DOI.

[105] Y. Song, D. Milam, and W. T. Hill III, *Long, narrow all-light atom guide*, Opt. Lett. **24** (1999), 1805, .

[106] F. Sorrentino, G. Ferrari, N. Poli, R. Drullinger, and G. M. Tino, *Laser cooling and trapping of atomic strontium for ultracold atoms physics, high-precision spectroscopy and quantum sensors*, Modern Physics Letters B **20** (2006), 1287, DOI.

[107] D. A. Steck, *Rubidium 87 d line data*, unpublished (2003), .

[108] S. Stellmer, M. K. Tey, Bo Huang, R. Grimm, and F. Schreck, *Bose-Einstein condensation of strontium*, Phys. Rev. Lett. **103** (2009), 200402, DOI.

[109] A. V. Taichenachev, V. I. Yudin, C. W. Oates, C. W. Hoyt, Z. W. Barber, and L. Hollberg, *Magnetic field-induced spectroscopy of forbidden optical transitions with application to lattice-based optical atomic clocks*, Phys. Rev. Lett. **96** (2006), 083001, DOI.

[110] Marco Giacinto Tarallo, *Development of a strontium optical lattice clock*, Ph.D. thesis, Università degli studi di Pisa, 2009.

[111] Meng Khoon Tey, S. Stellmer, R. Grimm, and F. Schreck, *Double-degenerate Bose-Fermi mixture of strontium*, Phys. Rev. A **82** (2010), 011608(R), DOI.

[112] O. Toader, T. Y. M. Chan, and S. John, *Photonic band gap architectures for holographic lithography*, Phys. Rev. Lett. **92** (2004), 043905, .

[113] A. Traverso, R. Chakraborty, Y. N. Martinez de Escobar, P. G. Mickelson, S. B. Nagel, M. Yan, and T. C. Killian, *Inelastic and elastic collision rates for triplet states of ultracold strontium*, Phys. Rev. A **79** (2009), 060702(R), DOI.

[114] D. V. van Coevorden, R. Sprik, A. Tip, and A. Lagendijk, *Photonic band gap structure of atomic lattices*, Phys. Rev. Lett. **77** (1996), 2412, .

[115] M. Weidemüller, A. Görlitz, Th. W. Hänsch, and A. Hemmerich, *Local and global properties of light-bound atomic lattices investigated by Bragg diffraction*, Phys. Rev. A **58** (1998), 4647, .

[116] M. Weidemüller, A. Hemmerich, A. Görlitz, T. Esslinger, and Th. W. Hänsch, *Bragg diffraction in an atomic lattice bound by light*, Phys. Rev. Lett. **75** (1995), 4583, .

[117] D. Wilkowski, *Runaway evaporation for optically dressed atoms*, eprints:arXiv1011.4372 (2010), .

[118] D. Wilkowski, M. Chalony, R. Kaiser, and A. Kastberg, *Low- and high-intensity velocity selective coherent population trapping in a two-level system*, Europhys. Lett. **86** (2009), 53001, DOI.

[119] D. J. Wineland, J. J. Bollinger, W. M. Itano, and D. J. Heinzen, *Squeezed atomic states and projection noise in spectroscopy*, Phys. Rev. A **50** (1994), 67, DOI.

[120] Jin-Hui Wu, M. Artoni, and G. C. La Rocca, *Controlling the photonic band structure of optically driven cold atoms*, J. Opt. Soc. Am. B **25** (2008), 1840, DOI.

[121] Xinye Xu, T. H. Loftus, J. L. Hall, A. Gallagher, and Jun Ye, *Cooling and trapping of atomic strontium*, J. Opt. Soc. Am. B **20** (2003), 968.

[122] Nan Yu and M. Tinto, *Gravitational wave detection with single-laser atom interferometers*, Gen. Relativ. Gravit. **43** (2011), 1943, DOI.

[123] P. Zhang, Sheng Liu, Cibo Lou, Fajun Xiao, Xiaosheng Wang, Jianlin Zhao, Jingjun Xu, and Zhigang Chen, *Incomplete brillouin-zone spectra and controlled Bragg reflection with ionic-type photonic lattices*, Phys. Rev. A **81** (2010), 041801(R), .

Index

μ-metal, 123

absorption signal, 67
atom-field coupling constant, 143

band pass filter, 235

cat eye laser, 235
cavity field decay rate, 142
cavity pumping rate, 143
cavity-to-free space ratio, 143
clock transitions, 267
collision
    fine changing, 133
    hyperfine changing, 133
cooperativity parameter, 143

dipole moment, 142
Doppler broadening, 82
Doppler cooling limit, 82

earth magnetic field, 77
eddy currents, 69

free spectral range, 142

gravimeter
    absolute, 258
    relative, 258
gravitational sag, 77

intensity decay rate, 142
intensity transmission, 142

lighthouse effect, 78

magnetic trap, 53

one-photon field amplitude, 142

partial pressure of strontium, 66

radiative escape, 133

saturation parameter, 144
scanning etalon, 65
self-induction, 69
superradiance, 267